ISSN 0911-5730
UVSOR-20
March 1993

UVSOR
ACTIVITY REPORT
1992

Ultraviolet Synchrotron Orbital Radiation Facility
Institute for Molecular Science

CONTENTS

ACTIVITIES

LIGHT SOURCE & BEAMLINES

GASES

SOLIDS

SURFACES

INSTRUMENTATION

FAR INFRARED

ABSTRACTS OF THE 46TH OKAZAKI CONFERENCE

APPENDIX

Control of the Bunch Length on the UVSOR Storage Ring [II]

Hiroyuki HAMA, Shiro TAKANO*) and Goro ISOYAMA
UVSOR Facility, Institute for Molecular Science, Myodaiji, Okazaki 444

The experimental study to make the bunch length of the electron beam short is in progress on the UVSOR storage ring by means of reducing a momentum compaction factor. A part of the preliminary results was reported in the last issue of the activity report.

The experiment has been carried out in the single-bunch mode at an electron energy of 600 MeV. At the injection point, the momentum compaction factor α was experimentally determined to be 0.035, and the bunch length was measured to be 260 ps (2σ)[1]. According to a model calculation[2], we synchronously changed excitation currents of the quadrupole (Q) magnets step by step to reduce α after the beam injection. A new accelerator control system[3] using μ-VAX computers with an application "UCOSS" has capacitated to make this experiment. To derive α at each operating point, the horizontal beam displacement as a function of the RF frequency and the synchrotron oscillation frequency (f_s) were measured. The bunch length was also measured directly using a fast photomultiplier with a single photon counting. The bunch length at a low beam current was successfully shortened down to ~40 ps, which was consistent with the other two measurements. In the very low α region, however, it was found out that effect of the second order term in the momentum compaction factor α_2 revealed itself, and then the beam lifetime became short. It is obviously a serious problem for stable operation with low α.

Because the second order term originates in the chromatic effect of the Q-magnets on the dispersion function, the effect of α_2 should be compensated with focusing sextupole (SF) magnets. The strength of the sextuple magnets was chosen to correct the chromaticities so far. Figure 1 shows the RF frequency dependence of f_s for various strengths of the SF-magnets at an operating point with α = 0.0009. Values of α_2 were derived by a fitting analysis with an analytical formula[4] including the α_2 term. A linear dependence of α_2 on the strength of the SF-magnets can be seen in the insert. In this case, the best correction was achieved when the SF strength was reduced to ~ 86 % of the initial value.

A direct measurement of bunch length with a streak camera[5] was in progress. The strength of SF-magnets was reduced to make α_2 nearly zero in the measurement, so that the momentum compaction factor was further reduced. In figure 2, the measured bunch length is plotted as a function of f_s which was measured simultaneously with the bunch length. A shape of a focusing image on a screen of the streak camera was taken account to analyze the data. Time resolution of the streak camera was estimated to be 16 ps, which is mainly due to time jitters of the streak trigger. Typical bunch profiles measured by the streak camera are shown in the inserts. The bunch length is almost proportional to the synchrotron oscillation frequency over the wide range, as predicted by theory. The shortest bunch length realized was 23 ps (~ 7 mm), and the estimated momentum compaction factor was 0.0003.

*) *Present address: SPring-8 Project Team, RIKEN, 2-1 Hirosawa, Wako 351-01, Japan*

References

1) A. Lin, H. Hama, S. Takano and G. Isoyama, Jpn. J. Appl. Phys. 31 (1992) 921.
2) J. Staples, LATTICE, LBL report No. 23939 (Lawrence Berkeley Laboratory, Berkeley, 1987).
3) N. Kanaya, H. Hama, J. Yamazaki, O. Matzudo and G. Isoyama, in preparation.
4) H. Hama, S. Takano and G. Isoyama, to be published in Nucl. Instr. and Meth.
5) Y. Tsuchiya, A. Takeshima, E. Inuzuka, K. Suzuki, M. Koishi and K. Kinoshita, Proc. of 16th Int. Cong. on High Speed Photography and Photonics (Strasbourg, 1984) Vol. 491.

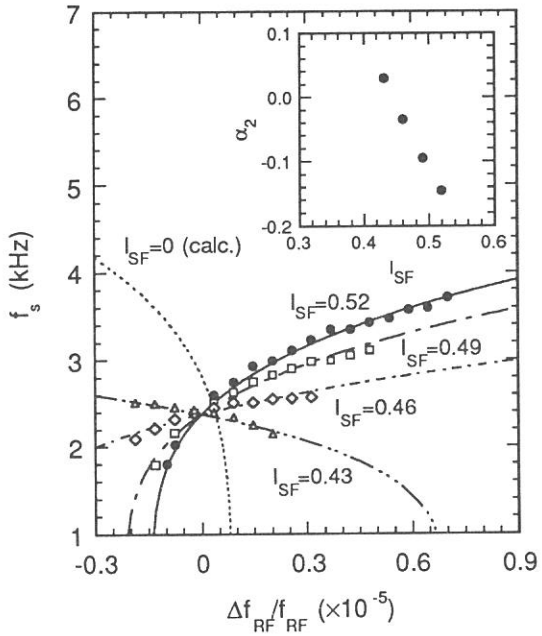

Fig. 1. Measured synchrotron oscillation frequency f_s as a function of the RF frequency for various strengths of the focusing sextupoles at the operation point with α = 0.0009. The theoretical curve for α_2 = + 0.518 is also shown by the dotted line. Experimantal values of the second order momentum compaction factor are plotted as a function of the strength of the sextupoles in the insert.

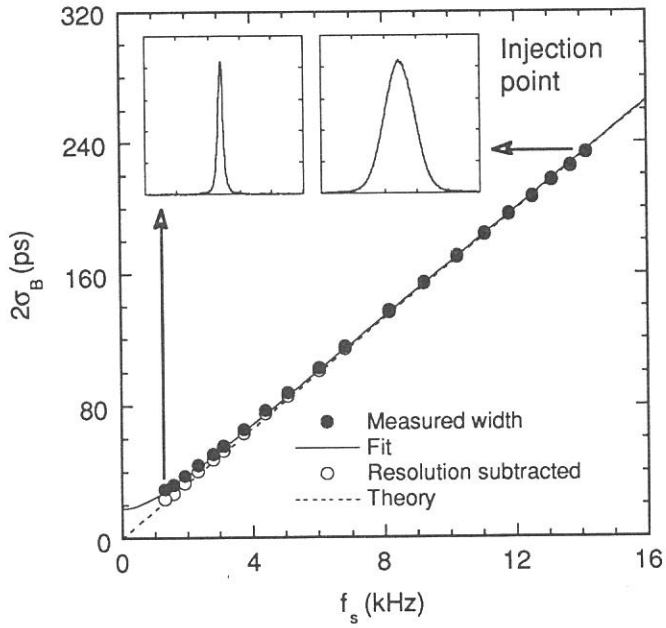

Fig. 2. Measured bunch length with the streak camara as a function of the synchrotron frequency observed simultaneously. The solid line is a fit taking account the time resolution of the streak camera. Typical bunch profiles are shown in the inserts.

Lasing of a Free Electron Laser in Visible on the UVSOR Storage Ring

Shiro TAKANO, Hiroyuki HAMA and Goro ISOYAMA
UVSOR Facility, Institute for Molecular Science
Myodaiji, Okazaki 444

Free electron laser (FEL) experiments are in progress on the UVSOR storage ring. FEL gain at a wavelength of 488 nm was measured with a conventional undulator at an electron energy of 500 MeV [1]. As the measured peak gain of 8×10^{-4} for the beam current of 10 mA/bunch was marginal to achieve lasing, the undulator was remodeled into an optical klystron (OK) in order to increase the gain. The gain with the OK was measured at the wavelength to be 0.4 % at 10 mA/bunch [2]. An optical resonator was installed for oscillation experiments, and the first lasing was obtained at a wavelength of 456 nm on March 8, 1992 [3].

The optical resonator consists of a pair of spherical mirrors separated by a distance of 13.3 m, which is a quarter of the circumference of the storage ring. As there is not enough room in the upstream of the OK, the optical cavity is asymmetric. Radii of curvature of the front and the rear mirrors are 8 and 6 m, respectively. The radius of the waist for the TEM_{00} mode is 0.48 mm. The filling factor calculated from overlap with the electron beam is 0.33. We have used mirrors coated with dielectric multilayer.

The geometrical axis of the optical cavity is aligned with the electron beam in the OK by using spontaneous radiation. In order to synchronize the light pulse stored in the cavity and electron

bunches, the cavity length is precisely tuned such that the width of the temporal profile of spontaneous radiation stored in the cavity is minimized.

For the oscillation experiments, the storage ring is operated in the two-bunch mode at the energy of 500 MeV. Figure 1 shows spectra of output light from the optical cavity for beam currents ranging from 21.5 down to 9 mA/bunch, which are measured with a monochromator equipped with a one-dimensional photodiode array. The laser line at λ= 456.6 nm is clearly seen in Fig.1 (a) and (b). The linewidth is approximately $\Delta\lambda$ = 0.2 nm (FWHM) after the monochromator resolution is subtracted. The relative linewidth $\Delta\lambda/\lambda$ is 4×10^{-4}. Figure 1 (c) and (d) show the spectra just above and below the lasing threshold, respectively. The macro-temporal structure of the laser light is observed with a PIN silicon photodiode. When the rf frequency is tuned to give the maximum output power, a quasi-periodic pulsed

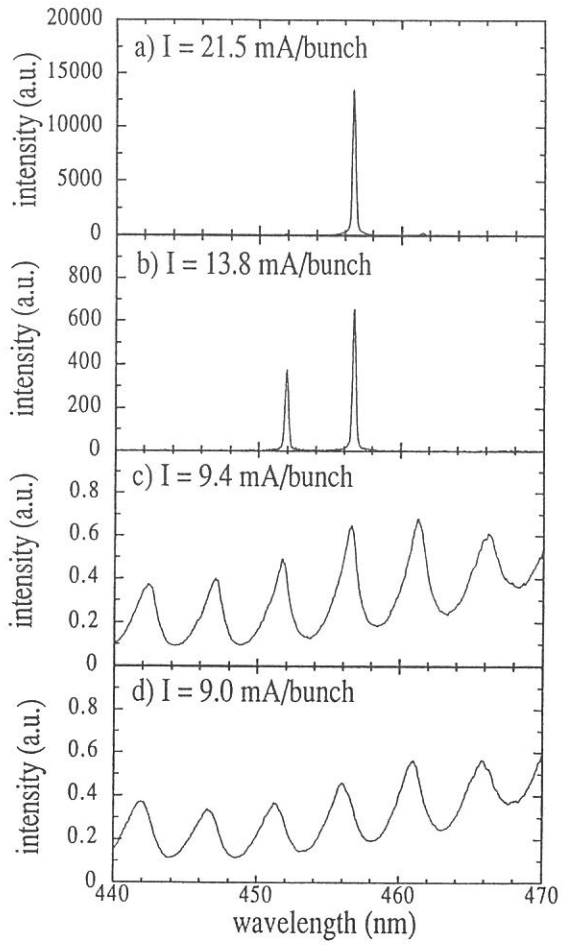

Fig. 1. Spectra of output light transmitted by the front mirror of the optical cavity.

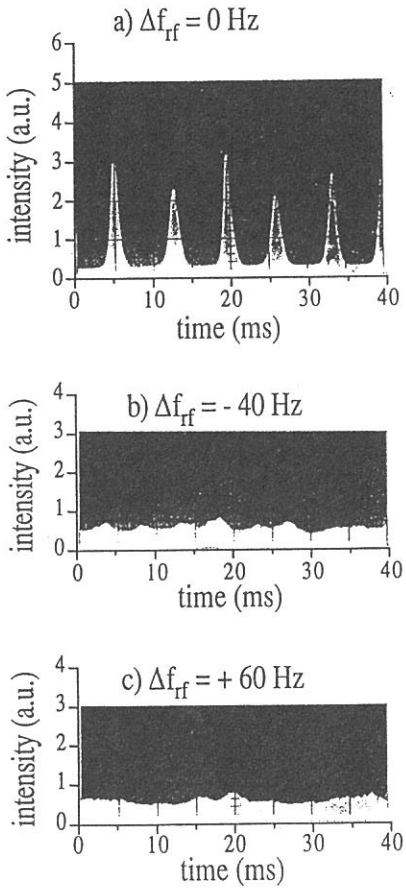

Fig. 2. Time profile of the laser light.

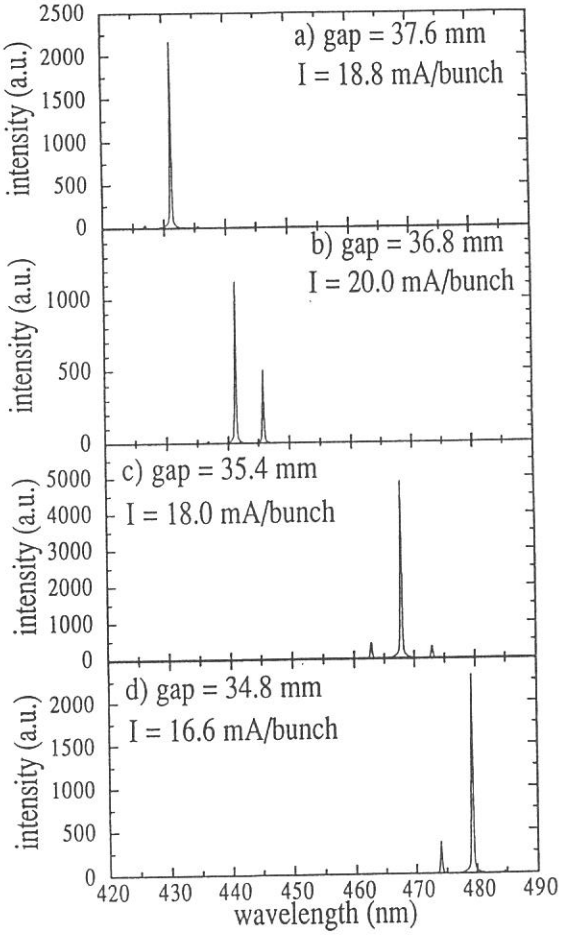

Fig. 3. Tunability of the laser wavelength.

structure is observed as shown in Fig. 2 (a). The rise time and the typical repetition period are approximately 1 and 7 ms, respectively. When the rf frequency is detuned, the CW structure appears as shown in Fig. 2 (b) and (c), though the intensity fluctuates. The maximum time-averaged output power is 0.2 mW when the beam current was 23 mA/bunch. From the measured duty ratio of macro pulse structure and the bunch length, the peak output power of the micro pulse is estimated to be more than 0.8 W. Lasing continues over the range from 430 to 480 nm when the magnet gap in the undulator sections is varied. Figure

3 shows some of the spectra of the laser light at various wavelengths.

References

[1] S. Takano, H. Hama, G. Isoyama, A. Lin and N.A. Vinokurov, Jpn. J. Appl. Phys. **31**(1992)2621.

[2] S. Takano, H. Hama and G. Isoyama, UVSOR Activity Report 1991, p. 4: S. Takano, H, Hama and G. Isoyama, submitted to Jpn. J. Appl. Phys.

[3] S. Takano, H. Hama and G. Isoyama, submitted to Nucl. Instr. and Meth. Phys. Res.

Apparatus for photoemission spectroscopy of solids and solid surfaces at BL2B1

Shin-ichiro TANAKA, Masao KAMADA and Yukihiro TAGUCHI*

Institute for Molecular Science, Okazaki 444
* College of Engineering, University of Osaka Prefecture, Mozu, Sakai, Osaka 591

We have constructed a new experimental system for the photoemission and absorption spectroscopy at BL2B1, where a 2-meter grazing incidence monochromator (Grasshopper Mark XV) has already been installed. It covers a photon energy range from 40 to 800 eV, and is suited to the core-level photoemission and absorption spectroscopy.

Figure 1 shows the schematic diagram of the apparatus. It consists of three chambers. Spectroscopic measurements are performed in the main chamber equipped with a double-pass CMA (Cylindrical Mirror Analyzer) with a coaxial electron gun, a LEED (Low Energy Electron Diffraction) optics, a quadrupole mass spectrometer, a gas doser, etc. The base pressure of the main chamber is $< 5\times10^{-11}$ Torr after a bakeout. The photoabsorption spectroscopy is measured via monitoring a total photoelectron with a picoammeter connected to the sample. The angle-integrated photemission spectroscopy is measured with the CMA. Constant initial state spectroscopy, constant final state spectroscopy, and Auger electron spectroscopy can also be measured. The time dependence of the incident light intensity and the transmission function of the monochromator is monitored with a gold grid located across the light beam.

The preparation of the samples is carried out in the preparation chamber which is equipped with a file, an evaporation source, and so on. The base pressure of this chamber is $< 1.5\times10^{-9}$ torr.

When samples are changed, the insertion chamber is opened to air, and pumped for ~1 hour. Then the sample can be transferred into the preparation chamber and the main chamber via a magnetically coupled linear-rotary motion device. The pressure of the main chamber is maintained below 4×10^{-9} Torr during the transfer and returns to $\sim1\times10^{-10}$ Torr in a few minuets after closing the valve.

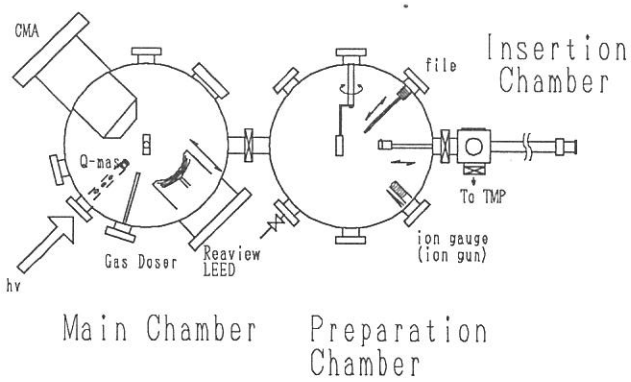

Figure 1

A Schematic diagram of an experimental apparatus at BL2B1

Beamline BL4B: Construction of an Apparatus for the Study of Synchrotron Radiation-Excited Semiconductor Processes

Tsuneo Urisu, Kazuhiko Mase, Haruhiko Ohashi, and Kosuke Shobatake
Institute for Molecular Science, Myodaiji, Okazaki 444

Synchrotron radiation (SR) is a powerful tool for studying surface physics and structure determination, and very active research is being undertaken in many SR facilities over the world. In recent years, another capability of SR, i.e. its application to microfabrication, is being explored. Its application to X-ray lithography is a typical example. Since semiconductor processes using SR have been expected to open its new potentialities of applying it as a fabrication tool, its research has attracted considerable attention from not only the technological viewpoints but also purely scientific ones of developing a new field in molecular science, i.e. surface photochemistry in the vacuum UV region /1/. In order to realize these goals we are now constructing an apparatus on beamline BL4b to study SR-excited semiconductor processes /2/.

The design for the whole apparatus has been just completed. It consists of five ultrahigh vacuum chambers, i.e. an etching chamber, an epitaxial growth or CVD chamber, an XPS surface analysis chamber, a sample storage chamber, and an air-lock chamber. The reaction mechanisms and dynamics of semiconductor processes will be the focus of our research using this apparatus. In addition to XPS, in-situ observations of adsorbed species by infrared absorption spectroscopy as well as detection of the desorbed ionic species by the time-of-flight mass spectroscopy are in preparation.

Figure 1 illustrates the top view of the apparatus connected to Beamline BL4B. SR beam is incident from the left side of the etching chamber. Design parameters are as follows:

Epitaxial chamber : Pumped by a 500 ℓ/sec turbomolecular pump(TMP). Expected base pressure: 1×10^{-9} Torr. Sample is heated by PBN/PG heater up to 1200 ℃, RHEED: Electron energy is 30 kV, Differentially pumped by 150 ℓ/sec TMP. IR port: BaF_2 window, incident angle, 82.5 $\pm$ 5 degrees.

Etching chamber : Pumped by 300 ℓ/sec TMP. Expected base pressure: 1×10^{-9} Torr. Sample heating and cooling: 100 K - 600 K, IR port: BaF_2 window, incident angle, 85 $\pm$ 5.

Sample storage chamber : Pumped by 300 ℓ/sec TMP. Expected base pressure: 1×10^{-9} Torr. Sample holders: A sample holder cleaned by heating up to 1200 ℃ using a PBN/PG heater. Three holders for sample storage. LEED is used for surface characterization.

Air-lock chamber : Pumped by 150 ℓ/sec TMP. Expected base pressure: 1×10^{-7} Torr. Sample holder: 4 holders.

XPS chamber : Pumped by a 270 ℓ/sec ion pump, a Ti sublimation pump, and a 150 ℓ/sec TMP. Base pressure: 1×10^{-10} Torr. XPS analyzer: spherical analyzer (VSW), using a Mg K_α X-ray source. IR port: BaF_2 window; incident angle: 82.5 $\pm$ 5 degrees.

REFERENCES

(1) T. Urisu, et. al., Applied Organometallic Chemistry 5, (1991) 229.

(2) H. Ohashi, et. al., UVSOR Activity Report (1991) 15.

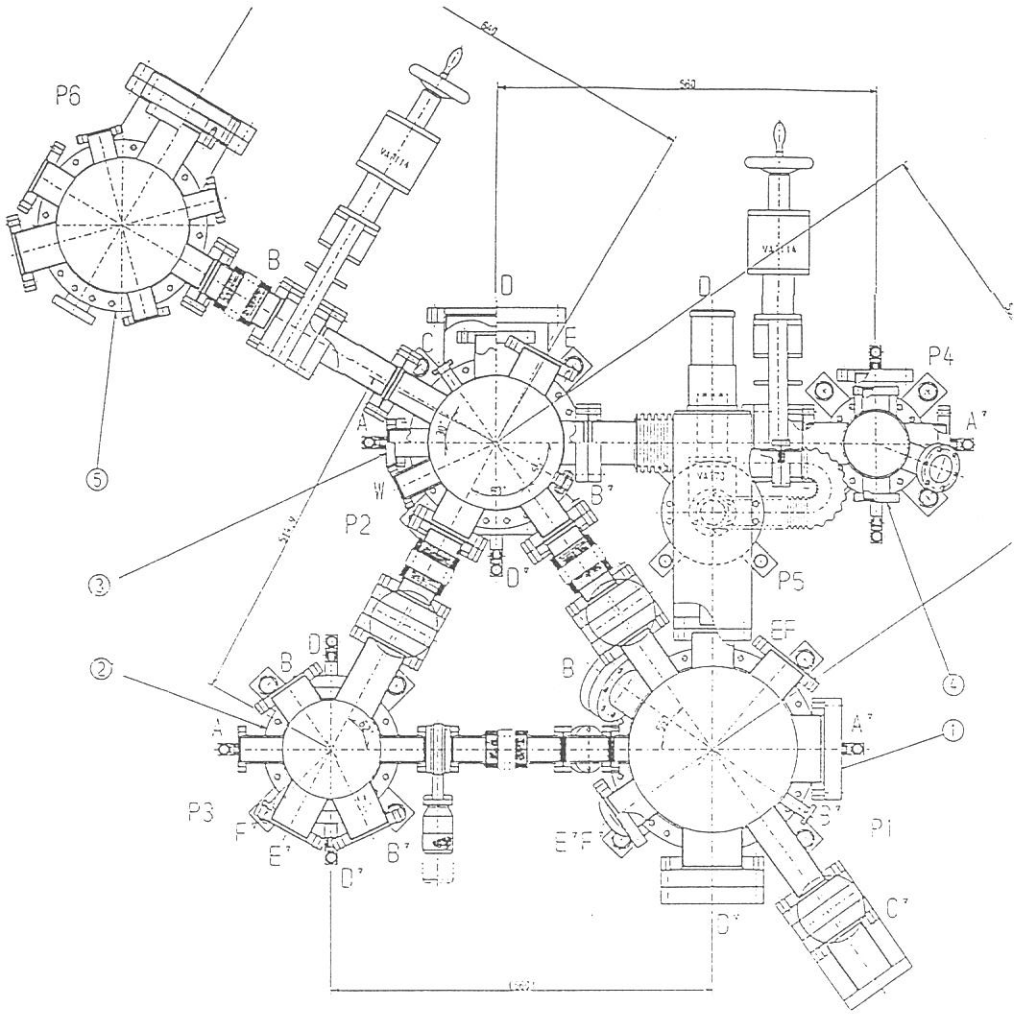

Fig. 1 Top view of the apparatus for the study of synchrotron radiation-excited semiconductor processes under construction on beamline BL4B. ① : Epitaxial chamber, ② : Etching chamber, ③ : Sample storage chamber, ④ : Air-lock chamber, ⑤ : XPS chamber.

A monochromator for measurement of fluorescence spectra of gases at the BL8B1 beamline of UVSOR

Shigeyoshi UMEMIYA[a], Eiji ISHIGURO[a], Toshio IBUKI[b],
Haruhiko OHASHI[c], Atsunari HIRAYA[c], Kusuo SAKAI[c], and Makoto WATANABE[c]

[a] Department of Applied Physics, Osaka City University, Sumiyoshi-ku, Osaka 558

[b] Kyoto University of Education, Fushimi-ku, Kyoto 612

[c] Institute for Molecular Science, Myodaiji, Okazaki 444

A VUV monochromator for fluorescence measurement was recently constructed and attached to an absorption cell behind a grazing incident monochromator in the BL8B1. Fig.1 shows the optical system. The absorption cell has a quartz window and a LiF window at both sides in the direction perpendicular to the incident beam. Fluorescence from the quartz window is focused by a quartz lens on an entrance slit of a Jobin-Yvon monochromator with a multichannel detector which is placed in the air, while that from the LiF window is dispersed by a 0.28 m spherical grating with 1200 l/mm in the vacuum chamber. Thus, the fluorescence spectra of gases in the region from 110 nm to 800 nm can be observed by this optical system.

We give here some examples of fluorescence observed with this apparatus. Figures 2 and 3 show the spectra of HCl which was excited by the zero order light of the grazing incident monochromator. The energy of the incident light extends from 70 eV to 280 eV with the maximum at 150 eV. Many sharp lines in the region above 300 nm can be assigned to emissions of atomic ions Cl^+ and two lines around 120 nm to H-Lyα and neutral Cl $^2P^o$-^2P. Broad bands in the region from 200 nm to 270 nm also are attributed to overlap of many atomic lines of ions Cl^+ and Cl^{++}, although they look like a molecular structure. Photoabsorption of the Cl-L edge starts at 200 eV and can be excited by the present incident white light, while the photoabsorption cross section of the valence shell of HCl is very weak around 200 eV. Valence excitation by a He resonance line of 58.4 nm(21.2 eV) yields the fluorescence of $HCl^+(A^2\Sigma^+ \rightarrow X^2\Pi)$[1,2] in the region from 250 to 450 nm. To the contrary, the relaxation paths following the Cl-L inner shell excitation leads to dissociation of HCl.

An another example of BrCN observed with the spherical grating monochromator is shown in fig.4. All lines in this region are due to neutral and ionic atoms of C and Br. The resolution is estimated to be approximately 100 at 200 nm.

References

1. T. Ibuki, N. Sato, and S. Iwata, J. Chem. Phys. **79**, 4805(1983).
2. B. P. Tsai and L. L. Parrella, J. Chem. Phys. **76**, 745(1982).

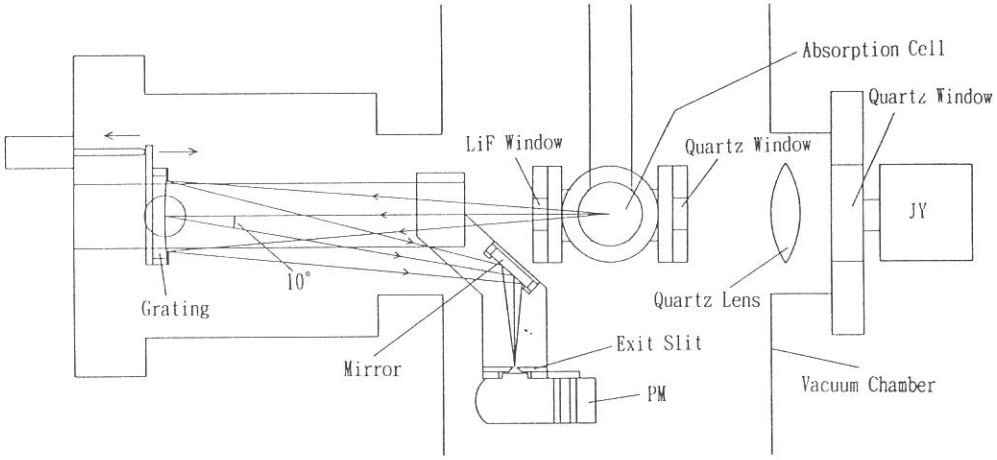

Fig. 1 Optical system for measurement of dispersed fluorescence
PM; photomultiplier, JY; Jobin-Yvon monochromator

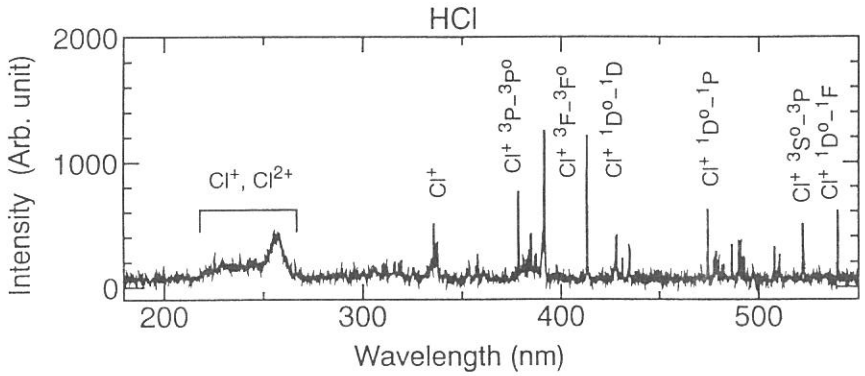

Fig. 2. Dispersed fluorescence spectrum of HCl in the region from 180 to 550 nm, measured with Jobin-Yvon monochromator in the air.

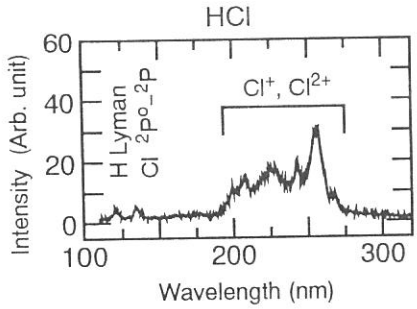

Fig. 3.
Dispersed fluorescence spectrum of HCl in the Vacuum UV and UV region

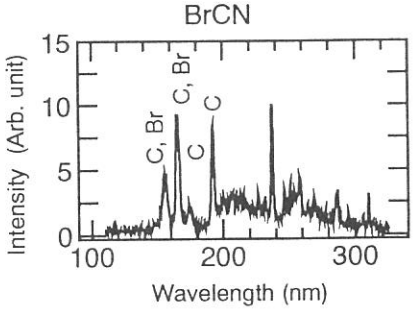

Fig. 4.
Dispersed fluorescence spectrum of BrCN in the Vacuum UV and UV region

Photoabsorption Spectra of Alkali Cyanide Molecules in the Vacuum Ultraviolet Region

Hisato YASUMATSU, Tamotsu KONDOW,
Department of Chemistry, Faculty of Science, The University of Tokyo, Hongo, Bunkyo-ku, Tokyo 113, Japan
Kaoru SUZUKI, Kiyohiko TABAYASHI and Kosuke SHOBATAKE
Institute for Molecular Science, Myodaiji, Okazaki 444, Japan

It has been discovered in the collisional energy transfer from metastable rare gas atoms, $Ar(^3P_{2,0})$ or $Kr(^3P_{2,0})$, to alkali cyanide molecules, MCN (M=Na, K, Rb), that there exist two types of dissociative states, which lead to the M+CN($B^2\Sigma^+$) channel; one is a repulsive state and the other is a predissociative excited ion-pair state [1]. In order to obtain information on dissociative states, the photoaborption spectra of MCN in the energy range of about 6~11 eV were measured by use of BL-2A beam line.

Figure 1 shows an experimental set-up. A 1 m *Seya-Namioka* monochromator was used to monochromatize the synchrotron orbit radiation (SOR). An absorption cell containing a sample was heated up to 1000 K to maintain a vapor pressure of about 100 mTorr. The absorption cell was windowless; stainless steel capillaries with an inner diameter of 2 mm and a length of 30 mm were mounted at both ends of the absorption cell. Argon gas was blown onto the lithium fluoride window separating the measurement chamber from the SOR source so as to prevent the sample from depositing on it.

Panels (a) and (b) of Fig. 2 show the absorption spectra of NaCN and RbCN, respectively. The spectra consist of (1) peaks centering at 6.5, 8 and 10 eV with a fwhm of about 2 eV, (2) intense and broader structures, and other peaks. The energies of the peaks (1) were found to be almost independent of M, while the absorption edge of the broad structure (2) was red-shifted in parallel with the ionization potential of M, I_p[M].

Figure 3 shows the schematic potential enrgy curves of MCN. The repulsive portions of the potential energy curves are mimicked from those of MCl, because the electron affinity of CN is almost the same as that of Cl, and the ion-pair states are governed by the Coulomb interaction at a sufficiently large distance between M and CN, R_{M-CN}. The Franck-Condon transitions to the repulsive states give rise to the broad peaks with a fwhm of 1.5~2.5 eV. It is assigned, therefore, that the peaks of 6.5, 8 and 10 eV originate from the Franck-Condon transition to the repulsive states correlating to the M+CN(X), the M+CN(A) and the M+CN(B) channels, respectively. The other peaks correspond to the transitions to M*+CN(X, A and B) channels. On the other hand, the energies of ion-pair states are specifically dependent on M because of the I_p[M] difference as shown in Fig. 3. The intense and broad structures associated with the ion-pair states are explained in terms of thier high density of states [2] in this energy range. Our *ab initio* calculations of the potential energy curves of CN^- [3] shows that the density of states of $(CN^-)^*$ is very large in the energy range above 6 eV.

References

[1] H. Yasumatsu, K. Suzuki and T. Kondow, *to be published.*

[2] The density of states of excited ion-pair states, $M^+ \cdot (CN^-)^*$, is approximated to be given by that of $(CN^-)^*$.

[3] H. Yasumatsu, S. Iwata and T. Kondow, *to be published.*

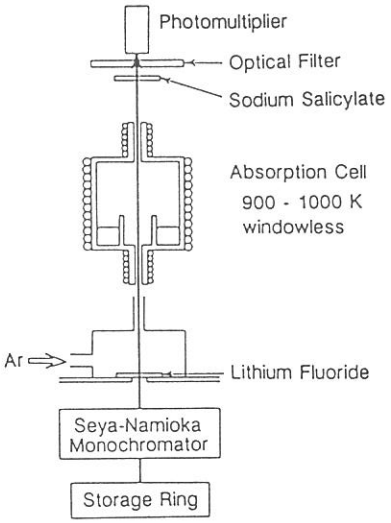

Figure 1: Schematic diagram of the apparatus.

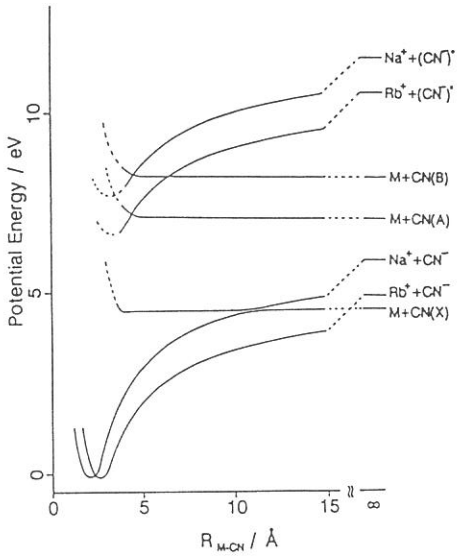

Figure 3: Schematic potential energy curves of MCN.

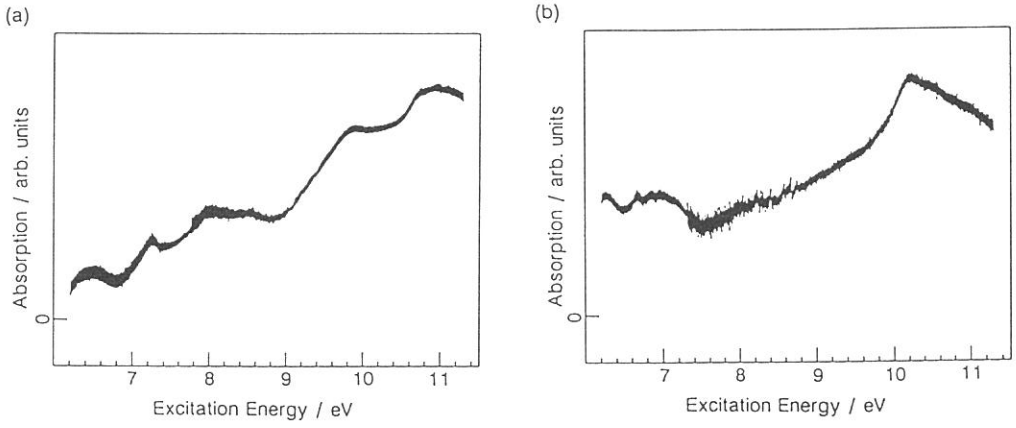

Figure 2: Absorption spectra of NaCN (panel (a)) and RbCN (panel (b)).

PHOTODISSOCIATION OF CYANOGEN IODIDE IN 105 - 175 nm REGION

Kazuhiro KANDA, Shunji KATSUMATA,
Takashi NAGATA*, Tamotsu KONDOW*,
Atsunari HIRAYA**, Kiyohiko TABAYASHI** and Kosuke SHOBATAKE**

Department of Fundamental Science, College of Science and Engineering, Iwaki Meisei University, Iwaki 970
* Department of Chemistry, Faculty of Science, The University of Tokyo, Bunkyo-ku 113
** Institute for Molecular Science, Myodaiji, Okazaki 444

When a cyanogen iodide (ICN) is photolyzed by a vacuum ultraviolet (VUV) radiation, a CN radical is formed in a variety of electronically excited states. The CN fragment produced in $A^2\Pi_i$ or $B^2\Sigma^+$ states immediately decays via radiative processes into the ground electronic state. In the present study, the quantum yields for the production of CN(A) and CN(B) in the photodissociation of ICN were determined in the wavelength range of 105 - 175 nm by monitoring the subsequent CN emission as a function of excitation energy. The measurement was performed at the BL2A station of UVSOR.

Figure 1 depicts the observed VUV absorption spectrum of ICN (upper panel) along with quantum yield curves for the CN^* production (lower panel). Those absorption bands are assignable to the Rydberg transitions.[1] While the yield curves show complex structures, close examination reveals following tendencies; (1) the curves have dips at the wavelengths where the absorption cross section reaches maxima, and (2) the two yield curves almost mimic each other. By considering the fact that the absorption spectrum has non-zero base line, the finding (1) indicates that underlying continuum makes contribution to the production of both CN(A) and CN(B). The finding (2) implies that CN(A) and CN(B) fragments are produced via identical precursor states of ICN, while the

branching fraction for the CN(A) production is 2-3 times larger than that for CN(B). The highest occupied molecular orbital of ICN, $2\pi(\pi_{C-N})$ bonding orbital, correlates to the 1π orbital of CN radical. Hence, the promotion of an electron from the 2π orbital possibly gives rise to a hole in the 1π orbital of the incipient CN radical, which asymptotically correlates to a free CN fragment in $A^2\Pi_i$ state. It is inferred from the orbital-correlation scheme that the underlying continuum is associated with transitions involving an configurational excitation of the 2π electron. The quantum yields decrease abruptly at ~114 nm as increasing the excitation energy. This sudden drop in the quantum yield is ascribed to the ionization process which starts to occur at 114 nm.

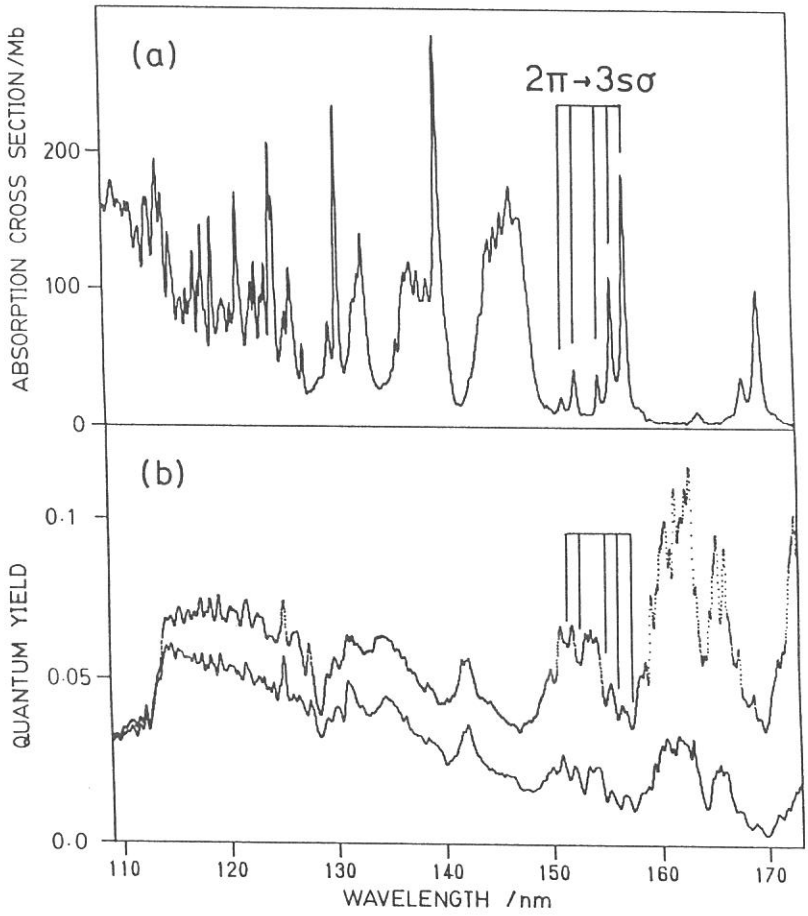

Fig. 1. (a) VUV absorption spectrum of ICN. (b) Quantum yield for the production of CN(A) (dotted line) and CN(B) (solid line) as a function of excitation wavelength.

[1] J. A. Myer and J. A. R. Samson, JCP, 52 (1970) 266.

Fluorescence Polarization of CN(B → X) Observed in Photodissociative Excitation of ClCN in the 105 - 145 nm Region

Mitsuhiko KONO, Kiyohiko TABAYASHI, and Kosuke SHOBATAKE

Institute for Molecular science, Myodaiji, Okazaki 444 Japan

Fluorescence polarization from $CN(B^2\Sigma^+)$ formed in photodissociative excitation process of ClCN was observed in the exciting wavelength region from 105 to 145 nm using synchrotron radiation as a polarized light source to study photodissociation dynamics. An absorption and fluorescence apparatus for vuv photochemical study constructed in the Beamline BL2A was used. The monochromated VUV light was introduced into a gas cell containing ClCN at 90 or 20 mtorr kept at room temperature. The intensity of the transparent light was measured in a conventional manner. The $CN(B^2\Sigma^+ \rightarrow X^2\Sigma^+)$ fluorescence emitted to the direction perpendicular to both the pointing vector and the polarization vector of the incident light. The degree of polarization for CN(B→X) fluorescence was measured using a Hinds' photoelastic modulator. The resolution was 0.10 nm for absorption and fluorescence excitation measurement and 0.30 nm for polarization measurement.

In order to facilitate the measurement of fluorescence polarization in a wide wavelength range the degrees of polarization were measured at reference wavelengths λ_{ref} = 125.4 and 133.0 nm, $P_{ref} = (I_{||} - I_{\perp})/(I_{||} + I_{\perp}) = 0.1270 \pm 0.0015$ and 0.0945 ± 0.0017, respectively, where $I_{||}$ and $I_{\perp}$ are the observed polarized fluorescence intensities parallel and perpendicular to the polarization vector of the incident light. At other wavelengths the fluorescence counts, $N_{||}$ and $N_{\perp}$ for parallel and perpendicular polarization to the electric vector were measured through two plate polarizers followed by each a photomultiplier tube (Hamamatsu R585) on a photon counting mode. The difference in the detection efficiencies for the two detectors were corrected for so that P_{ref} value determined using a photoelastic modulator agrees with the P_{ref} value with two polarizers, i.e. the degree of polarization at the reference wavelength, $P_{ref} = (N_{||} - cN_{\perp}) / (N_{||} + c\,N_{\perp})$, where c is the correction factor to be determined. Once the correction factor, c, is determined the degree of polarization at other wavelength than λ_{ref} is determined from $P = (N_{||} - c\,N_{\perp}) / (N_{||} + c\,N_{\perp})$, that is $I_{||} = N_{||}$ and $I_{\perp} = c\,N_{\perp}$ were adopted.

Figure 1 illustrates the degree of polarization for $CN(B^2\Sigma^+ \rightarrow X^2\Sigma^+)$ fluorescence, $P = (I_{||} - I_{\perp})/(I_{||} + I_{\perp})$, where $I_{||}$ and $I_{\perp}$ are the observed polarized fluorescence parallel and perpendicular to the polarization vector of the incident light against the wavelength of exciting light ranging in the region 105 nm to 145 nm. Figure 1 also shows absorption and fluorescence excitation spectra of ClCN gas in the cell. One finds that a) the degree of polarization is larger than 10 % above 111 nm and close to the limiting value of 1/ 7 and b) there appear undulatory structures around 116 nm and in the region from 120 to 126 nm. Compared with photodissociative excitation process of HCN and DCN molecules,[1] the dissociation seems to proceed via very short-lived

intermediates states, especially in the 117 - 130 nm region.

Since the sharp Rydberg progressions which appear in the 131 - 141 nm region are assigned to the transitions whose transition dipoles are perpendicular to the molecular axis, it is reasonable that the degrees of polarization become small at these peaks. However for the sharp Rydberg bands which appear in the 121 to 126 nm region and have been assigned to parallel transition, $4\sigma \rightarrow$ nsR the degree of polarization becomes smaller than the base values of polarization which is about P = 0.12. Probably the assignment should be changed from parallel to perpendicular transition.

Reference

1. K. Shobatake, A. Hiraya, K. Tabayashi, and T. Ibuki, *Vacuum Ultraviolet Photoionization and Photoemission of Molecules and Clusters*, Ed. by C. Y. Ng, (World Scientific Pub. Co., singapore, 1991) pp. 503-562.

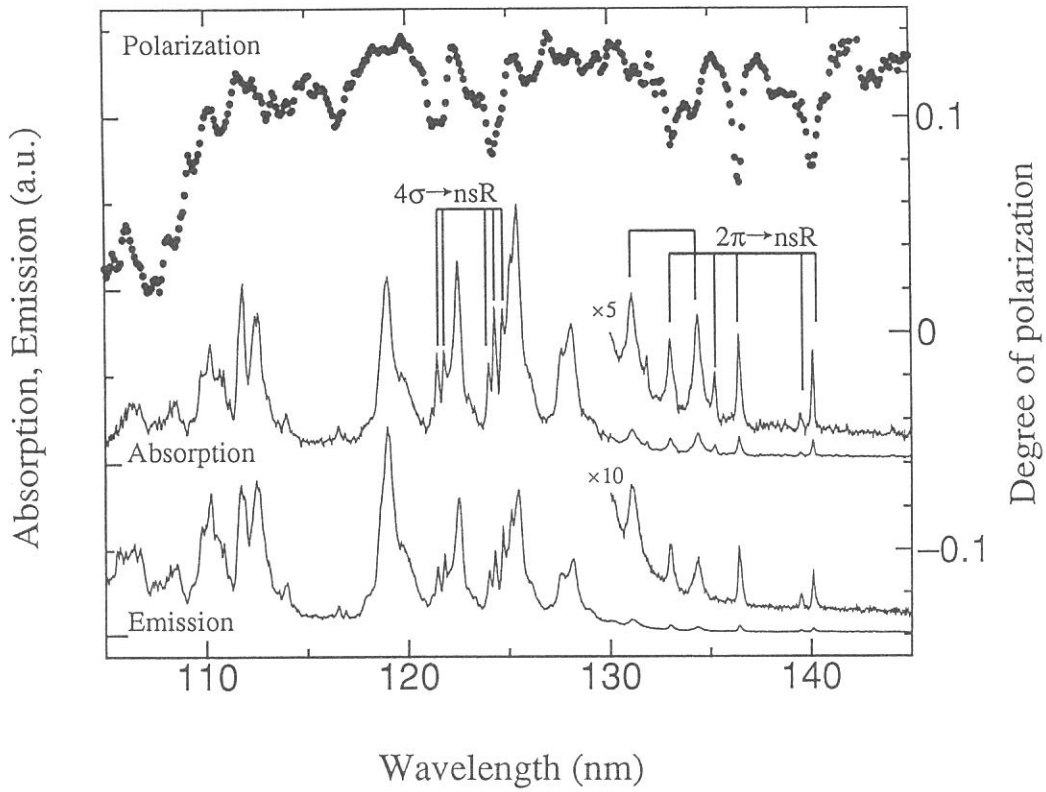

Figure 1. Absorption spectrum of ClCN, $CN(B^2\Sigma^+ \rightarrow X^2\Sigma^+)$ fluorescence excitation spectrum for the photodissociative excitation process $ClCN + h\nu \rightarrow Cl + CN(B^2\Sigma^+)$, and the degree of polarization $P = (I_{||} - I_{\perp})/(I_{||} + I_{\perp})$, plotted against exciting light wavelength ranging from 105 nm to 145 nm, where $I_{||}$ and $I_{\perp}$ are polarized fluorescence intensities parallel and perpendicular to the electric vector of the incident light. The resolution of the incident light for polarization measurement was 0.30 nm and 0.10 nm for the absorption and fluorescence excitation measurement.

Photo-induced Processes of Cl_2 ($1^1\Sigma^+_u$) State Studied by VUV/UV-Fluorescence Lifetime Measurements

Kiyohiko TABAYASHI,*† Mitsuhiko KONO,† Atsunari HIRAYA,*† and Kosuke SHOBATAKE*†

Institute for Molecular Science, and The Graduate University for Advanced Studies,† Myodaiji, Okazaki 444 Japan*

Photo-induced processes of excited Cl_2 in the presence of rare gas (Rg) third atoms are of fundamental importance in connection with our previous studies[1] on the excited state dynamics of Rg-Cl_2 van der Waals molecules generated in free jets. Here, VUV excitation light with a time duration of ca. 400 psec and a high repetition rate of 5.6 or 90.1 MHz (single-/multi-bunch operation of UVSOR) was successfully used for the time-resolved fluorescence measurements of Cl_2/Rg in a gas cell.

A typical time-decay curve for the fluorescence from ion-pair state of $Cl_2(1^1\Sigma^+_u)$ and that for excitation light are shown in **Figure 1**. The fluorescence for the bound-free transition $Cl_2(1^1\Sigma^+_u\text{-}X^1\Sigma^+_g)$ was collected in the region $185 < \lambda_{obs} < 215$ nm via a VUV monochromator and detected with a multichannel plate detector. Upon excitation to vibronic states ($1^1\Sigma^+_u$, $31 < v' < 41$) under the single collision condition (**Figure 2**), nearly a constant radiative decay of 2.65 nsec was obtained from a simple deconvolution analysis. **Figure 3** shows decay rates of Cl_2/Rg(Xe, Ne) system following λ_{ex}=137 nm excitation as a function of Rg partial pressure along with those of Cl_2/Ar case[2]. Collisional (total) quenching rate constants, $k(Xe) = 1.3\times10^{-9}$ and $k(Ne) = 1.4\times10^{-10}$ cm^3/sec are obtained. Since the reactive channel for $RgCl^*$ excimer formation is open only for Cl_2/Xe system in the excitation at $\lambda_{ex}\approx137$ nm, a comparable value of k(Xe) to k(Ar)= 9×10^{-10} cm^3/sec[2] indicates non-reactive collisional decays are quite effective for the excited ion-pare $Cl_2(1^1\Sigma^+_u)$ state. Relaxation to an intermediate $Cl_2(2^3\Pi_g)$ fluorescent state by collisional intersystem crossing is considered to be very important as one of the non-reactive quenching channels. Time-resolved fluorescence measurement for the $Cl_2(2^3\Pi_g)$ state as well as reaction product $XeCl^*(B)$ is under way to clarify the whole quenching mechanism of $Cl_2(1^1\Sigma^+_u)$ involved in Cl_2^*/Xe collision system.

References

[1] K. Shobatake, A. Hiraya, K. Tabayashi, and T. Ibuki, in *VUV Photoionization and Photodissociation of Molecules and Clusters*, C.Y. Ng ed. (World Sci.Pub. 1991), pp.503.

[2] T. Möller, B. Jordan, G. Zimmerer, D. Haaks, J. Le Calvé, and M.-C. Castex, Z. Phys. D **4**, 73 (1986).

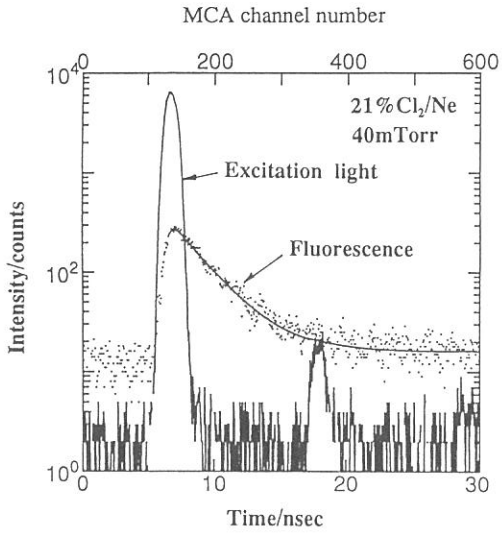

Figure 1. Time-decay profile for the $Cl_2(1^1\Sigma^+_u\text{-}X^1\Sigma^+_g)$ fluorescence upon excitation at 137nm and the time-profile of the scattered excitation light.

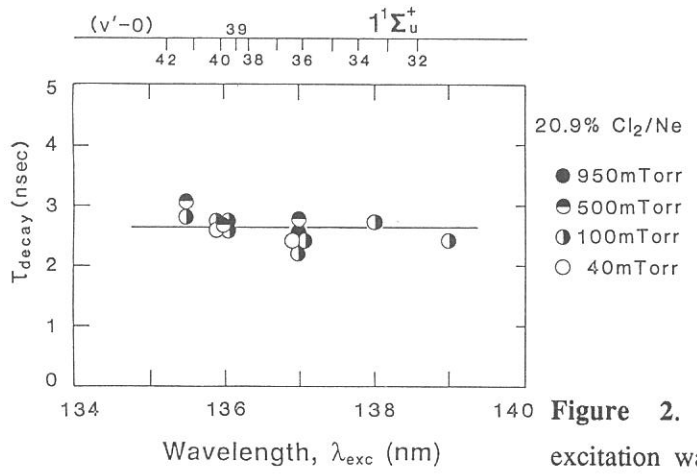

Figure 2. Radiative lifetime against excitation wavelength.

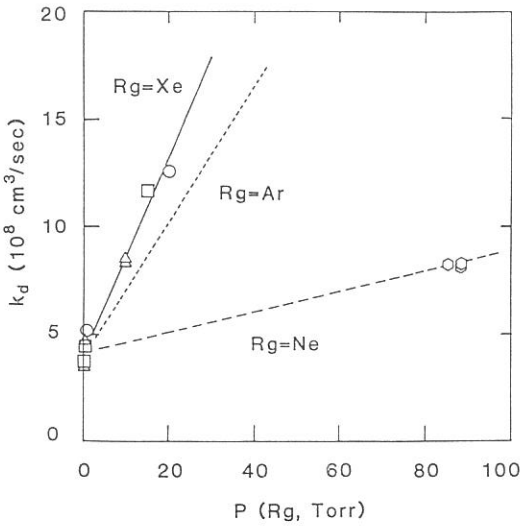

Figure 3. Decay rate for $Cl_2(1^1\Sigma^+_u\text{-}X^1\Sigma^+_g)$ fluorescence against Rg partial pressure upon excitation at 137nm.

PHOTOELECTRON SPECTRA OF ACETONE AND ACETONE DIMER

Kenji FURUYA,[1] Shunji KATSUMATA,[2] and Katsumi KIMURA[3]

[1]Institute for Molecular Science, Okazaki 444, and Department of Molecular Science and Technology, Kyushu University, Kasuga-shi, Fukuoka 816

[2]Department of Fundamental Science, Iwaki Meisei University, Iwaki-shi, Fukushima 970

[3]Institute for Molecular Science, Okazaki 444, and Japan Advanced Institute of Science and Technology, Tatsunokuchi, Ishikawa 923-12

In order to study the ionic states of acetone produced in a supersonic jet, we have carried out threshold photoelectron spectroscopy (TPES) with synchrotron radiation in the region 122.0 - 130.0 nm. Acetone has also been re-investigated with 58.4-nm He(I) photoelectron spectroscopy (PES). Figure 1 shows the PES [Fig. 1(a)] and the TPES [Fig. 1(b) and (c)] spectra. The energy resolutions are 21, 30, and 42 meV for spectra (a), (b), and (c), respectively. It has been found from Fig. 1 that the intensity of band 5 becomes stronger by lowering the resolution of the TPES analyzer. This fact cannot be explained in terms of the band broadening due to the lower resolution. Thus, we may conclude that there is an autoionizing state at 125.3 nm (9.893 ± 0.015 eV).

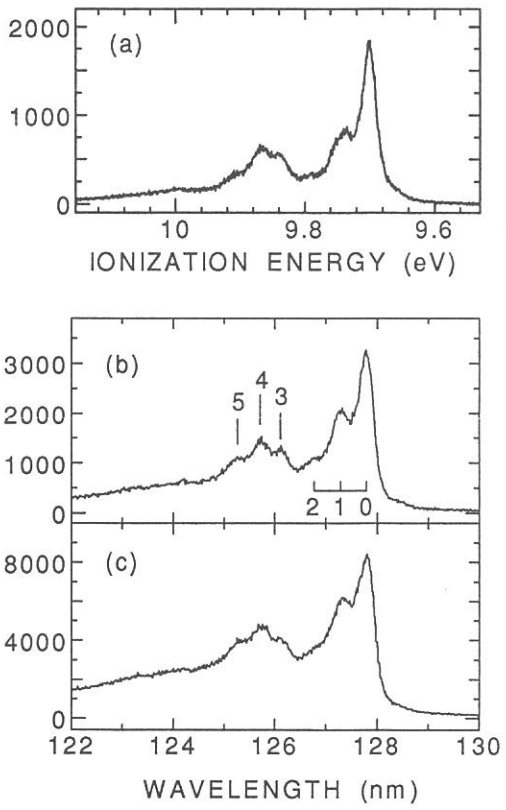

Fig.1 A He (I) photoelectron spectrum [(a)] and threshold photoelectron spectra [(b) and (c)] of acetone.

The threshold-photoelectron photoion coincidence (TPEPICO) spectra of acetone and its clusters were observed in the region 124.0 - 135.0 nm with an interval of 0.2 nm. A typical TPEPICO spectrum is shown in Fig. 2, observed at 131.0 nm (9.465 eV) which lies 0.235 eV below the adiabatic ionization potential of the acetone monomer (9.70 eV). The monomer cation peak in Fig. 2 is attributed to scattered light arising from some imperfection of the grating.

In the present experiments, the trimer and the tetramer cation intensities were much weaker than the dimer cation intensity (almost noise level) in all the observed TPEPICO spectra, as shown in Fig. 2. Thus, the contribution of larger clusters to the dimer cation peak observed in all the TPEPICO spectra is negligibly small. The solid curve in Fig. 3 was obtained by plotting the total dimer cation counts against the excitation wavelength, giving rise to intensity distribution corresponding to a TPES spectrum of the non-dissociative acetone dimer. The plotted curve may be called a 'TPEPICO excitation spectrum'. The

photoionization efficiency (PIE) curve of the dimer cation observed by Trott et al.[1] is shown in Fig. 3 by a dotted curve for comparison. From the TPEPICO excitation spectrum, the appearance ionization potential of the dimer cation has been evaluated to be 9.210 ± 0.015 eV. This value is slightly lower than that (9.26 ± 0.03 eV) evaluated by Trott et al.[1]

In the TPEPICO excitation spectrum shown in Fig. 3, there are two bands; one is a broad band with a peak at 129.6 nm, and the other is a satellite band with a peak at 127.2 nm. The latter peak position is identical to the PIE peak position. In contrast to the sharp vibrational bands of the monomer, the 129.6 nm band shows long tails, to either side of the band maximum implying that the potential minimum of the dimer cation is much different from that of the neutral dimer, and that the Franck-Condon factor of direct ionization is not zero for a very wide energy region.

The second electronic state of the acetone monomer cation is located at 12.59 eV (98.47 nm), much higher than the maximum positions, 9.747 eV (127.2 nm) and 9.567 (129.6 nm), observed in the present TPEPICO excitation spectrum. The difference is too large to explain the dimer production. Thus it is not expected that the two observed bands are related to the second electronic state of the acetone monomer. Since the upper state of the charge resonance states produced from the interaction between the two kinds of acetone dimer cations, acetone-$(acetone)^+$ and $(acetone)^+$-acetone in the electronic ground states, has a repulsive potential well, the upper state should not be observed in the present dimer TPEPICO excitation spectrum. The band shape observed at 127.2 nm in the PIE spectrum implies that this band cannot be due to the dimer cation. Therefore, we can conclude that the bands observed at 127.2 and 129.6 nm in the TPEPICO excitation spectrum are assigned to a Rydberg state of the neutral dimer and the electronic ground state of the dimer cation, respectively.

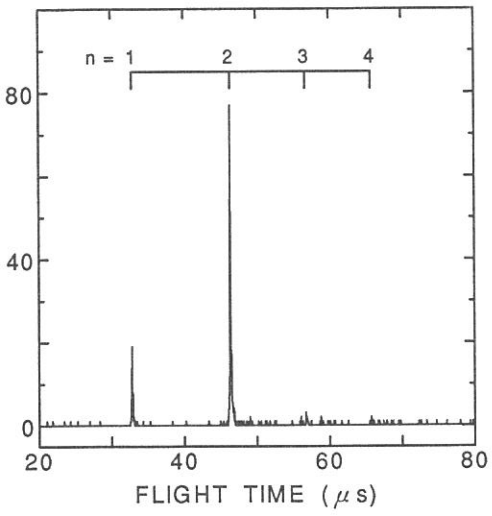

Fig.2 A threshold-photoelectron photoion coincidence (TPEPICO) spectrum of acetone clusters observed at 131.0 nm.

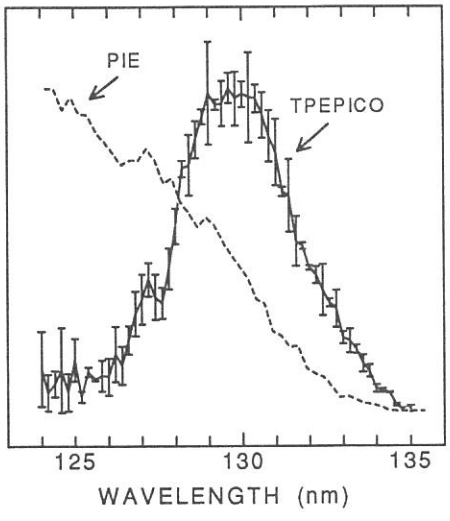

Fig.3 TPEPICO excitation (solid curve) and PIE (dotted curve) spectra of the acetone dimer. The PIE spectrum was taken from ref.[1].

[1]W. M. Trott, N. C. Blais, and E. A. Walters, *J. Chem. Phys.*, **69**, 3150 (1978).

IMPROVEMENT OF PHOTOELECTRON-PHOTOELECTRON COINCIDENCE SPECTROMETER AND AN INVESTIGATION OF DOUBLE IONIZATION PROCESSES BY EXCITATION ABOVE THE *3d* ELECTRON IONIZATION THRESHOLD REGION OF KRYPTON

Katsuhiko OKUYAMA, Eiken NAKAMURA, Kenji FURUYA[a], and Katsumi KIMURA[b]

Institute for Molecular Science, Okazaki 444

[a] Department of molecular science and technology, Kyushu Univ., Kasugashi Fukuoka 816

[b] Japan advanced institute of science and technology, Tatsunoguchi Ishikawa 923-12

Recently we have obtained successful results concerning a single-photon double-ionization process in Xe atom by means of a photoelectron-photoelectron coincidence (PEPECO) apparatus equipped with a magnetic-bottle time-of-flight (TOF) analyzer and the using the monochromatic orbiting radiation from the 25-pole undulator on beamline 3A2.[1] In order to expand our field of research to molecular systems as well as investigating a double-photoionization process in greater detail, we have initiated a series of improvements on the PEPECO apparatus. Firstly, we have introduced a new rear mirror that provides a suitable focal position for our apparatus, which has made the photon density 20-times higher than previously and has increased the coincident rate. Secondly, the photoelectron flight length of the short TOF tube constructed on the opposite side of the main TOF tube has increased from 4 cm to 14 cm and a small turbo molecular pump has been introduced to pump the short TOF tube. These improvements have resulted in a significant improvement in spectral resolution.

By using the PEPECO spectrometer improved, we investigated the double-ionization processes by photoexcitation just above the *3d* electron ionization threshold region of Kr atom. Fig. 1 shows the PEPECO spectrum of Kr atom at 124.5 A (99.6eV) with intensities recorded as dot density, of which horizontal and vertical axes show the times of flight on a linear scale in the short and long TOF analyzer, respectively. The excitation wavelength corresponds to 4.6 eV and 5.8 eV above $3d_{5/2}$ and $3d_{3/2}$ electron removal ionization threshold, respectively.[2] The double-cross structure observed on the spectrum clearly indicates that the double phtoionization process of Kr excited by 124.5 A single-photon chiefly occurs as indirect mechanism via two $3d^{-1}$ states. Direct double

ionization process, yielding the electronic ground terms of Kr^{+2}, is identified as minor process (20%) superimposing on the major double cross structure.

References

1) K.Okuyama, J.H.D.Eland, and K.Kimura, *Phys. Rev. A,* **41** 4930 (1990).

2) G.C.King, M.Tronc, F.H.Read, and R.C.Bradford, *J. Phys. B : Atom Molec. Phys.,* **10** 2479 (1977).

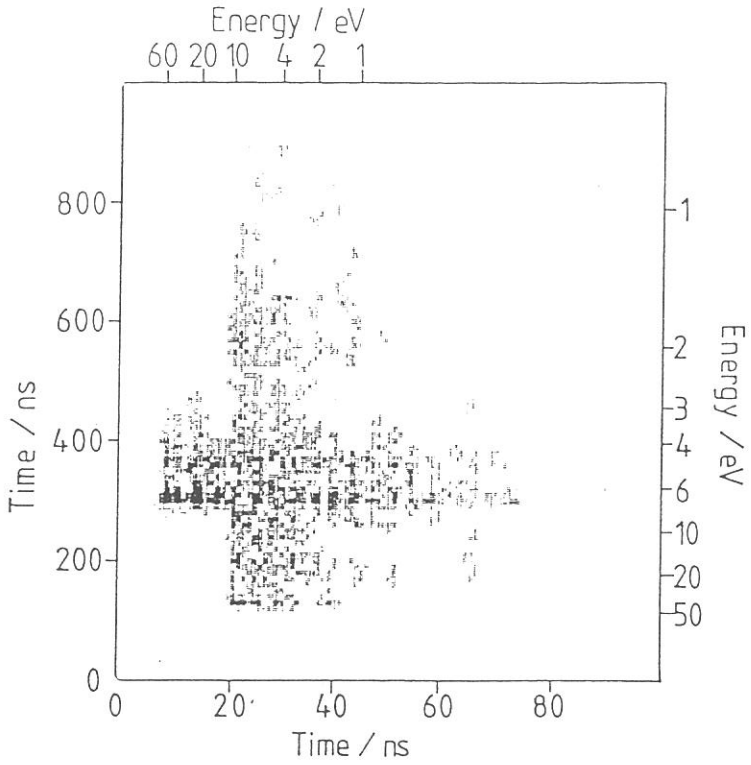

Figure 1 PEPECO spectrum of krypton at 124.5 A (99.6 eV) with intensities recorded as dot densities.

SINGLE AND DOUBLE PHOTOIONIZATION CROSS SECTIONS OF NO AND IONIC FRAGMENTATION OF NO^+ AND NO^{2+}

Toshio MASUOKA

Department of Applied Physics, Osaka City University, Sumiyoshi, Osaka 558

Single and double photoionization processes of nitric oxide (NO) have been studied in the photon energy region 37-100 eV by use of time-of-flight mass spectrometry and the photoion-photoion coincidence (PIPICO) method together with synchrotron radiation. The single (σ^+) and double (σ^{2+}) photoionization cross sections of NO are determined by a newly developed method.[1] The results are shown in Fig. 1 as a function of photon energy. The total cross section is from Ref. 2. It is emphasized that the double photoionization cross section reported in Fig. 1 includes both the dissociative and nondissociative processes of the precursor NO^{2+}. The threshold for the dissociative double photoionization was found to be 41.0 + 0.3 eV.

Ion branching ratios and the partial cross sections for the individual ions (NO^+, N^+, and O^+) produced from the precursor NO^+ and those (N^++O^+, NO^{2+}, N^{2+}, and O^{2+}) from NO^{2+} are also obtained.

The dissociation ratios of the singly and doubly charged precursors are shown in Fig. 2. It is interesting to note that the dissociation ratio of NO^{2+} reaches an asymptotic value very close to 0.85 at about 47 eV. The ground state of NO^{2+}, $X^2\Sigma^+$, is known to be nondissociative, and the first ($A^2\Pi$) and the second ($B^2\Sigma^+$) excited states to be partially bound. If only these bound states are the source for the (meta)stable NO^{2+}, the dissociation ratio should increase at higher photon energies. Obviously, the results in Fig. 2 provide an evidence for the presence of bound electronic states at higher photon energies and/or autoionization to the low-lying bound states of

NO^{2+}. On the other hand, the dissociation ratio of NO^+ decreases above 42.5 eV. This provably means that the Rydberg states converging to the low-lying electronic states of NO^{2+} are nondissociative and produce the (meta)stable NO^+. Above about 58 eV the dissociation ratio of NO^+ increases. However, the nondissociative process is still dominant even at higher photon energies. This strongly suggests that the majority of the high-lying electronic states of NO^+ are nondissociative.

References

1) T. Masuoka and H. Doi, Phys. Rev. A 1993, No. 1.

2) Y. Iida, F. Carnovale et al., Chem. Phys., 105, 211 (1986).

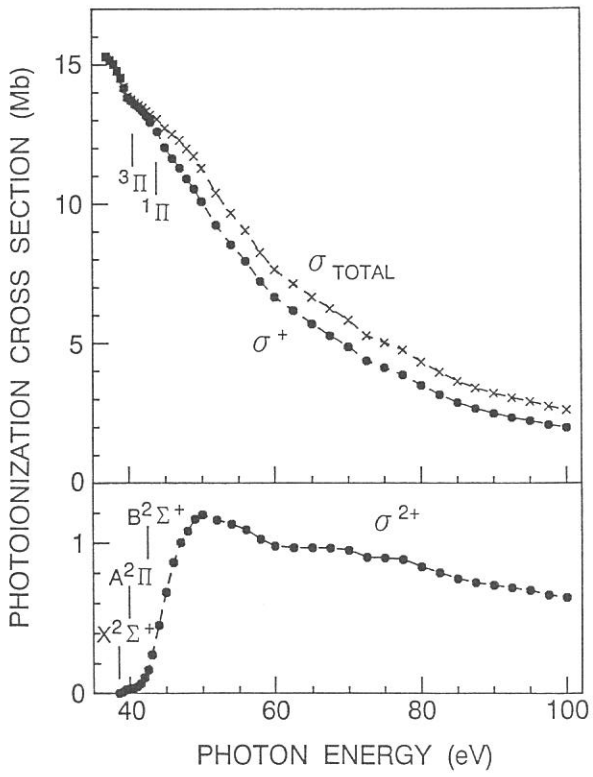

FIG. 1 Single (σ^+) and double (σ^{2+}) photoionization cross sections of NO.

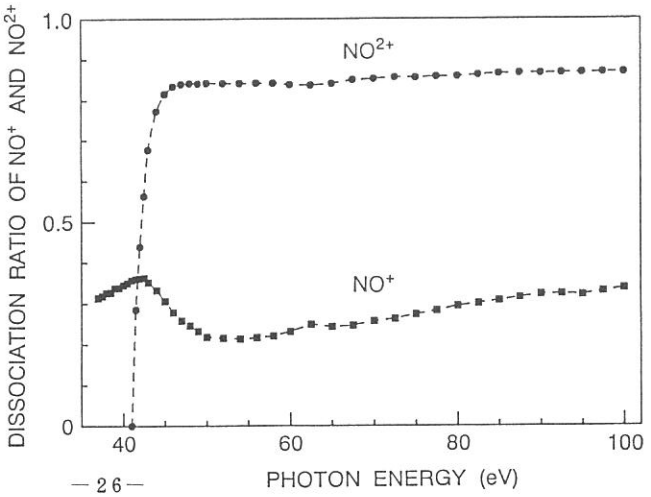

FIG. 2 Dissociation ratios of the precursors NO^+ and NO^{2+}.

DISSOCIATIVE MULTIPLE PHOTOIONIZATION OF BrCN AND ICN IN THE VALENCE SHELL AND n*d*(*n*=3,4) REGIONS

Toshio IBUKI, Inosuke KOYANO* and Toshio MASUOKA**

Kyoto University of Education, Fukakusa, Fushimi-ku 612
**Department of Material Science, Himeji Institute of Technology*
Kanaji, Kamigohri, Hyohgo 678-12
***Department of Applied Physics, Osaka City University, Sumiyoshi-ku, Osaka 558*

The multiple photoionization processes of BrCN and ICN in the valence and n*d* (n=3,4) inner shell region have been studied using photoion-photoion coincidence (PIPICO) techniques in the photon energy region of 40-130 eV at BL3A2 station of UVSOR. Figures 1 and 2 show the PIPICO branching ratios of the doubly charged BrCN and ICN, respectively, and those of the triply charged molecular ions are depicted in figs. 3 and 4. We can see some remarkable features from these figures:

(A) Doubly charged cation is formed by a single photon excitation of valence orbital electrons.

(A1) The decay channels of the doubly charged $BrCN^{2+}$ in fig. 1 change smoothly with increasing photon energy while those of ICN^{2+} are strongly affected at the ionization potential of $(4d)^{-1}$ as shown in fig. 2.

(A2) Neither (C^+ + N^+) nor (IC^+ + N^+) ion pair, which is formed in BrCN (see fig. 1), is observed in the ICN double photoionization.

(B) Triply charged ion precursors presumably arise primarily form double Auger decomposition processes of the initial n*d* hole states (see figs. 3 and 4).

(B1) The following three dissociation channels are observed for the triply charged cations: X^{2+} + CN^+ (1), X^{2+} + N^+ (2), and X^{2+} + C^+. (3)

(B2) The threshold energies of reactions (1)-(3) for X=Br are 70±1 eV, while for X=I the onset of reaction (1) is 59±1 and those of (2) and (3) lie 70±1 eV. The energy difference of about 10 eV between reactions (1) and (2) (and/or (3)) for X=I is very close to the bond energy of C≡N radical.

The above observations suggest that $BrCN^{2+}$ and $BrCN^{3+}$ seem to decompose explosively, while the multiply charged ICN may decompose successively.

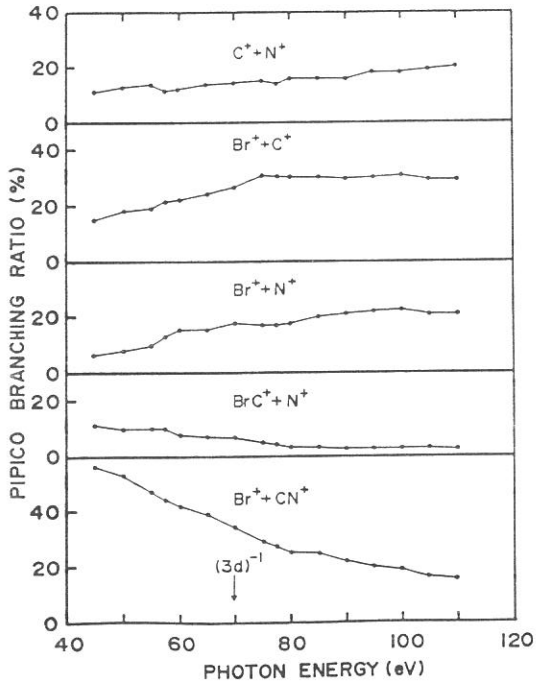

Fig.1. Photoionization branching ratios for doubly charged $BrCN^{2+}$.

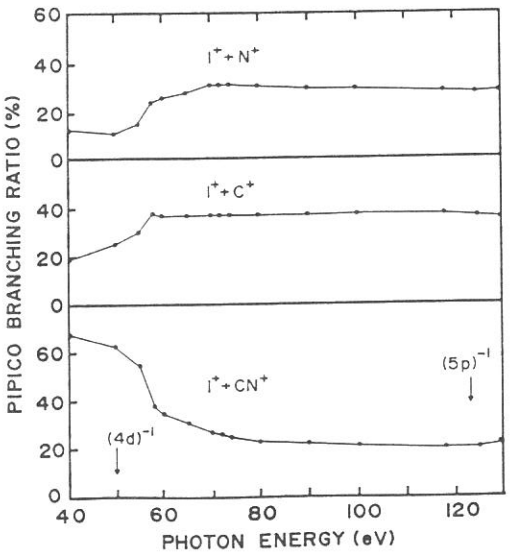

Fig.2. Photoionization branching ratios for doubly charged ICN^{2+}.

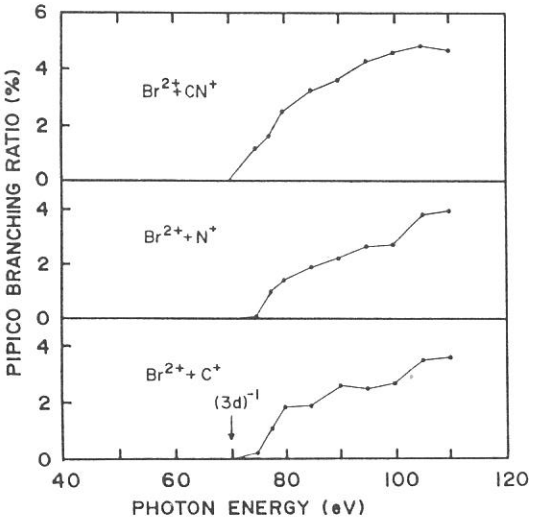

Fig.3. Photoionization branching ratios for triply charged $BrCN^{3+}$.

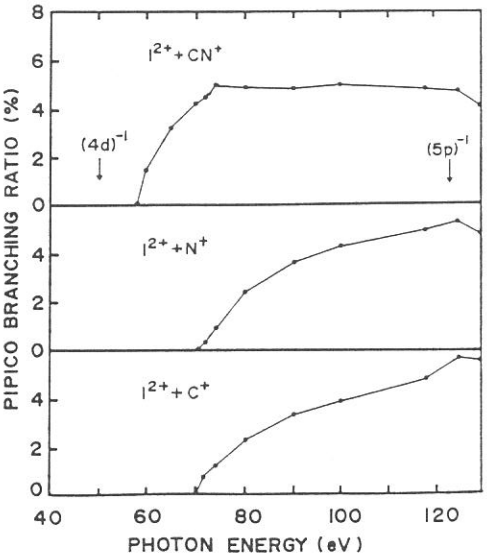

Fig.4. Photoionization branching ratios for triply charged ICN^{3+}.

Dissociation dynamics of SO^{2+} and CH_3F^{2+} studied by the triple photoelectron-photoion-photoion coincidence (PEPIPICO) method

Toshio Masuoka

Department of Applied Physics, Osaka City University,

Sumiyoshi-ku, Osaka 558

Multiple ionization of molecules has been extensively studied in recent years by using coincidence methods such as photoelectron-photoion (PEPICO), photoion-photoion (PIPICO), photoelectron-photoelectron (PEPECO), photoion-fluorescent photon (PIFCO), and photoelectron-photoion-photoion (PEPIPICO, or PE2PICO) coincidence.[1] These methods, which are essential to correlate two or more particles from each single ionization event, have provided much information on the multiple ionization of molecules. Among these, the PEPIPICO method has been shown to be a powerful technique to study the dissociation reactions of doubly and multiply charged molecules into three fragments.[2] Three-dimensional flight time distributions measured for dissociative double ionization clearly show the momentum distributions (speed and angle) of the fragments; thereby enabling determination of the charge separation mechanisms.

The dissociation dynamics of doubly and triply charged sulfur dioxide (SO_2) and methyl fluoride (CH_3F) are studied here by this technique over a photon energy region of 46-80 eV with the use of monochromatized synchrotron radiation. It was found that for the three-body dissociation of the type $ABC^{2+} \rightarrow A^+ + B^+ + C$, the dissociation mechanism is not dependent on the excitation energies in this region. This phenomenon suggests the presence of two site-specific positive holes each of which is related to a particular dissociation pathway. It is additionally concluded that atomization of the precursors is a dominant process in SO_2 at higher excitation energies.

Although several methyl compounds have recently been studied by the

PEPIPICO technique, the results for methyl fluoride have not yet been reported. Figure 1 shows a PEPIPICO distribution in the t_1 - t_2 plane at an excitation energy of 80 eV. Fourteen islands are observed, four of which have not been identified by previous PIPICO measurements.[3] The unidentified channels are CH_3^+, CH_2^+, CH^+, and C^+, each being in coincidence with F^+. It can be seen in Fig. 1 that the island size is very small in all the ionpair formations that include H^+ and H_2^+ ions; a result of the H^+ and H_2^+ ions taking almost all the energy but carrying very little momentum. Accordingly, it is difficult to obtain a definite slope for these islands and thus no analysis was made. The $CH_2^+ + F^+$ channel appears to be sequential via CH_3^+, since its slope is slightly less than 1. Similarly, the $H^+ + F^+$ channel has been suggested as being sequential via CH_3^+.[3] The $CH^+ + F^+$ and $C^+ + F^+$ channels are too weak to obtain meaningful island slope.

REFERENCES
1. J. H. D. Eland, Vacuum Ultraviolet Photoionization and Photodissociation of Molecules and Clusters, edited by C. Y. Ng (World Sci., Singapore, 1991), p. 297 and references therein.
2. J. H. D. Eland, F. S. Wort, and R. N. Royds, J. Electron Spectrosc. Relat. Phenom. **41**, 297 (1986).
3. T. Masuoka and I. Koyano, J. Chem. Phys. **95**, 1619 (1991).

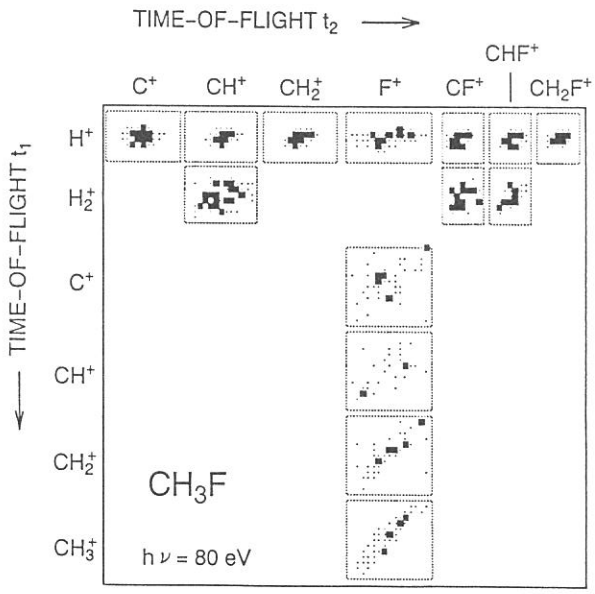

FIG. 1. TOF distributions for the dissociative double photoionization of CH_3F. Only a portion of each island is shown. Coincidences greater than 70% of the maximum intensity for each process are represented by solid rectangles; those greater than 40% and less than 70% are shown by dots.

IONIC FRAGMENTATION PROCESSES FOLLOWING Si:2p CORE LEVEL PHOTOEXCITATION AND PHOTOIONIZATION OF TETRACHLOROSILANE

Shin-ichi NAGAOKA, Toshio MASUOKA,[+] and Inosuke KOYANO[#]

Department of Chemistry, Faculty of Science, Ehime University, Matsuyama 790

[+]Department of Applied Physics, Osaka City University, Sumiyoshi, Osaka 558

[#]Department of Material Science, Faculty of Science, Himeji Institute of Technology, 1479-1 Kanaji, Kamigohri, Hyogo 678-12

In recent years, relaxation processes following core excitation and ionization in molecules have been a topic of much interest. We have investigated fragmentation following photoexcitation and photoionization of tetrachlorosilane (TCS) in the range of Si:2p excitation and ionization by means of the photoelectron-photoion and photoion-photoion coincidence methods (PEPICO and PIPICO methods, respectively).

The experiments were performed using a time-of-flight spectrometer with variable path length, coupled to a constant-deviation grazing incidence monochromator installed on the BL3A2 beam line of the UVSOR synchrotron radiation facility in Okazaki.[1]

The total photoionizaion efficiency curve of TCS has three peaks near the 2p core-ionization threshold of the silicon atom (Fig. 1). These peaks were assigned to the excitation of an Si:2p electron into $8a_1$, $9t_2$, and 4e orbitals below the threshold. There is an alternative interpretation (doubly excited state) for the peak seen at 110.1 eV. The Si:2p threshold of TCS is located at 110.17 eV. Resonant Auger processes follow the excitation at these peaks. Once an Si:2p core electron is initially excited (1 hole and 1 excited electron), the molecule is usually left with two holes in (a) valence orbital(s) and an excited electron in a virtual orbital. The two valence holes tend to fragment the system extensively.

Various ion pairs arise from Coulomb explosion processes from the dissociation of the unstable doubly charged ion.

Figure 2 shows an example of the photoionization mass spectra in the PEPICO mode. It was found that $I_{ion}/I_{tot\text{-}ion}$ for Si^+ and Cl^+ shows two broad peaks, one around 105 eV and the other around 110 eV. In contrast, $I_{ion}/I_{tot\text{-}ion}$ for all other ions decreases around these energies. It was also found that $I_{PIPICO}/I_{tot\text{-}PIPICO}$ for Si^+-Cl^+ shows pronounced peaks around 105 and 110 eV, whereas those for Cl^+-$SiCl_n^+$ (n = 1-3) show corresponding dips around these photon energies. The fragmentation scheme leading to the production of the ion pairs in TCS may be described as follows:

$$SiCl_4 + h\nu \rightarrow SiCl_4^{2+} + 2e \rightarrow Si^+ + Cl^+ + n.p.$$

1. T. Masuoka, T. Horigome, and I. Koyano, Rev. Sci. Instr. 60, 2179 (1989); E. Ishiguro, M. Suzui, J. Yamazaki, E. Nakamura, K. Sakai, O. Matsudo, N. Mizutani, K. Fukui, and M. Watanabe, Rev. Sci. Instr. 60, 2105 (1989).

Fig. 1 (left-hand side) Total photoionization efficiency curve of TCS in the range 100-115 eV.
Fig. 2 (right-hand side) Photoionization mass spectrum of TCS taken by excitation at 104.7 eV in the PEPICO mode.

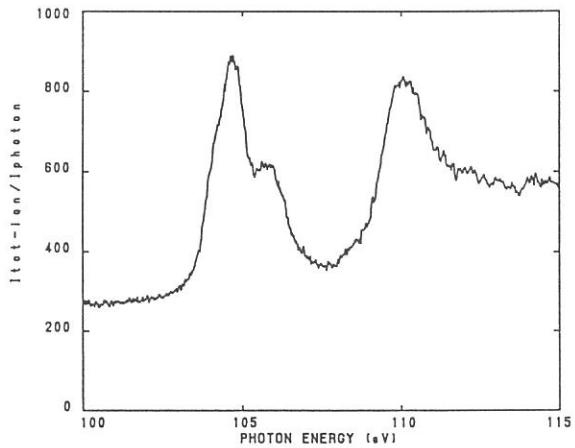

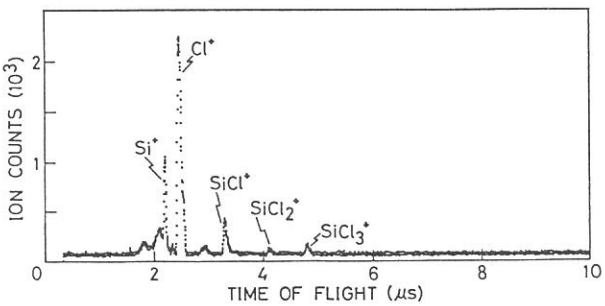

Dissociative Ionization Following Valence and Si:2*p* Core Level Photoexcitation of $HSi(CH_3)_3$ in the Photon Energy Range 24 - 133 eV

Bong Hyun Boo,[a] Inosuke Koyano,[b] Toshio Masuoka,[c] and Eiken Nakamura[d]

[a]*Department of Chemistry, Chungnam National University, Taejon 305-764, and Center for Molecular Science, 373-1 Kusung-dong Yusung-gu, Taejon 305-701, Korea*

[b]*Department of Material Science, Himeji Institute of Technology, 1479-1 Kanaji, Kamigohri, Hyogo 678-12*

[c]*Department of Applied Physics, Osaka City University, Sumiyoshi-ku, Osaka 558*

[d]*UVSOR, Institute for Molecular Science, Myodaiji, Okazaki 444*

Dissociation processes of $HSi(CH_3)_3$ have been investigated in the valence and Si:2*p* core-level photoionization by use of synchrotron radiation and the photoelectron-photoion coincidence (PEPICO) and photoion-photoion coincidence (PIPICO) techniques. Metastable $SiC_2H_n^{2+}$ is observed in the energy range E > 39 eV, respectively. Along with this dication, various monocations such as H^+, H_2^+, CH_n^+ (n=0-4) and $SiC_mH_n^+$ (m=0-3, n=0-9) are also observed. The ion branching and PIPICO ratios are measured as a function of the incident photon energy. Variation of the ion and the PIPICO branching ratios with the incident photon energy is shown in Figs. 1 and 2, respectively.

At the lowest energy examined, E = 24.00 eV, the most predominant process in the dissociative single photoionization of $HSi(CH_3)_3$ is the Si-C bond rupture forming $HSi(CH_3)_2^+$.

$HSi(CH_3)_3 + h\nu \rightarrow HSi(CH_3)_3^+ + e$ (valence ionization)

$HSi(CH_3)_3^+ \rightarrow HSi(CH_3)_2^+ + CH_3$

The ion branching ratio for H^+ rises beginning around 27 eV. Clear features are observed in the ion branching ratios for H^+ and H_2^+ in the energy ranges 95 < E < 110 eV and 100 < E <108 eV, respectively. Also in the PIPICO ratio data given in Fig. 2, processes 1, 2 and 3 are observed around 100 eV.

$HSi(CH_3)_3 + h\nu \rightarrow HSi(CH_3)_3^+ + e$ (Si:2*p* photoionization)

$HSi(CH_3)_3^+ \rightarrow HSi(CH_3)_3^{2+} + e$ (Auger) (1)

$HSi(CH_3)_3^{2+} \rightarrow CH_m^+ + SiC_nH_p^+$ (n=0-2) + n.p. (2)

$\rightarrow H^+ + SiC_nH_p^+$ (n=0-2) + n.p. (3)

where n.p. denotes the neutral products associated with the ionic products. Thus this energy corresponds to the Si:2*p* photoexcitation. In the range E > 100 eV, the source of CH_3^+ is mainly the dissociation channel, reaction 2. At energies beginning about 65 eV, the ion branching ratio of CH_3^+ slightly decreases. This decrease is correlated with the increase in the ion branching ratio of CH_n^+ (n=0-2). The core-level photoionization is observed to produce quite different fragmentation patterns showing the selective reactivities toward the Si-H and Si-C bonds giving rise to the bond cleavages. The core ionization of the localized Si:2*p* orbital results in the deposition of the internal energy to the silicon center, this internal

energy could be consumed to break the Si-H and/or Si-C bonds.

The valence double ionization and Si:2*p* core ionization thresholds are estimated to be ≈25 eV and 102 ± 1 eV, respectively. The Si:2*p* ionization threshold is similar to the $Si2p_{3/2}$ ionization energy of 111.6 eV in SiF_4.[1]

Reference

1. Aksela, K.; Tan, K. H.; Aksela, H.; Bankroft, G. M. *Phys. Rev. A 33*, **1986**, 258.

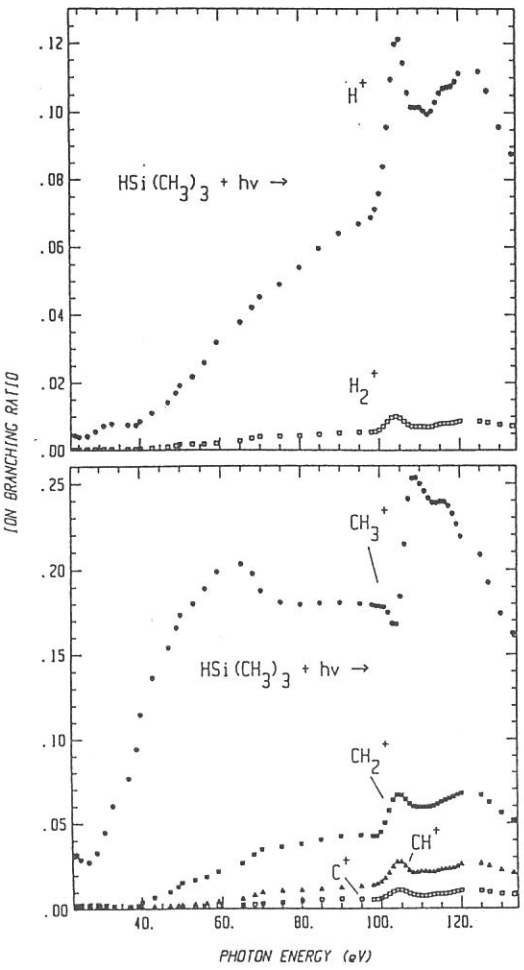

Figure 1. Ratios of integrated intensities of ion peaks in TOF mass spectrum to total photon intensity ($I_{ion}/I_{tot\text{-}ion}$) in $HSi(CH_3)_3$ as a function of photon energy.

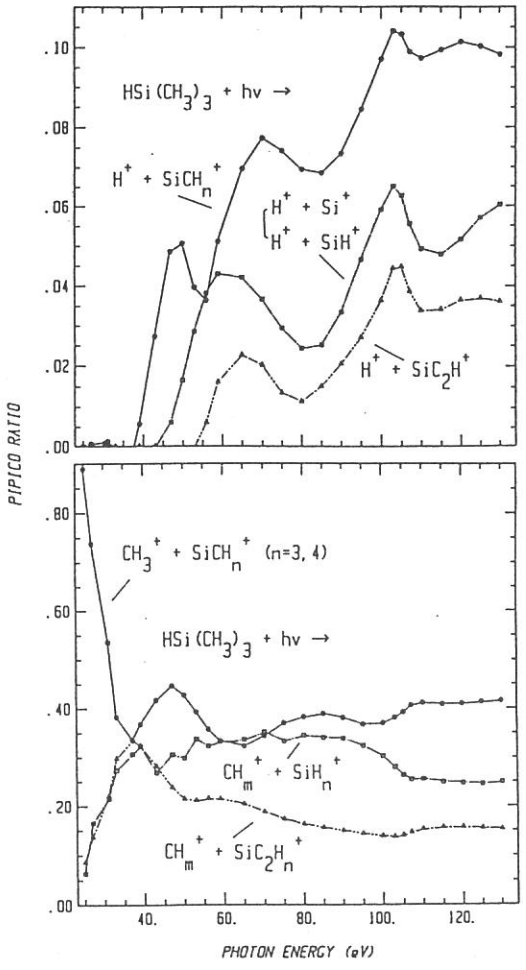

Figure 2. Ratios of integrated intensities of ion pairs in PIPICO spectrum to total double photo-ionization ($I_{PIPICO}/I_{tot\text{-}PIPICO}$) in $HSi(CH_3)_3$ as a function of photon energy.

POSITIVE ION-NEGATIVE ION COINCIDENCE SPECTROSCOPY OF O_2

Hiroaki YOSHIDA, Hideo HATTORI, and Koichiro MITSUKE

Department of Vacuum UV Photoscience, Institute for Molecular Science, Myodaiji, Okazaki 444

A new coincidence technique is developed for studying the ion-pair formation processes in the vacuum ultraviolet using synchrotron radiation. This technique utilizes the flight-time correlation of a pair of positive and negative ions produced by single photon excitation. The ion-pair formation from O_2 is studied for examining the performance of the apparatus.

Experiments are made by using synchrotron radiation emitted from beam line BL2B2 installed in the UVSOR storage ring. Figure 1 shows the schematic diagram of the time-of-flight mass spectrometer (TOFMS) and the data acquisition system. A sample gas is expanded into a beam expansion chamber from a nozzle of 100-μm diameter at room temperature of 298$\pm$3K and a stagnation pressure of 25 torr. The molecular beam is introduced through a conical skimmer into a photoionization chamber pumped to 10^{-6} torr when the beam is on. Ion pairs are formed by interaction with a monochromatized VUV photon beam at the photoexcitation region. Ion pairs thus produced are accelerated by an electrostatic field applied in the perpendicular direction to axes of both molecular beam and photon beam. Positive ions are mass-separated by a single-field type of TOFMS, while negative ions by a double-field type. The positive-ion signal is fed into the start input of a time-to-amplitude converter and the negative-ion signal into the stop input. Flight-time difference thus obtained is accumulated in a multichannel analyzer. Upon detection of a positive ion, a gate pulse voltage is applied to grid G2 to prevent electrons from penetrating the flight tube beyond G2. Application of this gate pulse is very effective in suppressing the false coincidence counts.

Figure 2 shows a coincidence spectrum of O^+ and O^- produced from O_2 at the photon wavelength of 709.5 Å (photon energy $E_{h\nu}$ = 17.47 eV). This energy is 0.2 eV distant from the threshold at 17.27 eV (717.8 Å) for the lowest ion-pair formation channel, $O_2(^3\Sigma_g^-) + h\nu \rightarrow O^+(^4S_u) + O^-(^2P_u)$. The background count is ascribed to the false coincidence signals, mainly arising from the start input of O_2^+ signals and the stop

input of electrons signals. The sharp peak observed at 14.22 μs is assigned to the coincidence peak due to the ion pairs produced by a single photoexcitation event. This assignment is supported by the following corroborating evidence. First, we clock the flight times separately for O^+ and O^- from photoexcitation region to the detectors by applying a pulse voltage to grid G2. The flight-time difference is estimated to be 14.4$\pm$0.5 μs, which is in good agreement with the position of the coincidence peak in Figure 2. Second, we measure the photodissociation efficiency curve for the ion-pair formation process by scanning the photon wavelength. This curve is compared with the efficiency curve of O^- measured by using molecular-beam photoionization apparatus on the beam line BL3B in the UVSOR facility. Several structures are commonly observed in the two curves.

Figure 1.

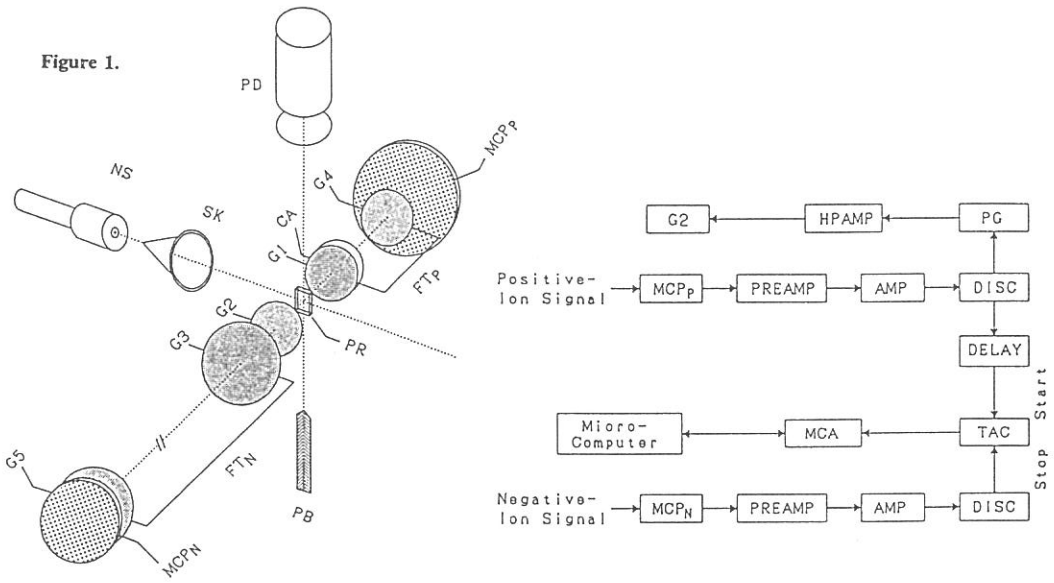

Figure 2.

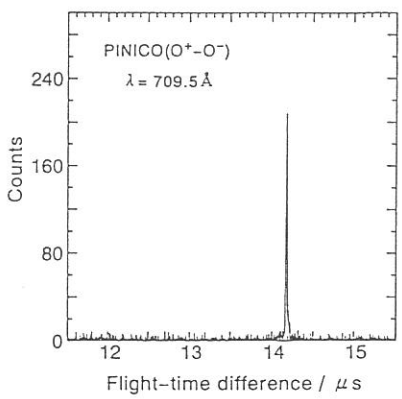

Figure 1. Schematic diagram of the time-of-flight mass spectrometers and data acquisition system for coincidence spectroscopy. (NS) nozzle source; (SK) conical skimmer; (PR) photoexcitation region; (PB) monochromatized photon beam; (PD) photon detector; (G1-G5) grids; (CA) capillary array plate; (FT_P) flight tube for positive ions; (FT_N) flight tube for negative ions; (MCP_P) microchannel plates for positive-ion detection; (MCP_N) microchannel plates for negative-ion detection; (PREAMP) pre-amplifier; (AMP) main-amplifier; (DISC) discriminator; (TAC) time-to-amplitude converter; (DELAY) delay circuit; (MCA) multichannel analyzer; (PG) pulse generator; (HPAMP) high-speed power amplifier.

Figure 2. Coincidence spectrum of O^+ and O^- produced from O_2 measured at the photon wavelength of 709.5 Å.

NEGATIVE-ION MASS SPECTROMETRIC STUDY OF ION-PAIR FORMATION IN THE VACUUM ULTRAVIOLET. $SO_2 \longrightarrow O^- + SO^+$, $O^- + S^+ + O$

Koichiro MITSUKE,[α] Shinzo SUZUKI,[β] Takashi IMAMURA,[γ] and Inosuke KOYANO[δ]

[α] Department of Vacuum UV Photoscience, Institute for Molecular Science, Myodaiji, Okazaki 444

[β] Department of Chemistry, Tokyo Metropolitan University, Minami-Osawa, Hachioji, Tokyo 192-03

[γ] Atmospheric Environment Division, National Institute for Environment Studies, Onogawa, Tsukuba, 305

[δ] Department of Material Science, Himeji Institute of Technology, 1479-1 Kanaji, Kamigohri, Hyogo 678-12

Photoexcitation of molecules to highly-excited states is often accompanied by dissociation into a pair of positive and negative ions in the photon energy range of 10 - 50 eV. The detection of negative ions produced by such ion-pair processes provides a sensitive probe to investigate the properties of Rydberg states lying in the vacuum ultraviolet. The present report describes ion-pair formation from photoexcitation of SO_2,

$$SO_2 + h\nu \longrightarrow O^- + SO^+, \quad (1)$$

$$SO_2 + h\nu \longrightarrow O^- + S^+ + O \quad (2)$$

studied by mass spectrometry using synchrotron radiation in the 15 - 35 eV photon energy range.[1] Negative ions O^- from SO_2 has been observed.

Figure 1 shows the O^- photodissociation efficiency curve. The appearance energy for O^- is in good agreement with the thermochemical threshold of 14.49 eV for the formation of $O^-(^2P_u) + SO^+(\tilde{X}\,^2\Pi)$. The cross section for process (1) at ~765 Å is estimated to be $(2.6\pm1)\times10^{-20}$cm^2 from a comparison between the count rate of O^- produced by process (1) and that of O^- produced from O_2. The quantum yield for process (1) is then obtained to be $(6.4\pm2.5)\times10^{-4}$ at ~765 Å from the total photoabsorption cross section for SO_2, 4.1×10^{-17}cm^2.

The efficiency curve can be divided into two regions: Region I [680 - 860 Å] containing sharp peaks, and Region II [370 - 680 Å] in which two broad peaks with maxima at ~610 and ~550 Å exist. The O^- efficiency rises markedly at the wavelengths of 622 and 570 Å . These onsets are attributed to the formation of triplets of fragments: $O^-(^2P_u) + S^+(^4S_u) + O(^3P_g)$ and $O^-(^2P_u) + S^+(^2D_u) + O(^3P_g)$. Region I appears to consist of a number of vibrational progressions which may be assigned to Rydberg states with

a variety of symmetry and principal quantum numbers. We can extract and assign three vibrational progressions in the symmetric stretching mode ν_1 for the *s*-type Rydberg states converging to SO_2^+ ($\tilde{D}\ ^2A_1$). Term values, effective principal quantum numbers, and quantum defects are calculated by using a Rydberg formula. Some of the vibrational progressions reported in the photoionization efficiency curve[2] of SO_2^+ from SO_2 are not discernible in our O^- efficiency curve. We can explain this discrepancy in terms of the specificity of the Rydberg states in the autoionization branching.

1) K. Mitsuke, S. Suzuki, T. Imamura, and I. Koyano, J. Org. Mass Spectrom. to be published.

2) J. Erickson and C. Y. Ng, J. Chem. Phys. **75,** 1650 (1981); C. Y. R. Wu and C. Y. Ng, J. Chem. Phys. **76,** 4406 (1982).

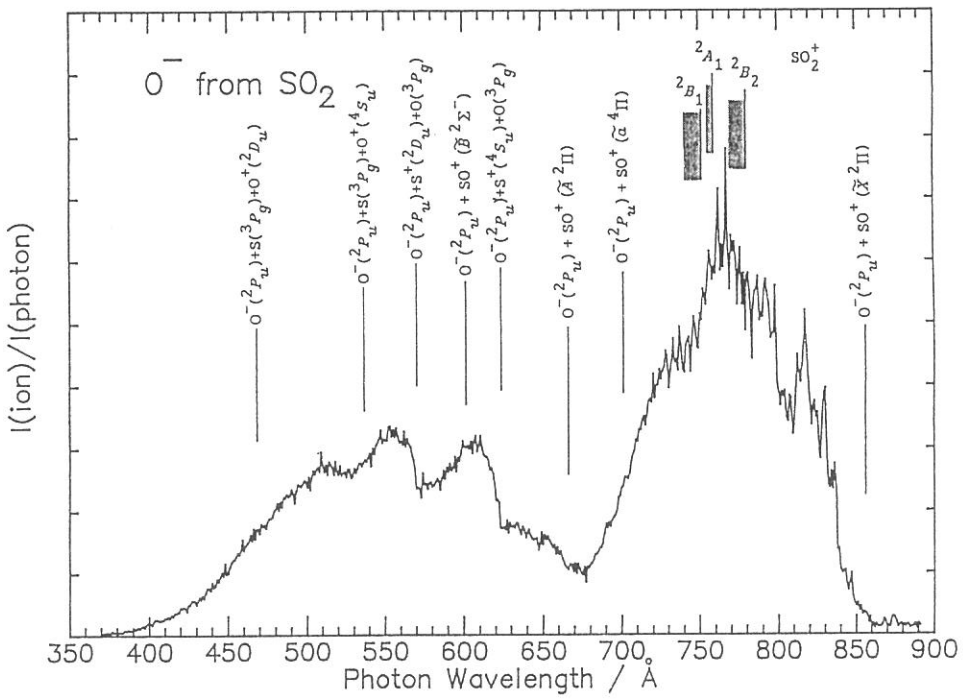

Figure 1. Photodissociation efficiency curve of O^- produced from SO_2 taken at a wavelength resolution (FWHM) of 0.8 Å and wavelength intervals of 1 Å. The vertical lines indicate the ionization limits for SO_2^+ ($\tilde{C}\ ^2B_2$, $\tilde{D}\ ^2A_1$, and $\tilde{E}\ ^2B_1$) and the thermochemical thresholds for possible ion-pair channels (Ref. 1).

ION-PAIR FORMATION FROM HYDROCARBONS BY PREDISSOCIATION OF RYDBERG STATES WITH C(2s)-HOLE CHARACTER

Hideo HATTORI, Hiroaki YOSHIDA, and Koichiro MITSUKE

Department of Vacuum UV Photoscience, Institute for Molecular Science, Myodaiji, Okazaki 444

Ion-pair formation induced by photoexcitation of saturated hydrocarbons ($RH+h\nu \rightarrow RH^{**} \rightarrow H^- + R^+$, $R=C_nH_{2n+1}$ n=1-5) has been studied by negative-ion mass spectrometry. We use monochromatized photon beam in the wavelength range of 400-1000Å at the beam line BL3B. All kinds of hydrocarbons are found to undergo predissociation into ion pairs with the cross section of 8.0×10^{-22} $-1.0\times10^{-20}cm^2$, when they are superexcited to Rydberg states formed by promotion of an electron in a molecular orbital composed of carbon 2s-type atomic orbitals.

Figure 1 shows the H^- photodissociation efficiency curve of ethane. Most of the peaks are assigned as resulting from transitions to the Rydberg states with C(2s)-hole character. A series of peaks observed in the energy range of 18.5-20.0eV correspond to vibrational progressions of the Rydberg states, $2a_{2u} \rightarrow$4s, 5s. We assign these peaks to the $v \geqq 0$ vibrational states of the ν_1(C-H stretching) and ν_3(C-C stretching) modes, as indicated in Fig.1(b), since their spacings are in good agreement with those for the $(2a_{2u})^{-1}$ band in He II photoelectron spectrum of C_2H_6.[1)]

Figures 2 and 3 show the photodissociation efficiency curves of H^- produced from propane and n-butane, respectively. Assignments of the Rydberg states which make peaks are indicated. We wish to point out that the ion-pair formation proceeds exclusively via the Rydberg states produced by promotion of a C(2s) electron. In all efficiency curves, there is not a peak over the whole energy range where the Rydberg states with excitation of an outer-valence electron are present. This finding can be interpreted as that other competitive decay pathways are dominant for these Rydberg states. Namely, Rydberg states with relatively lower excitation energies may have propensity to autoionize or predissociate into neutral fragments. Many molecular orbitals closely lie from -10 to -15eV, so that the energy widths for autoionization of such Rydberg states become large due to considerable overlap between the initially excited orbital and the target occupied orbital to be ionized.

As suggested by the efficiency curve of propane (Fig.2), predissociation into ion pairs

is markedly suppressed from the Rydberg states formed by promotion of an electron accommodated in the deepest inner-valence orbital, $3a_1$. Since this orbital has large overlap with the shallower $4a_1$ orbital, the lifetime of the Rydberg states converging to the $(3a_1)^{-1}$ ionic state is expected to be much shorter with respect to autoionization into the $(4a_1)^{-1}$ ionic state than with respect to conversion to the ion-pair state. Hence, these Rydberg states do not effectively predissociate into ion pairs in spite of their C(2s)-hole character. A similar phenomenon is observed for the Rydberg states of n-butane converging to the $(3a_g)^{-1}$ ionic state. (Fig.3)

1) J.W.Rabalais, and A.Katrib, Mol. Phys. 27, 923 (1974).

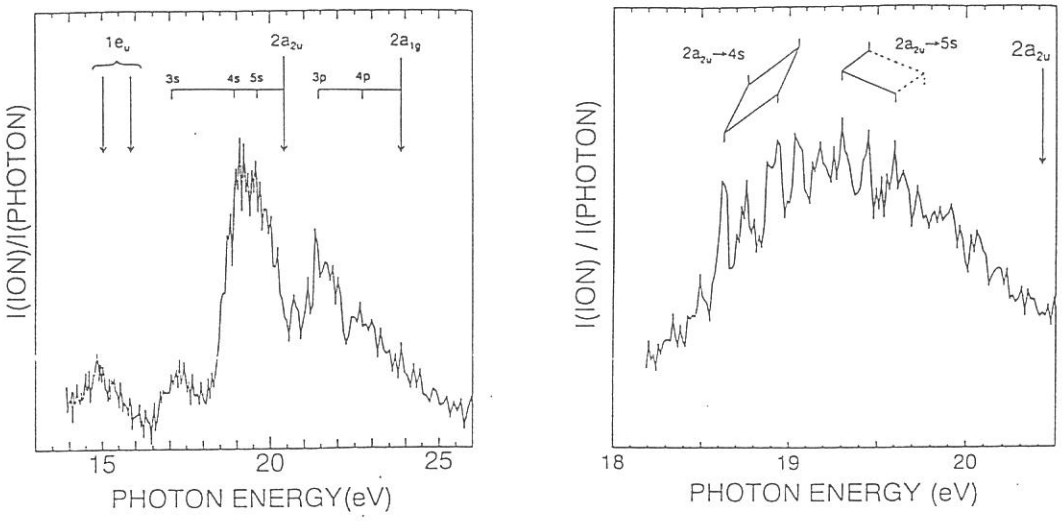

Figure 1 Photodissociation efficiency curves of H^- produced from ethane (a) with intervals of 2Å, and (b) with intervals of 0.5Å. The vertical IPs for molecular orbitals and assignments of the Rydberg states are indicated.

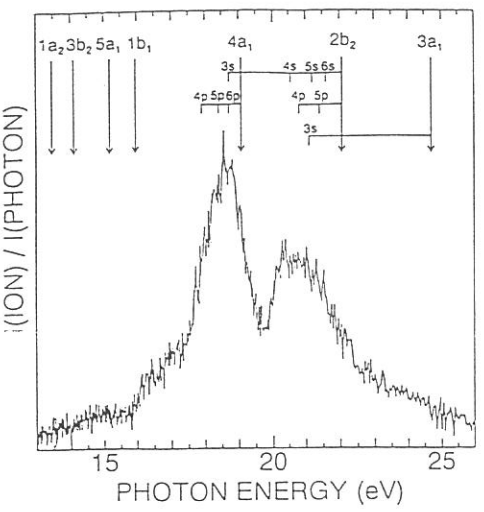

Figure 2 Photodissociation efficiency curves of H^- produced from propane.

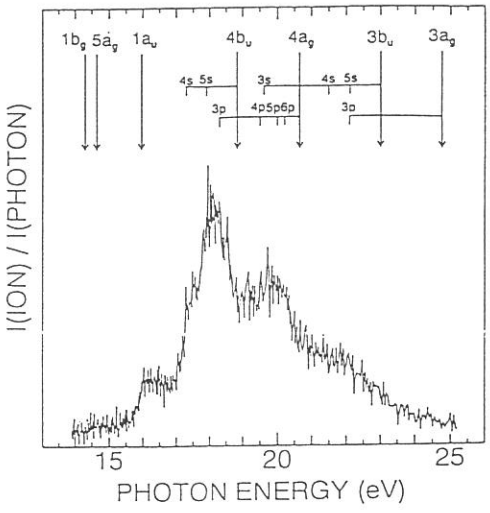

Figure 3 Photodissociation efficiency curves of H^- produced from n-butane.

VUV Reflectivity Spectra of Rare-Earth Sesquioxides II

Fumitaka ARAI, Shin-ichi KIMURA, Yasuhiko SATO,
Mikihiko IKEZAWA, Yuki CHIBA and Mareo ISHIGAME

Research Institute for Scientific Measurements, Tohoku University, Aoba-ku, Sendai 980

Rare-earth elements are characterized by the 4*f* electrons, and their compounds have some interesting properties such as the mixed valence state. So we measured a series of rare-earth sesquioxides (R_2O_3's), which are typical insulator compounds, for the purpose of investigating the fundamental electronic state of the rare-earth compounds. We have already reported the VUV reflectivity spectra of four kinds of R_2O_3 single crystals (R=La, Nd, Gd and Y) [1]. In this report, we measured the reflectivity spectra of another four kinds of R_2O_3 single crystals (R=Er, Tm, Yb and Lu) for the first time in the photon energy region between 4 eV and 35 eV at 300K at the beamline BL7B. We discuss the electronic structure of these materials including the 4*f* multiplet structure.

We made single crystals of all samples by the floating zone method using a Xe-arc lamp image furnace. All compounds form bcc type crystal structure, which is called the C-type. We measured the reflectivity spectra using the cleavage surface along to the (111)-plane.

Figure 1 shows reflectivity spectra of five kinds of R_2O_3 materials (R=Y, Er, Tm, Yb and Lu). Y_2O_3 has no 4*f* electron and has the same bcc crystal structure as other R_2O_3. We adopted Y_2O_3 as the reference material of R_2O_3 because the ionic radius of Y^{3+} is almost the same as that of Er^{3+}, Tm^{3+}, Yb^{3+} and Lu^{3+}. All spectra are similar to one another. This means that the origin of the main structure of these spectra is almost equal to one another.

We will make a detailed analysis using the optical conductivity spectra (Figure 2), which are derived from the Kramers-Kronig transformation of the reflectivity spectra in Figure 1. There are three peak structures in common, which are located around 10 eV (here called a), 18 eV (b) and 30 eV (c). In our previous papers, we have explained that the origin of the main part of the structure a is the excitation from the valence band (O-2*p*) to the conduction band (R-5*d*), that of the peak a' is the exciton of the peak a, and that of the peak c is the intra-atomic excitation from R-$5p_{3/2}$ to R-5*d* states [1, 2]. The structure due to the transition from R-$5p_{1/2}$ to R-5*d* is not seen in this figure because this peak is expected to be out of the observed energy range at about 38 eV. The origin of the peak b is considered to be the transition from O-2*s* to R-5*d* states, because this energy position and structure are almost the same among the materials and the energy position is expected from the atomic states of rare-earth and oxygen [3].

It can be seen that the detailed structure of peak a in each R_2O_3 spectrum is different from one another. It is obvious that the reason for this is the difference of the expanse of the R-4*f* states due to the 4*f* multiplet. The peak structure due to the transition from O-2*p* to Y-4*d* is thought to be almost equal to that from O-2*p* to R-5*d* because the band shape of 4*d* in Y_2O_3 is as almost same as that of 5*d* in R_2O_3. Therefore the difference structure of the peak a among each R_2O_3 is thought to be due to the expanse of R-4*f* electrons. We show the 4*f* multiplet structure which is estimated from the theoretical expectation [4] in Figure 2. The peak structure of R_2O_3 which is different from that of Y_2O_3 around 10 eV is thought to be explained by the R-4*f* multiplet structure. However, the peaks of R_2O_3 at about 7 eV indicated by a" are located at almost same energy position in each R_2O_3 spectrum, and can't be explained by this consideration. These peaks are thought to be due to the exciton of the transition from R-4*f* to R-5*d*.

References
[1] S. Kimura, F. Arai, M. Ikezawa, Y. Chiba and M. Ishigame, UVSOR Activity Report 1991, 86 (1992).
[2] S. Kimura, T. Nanba, T. Tomikawa, S. Kunii and T. Kasuya, Phys. Rev. **B46**, 12196 (1992)
[3] C. E. Moore, *Atomic Energy Levels vol. 1 and 3*, (U. S. Government Printing Office, Washington D. C., 1949)
[4] M. Campagna, G. K. Wertheim and Y. Bear, *Photoemission in Solids II*, L. Ley and M. Cardona (eds.) (Springer–Verlag, 222 1979)

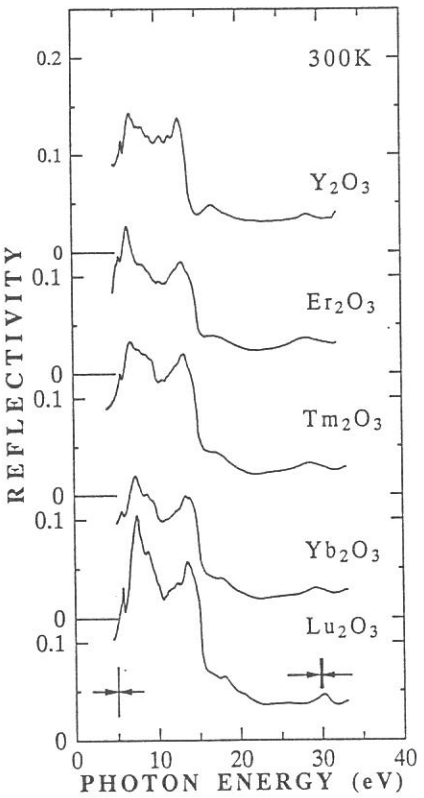

Fig.1. Reflectivity spectra of R_2O_3(R=Y,Er,Tm,Yb and Lu) single crystals in the photon energy region between 4 eV and 35 eV at 300K.

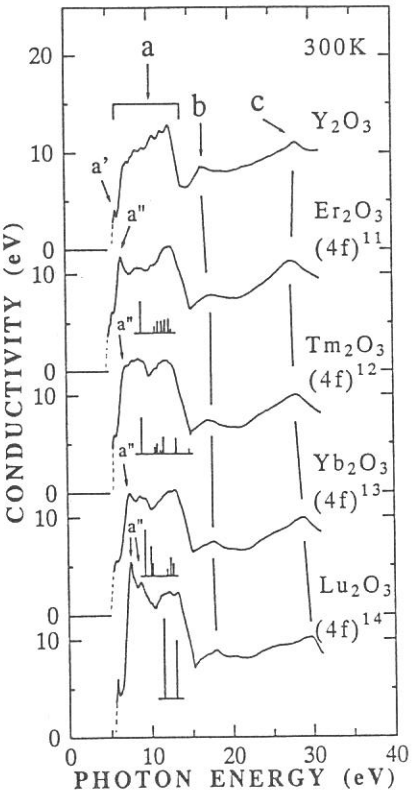

Fig.2. Optical conductivity spectra of R_2O_3's from the Kramers–Kronig transformation of the reflectivity spectra and 4*f* multiplet structures derived from theory (refer to [4]).

GENERATION OF OXYGEN DEFICIENT DEFECTS IN SYNTHETIC SILICA GLASS BY QUENCHING

Shigetosi Hayashi, Hiroshi Kawazoe*
Fine Ceramics Research Laboratory, Advanced Technology Research Laboratories of Sumitomo Metal Industries Ltd., 16-1 Sunayama, Hasaki, Kashima-gun, Ibaraki 314-02
*Research Laboratory of Engineering Materials, Tokyo Institute of Technology, Midori-ku, Yokohama 227

Informations on the generation mechanism and the properties of oxygen deficient defects in synthetic silica glass are very important in the use of the glass as optics in ultra-violet regions. We already reported that ≡Si-Si≡ (one type of the oxygen deficient defects) is generated by chlorine evaporation during sintering of the porous silica glass obtained by VAD (Vapor-phase Axial Deposition) method with several tens of ppm chlorine.

Another generation mechanism of ≡Si-Si≡ in synthetic silica glass was found in the present study. Samples were prepared by quenching the consolidated silica glass plates (from 1000 ℃ to 1500 ℃) These silica glasses contain less than 20 ppm of OH groups and less than 1 ppm of Cl. Absorption spectra of the samples were measured at the beam line BL1B.

Fig.1 shows absorption spectra of quenched silica glasses. In the sample heated at 1000 ℃ no optical absorption peak was observed, but in samples heated at higher temperature 7.6 eV absorption intensity (≡Si-Si≡) increased as raising their heating temperature.

Fig.2 shows Arrhenius' plots of the yields of ≡Si-Si≡ defects calculated by using absorption cross section 6 10^{-17} cm^2. It seems that the defects were generated by the thermally activated process.

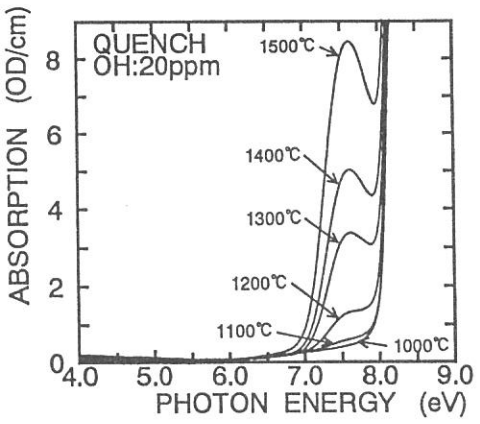

Fig.1 Generation of 7.6eV-absorption band in low OH-silica glass by quenching.

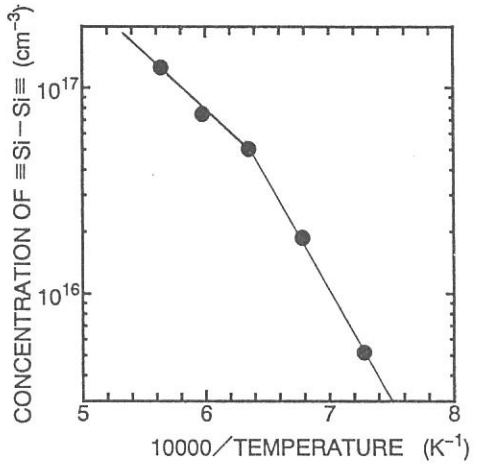

Fig.2 Arrhenius' plots of ≡Si-Si≡ yields in synthetic silica glasses by quenching.

CONVERSION OF OXYGEN VACANCY INTO E' CENTER INDUCED BY EXCIMER LASER IRRADIATION IN HIGH-PURITY SILICA

Hiroyuki NISHIKAWA, Takayuki SOTA, and Yoshimichi OHKI
Department of Electrical Engineering, Waseda University
3-4-1 Ohkubo, Shinjuku-ku, Tokyo 169

Optical absorption in ultraviolet (uv)-vacuum uv (vuv) regions were measured on high-purity silicas irradiated by excimer lasers. Samples investigated are oxygen-deficient silicas with low-OH ([OH]<1 ppm) and high-OH ([OH]≈ 20 ppm) concentrations. Irradiation was carried out with ArF (6.4 eV) or F_2 (7.9 eV) excimer laser at room temperature. Vacuum-uv-transmission measurements were done using synchrotron radiation from UVSOR as a light source. Shown in Figs.1 and 2 are uv-vuv absorption spectra obtained for the low-OH and high-OH oxygen-deficient silicas, respectively, after irradiation with 6.4-eV or 7.9-eV photons. Although the appearance of absorption bands at 5.0 and 5.8 eV can be seen, no significant change is observed in an absorption band at 7.6 eV in the low-OH sample. On the other hand, the decay of the 7.6-eV band is observed in conjunction with a significant growth of the 5.8-eV band in the high-OH sample, as shown in Fig.2. The 5.8-eV and 7.6-eV bands are considered to be due to E' center (≡Si·)[1] and oxygen vacancy (≡Si-Si≡)[2], respectively. Therefore, these results indicate that the conversion of the oxygen vacancies into E' centers is enhanced in the presence of hydrogen. The following mechanism is considered to be responsible for the conversion of the oxygen vacancy:

$$\equiv Si\text{-}Si\equiv + \cdot H \rightarrow \equiv Si\text{-}H \quad \equiv Si\cdot \qquad (1).$$

This mechanism involving the formation of the E' variant ($\equiv Si\text{-}H$ $\equiv Si\cdot$) in the high-OH sample is supported by the observation of a peak shift relative to the 5.8-eV band of the E'_{γ} center ($\equiv Si\cdot\ ^{+}Si\equiv$) by 0.1 eV to the lower energy.

References

1. C.M. Nelson and R.A. Weeks, J. Am. Ceram. Soc. 43, 396 (1960).

2. R. Tohmon et al. Phys. Rev. B 39, 1337 (1989).

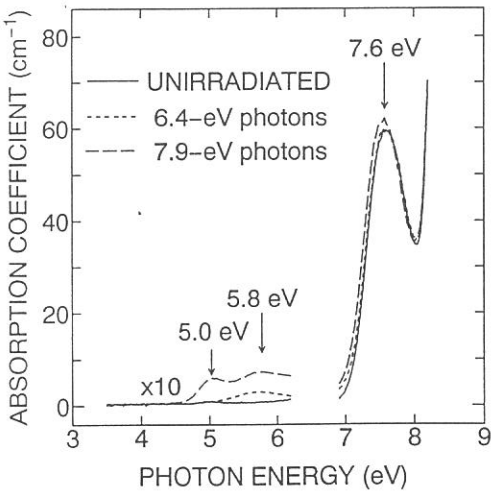

FIG.1 UV-VUV spectra of low-OH oxygen-deficient silica ([OH]<1 ppm) irradiated by 6.4-eV or 7.9-eV excimer laser

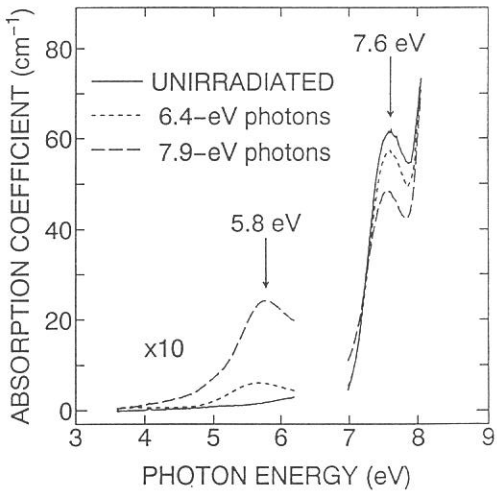

FIG.2 UV-VUV spectra of high-OH oxygen-deficient silica ([OH]≈20 ppm) irradiated by 6.4-eV or 7.9-eV excimer laser

REFLECTION SPECTRA OF Pb HALIDES AND BiI_3 IN THE 5*d* CORE EXCITON REGION

Masami FUJITA, Hideyuki NAKAGAWA,[+] Atsuhiko KASHINO,[+]
Kazutoshi FUKUI,[+] Takeshi MIYANAGA[++] and Makoto WATANABE[+++]

Maritime Safety Academy, Wakaba, Kure 737
[+]*Department of Electrical and Electronics Engineering, Faculty of Engineering, Fukui University, Fukui 910*
[++]*Department of Physics, Faculty of Education, Wakayama University, Wakayama 640*
[+++]*Institute for Molecular Science, Myodaiji, Okazaki 444*

The crystal structure of $PbCl_2$ and $PbBr_2$ belongs to orthorhombic (D_{2h}^{16}, *Pmnb*), while that of PbI_2 belongs to hexagonal (D_{3d}^{3}). BiI_3 has a rhombohedral (C_{3i}^{2}) crystal structure. The peaks due to the Pb^{2+} 5*d* core exciton are observed in the optical spectra of Pb halides in the 20-25 eV region.[1-3] In BiI_3, the Bi^{3+} 5*d* core exciton peaks are found in the 25-30 eV region.[1] In the present study, reflection spectra of these crystals were measured in order to investigate the crystal field effect on the core exciton.

Figure 1 shows reflection spectrum of BiI_3 single crystal below 12 eV. First exciton peak is seen at 2.0 eV. Sharp peak is also observed at 3.8 eV. Spectral features below 6 eV agree with those by previous study.[4] No distinct structure is observed between 10 and 25 eV.

In Fig. 2 are shown reflection spectra of Pb halides (upper part) and BiI_3 (lower part) in the metal 5*d* core exciton region. In addition to the three main peaks 1, 2 and 3, the small peak 0 is found in the low energy side of the peak 1 in each crystal. Weak shoulder 1' is observed at the high energy side of the peak 1 in PbI_2 and at the low energy side of the peak 1 in BiI_3. The structures 3 in PbI_2 and BiI_3 are broader than in $PbCl_2$ and $PbBr_2$.

The peaks 1, 2 and 3 are assigned to the transitions from the $^1S_0$ ground state to the $^3P_1$, $^1P_1$ and $^3D_1$ states, respectively. Energy splittings and relative intensities of these peaks in $PbCl_2$ and $PbBr_2$ are explained well based on the atomic excitation picture neglecting the crystal field effect.[3] This means that the anisotropic crystal field in $PbCl_2$ and $PbBr_2$ is weaker than in PbI_2 and BiI_3. The peak 0 in each material and the structure 1' in PbI_2 and BiI_3 are attributed to the transitions allowed by the anisotropic crystal field

effect. Broadness of the peak 3 in PbI_2 and BiI_3 is also ascribed to the crystal field effect. The splitting of the Pb^{2+} 6*p* level in PbI_2 due to the crystal field potential is supposed to be about 1 eV in order to explain the spectrum of PbI_2.

References

1) J. Bordas, J. Robertson and A. Jakobsson: J. Phys. C 11(1978)2607.
2) T. Hayashi, K. Toyoda and M. Itoh: J. Phys. Soc. Jpn. 57(1988)1861.
3) M. Fujita, H. Nakagawa, K. Fukui, H. Matsumoto, T. Miyanaga and M. Watanabe: J. Phys. Soc. Jpn. 60(1991)4393.
4) T. Komatsu and Y. Kaifu: J. Phys. Soc. Jpn. 40(1976)1062.

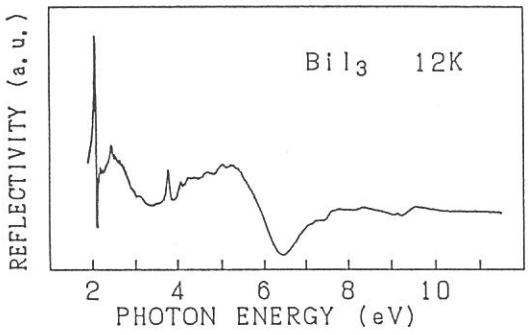

Fig. 1. Reflection spectrum of BiI_3 below 12 eV.

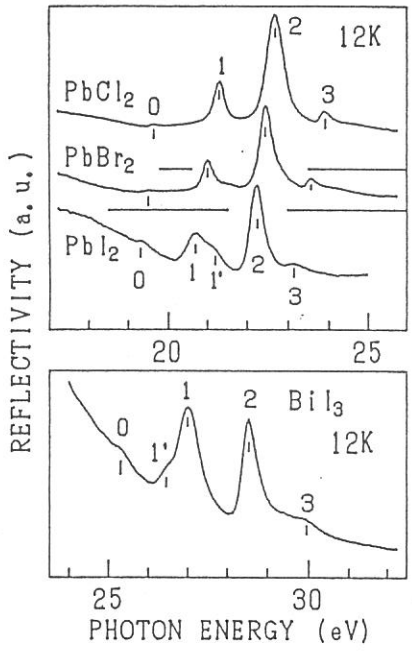

Fig. 2. Reflection spectra of Pb halides (upper part) and BiI_3 (lower part) in the 5*d* core exciton region.

VACUUM ULTRAVIOLET REFLECTANCE SPECTRA OF Mn_2Sb, MnAlGe, Superlattices (Mn/Sb, Fe/Gd, Fe/Nd) AND INTERCALATION COMPOUNDS (M_xTiS_2(M:Ni,Fe))

Shigemasa SUGA, Akio KIMURA, Tomohiro MATSUSHITA,
Yasuaki MORI, Hiroaki SHIGEOKA and Shin Imada

Department of Material Physics, Osaka Universitsy
Toyonaka, Osaka 560

The electronic structures of Cu_2Sb type compounds, magnetic superlattices and TiS_2 intercalation compounds were studied by means of the vacuum ultraviolet reflectance spectroscopy by use of synchrotron radiation from UVSOR electron storage ring. The measurement was done at BL-1B of UVSOR equipped with a Seya-Namioka monochromator. The higher order light was suppressed by use of pyrex, SiO_2 and LiF filters in the wavelength regions above 3000, 1500 and 1000 A. The incidence angle was set to 22.5 degrees and the p reflectance was measured by a photomultiplier. All measurement was done at room temperature. Cleaved surfaces were employed for the intercalation compounds and the as grown surfaces were used for the superlattices. For Cu_2Sb type materials polished surfaces were prepared for the reflectance measurement. The reflectance spectra were obtained by normalizing the spectra by the spectrum of the monochromator output.

Figure 1 shows the reflectance spectrum of $Fe_{1/3}TiS_2$ compared with that of the TiS_2. Since the electronic structure of TiS_2 has been well studied by many authors, the reflectance spectrum can be rather easily understood. The spectrum in the 2-30eV region can be separated into 4 regions with distinct dip structures:(I) the region extending up to 3eV, (II) the region up to 8eV, (III) the region extending up to about 12eV and finally the region extending from 12eV beyond 20eV (IV). According to the band calculation,[1] the transitions between S 3p valence bands and the lower Ti 3d conduction bands which have "t_{2g}" symmetry are dominant in the region I. The region II consists of the transitions from the S 3p valence bands to the higher Ti 3d states with "e_g" symmetry. The transition between the bonding and antibonding orbitals occur in the region III. In the spectrum of $Fe_{1/3}TiS_2$, the sharp peak around 3.5 eV appears in the energy region II. This structure may be related to the Fe 3d state.

The reflectance spectra of the superlattices, Mn/Sb, Fe/Nd and Fe/Gd as well as Mn_2Sb and MnAlGe are summarized in Figs.2 and 3. The similarity between the two spectra of Fe/Nd and Fe/Gd compared with that of Mn/Sb suggests that the spectra in the energy region up to 20eV is mostly governed by the excitation associated with Fe.

Reference
1) A.Zunger and A.J.Freeman, Phys. Rev. B **16**, 906 (1977).

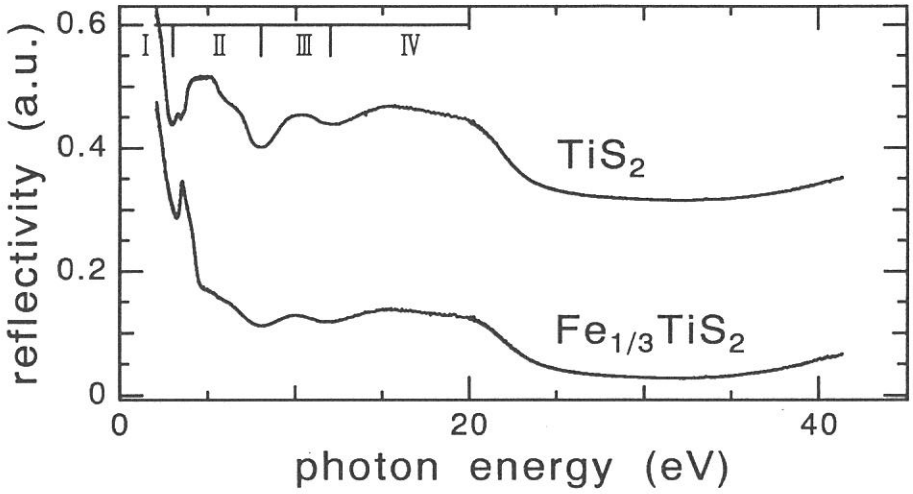

Fig.1

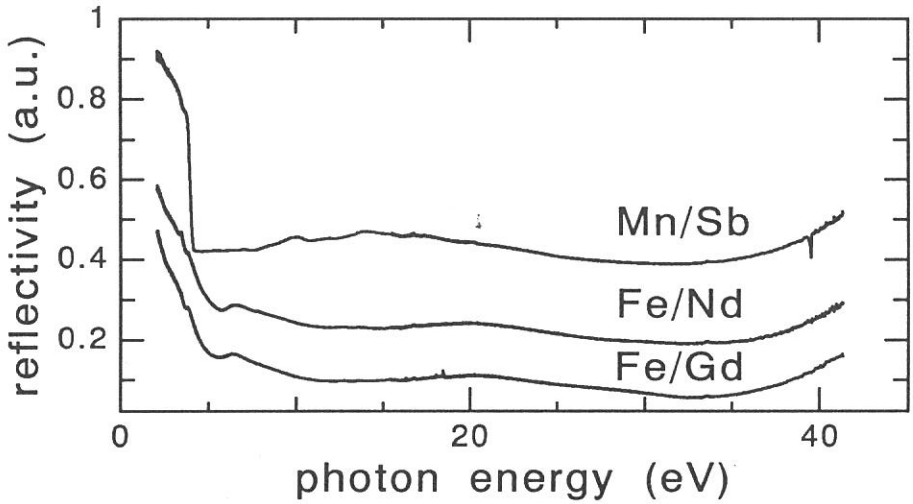

Fig.2

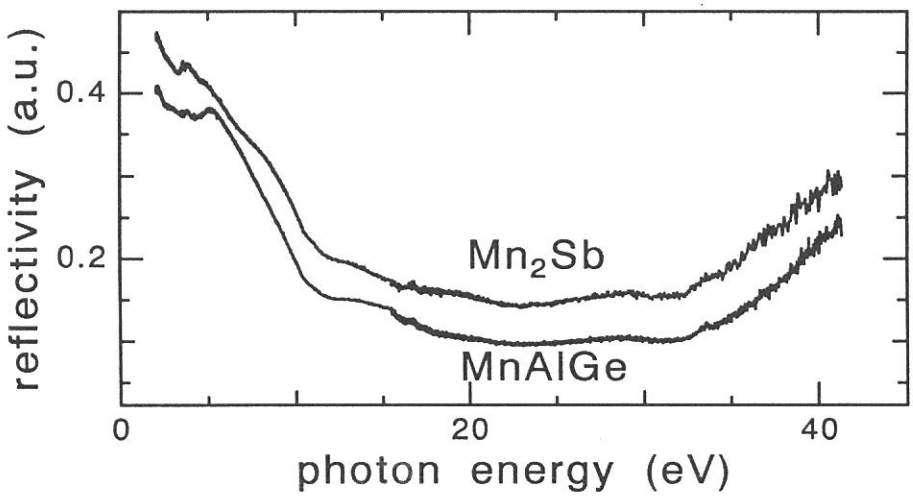

Fig.3

Contribution of Eu^{2+} to PSL Center Formation in $BaFBr:Eu^{2+}$ Single Crystal

Yasuo Iwabuchi, Nobufumi Mori,Terumi Matsuda
Tadaoki Mitani[1], Shigeo Shionoya[2]

Fuji Photo Film Co.,Ltd., Technology Development Center, Miyanodai, Kaisei, Kanagawa, 258 Japan
[1]Institute for Molecular Science, Myodaiji, Okazaki, 444 Japan
[2]Tokyo Engineering University, Department of Electronics, Hachioji, Tokyo, 192 Japan

Previous investigations showed that PSL centers are created efficiently at the energy of exciton formation in $BaFBr:Eu^{2+}$ single crystal.[1] Moreover, at the low energy side of the exciton band, a shoulder-like structure is observed. To clarify an origin of this structure,we measured the change of this structure with increasing the concentration of Eu^{2+}.

$BaFBr:Eu^{2+}$ single crystals were grown by the horizontal Bridgman method in a graphite boat. The various single crystals different in the Eu^{2+} concentration were made by changing the quantity of additional Eu^{2+} at preparation. The measurements using vacuum ultra violet (VUV) light were performed at the beam line BL-7B. The PSL center formation spectra which represents an efficiency of PSL center creation, were measured as follows. The samples were irradiated by chopped He-Ne laser at 10 Hz (633nm:NEC) as scanning the VUV light, and detected the signal of Eu^{2+} luminescence which was synchronized with chopped He-Ne laser excitation by using lock-in amplifier. Eliminating second diffractive light, VUV light was passed through a quartz filter. The electric vector E of the excitation light was always perpendicular to the c-axis of the single crystal.

Figure1 shows PSL center formation spectra in $BaFBr:Eu^{2+}$ single crystals of different concentration of Eu^{2+} at LNT. The concentration of doped Eu^{2+} analyzed by ICP method is (a)0.58% (b)0.15% (c)0.028% respectively. Spectra were normalized at the peak intensity concerning to the first exciton band at 7.2 eV. It is seen that the intensity of the structure at 6.6 eV grows as the concentration of Eu^{2+} increasing. The inset shows the relationship between the analyzed Eu^{2+} concentration in the $BaFBr:Eu^{2+}$ single crystal and the intensity of the structure at 6.6 eV.

As we can see the linear relationship, it is clear that the structure at 6.6 eV is due to the Eu^{2+}.

As to this structure at the low energy side of the exciton, the process of Eu^{2+} ionization is considered from the energy level scheme of $BaFBr:Eu^{2+}$.[2] That is to say, an electron generated by Eu^{2+} ionization is trapped by F^{+} center to form F center and Eu^{3+}. An ionization of Eu^{2+} was observed in alkaline-earth halides such as CaF_2[3], SrF_2, BaF_2[4], so it is sufficiently considered that the ionization of Eu^{2+} occurs in $BaFBr:Eu^{2+}$.

Reference

[1] Y.Iwabuchi, N.Mori, T.Matsuda, T.Mitani and S.Shionoya, UVSOR Activity Report 19 (1992) 128

[2] K.Takahashi, K.Kohda, J.Miyahara, Y.Kanemitsu, K.Amitani and S.Shionoya, J.Lumin. 31&32 (1984) 266

[3] C.Pendrini, F.Rogemond and D.S.McClure, J. Appl. Phys. 59 (1986) 1196

[4] B.Moine, C.Pedrni and B.Courtois, J.Lumin. 50 (1991) 31

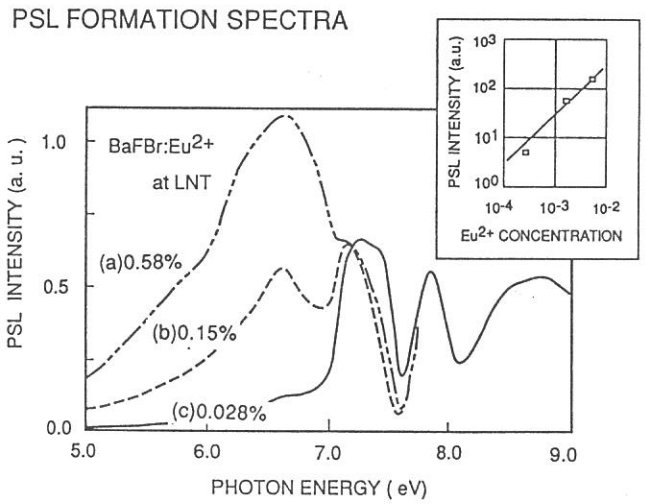

Figure 1 PSL center formation spectra in BaFBr single crystals of different concentration of Eu^{2+} at LNT. The concentration of doped Eu^{2+} is (a)0.58% (b)0.15% (c)0.028% respectively. Inset shows the relationship between the analyzed Eu^{2+} concentration in the $BaFBr:Eu^{2+}$ single crystal and the intensity of the structure at 6.6 eV .

Self-Trapped Excitons in $CdBr_2$ and $CdCl_2$

Hideyuki NAKAGAWA, Atsuhiko KASHINO, Junji YAMADA, Kazutoshi FUKUI, Takeshi MIYANAGA [A], Masami FUJITA [B], Makoto WATANABE [C]

Department of Electrical and Electronics Engineering, Fukui University, Fukui 910, Japan
[A] *Department of Physics, Faculty of Education, Wakayama University, Wakayama 640, Japan*
[B] *Maritime Safety Academy, Kure 737, Japan*
[C] *Institute for Molecular Science, Myodaiji, Okazaki 444, Japan*

Cadmium chloride and bromide are typical ionic crystals of layer structure, where one Cd^{2+}-ion sheet is sandwiched between two halogen ion sheets. A cadmium ion sits at the center of an octahedron composed of six halogen ions located at the vertices. The top of the valence band consists mainly of halogen np (n=3 or 4) orbitals while the bottom of the conduction band has cadmium 5s character. The lowest excitonic absorption corresponds to the transition from halogen np to cadmium 5s levels. Two luminescence bands are produced with excitation in the fundamental absorption region, that is, the one appears in near uv-region (UV-emission) and the other in yellow-region (Y-emission). They are associated with radiative decay of self-trapped excitons (STE). The STE-states in CdX_2(X=Cl or Br) are believed to be identical with the excited states of the $\left[Cd^{2+}X_6^-\right]^{4-}$-complex molecular ions which are formed through exciton-phonon interaction.

Decay profiles of UV and Y emission bands in $CdBr_2$ and $CdCl_2$ are shown in Fig. 1. Excitation was made with single-bunched pulses at 36 eV from an undulator of UVSOR which have 0.5 ns pulse duration and 178 ns pulse interval. The exsistence of long lived decay components gives rise to the piling-up of luminescence intensity. The decay curve of the UV-emission consists of two decay components, the fast(τ_F=11 ns for $CdBr_2$ and 2.0 ns for $CdCl_2$) and the slow($\tau_S \gg 178$ ns) ones. They are sttributed to the parity-allowed radiative decay of the spin singlet and triplet STE's. Detailed examination on the triplet components with use of N_2 gas laser pulses elucidates that the slow decay component is further decomposed into three ones, which indecates that the triplet STE state splits into three level system due to the spin-orbit and exciton-lattice interactions.

The decay curve of the Y-emission contains only the slow component, which is further decomposed into three decay components and is connected to the parity-forbidden radiative decay of STE's.

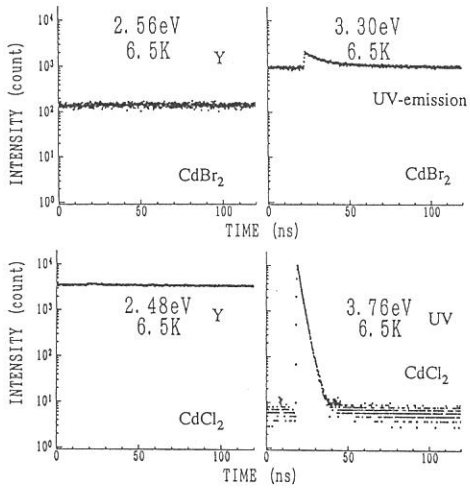

Fig.1 Decay curves of UV and Y emission bands in $CdBr_2$ and $CdCl_2$. Excitation was made with undulator radiation at 36eV. Piling-up arises from the existence of slow components with longer decay time than the pulse interval 178ns.

TIME-RESOLVED MEASUREMENTS OF EXCITATION SPECTRA FOR INTRINSIC EMISSION IN ALKALI IODIDES

Tamao MATSUMOTO, Akinori MIYAMOTO and Ken-ichi KAN'NO

Department of Physics, Kyoto University

We previously reported that the intrinsic emission bands of type I[1] in alkali halides, which are attributed to on-center self-trapped excitons (STE), consist of fluorescent (singlet) and phosphorescent (triplet) components.[2] In the present work, excitation spectrum for each component of these composite bands has been studied in three iodides; 4.21eV band (π_I) in NaI, 4.14eV band (σ) in KI and 3.90eV band (σ) in RbI. Spectra were obtained below and above the temperature at which resonance emission of free excitons (FE) disappears, using the time-resolved detection system of luminescence equipped at BL1B[2].

In Fig. 1 are shown excitation spectra obtained around 15K. Solid curves indicate singlet component and dotted curves indicate triplet components. By chain curves are shown excitation spectra for triplet emission bands from two different configurations of off-center STE's; 3.29eV band (π_{II}) in KI and 2.21eV band (π_{III}) in RbI. All excitation spectra are normalized at 7.0eV. Absorption spectra obtained by Teegarden and Baldini[3] are also shown by broken curves along with arrows indicating the energy positions of n=1 FE, n=2 FE and the onset of band-to-band transition. Both components of type I emission bands are efficiently excited in the whole energy region of band-to-band transition. Excitation spectra for them coincide above 7.0eV in NaI. In KI and RbI, excitation spectra for them and for π_{II} or π_{III} band coincide above 6.5eV. In the energy region between n=1 and n=2 FE, no intrinsic emission bands are excited efficiently. We observed emission bands related to impurities under excitation into this energy region.

In Fig. 2 are shown excitation spectra taken at higher temperature. As for NaI, only excitation spectrum for the triplet component is shown because singlet component disappears at this temperature. Shapes of all excitation spectra in band-to-band transition region are almost similar to those at low temperatures. Between n=1 and n=2 FE energy, however, π bands of three iodides are efficiently excited contrary to the result at low temperature. On the other hand, both components of σ bands in KI and RbI are still not efficiently excited there.

---

[1]K.Kan'no, K.Tanaka and T.Hayashi: Rev.Solid State Science **4,** 383 (1990)
[2]T. Matsumoto, T.Kawata, A.Miyamoto and K.Kan'no:J.Pys.Soc.Jpn. **61**,4229 (1992)
[3]K.Teegarden and G.Baldini: Phys.Rev. **155**,896 (1967)

At low temperature, it is clear that emission yield in the energy region between n=1 and n=2 FE are depressed by the presence of impurities. The n=1 FE, whose diffusion length is sufficiently large in iodides at low temperature,[4] are likely to have chances of being caught by impurities on their long free path.

At higher temperature, total intensity of intrinsic luminescence increases in three iodides in the energy region between n=1 and n=2 FE, reflecting the situation that almost all n=1 FE's immediately relax into STE state. In KI and RbI, it should be remarked that emission bands from off-center configuration increase but that both components of emission bands from on-center configuration do not. This suggests that n=1 FE preferentially relax into off-center configuration. The electron wavefunction of on-center STE is likely to be very diffuse.[5] We imagine that n=1 FE with small radius would not relax into on-center configuration when it can relax into off-center configuration.

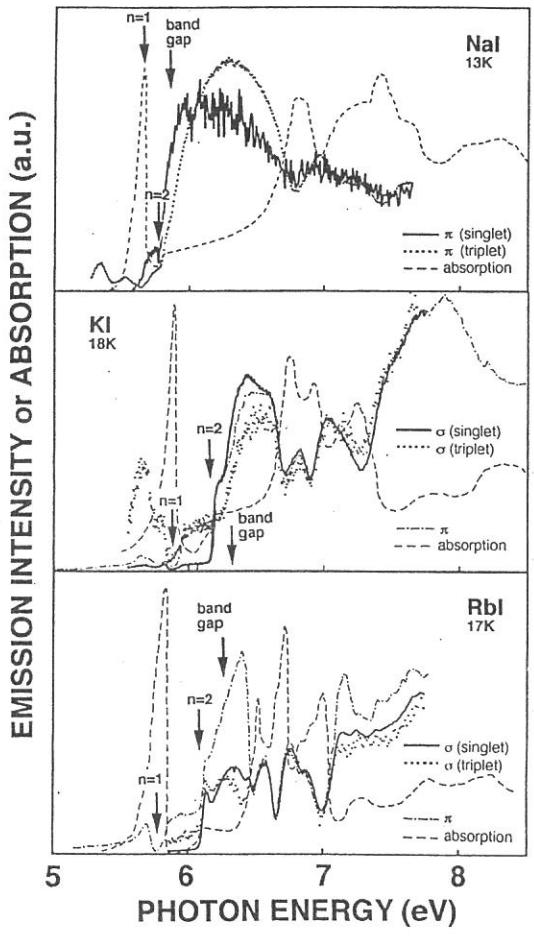

Fig. 1

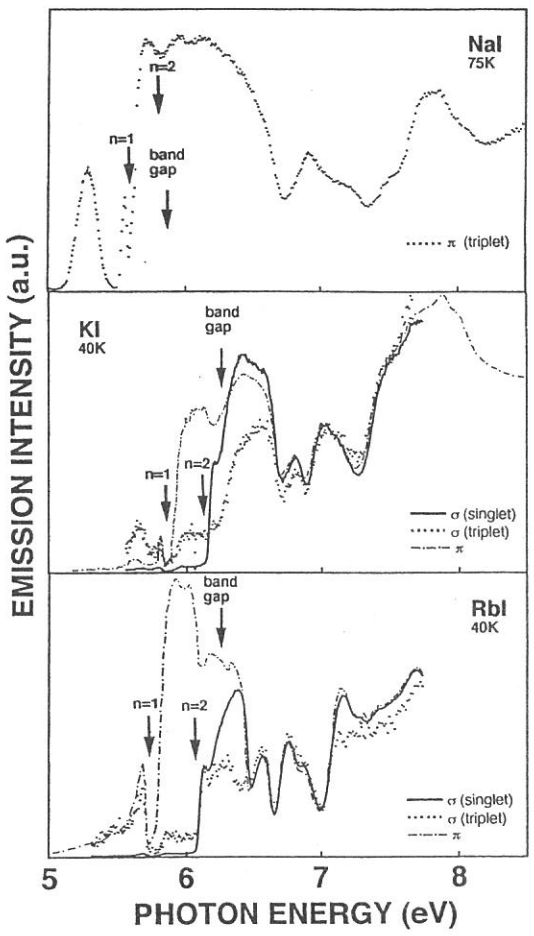

Fig. 2

[4]H.Nishimura: in Defect processes induced by electronic excitation in insulators, Edited by N. Itoh, p.56, World Scientific, (1989)
[5]T.Kawata, T.Mukai, T.Matsumoto and K.Kan'no: Proceedings of ICDIM92 (in press)

TEMPORAL BEHAVIOR OF THE RESONANT LUMINESCENCE OF EXCITONS IN KI AND RbI

Tetsusuke HAYASHI, Masayuki WATANABE, Ping GU*, and Toru TSUJIBAYASHI**

Faculty of Integrated Human Studies, Kyoto University, Kyoto 606-01.

**Department of Physics, Kyoto University, Kyoto 606-01.*

***Osaka Dental University, Hirakata, Osaka 573.*

Photo-excitation in the lowest (n=1) exciton absorption band of alkali iodide crystals induces resonant luminescence of free excitons (FE) together with the luminescence of self-trapped excitons (STE). The efficiency of the FE luminescence relative to the STE luminescence is less than 1×10^{-2}. It has been accepted that the FE state is separated from the STE state by an adiabatic potential barrier and a large part of FE at low temperatures relax to the STE state due to a tunneling process through the barrier.[1] In Fig.1 and 2 are shown the luminescence spectra of FE in KI and RbI. The main band at 5.828 eV in KI and that at 5.729 eV in RbI were identified recently as the emission from the triplet (J=2) state of FE.[2,3] We can observe a weak singlet emission on the high energy side of the main band. We have measured, for the first time, the temporal behavior of the triplet emission of FE, and examined the dynamical process of exciton relaxation.

Measurements were performed with BL1B of UVSOR under normal operation. The luminescence signal was collected through lenses set inside and outside of a sample chamber, and was dispersed with a single-path monochromator. Decay curves were measured with the time-correlated single photon counting method by using a MCP photomultiplier and a TAC system.

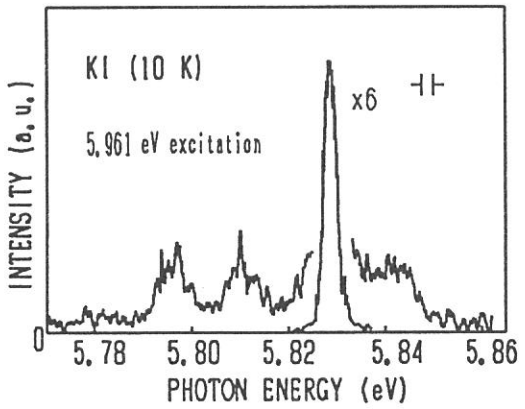

Fig.1 Emission spectrum of FE in KI at 10K.

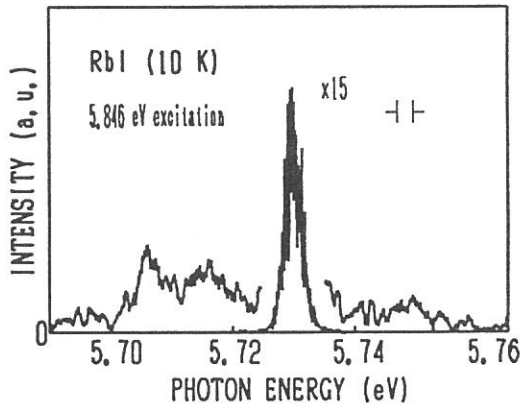

Fig.2 Emission spectrum of FE in RbI at 10K.

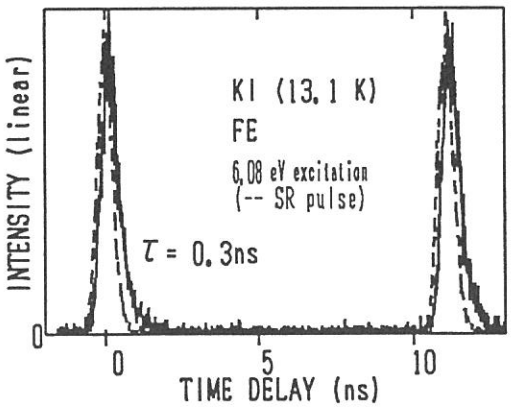

Fig.3 Temporal behavior of the FE luminescence in KI at 13.1K.

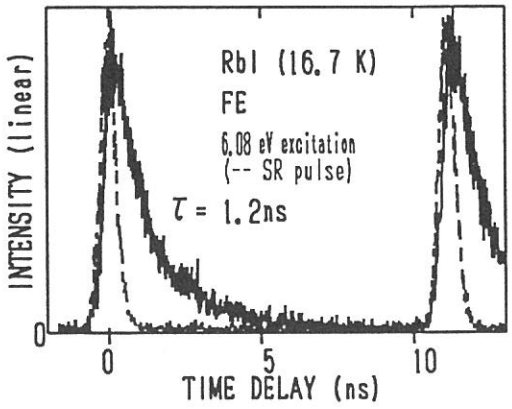

Fig.4 Temporal behavior of the FE luminescence in RbI at 16.7K.

The decay profiles of the FE luminescence at around 15 K in KI and RbI are presented in Figs.3 and 4. The excitation photon energy was 6.08 eV. The emission signals due to the two successive excitation pulses are shown together with the time response of the excitation pulse (dotted curve). The decay times of 0.3 ns for KI and 1.2 ns for RbI are obtained from the convolution analysis. We have obtained the yield of the FE luminescence of 2.5×10^{-3} for KI and 8.3×10^{-3} for RbI from the conventional measurement of the emission spectra on assuming the total luminescence efficiency to be unity. We can see that the difference in the luminescence yield between KI and RbI is roughly corresponding to the difference in the decay time. That is, the observed decay times are not the radiative lifetimes of FE, but they are determined by the self-trapping rate. The radiative lifetime of FE could be longer than 100 ns, which supports the identification of the relevant state of the FE luminescence as the triplet state.

References

1) K. Nasu and Y. Toyozawa: J. Phys. Soc. Jpn. **50** (1981) 235.
2) K. Tanimura and N. Itoh: Phys. Rev. **B45** (1992) 9417.
3) T. Kishigami-Tsujibayashi, K. Toyoda, and T. Hayashi: Phys. Rev. **B45** (1992) 13737.

VARIATION OF DECAY CURVES FOR AUGER-FREE LUMINESCENCE FROM BaF_2 AND CsCl CRYSTALS AGAINST EXCITING PHOTON ENERGY

Yoshihiko NUNOYA, Jian-zhi RUAN(GEN) and Shinzou KUBOTA

Rikkyo University, Nishi-Ikebukuro 3, Tokyo, 171

Decay curves for Auger-free luminescence from BaF_2 and CsCl crystals have been measured over the range of incident photon energy $h\nu$ from the threshold E_{th} of the luminescence to 30 eV. Motivation for this study is to explain the non-single exponential decay in luminescence intensity from BaF_2 and CsCl crystals under excitation of uv photons, as shown in Fig.1.[1] We should note that under excitation with 22 eV photons the decay curve for the 5.6 eV band from BaF_2 crystal has a short decay component with decaytime of 0.4 ± 0.1 ns together with the main decay component of 0.83± 0.02 ns. Under excitation of high-energy electrons due to 511 keV photons, the decay shows a single exponential decay with a decay time of 0.90 ± 0.05 ns. The difference in decay curves of the 4.5 eV band from CsCl is also observed in CsCl, as shown in Fig.1.

The experiment was carried out by using a 1-m Seya-Namioka monochromator at BL7B beam line of UVSOR. The experimental set up is similar to that described in Ref.2. Decay curves were measured by using 5.632 MHz UVSOR single bunch operation. Energy resolved luminescence photons were detected by a MCPPM (Hamamatsu R1564U-30).

For $E_{th} < h\nu < 20$ eV and $h\nu > 27$ ev, the measured decay curves of the 5.6 eV band from BaF_2 crystal show a single exponential decay down to the intensity of 1/500 of the peak intensity. The decay time is found to be 0.83 ±0.02 ns. For 20 eV < $h\nu$ < 26 eV a short component of decay time of 0.4 ns is observed together with the main decay component of 0.83 ns. The short component is also observed from BaF_2 crystal at liquid nitrogen temperature. The origin of the short decay component is unknown.

Decay curves of the 4.5 eV band from CsCl at room temperature have at least two exponential decay components with decay time of 0.6 ± 0.1 ns and 1.55 ± 0.05 ns. No appreciable energy dependence in decay curves is observed in the energy range from E_{th} to 30 eV which are related to different absorption coefficients. By considering no energy dependence in decay curves, the non-single exponential decay observed here can not be linked to the surface effect.[3] The surface

effect has been proposed to explain the faster decrease in luminescence intensity of the 4.5 eV band from CsCl under Cs^+ 4d core excitation of 80 eV < hν < 140 eV with increasing absorption coefficient. Under Cs^+ 4d core excitation decay curves have at least two exponential decay components of a short component with 0.1 - 0.2 ns decaytime and a second component with 1 - 1.5 ns decaytime. The decay curve under Cs^+ 4d core excitation is faster than that of uv photon excitation.

References:
1.S.Kubota, Proceedings of the tenth international conference on vacuum ultraviolet physics, Paris, 1992 (World Scientific Publication), in press.
2. S.Kubota, M.Itoh, J.Ruan(Gen), S.Sakuragi and S.Hashimoto, Phys. Rev. Letters (1988)183.
3. S.Kubota, M.MacDonald and I.H.MunroJ.Lum. 48 & 49(1991)589.

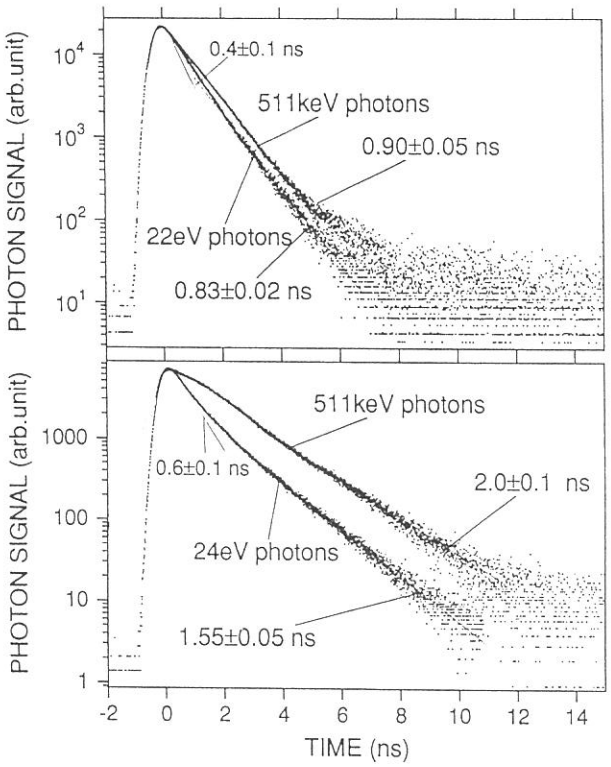

Fig.1. Decay curves for the 4.5 eV band from CsCl and for the 5.6 eV band from BaF_2 under uv photons and high-energy electron excitation by using 511 kev photons.

LIGHT AMPLIFICATION DUE TO POPULATION INVERSION BETWEEN THE VALENCE AND OUTERMOST-CORE BANDS IN BaF_2

Minoru ITOH and Hiroshi ITOH*

Faculty of Engineering, Shinshu University, Nagano 380
**Faculty of Education, Kagawa University, Takamatsu 760*

In BaF_2, a core hole created in the Ba^{2+} $5p$ band decays primarily through the radiative recombination with an F^- $2p$ valence electron, because the Auger decay process is energetically impossible. The resulting luminescence has been called "Auger-free (AF) luminescence ".[1] We notice that both the valence and core bands are completely filled with electrons at thermal equilibrium. As a result, it is likely that an inverted population between these two levels is easily realized at any intensity of excitation through which some electrons are elevated from the core band to the conduction band, leading to a laser oscillation of AF luminescence.

The present experiment was performed at room temperature by using an undulator radiation from the UVSOR ring as a pumping source. A 1-mm-thick plate of BaF_2 was mounted on a rotatable sample holder installed in a vacuum chamber. A flat multiple-dielectric coated mirror (R = 100% at 217 nm) and a quartz plate were placed close to the sample in the direction perpendicular to the exciting beam; see the inset in Fig. 1. Thus it was possible to form an optical cavity by suitably adjusting the orientation of the dielectric mirror. Without using lenses, the luminescence was observed through a grating monochromator, the entrance slit of which was 70 cm away from the sample.

Figure 1 shows luminescence spectra of BaF_2 measured under the core-band excitation with 36.0-eV photons; (a) no collimation and (b) best collimation. A broad band around 300 nm is due to the radiative annihilation of a self-trapped exciton. In (a), two emission bands are seen at 219 and 195 nm. These bands have been assigned to the AF luminescence of BaF_2. It is clear that the peak intensity of the 219-nm band is enhanced when the mirror is adjusted for best attainable collimation. In Fig. 2 we present decay behaviors of the 219-nm band taken under (a) no collimation and (b) best collimation. A pulse shape of the exciting light is also shown as (c) for reference. In (a), the luminescence exhibits a single-exponential decay, with a time constant of 0.8 ns. By adjusting the collimating mirror, the decay time becomes slightly fast [(b)]. However, such an appre-

ciable sharpening of the decay profile was not observable if the intensity of the undulator radiation was reduced to $\sim 1/3$ of the maximum value.

These observations suggest a possibility of the light amplification of AF luminescence (185-240 nm) in BaF_2. Although the data are still preliminary, the present work has demonstrated a new type of laser operation in which the core-valence transition plays an important role.[2)]

References

1) M. Itoh, S. Kubota, J. Ruan(Gen) and S. Hashimoto: Rev. Solid State Sci. **4** (1990) 467.

2) M. Itoh and H. Itoh: Phys. Rev. **B 46** (1992) 15509.

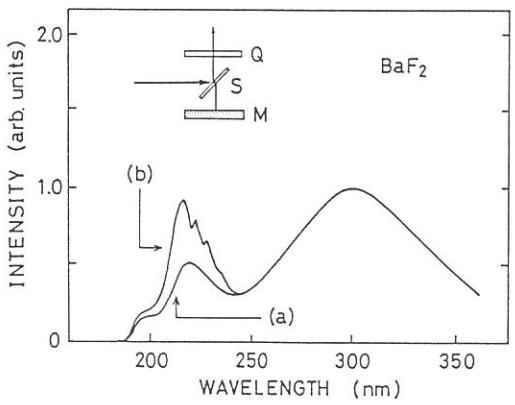

Fig.1. Luminescence spectra of BaF_2 excited with undulator radiation at 36.0 eV. The inset shows a cavity configuration (Q, quartz plate; S, BaF_2 crystal; M, adjustable mirror).

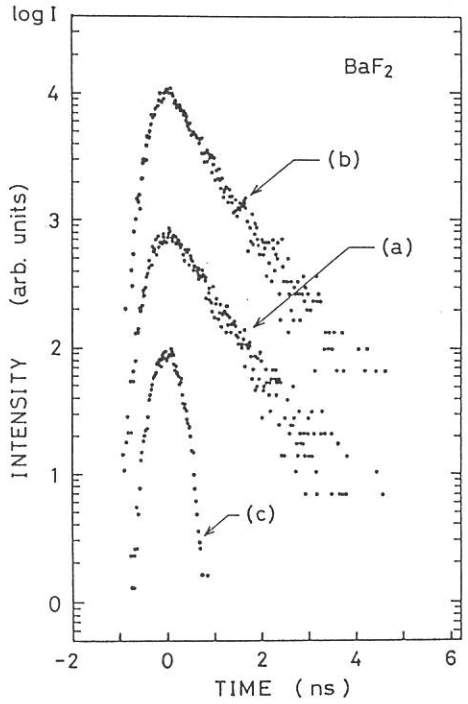

Fig.2. Decay profiles of the 219-nm band in BaF_2 [(a) and (b)]. A pulse shape of the exciting light is also shown as (c). For illustration purposes, the curves (a),(b) and (c) are shifted by one order, respectively.

XANES and EXAFS study of K_3C_{60}

Kazuyuki TOHJI and Hisanori SHINOHARA*

Department of Resources Engineering, Tohoku University, Sendai 980, Japan.
*Department of Chemistry for materials, Mi'e University, Tsu 514, Japan.

The Potassium L-edge EXAFS spectrum of microcrystalline potassium-doped K_3C_{60} has been measured using 250-500 eV synchrotron radiation. EXAFS is particularly useful to obtain the information of local structures around potassium in K_3C_{60}.

The XANES and EXAFS experiments have been performed on the BL-2B1 Beam Line of UVSOR at the Institute for Molecular Science. The beam line is equipped with a grasshopper monochromator. The energy resolution of the monochromator with the grating(600 lines/mm mechanically ruled grating) is 0.8 eV around the potassium L_{III} edge. In order to eliminate intensity variation due to carbon contaminants deposited on the optical elements, The background normalization-subtraction procedure is employed[1]. The background features are eliminated by subtracting the signal stemming from the Au-coated grid reference from that of C_{60} deposited on the Au substrate. This ensures optimum cancellation of all background structures. Energy calibration is performed by use of two transmission minima at 284.7 and 291.0 eV, which come from the carbon contamination.

Details of the production of fullerene-rich carbon soot by the contact arc method[2] have been described previously. Briefly, an arc between two graphite rods(13.5 mm in diameter) is sparked at 200-250 A in direct current (DC) mode in a He pressure of 100 Torr. Separation and purification of C_{60} are attained by column chromatography on neutral alumina (ICN Biomedicals Akt.I) with hexane/toluene solvent.

Fig.1 shows a XANES spectrum of potassium-doped K_3C_{60} microcrystals. The spectrum shows the carbon K-edge π^* resonance and σ^* resonance which are partly overlapped with the potassium L-edge absorption. The intensity of the potassium L-edge absorption increases as the number of potassium atoms (n) in K_nC_{60} . The results are consistent with a recent report on the XANES spectra on the same system with much higher spectral resolution[3].

Fig.2 exhibits EXAFS features of K_3C_{60} which are present at much higher energy regions. Fig.3 shows the extracts EXAFS oscillation $\chi(k)$ which is obtained after subtraction of the smooth X-ray absorption background and normalization[4-5]. Here, the wave vector k is defined by the following equation:

$k = \sqrt{2m(E-E_0)/h^2}$,

where E is the energy of the incident X-ray beam and E_0 is the threshold energy of L_{III} absorption of potassium atoms. The E_0 value was set to be 293 eV in the present analysis. The function $k^3\chi(k)$ was Fourier transformed over the range of $3.0<k<7.4$. The obtained magnitude, FT, is shown in the side of Fig.3. In the present calculations the values for the back scattering amplitude and the phase shift reported by Teo and Lee were used[6]. The obtained nearest-neighbor K-C distance is 3.06 A. The present value

is shorter than that obtained by an X-ray powder pattern analysis of K_3C_{60} (3.27 A for tetrahedral site), where the C_{60} molecules are assumed to be locked into a fixed position. The nearest-neighbor K-C distance decreases if the C_{60} molecules rotate in the K_3C_{60} crystals. The present results imply that the C_{60} molecules rotate in a cooperative manner (jump motion).

References
1) J. Store, R. Jaeger, Phys. Rev. B, 26, 4111, (1982).
2) R.E. Haufler, et al., Mat. Res. Soc. Proc. 206, 627, (1991).
3) C.T. Chen, et al., Nature, 352, 603 (1991).
4) F.W. Lytle, et al., Phys. Rev. B, 11, 4825, (1975).
5) K. Tohji, et. al., J. Am. Chem. Soc., 106, 612, (1984).
6) B.K. Teo and P.A. Lee, J. Am. Chem. Soc., 101, 2815, (1979).

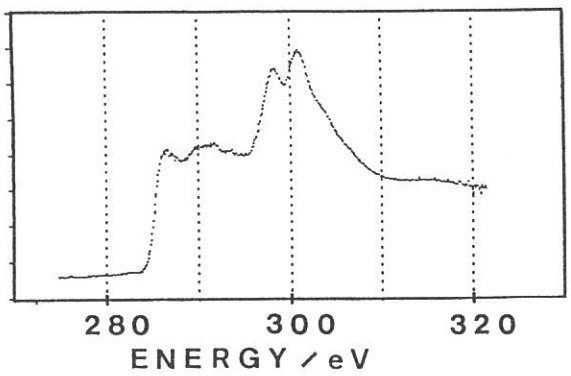

Fig.1
XANES spectrum of potassium-doped C_{60}. The intense peaks around 300 eV are due to potassium L-edge absorption. The K_3C_{60} sample is prepared ex-situ and shows a superconducting transition at 19 K.

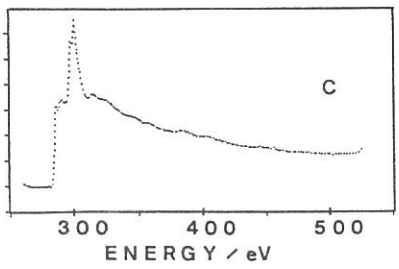

Fig.2
EXAFS feature of micro-crystalline K_3C_{60} at room temperature.

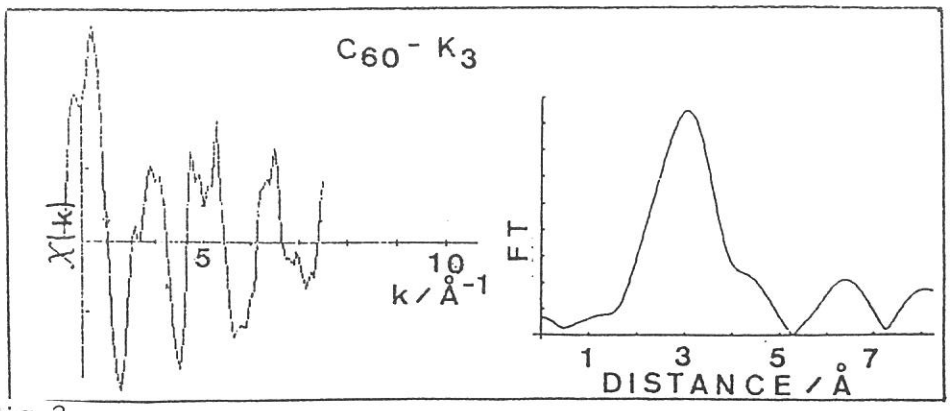

Fig.3
Extracted oscillation of Fig.2 and its Fourier transform.

Ni $L_{2,3}$ Absorption Spectra of $NiPS_3$

K.NOGUCHI, S.NAKAI, A.KAMATA, K.MATSUDA and K.SANO

Faculty of Engineering, Utsunomiya University, Utsunomiya 321

A layered 3*d* transition-metal thiophosphate crystallizes in the crystal structure belongs to the monoclinic space group with 4 formula units per unit cell and is related to the $CdCl_2$ structure. The sulfur atoms in the compound are cubically closed-packed, and the metal atoms and the phosphorus-phosphorus pairs occupy the cadmium positions. Furthermore, the crystal is constructed of a stack of sandwich layers each of which is weakly bonded by van der Waals forces. With in the layers the metal atoms are surrounded octahedrally by six sulfur atoms. The only difference is that a P_2 pair in $NiPS_3$ occupies one of the three metal-sites of the layered transition metal disulfides[1]. In this study, we have measured the linear polarized Ni $L_{2,3}$ absorption spectra in $NiPS_3$ single crystals.

Measurements have been performed by using synchrotron radiation at the BL-7A line of the Ultraviolet Synchrotron Radiation Facility (UV-SOR), Institute for Molecular Science. We have used a double crystal Beryl ($10\bar{1}0$) monochromator with an energy resolution about 0.4 eV at Ni *L* absorption peak. Spectra were measured by means of photoelectric yield from single crystal surfaces. The sample of $NiPS_3$ was cleaved in a vacuum by pealing off with Scotch tape along the sample surface (ab plane).

Figure 1 shows Ni 2*p* XAS spectra of $NiPS_3$. The upper solid curve (θ=70°) was taken for the polarization of electric field nearly parallel to the c-axis (E//c), and the lower dotted one (θ=0°) was taken parallel to the ab plane (E//ab). These spectra were normalized to the background. The first peak which appeared about 852eV corresponds to $2p_{3/2}$ absorption peak, and the second one which appeared about 870eV to $2p_{1/2}$ absorption peak. The satellite structure was appeared around 857eV. In Fig. 1, the polarization dependency is not clearly seen.

The $L_{2,3}$ absorption spectra are interpreted in terms of the multiplet structure which results from the interaction between a 2*p* hole and 3*d* electrons of localized metal ions[2]. It is well known that in a purely ionic configuration and in D_{Oh} symmetry the crystal field together with the *d*-*d* Coulomb interaction cause the ground state of a d^8 ion to be A_{2g} (ϵ_g). This state can mix with states $d^9\underline{L}$ and $d^{10}\underline{L}\,\underline{L}'$ of A_{2g} symmetry, where $\underline{L}$ denotes a ligand hole. The initial state covalency is related to the amount of d^8, $d^9\underline{L}$ and $d^{10}\underline{L}\,\underline{L}'$ character in ground state. The final state after absorption are of the form $\underline{c}\,d^9$ and $\underline{c}\,d^{10}\underline{L}$, where $\underline{c}$ denotes a core hole.

van der Laan et al.[3] reported the decrease in multiplet splitting which appeared in Ni $2p$ absorption spectra of Ni dihalides with decreasing anion electronegativity because of covalent mixing in both the initial and final states. Then, the relative intensities of the multiplet are reflect the covalent mixing. Comparing our experimental spectra with the calculated results by van der Laan, we can obtain the mixing amount of ground state for $NiPS_3$; the value of $3d$, $3d^9\underline{L}$, and $3d^{10}\underline{L}\,\underline{L}'$ characters as 0.47, 0.44 and 0.09, respectively.

However, the polarization dependency is not so clear in our result, so, improved experiments have to be done in future.

References

1) F.Hulliger , Physics and Chemistry of Materials with Layered Structures, ed. F.Levy (D.Reidel Pub. Com., Dordrecht,1967) Vol.5, P.217

2) S.Nakai et al. , J.Phys Soc. Jpn. 54 (1985) 4034

3) G.van der Laan et al., Phys. Rev. B33 (1986) 4253

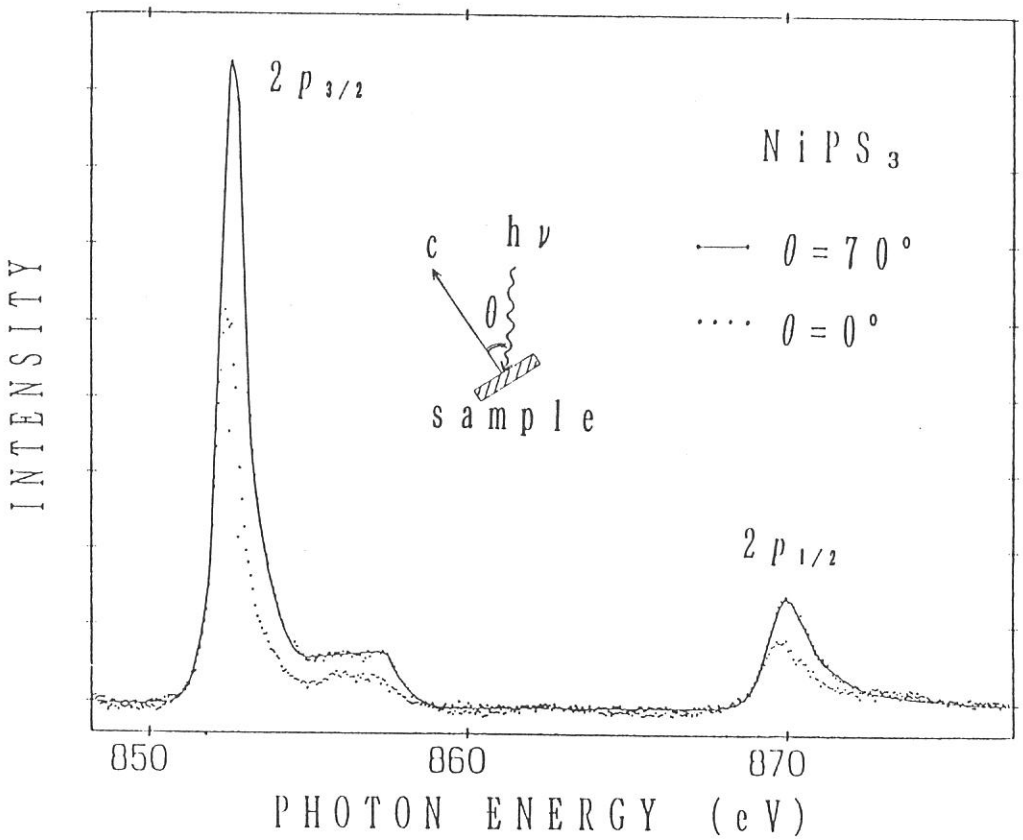

Fig. 1

Ni L-edge absorption spectra in Ni-MgO solid solutions

Tomoko HANADA, Tsunehiro TANAKA, Hisao YOSHIDA,
Takuzo FUNABIKI, and Satohiro YOSHIDA

Division of Molecular Engineering, Kyoto University, Kyoto 606

So far, we have studied solubility of Ni atoms into MgO matrix. We have found that nickel-ions-impregnated MgO powder forms a solid solution easily by calcination at 773 K at any ratio of Ni and Mg. Previous studies for Ni-MgO solid solutions concluded that nickel ions exist in divalent state in solid solutions of low nickel concentration. In fact, in our case, when the nickel concentration is lower than 50 % (Ni % = mole of Ni / (mole of Ni + mole of Mg) × 100) , the solid solution is pale green, indicating that nickel ions are present as Ni^{2+}. But at 50 %, the color is dark gray and gets darker with an increase in Ni concentration. Such a change in the color suggests that divalent and trivalent nickel ions coexist in the solid solutions. In the study of catalysis by the solid solutions, the quantitative analysis of divalent and trivalent nickel ions is very important. However, XPS can not be applied for the analysis because of little difference in the binding energy between Ni^{2+} and Ni^{3+}.

In this work, we measured $L_{3,2}$-edge XAFS including the bands due to $2p \rightarrow 3d$ transition and investigated a relation between the valence of nickel atoms and XAFS spectra, since the valence of nickel atom relates to the $2p \rightarrow 3d$ transition cross section.

Samples were prepared by impregnation of MgO powder with an $Ni(NO_3)_2$ aqueous solution, followed by calcination at 773 K for four hours in a dried air stream. Concentration of Ni ions was determined by X-ray fluorescence method.

Ni $L_{3,2}$-edge absorption measurements were carried out on BL-7A at UVSOR with a ring energy of 750 MeV and a stored current of 80-200 mA in a mode of total electron yields. Besides the samples, we recorded XAFS of $NiO(Ni^{2+})$ and $Ni_2O_3(Ni^{3+})$ as references. A double crystal beryl monochromater was used, and energy calibration was carried out using Al K-edge.

For all the samples including NiO and Ni_2O_3 references, spectra were very similar to each other. Figure 1 shows the spectrum of Ni $L_{3,2}$ absorption for $Ni_{0.5}Mg_{0.5}$ binary oxide as an example. Peaks are seen at around 853 and 855 eV in L_3-edge region, at around 870 and 871 eV in L_2-edge region. The positions of these peaks are the same for all samples within a resolution of the monochromater. That is, we could not observe any chemical shifts.

The white line in L_3-edge spectrum, the prominent peak at 853 eV, is assigned to $2p_{3/2} \rightarrow 3d$ transition. An Ni^{3+} ion has more unoccupied 3d orbitals than an Ni^{2+} ion and it is generally expected that the intensity of the white line associated with Ni^{3+} is higher than that associated with Ni^{2+}. To evaluate the intensity, we subtracted the backgrounds from recorded spectra and carried out deconvolution of the resultant spectra with Lorenzians. A typical deconvoluted spectrum is

shown in Fig. 2. Unfortunately, we failed the precise evaluation of intensity because of missing of an adequate normalizing procedure. However, we found that full width at half maximum (FWHM) of the white line changes with increasing nickel concentration as shown in Fig. 3. When nickel concentration is below10 %, samples are pale green, and FWHMs are found to be close to that of NiO(1.1 eV). Thus we suppose that nickel ions are almost divalent in these solid solutions. On the other hand, with an increase in the concentration, FWHM becomes larger, and converges on 1.25 eV above for samples contaning Ni ions 40 %. The broadening in the white line may result from formation of Ni^{3+} ions.

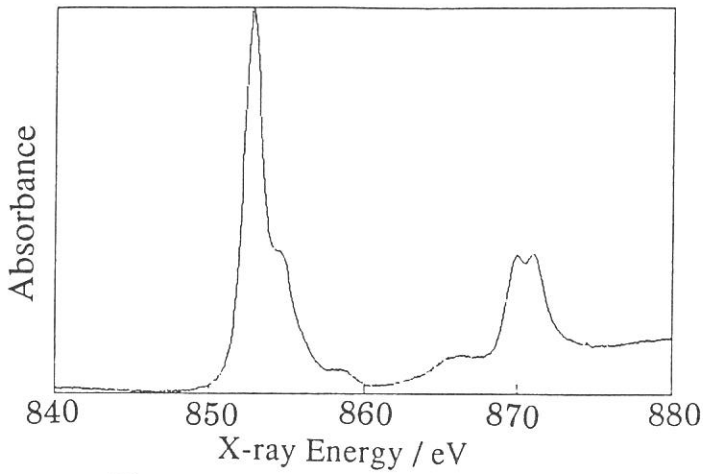

Fig.1 Ni $L_{3,2}$-edge absorption spectrum of $Ni_{0.5}Mg_{0.5}$ binary oxide.

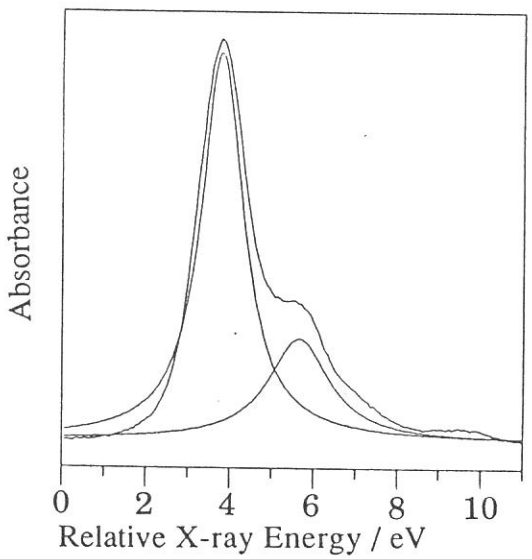

Fig.2 Ni L_3-edge absorption spectrum and its deconvoluted spectrum of $Ni_{0.5}Mg_{0.5}$ binary oxide. Energy offset is taken to be 849.0 eV.

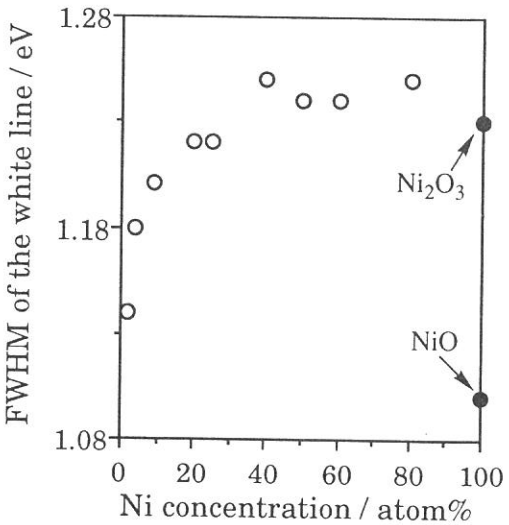

Fig.3 Variation of FWHM of the white line with Ni concentration in Ni_xMg_{1-x} binary oxide.

Cu $L_{2,3}$-edge Absorption Spectra of Cu-Au Alloys

T.K. SHAM[1,2,*], A. HIRAYA[1] and M. WATANABE[1]

1. UVSOR, Institute for Molecular Science, Myodaiji, Okazaki 444
2. Department of Chemistry, University of Western Ontario, London, Ontario, N6A 5B7 Canada

Electronic charge redistribution upon alloying of Au and Cu has been a subject of considerable interest for many decades in connection with the study of Friedel charge screening, effect of d-d interaction upon dilution and the local charge redistribution in view of chemical effects such as electronegativity difference. The perhaps most intriguing spectroscopic observation of these alloys has been the opposite trends exhibited by the Mossbauer isomer shifts and the photoelectron Au 4f binding energy shifts on the basis of simple electronegativity predictions. A charge compensation model has been proposed to explain this discrepancy[1]. In this model, Au loses d charge and this loss is overcompensated by a gain of s charge so that the net charge flow onto the Au site is in accord with electronegativity predictions. The d charge depletion at the Au site in Cu-Au alloys has recently been confirmed by X-ray absorption measurements of the Au $L_{2,3}$ edge whitelines[2]. Despite these observations, the nature of charge redistribution at the Cu site is not fully understood, although electronegativity argument suggests that Cu is expected to lose charge. The objective of this experiment is to make high resolution measurements of the near edge structure of the Cu L-edge in a series of Au-Cu alloys. In this report, preliminary results are presented and their implications discussed.

X-ray absorption measurements were performed at the BL1A beamline which is equipped with a double crystal monochromator. A set of beryl crystals (2d= 15.965 Å) was used. At the Cu $L_{3,2}$ edge, the overall spectrometer resolution is $<$ 1 eV. Absorption spectra were simultaneously recorded in three modes: total electron yield (TEY) with specimen current, total electron yield with a multichannel plate (MCP) and X-ray fluorescence yield (FLY) with a gas (Ar/CH_4) proportion counter. Normal incidence of the photon beam onto the sample with the fluorescence detector and the MCP positioned at 45 degree from the incident beam was used to record the data. Both TEY give identical spectra while TEY and FLY exhibit a drastic difference in the sensitivity of sampling depth with FLY being more sensitive to the bulk.

Samples of Cu, Cu_3Au (order and disordered), CuAu (ordered and disordered) and $CuAu_3$ have been studied. The specimens are metal foils of which the surface was scraped prior to their introduction into the vacuum chamber and was scraped again in-situ with a diamond file before each measurement. Fig.1 shows the Cu L-edge of a Cu_3Au sample before and after scraping. It is apparent that the surface is covered with oxide before scraping and after scraping the TEY spectra are still sensitive to the oxide remaining on the surface while the FLY spectrum is essentially bulk-like with no detectable oxide.

Fig.2 shows the Cu L-edge TEY spectra of several clean samples. It can been seen from fig.2 that the Cu L-edge has rich structures with an apparent whiteline at the threshold. These structures are often not seen in low resolution spectrum[3]. The presence of the whiteline (first peak in the $L_{3,2}$ edge) is not totally surprising since there exists some unoccupied densities of d states above the Fermi level due to s-p-d rehybridization, and a p

it can be revealed that the Cu deposit is dispersed and contains a mixture of CuO, Cu_2O and Cu with mostly oxide on the surface. This is deduced from the comparison of the TEY (more surface sensitive) and the FLY (more bulk sensitive) spectra. This observation is not surprising since the oxidation reduction reaction (hydrogen is oxidized in this case) was carried out in solution in ambient atmosphere and the Cu/porous silicon samples had been stored in ambient atmosphere prior to the measurement. The feature at ~ 57.2 deg Bragg angle (~920 eV) is the signal from the Si substrate due to second order radiation. Detailed analysis is now in progress.

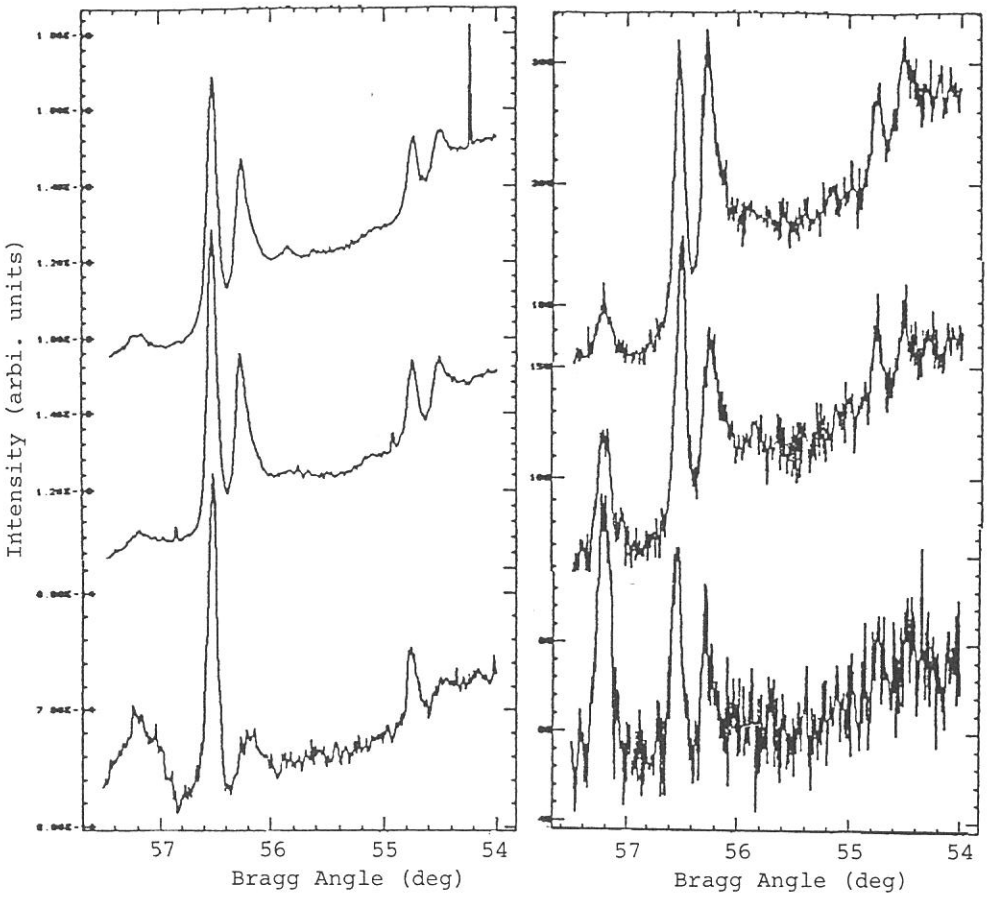

Fig.2 TEY (left panel) and FLY (right panel) spectra of copper on porous silicon. The initial concentrations of copper sulphate are (from top to bottom): 0.1 M, 0.01 M and 0.001 M

* JSPS (Japan Society for the Promotion of Science) Visiting Fellow, 1992.

1. M.J Sailor and K.L. Kavanagh, Adv. Mater. 4, 432(1992).
2. L.T. Canham, Appl. Phys. Lett., 57, 1046(1990).
3. I. Coulthard, J.W. Lorimer and T.K. Sham, Abstract 824RNP, 118th Meeting, The Electrochemical Society, Toronto, Oct. 1992; and to be published.

Reductive Dispersion of Cu on Porous Silicon: A Cu L-edge Study

T.K. SHAM[1,2,*], A. HIRAYA[1], and M. WATANABE[1]

1. UVSOR, Institute for Molecular Science, Myodaiji, Okazaki 444
2. Department of Chemistry, University of Western Ontario, London, Ontario, N6A 5B7 Canada

Porous silicon, silicon with high porosity and nano-crystalline structures has recently attracted much attention[1] partly because of its intense luminescence in the visible[2] and partly because of the fact that it is easy to make electrochemically. We became interested in porous silicon in connection with synchrotron light induced optical luminescence and its potential application in optoelectronics as well as the reductive dispersion of Cu and noble metals on the vast surface area of porous silicon[3].

In this report, we present preliminary results of the Cu L-edge spectra of a series of Cu films dispersed on porous silicon substrate from aqueous solution of $CuSO_4$. The measurements were carried out at the BL1A beamline using beryl crystals as the monochromator (2d = 15.965 Å). Porous silicon was prepared electrochemically on a p-type Si(100) wafer with a current density of 20 mA/cm^2 for 20 minutes. Cu films were prepared by immersing the specimen into $CuSO_4$ solutions with concentrations of 0.1 M, 0.01 M, and 0.001M[3]. Total electron yield (TEY) and fluorescence yield (FLY) were simultaneously used to record the Cu absorption spectrum at the Cu $L_{3,2}$ edge. Cu, Cu_2O and CuO were used as model compounds. The corresponding spectra are shown in Fig.1

Fig. 2 shows the TEY and FLY spectra of Cu deposited on porous silicon. A couple of features are noted. First, there is a significant amount of Cu on the porous silicon surface indicating the very large surface area. Second, comparing to Fig.1,

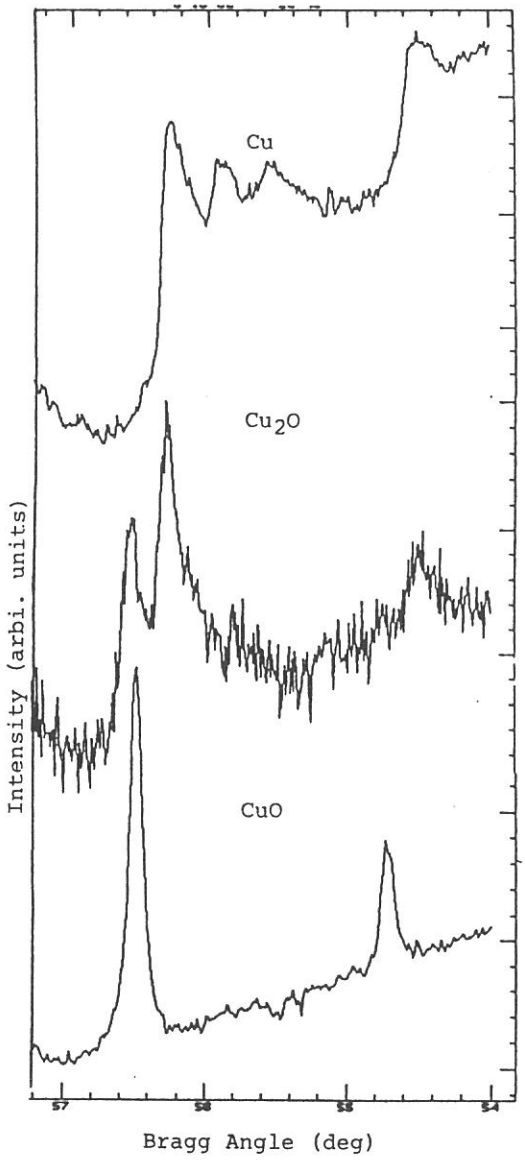

Fig 1. From top to bottom: Cu $L_{3,2}$ edge spectrum of Cu, Cu_2O and CuO.

to d dipole transition probes the d character. Two features are noteworthy from Fig.1. First, the whiteline becomes slightly less intense upon dilution of Cu in Au indicating that Cu gains some d charge upon alloying. Since Au is the most electronegative metallic element and gains charge overall in Cu-Au alloys, this observation implies that Cu loses sp charge and this is partially compensated by a d charge gain. The trend however is less dramatic than observed previously at the Au site[2]. Second, the oscillations beyond the whiteline become closer in energy as Cu becomes dilute. The origin of this is presently under investigation.

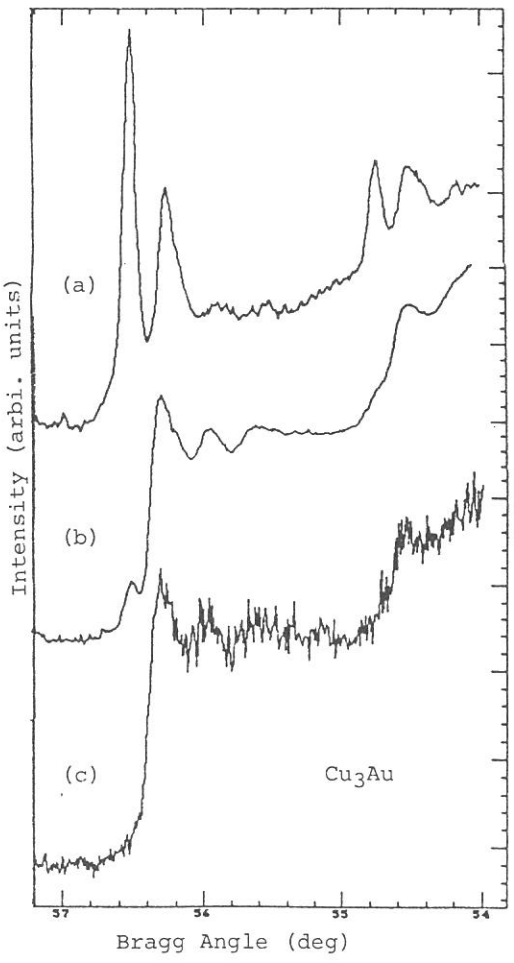

Fig.1 Cu_3Au spectra: (a) before scraping (TEY) (b) TEY and (c) FLY after scraping; Photon energy(eV)=776.5/sinθ

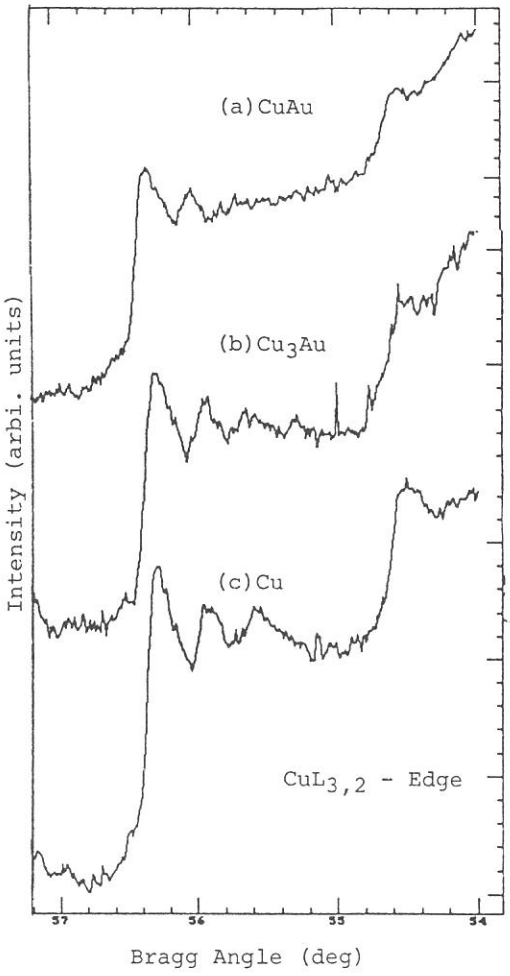

Fig.2 (a) CuAu, (b) Cu_3Au, (c) Cu; Photon energy (eV)= 776.5/sinθ

* JSPS (Japan Society for the Promotion of Science) Visiting Fellow, 1992

1. R.E. Watson, J. Hudis and M.L. Perlman, Phys. Rev. B4, 4139(1971).
2. T.K. Sham, Y.M. Yiu, M. Kuhn and K.H. Tan Phys. Rev. B41, 11881(1990).
3. G. Meitzner, D.A. Fischer and J.H. Sinfelt, Catalysis Letters, 15 219(1992).

Polarized Cu *L* Absorption Spectra of $Bi_2Sr_2Ca_{1-x}Y_xCu_2O_8$ (x=0.0,0.6)

Kimikazu SANO, Shun-ichi NAKAI, Atsushi KAMATA, Kunio MATSUDA,
Kazuhiro NOGUCHI, Hiroyoshi ISHII*, and Ikuyo SHIOZAKI*

Faculty of Engineering, Utsunomiya University, Utsunomiya 321
**Department of Physics, Tokyo Metropolitan University, Hachioji 192-03*

The cuprate oxide superconductors exhibit superconducting phenomenon when holes are doped into the compound. It is generally accepted that the doped holes are mainly located in O $2p_{x,y}$ and Cu $3d_{x^2-y^2}$ orbitals in the two-dimensional CuO_2 plane. The polarization dependency of X-ray absorption spectroscopy [1,2] (XAS) and high energy electron energy loss spectroscopy[3,4] (EELS) at O site, have shown the doped holes exist in the O $2p_{x,y}$ orbitals. On the other hand,concerning Cu $2p$ spectra which reveal information about Cu $3d$ orbitals, each experiment has shown different results. Bianconi et al.[5] and Abbate et al.[6] by using XAS measurements, have reported the peak energy shift about 0.3-0.5eV between Cu $3d_{x^2-y^2}$ and Cu $3d_{3z^2-r^2}$ components, though EELS by Nücker et al.[7] and XAS by Suzuki et al.[8] have shown no peak shift. These discrepancies are very important because the measurements provide direct information about unoccupied electronic states on the Cu $3d_{x^2-y^2}$ and the Cu $3d_{3z^2-r^2}$ orbitals. In order to clarify these discrepancies in the experiments, we have measured the linear polarized Cu $2p$ XAS spectra in $Bi_2Sr_2Ca_{1-x}Y_xCu_2O_8$ (x=0.0,0.6) single crystals.

The XAS measurement has been performed on the BL-7A at UVSOR facility with an energy resolution about 0.4eV at Cu *L* absorption peak. Spectra were measured by means of total electron yield from single crystal surfaces. The $Bi_2Sr_2CaCu_2O_8$ (x=0.0) is a superconductor sample which has a transition temperature of 80K, and non superconductor sample $Bi_2Sr_2Ca_{0.4}Y_{0.6}Cu_2O_8$ (x=0.6) shows a semiconducting behavior. These samples have been cleaved in a vacuum by pealing off with scotch tape to obtain clean surfaces.

Figure 1 shows the polarized Cu $2p$ XAS spectra of $Bi_2Sr_2CaCu_2O_8$(a) and $Bi_2Sr_2Ca_{0.4}Y_{0.6}Cu_2O_8$(b) single crystals. θ is the incidence angle of synchrotron radiation light, as indicated in figure 1. The spectra at θ=0° were taken for the polarization of electric field parallel to the CuO_2 plane and spectra at θ=80° were taken for almost perpendicular to CuO_2 plane. The spectra were normalized to the background below the absorption edge. In figure 1, both the spectra show the large polarization dependency and the energy shift between two incidence angles was about 0.5eV for x=0.0 and 0.3eV for x=0.6 sample. The intensity ratio was estimated to be about 7% and 22%, respectively. In our experiment, the energy shifts in the Cu $2p$ XAS spectra of both samples are commonly observed, therefore, it is considered that this effect is mainly related to the crystal structure of the sample.

Recently, C. T. Chen[9] measured Cu *L* XAS spectra for the same sample by means of total electron yield (TEY) and fluorescence yield (FY) method, and observed the peak energy shift in the TEY spectra but no shift in the FY spectra. Though TEY method is surface sensitive measurement, FY is bulk sensitive. Accordingly, our experimental results may not give information of bulk electronic structure in the sample. Therefore, the origin of the energy shift with angle is not fully understood at present. With respect to the intensity ratio with two incidence angles, our experimental results suggest a strong two-dimensionality of the electronic structure in $Bi_2Sr_2CaCu_2O_8$ as compared with $Bi_2Sr_2Ca_{0.4}Y_{0.6}Cu_2O_8$.

References
1) H.Matsuyama et al., Physca C160 (1989) 567.
2) C.T.Chen et al., Phys. Rev. Lett. 66 (1991) 104.
3) N.Nücker et al., Phys. Rev. B37 (1988) 5158.
4) H.Romberg et al., Phys. Rev. B32 (1990) 8868.
5) A.Bianconi et al., Phys. Rev. B44 (1991) 10126.
6) M.Abbate et al., Phys. Rev. B42 (1990) 7914.
7) N.Nücker et al., Phys. Rev. B39 (1989) 6619.
8) S.Suzuki et al., Phys. Rev. B44 (1991) 5381.
9) C.T.Chen, Private Communication.

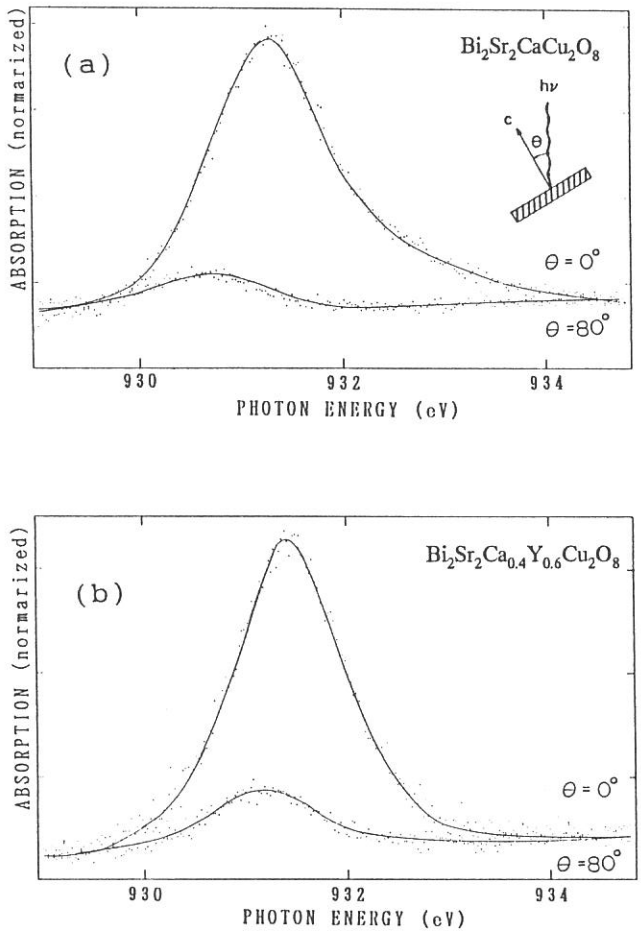

Fig.1 (a) Polarization dependency in the Cu 2*p* XAS spectra of $Bi_2Sr_2CaCu_2O_8$.

(b) Polarization dependency in the Cu 2*p* XAS spectra of $Bi_2Sr_2Ca_{0.4}Y_{0.6}Cu_2O_8$.

Cu $L_{III,II}$-EDGE X-RAY ABSORPTION SPECTROSCOPY STUDIES OF (Bi, Pb)-Sr-Ca-Cu-O: THE T_c VARIATION OF SUPERCONDUCTING COMPOUNDS

W. F. Pong,[1] H. L. Tong,[2] P.K. Tseng,[2] C. H. Chou,[2] J. B. Shi,[3] H. C. Ku,[4] A. Hiraya,[5] M. Watanabe.[5]

(1) Dept. of Phys. Tamkang U., Tamsui, Taiwan, (2) Dept. of Phys. Natl. Taiwan U., Taipei, Taiwan, (3) Dept. of Electronic Eng., Feng Chia U., Taichung, Taiwan, (4) Dept. of Phys., Natl. Tsing Hua U., Hsinchu, Taiwan, (5) Institute for Molecular Science, Okazaki, Japan.

We have measured the *x*-ray absorption spectra of Cu $L_{III,II}$-edge for the T_c variation of superconducting (Bi, Pb)-Sr-Ca-Cu-O compounds (Pb-BSCCO) at room temperature. The samples were measured using total electron yield mode with an electron multiplier under a base pressure of less than $5x10^{-8}$ torr, and the data was collected using a double-crystal beryl $(10\bar{1}0)$ monochromator.

Fig. 1 shows the Cu $L_{III,II}$-edge absorption spectra of the CuO and Pb-BSCCO compounds. The white line peak energies of CuO, Pb-BSCCO compounds, their corresponding full width at half maximum (FWHM), as well the relative integrated intensity of the peaks (from -2 to +2 eV relative to threshold of Cu $L_{III,II}$-edge) are summaried in Table I. The maximum white line peak of Cu $L_{III,II}$ in CuO are 931.3±0.3 and 951.2±0.3 eV, respectively. According to the dipole-selected transition rules, the origin of white line peaks at the Cu $L_{III,II}$ edges are attributed to atomic-like transitions from the ground state Cu 2p photoelectron being excited to the final state Cu 3d. This is due to hybridized Cu(3d) - O(2p) electron transfer which occurs from the 3d orbitals in Cu to the O atoms to give some unoccupied d states. For non-superconducting and various T_c superconducting Pb-BSCCO compounds, a sharp resonance white line denotes both Cu $L_{III,II}$ with a threshold similar to CuO, are evidently coincident with the prominent peaks at ~931 and ~951 eV. The main peaks in the spectra of the Pb-BSCCO are clearly similar to the CuO curve, this reveals a predominant Cu^{+2} ground state in Pb-BSCCO. Details of the *x*-ray absorption studies for Pb-BSCCO compounds will be reported in the future.

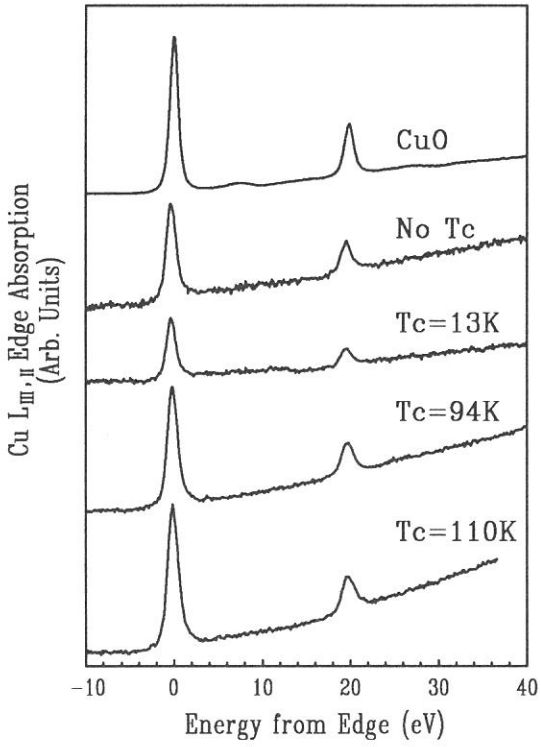

Fig. 1 Normalized Cu $L_{III,II}$ absorption spectra for CuO, and various T_c Pb-BSCCO compounds. The zero energy corresponds to 931.3 eV.

Compounds	$E_0(L_{III})$	FWHM	I_{III}	$E_0(L_{II})$	FWHM	I_{II}	$E_0(L_{II}) - E_0(L_{III})$	I_{III}/I_{II}
No Tc	931.0	1.3	102	950.9	1.3	36	19.9	2.9
Tc≈13K	931.0	1.2	59	950.9	1.5	18	19.9	3.3
Tc≈94K	931.1	1.3	128	951.0	1.6	38	19.9	3.4
Tc≈110K	931.1	1.4	151	951.1	1.7	50	20.0	3.0
CuO	931.3	1.1	1453	951.2	1.2	492	19.9	3.0

Tab. I Energy position (E_0) (±0.3 eV), full width at half maximum (FWHM) (±0.1 eV), and ($I_{III,II}$) relative integrated intensity of the white line peaks in the Cu $L_{III,II}$ near-edge absorption spectra.

TRIAL FOR MEASUREMENTS OF Ca K, Sr L, AND Cu L ABSORPTION EDGES FOR Bi-BASED HIGH-Tc SUPERCONDUCTORS

Rika SEKINE[1,2], Yasuhiro MURAKOSHI[1,3], and Maki KAWAI[2]

[1]Research Laboratory of Engineering Materials, Tokyo Institute of Technology, Yokohama, 227
[2]The Institute of Physical and Chemical Research (RIKEN), Wako, 351-01
[3]Tokyo Gakugei University, Koganei, 184.

The Tc values of high-Tc superconducting oxides are affected by the hole concentration. In the Bi 2212 phase, the hole carrier, which is controlled by the amount of oxygen, is supplied from the Bi-O layer to the Cu-O_2 layers through the Sr-O layers. Therefore, when the oxygen is reduced, not only the changes in hole carrier concentration but also changes in oxygen position may affect the mechanism of carrier supply and the Tc values. X-ray absorption spectra (XANES and EXAFS) of metal atoms can give us the information on the local structure of oxygen, i,e, coordination number and distance around each metal atom. In this study, we try to investigate the soft X-ray absorption edge regions, Ca K, Sr $L_{II,III}$, and Cu L_{III} for Bi2212 phases.

The Bi2212 samples ($Bi_{2.2}(Sr_{0.9-y}Ca_y)_2Ca_{1.0}Cu_{2.0}O_{8.1+\delta}$ with y=0, 0.4) were sintered in dry air for 144-240 hours at 810-840℃ as previously reported. [1] Some of the sintered samples were annealed in Ar at 600 ℃ for 48 hours and others in O_2 at 600 ℃ for 48 hours. Single crystal of Bi 2212 phase, which was supplied by Shigaki et al., was prepared by traveling solvent floating zone method. [2] Measurements were carried out at the beam line 7A of the UVSOR storage ring in the Institute for Molecular Science at room temperature in UHV chamber. Photon energy with the energy range of 900-4200 eV was used. Double crystal Ge(220), beryl, and InSb monochrometers are used for Ca K (3800-4200 keV), Cu L(920-980 eV), and Sr L(1920-2130 eV) edges, respectively. The X-ray absorption spectra have been measured by recording the total electron yield.

Figure 1 shows examples of Ca K-egde absorption spectra for (a) $CaCO_3$, which was used as a reference compound, and (b) Bi2212 sample with y=0.4. As shown in Fig.1(a), in higher energy regions than 4300 eV, the effects of harmonics could not be eliminated. Therefore, we focussed interests on only the XANES region in Fig.1(b). Since we cannot record spectra in sufficient S/N ration with the present equipment, we abandoned the measurement for the Ca K-edge region.

Figure 2 shows Sr $L_{II,III}$-edge spectrum for the single crystal of $Bi_{2.0}Sr_{1.8}Ca_{1.0}Cu_{2.0}O_{8+\delta}$. The L_{II} and L_{III} edges are

too near to separately discuss the EXAFS oscillations. Therefore, we only focused interests on the changes in the energy for Sr L_{III} edge. The edge energy was observed from 1943.01-1943.11 for each samples with different y values or different treatment, which is considered to be almost the same in limited energy resolution.

Figure 3 shows Cu L_{III} spectrum with emittance angle of 50 degree respect to perpendicular. There have been pointed out that at least two components exist for high-Tc cuprate compounds in Cu L_{III} region around 931 eV and 933 eV. Furthermore strong angular dependence in intensity ratio for these two peaks are also pointed out. However, we cannot clearly observe the latter peak or angular dependence. The peak energy for the former one changes from 931.4 to 931.6 eV for different samples, however, it seems that the shift depends not on the intrinsic energy state of each sample but on surface energy state which is sensitive to impurities or damages induced by air ambient or X-ray irradiation that samples are exposed during measurements.

The authors are indebted to M. Watanabe, O. Matsudo, and J.Yamazaki, UVSOR, the Institute for Molecular Science.

References

1 S. Kambe, T. Matsuoka, M. Takahashi, M. Kawai, and T. Kawai, Phys. Rev. B, 42 (1990) 2669.

2. I. Shigaki, K. Kitahama, K. Shibutani S. Hayashi, R. Ogawa, Y. Kawate, T. Kawai, S. Kawai, M. Matsumoto, and J. Shira fuji, Jpn. J. Appl. Phys., 29 (1990) L2103.

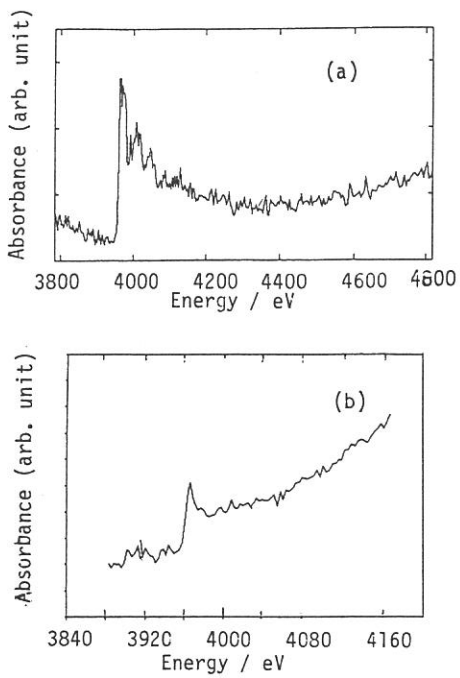

Fig. 1. Ca K-edge absorption spectra. (a)$CaCO_3$, and (b) $Bi_{2.2}Sr_{1.0}Ca_{1.8}Cu_{2.0}O_{8+\delta}$.

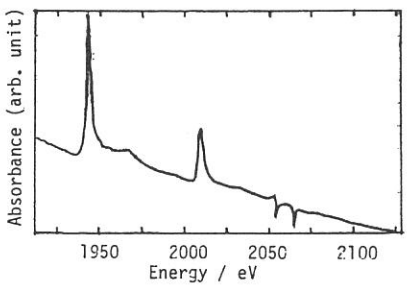

Fig. 2 Sr L_{II} (~2100 eV)- and L_{III} (~1940 eV)-edge absorption spectrum for single crystal of $Bi_{2.0}Sr_{1.8}Ca_{1.0}Cu_{2.0}O_{8+\delta}$.

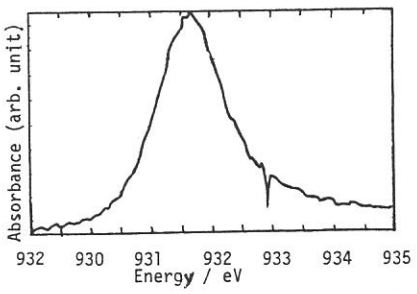

Fig. 3 Cu L_{III}-edge absorption spectrum for single crystal of $Bi_{2.0}Sr_{1.8}Ca_{1.0}Cu_{2.0}O_{8+\delta}$.

XAFS Study of Na-doped Nb_2O_5 Catalysts

Sadao Hasegawa*, Hirofumi Aritani* , Masahiko Morooka*, Yasue Sasaki* and Tsunehiro Tanaka**

*Department of Chemistry, Tokyo Gakugei University, Koganei, Tokyo 184

**Department of Hydrocarbon Chemistry, Faculty of Engineering, Kyoto University, Kyoto 606

1. Introduction

In our previous report[1,2], Na-doped Al_2O_3 catalyst has been exhibited a basic property. A sodium ion on the surface acts as an electron donor for the surface oxygen. It was deduced on the basis of XANES of sodium halides that the ionicity of a Na-O bond in that catalysts relates to the energy position of the primary peak, which is consistent with the catalytic performance.

In this report, the effect of Na-loading on the surface of bulk Nb_2O_5 and Al_2O_3-supported Nb_2O_5 catalysts have been investigated.

2. Experimental

Na-loaded Nb_2O_5 were prepared by impregnating niobium pentoxide with the ethanol solution of sodium ethoxide. Nb_2O_5 catalyst was prepared by the calcination of hydrated niobium pentoxide in air at 773K. Its structure was determined to be rhombic Nb_2O_5 by X-ray diffraction. Al_2O_3-supported niobium oxide catalysts were prepared by impregnating alumina powder (Nb_2O_5 10wt% on Al_2O_3) at 363K. All catalysts were followed by drying and calcining in air at various temperature.

The Na K-edge absorption spectra of the catalysts were measured at BL-7A soft X-ray beam line with UVSOR facilities, when used a beryl two-crystal monochrometer.

Table 1 Results of Isomerization of 1-butene. *1

catalysts	Composition / % 1-butene	2-butene cis-	2-butene trans-	selectivity*2
Nb_2O_5	50.4	26.0	23.6	1.1
Na/Nb_2O_5 *3	100	-	-	-
Nb_2O_5/Al_2O_3*4	27.1	27.6	45.4	0.6
$Na/Nb_2O_5/Al_2O_3$*4*5	65.6	28.5	5.9	4.9

*1 Reacted at 423K for 120min. *2 Value of cis/trans-2-butene.
*3 Na content is 10wt%. *4 Nb_2O_5 is 10 wt% on Al_2O_3.
*5 Na content is 2mmol/g.

3. Results and Discussion

Fig.1 shows the Na K-edge XANES pattern of Na-loaded catalysts. In the case of Na-loaded bulk Nb_2O_5, XANES pattern was different from the case of Na-loaded Al_2O_3 and no formation of basic site was observed on the surface, because cubic sodium niobate ($NaNbO_3$) was formed by calcination at 773K, which was determined by X-ray diffraction. This facts were agreed the results that no reactivity during 1-butene isomerization (Table 1) was observed.

In another case of Na-loaded Nb_2O_5/Al_2O_3, XANES pattern was different from Na-loaded bulk Nb_2O_5. It was exhibited a basic property by the reaction of 1-butene isomerization. As shown in Fig.2, Na-O bond length by the FT of k^3-weighted Na K-edge EXAFS in Na-loaded Nb_2O_5/Al_2O_3 was found to be 0.13nm. In the case of Na-loaded bulk Nb_2O_5, Na-O bond length was observed at 0.18nm. It posesses that the effect of Na-loading on Nb_2O_5/Al_2O_3 was not crystalyzed but formed nearly Na-O bond on the surface. These results possess that the bond length of Na-O in Na-loaded Nb_2O_5/Al_2O_3 catalyst was different from the case of cubic structure of sodium niobate, and existed the type of basic Na-O site on the surface. Such as Na non-loaded Nb_2O_5/Al_2O_3 catalyst was observed acidic property, in contrast, Na-loaded Nb_2O_5/Al_2O_3 was observed basic property.

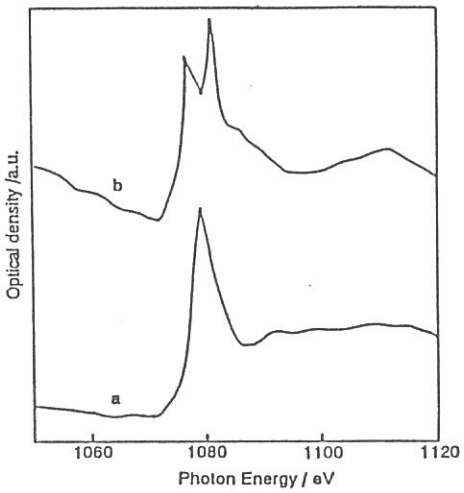

Fig.1 Na K-edge XANES pattern of sodium-loaded (a) bulk Nb_2O_5 and (b) Nb_2O_5/Al_2O_3.

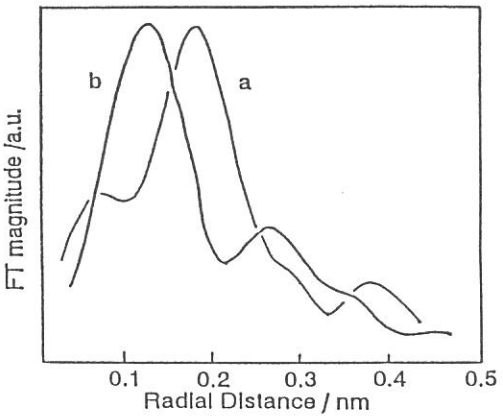

Fig.2 Fourier transform of k^3-weighted EXAFS of sodium-loaded (a) Nb_2O_5 and (b) Nb_2O_5/Al_2O_3.

1. N. Yoshihara, T. Kitagawa, I. Ihara, S. Hasegawa, T. Hasegawa, Bull. Chem. Soc. Jpn., 65 (1992) 1185.
2. S. Hasegawa, M. Morooka, H. Aritani, H. Yoshida, T. Tanaka, Jpn. J. Appl. Phys., in press.

X-RAY EXCITED LUMINESCENCE YIELD SPECTRA OF NaBr AND NaBr:Cu SINGLE CRYSTALS AT Na K-EDGE

Takatoshi MURATA, Katsuyuki HARADA, Atsunari HIRAYA[1], and Makoto WATANABE[1]

Department of Physics, Kyoto University of Education, Fukakusa, Fushimi, Kyoto 612

[1] *UVSOR, Institute for Molecular Science, Myodaiji, Okazaki 444*

The x-ray excited optical luminescence (XEOL) is one of the de-excitation processes following the excitation. The extensive study on the XEOL yield of CaF_2 has been performed by the present authors[1,2]. They found that the bi-directional edge jumps occur depending on the method of the preparation of the sample and also on the temperature. They succeeded to reproduce the observed yield spectra by the calculation using phenomenological theory proposed by Emura *et al.*[1,2]

The origin of the luminescence is the multiple production of the low-energy electrons by the incoming high-energy photons or particles. In some cases, it is possible to observe separated luminescence bands caused by the doped impurities and by the bulk. This means that there are different channels of the energy transfer of the produced low-energy electrons and holes with Auger effect. We present here examples of Cu-activated NaBr which emits two luminescence bands; one at 3.4 eV by Cu^+ impurities, and another at 4.5 eV by bulk NaBr, and non-activated NaBr which luminesces only 4.5 eV.

Luminescence yield measurements of NaBr and NaBr:Cu cleaved single crystal samples for the Na K edge excitation were performed at the BL1A, using a double crystal monochromator with two beryl flat crystals[3]. Interference filters were used to separate the emission band of the bulk and that from Cu impurities. Luminescence signal was detected with a Hamamatsu R955 photomultiplier.

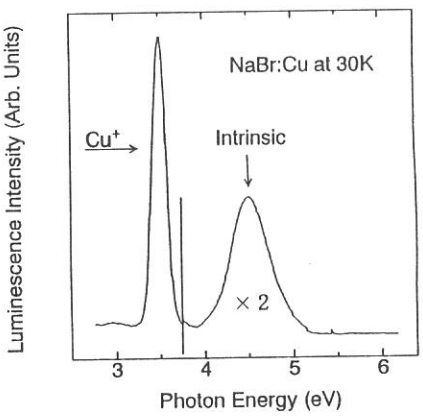

Fig. 1 Optical luminescence spectrum of NaBr:Cu at 30K.

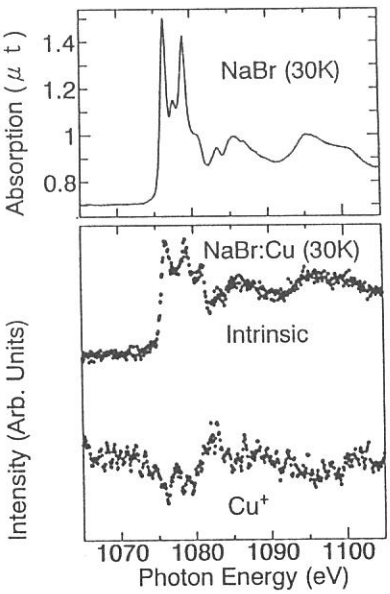

Fig. 2 Absorption spectrum of NaBr and yield spectra at 30 K.

Figure 1 shows the optical luminescence spectrum of NaBr:Cu at 30 K. The shape of the spectrum does not change with exciting x-ray energy. The emission band at 4.5 eV ($\sim$ 275 nm) is the intrinsic luminescence caused by the electron-hole recombination of the relaxed excited states. The band at 365 nm ($\sim$ 3.4 eV) is due to the transition from $3d$ to $3s$ state of Cu^+ ion. Figure 2 shows the luminescence yield spectra of the sample of the NaBr:Cu crystal with Na K-edge-excitation at 30 K. The absorption spectra of NaBr[4] is shown at the top. Although the signals of the yield spectra are noisy, both spectral features reproduce the absorption spectrum fairly well except for the direction of the edge-jump at the Na K-edge; it is normal for the intrinsic luminescence, and inverted for the impurity luminescence. In the case of NaBr pure crystal, a negative jump was observed as in the case of NaCl[3]. The total feature of these yield spectra is similar in the case of the Br K-edge excitation[5].

According to the phenomenological theory by Emura *et al.*[2], the ratio R of the luminescence intensities above and below the energy of the K absorption edge is expressed as follows:

$$R = \frac{1 - e^{-(\mu+\mu')t}}{1 - e^{-\mu t}} \times \frac{\mu + \mu' B}{\mu + \mu'}, \tag{1}$$

with $B \equiv \eta'/\eta$. Here μ and μ' denote the linear absorption coefficients due to the L-and K-edges, respectively, and η and η' are the effective yields of the luminescence for the excited electrons from L-shell and K-shell, respectively. The parameter t means the escape depth of the luminescence.

The negative features mean that the high-energy electrons excited from outer core states by x-rays at Na K-edge region contributes more to the optical luminescence than those from inner core states in ordinary cases. The positive jumps observed in the intrinsic luminescence yield for Cu-contained NaBr indicate that the contribution of the K-electrons is superior. The high energy electrons excited from L-states transfer energies mainly through the luminescence channel to the impurity. Accordingly, the relative contribution of the K-electrons to the intrinsic luminescence channel increases. Detailed discussion is made elsewhere[5].

REFERENCES

1) T. Murata, K. Harada, S. Emura, M. Nomura, K. R. Bauchspießand H. Maeda: To be published in Jpn. J. Appl. Phys. Suppl. (1993).

2) S. Emura, T. Moriga, J. Takizawa, M. Nomura, K. R Bauchspieß, T. Murata, K. Harada, and H. Maeda: To be published in Phys. Rev. B.

3) A. Hiraya, T. Horigome, N. Okada, N. Mizutani, K. Sakai, O. Matsudo, M. Hasumoto, K. Fukui and M. Watanabe: Rev. Sci. Instrum. **63** (1992) 1264.

4) T. Matsukawa S. Naoe, T. Murata and T. Mori: J. Phys. Soc. Jpn. **57** (1988) 2916.

5) T. Murata, K. Harada, S. Emura, M. Nomura, K. R. Bauchspieß, H. Maeda, A. Hiraya, and M. Watanabe: To be published in Jpn. J. Appl. Phys. Suppl. (1993).

Mg K-edge XANES Study of Mgnesium Oxide Species Supported on Silica prepared by Sol-gel Method

Hisao YOSHIDA, Tsunehiro TANAKA, Tomoko HANADA,
Takuzo FUNABIKI and Satohiro YOSHIDA

Division of Molecular Engineering, Kyoto University, Kyoto 606-01

It is widely known that catalytic activity of supported metal oxide is often different from that of the corresponding unsupported metal oxides. This has been understood to be due to not only the enlargement of surface area of metal oxide but also the qualitative change of active sites. The electronic and/or geometric state of active sites is presumably quite different from that in unsupported one. The effect of loading on its catalysis varies with kinds of material of support, loaded amount and the method of preparation. In the case of silica support, the difference of preparation method results in different activity.

Thermal change in the structure of an MgO/SiO_2 (MS) catalyst which show a high activity for fine chemical synthesis has already been reported[1]. In a previous study, we used silica as a support supplied by Fuji-Divison Chem. Co., while in the present study we prepared amorphous silica by hydrolysis of tetraethyl orthosilicate by a sol-gel method as described elsewhere[2]. Because the commercial silica contains inpurities which may lead us to a wrong conclusion about the property of silica, we adopted a sol-gel method to obtain pure silica. Here, we would like to clarify the effect of this silica support on the structure of surface magnesium oxide species by investigating Mg K-edge XANES.

The preparation of the samples and X-ray absorption experiments were carried out as described in the previous report[1]. The structure of MgO species in the highly loaded (> 20 wt%) MgO/SiO_2 was found to be the same as that of bulk MgO with rock salt structure by XANES analysis mentioned later, although XRD pattern showed a broad X-ray diffraction peak by the MgO (200) plane. In the case of low loaded (< 5 wt%) MgO/SiO_2, there were no appreciable peaks in the XRD pattern. Therefore, we have expected that the magnesium oxide is highly dispersed to form surface MgO species with a different structure from that of the bulk. The surface concentration of MgO estimated by XPS increased linearly with the loading of MgO up to 5 wt%, indicating that such highly dispersed MgO is dominant in the samples.

However, all the samples calcined at 500 °C in air (MS5) gave approximately the same XANES spectra regardless of the loading as those of Mg ions located at a center of a regular octahedron of oxygen ions as shown in Fig.1 a), b) and c). This suggests that magnesium ions are present in micro particles of MgO or in two dimentional array of MgO_6 octahedra even in the case of low loaded amounts of MgO. If MgO particles are formed, it is promising that the samples function as a solid base catalysts.

When the samples were calcined at 800 °C, 20MS8 and 5MS8 exhibited the

spectra identical to MS5 samples as illustrated in fig.1 d) and e). On the other hand, XANES feature of 1MS8 as shown in Fig.1 f) was appreciably different from that of 1MS5. In particular, resonance absorption at around 1325 eV was changed significantly. This change indicates that the structure of the MgO micro particle or the raft-like species has changed by calcination at 800 °C. We have recently found that on the 1wt% MgO loading sample evacuated at 800 °C, a new type of magnesium oxide species formed, which exhibited a photoluminescence spectrum with a fine structure[3] associated with an Mg-O bond in isolated MgO species interacted with the silica surface. Correspondingly, the change of XANES would result mainly from a distortion of coordination caused by the interaction of the isolated MgO species with silica surface in which Si^{4+} is coordinated tetrahydrally with oxygen anions.

In the previous study[1], drastic thermal structure-change of MgO species supported on the commercial silica by 17wt% was reported. However, in this study in which a sol-gel method was adopted for silica preparation, such change was not observed. The detailed study of the difference between these silica samples is now in progress.

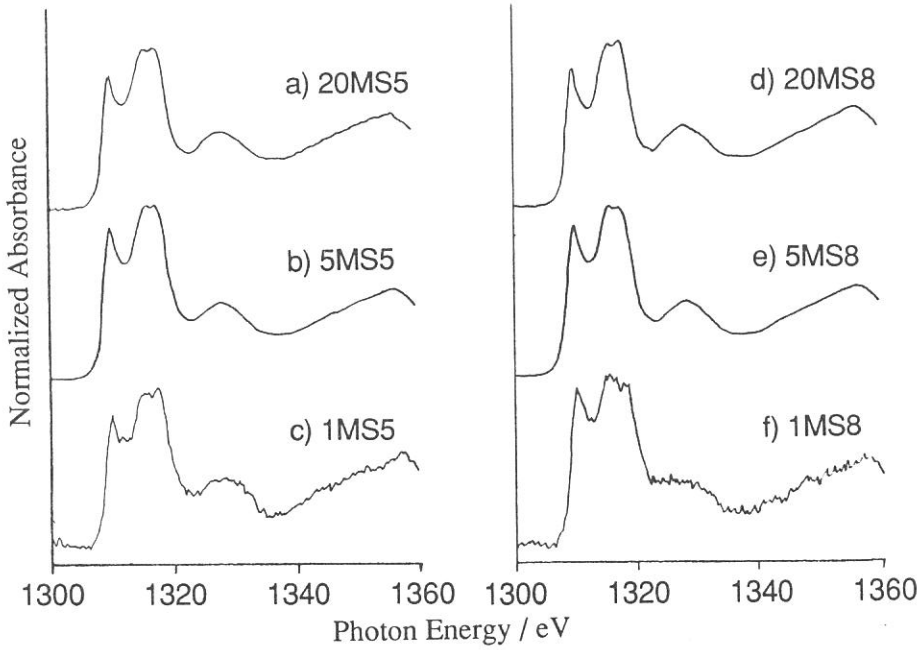

Fig.1 Mg K-edge XANES of the xMSy samples. x stands for loading amount (/wt%MgO), and y stands for calcination temperature (/100 °C).

1) T.Tanaka, H.Tsuji, G.Zhang, M.Sakuraba and H.Hattori, UVSOR ACTIVITY REPORT 1990,p81.

2) S.Yoshida, T.Matsuzaki, T.Kashiwazaki, M.Mori and K.Tarama, *Bull. Chem. Soc. Jpn.*,1974,**47**,1564.

3) T.Tanaka, H.Yoshida, K.Nakatsuka, T.Funabiki and S.Yoshida, *J. Chem. Soc. Faraday Trans.*, 1992,**88**,2297.

Mg K-EDGE STUDY ON ALKALI MODIFIED MgO CATALYSTS

HIDETO TSUJI, TSUKASA HISAZAKI, FUYUKI YAGI and HIDESHI HATTORI

Department chemistry, Faculty of Scienece, Hokkaido University, Sapporo, 060

INTRODUCTION Modification of MgO catalyst with alkali metal cations results in the activity higher than that of non-modified MgO for many base-catalyzed chemical reactions[1]. It is considered that the effect of modification by addition of guest ions on the catalytic property is caused by variation of reactive sites such as surface defects or change of partial charge on O anion of MgO surface. In any case the difference in electronic structure of MgO surface should be found. The considerable XPS studies on the electronic state of MgO surface with regard to the effect of alkali modification were carried out. However, the difference in the electronic state of matrix MgO caused by the modification with alkali was not observed clearly.

Previously we reported Mg K-edge XANES of MgO and Na^+ added MgO and found the distinct change of absorption edge structure[2]. In the present study, the electronic states of MgO influenced by addition of alkali metal cations, Li^+, K^+ and Rb^+, were investigated by Mg K-edge X-ray absorption spectroscory. We generalize the effect of alkali modification on MgO matrix and discuss the results in relation to base-catalytic actions.

EXPERIMENTAL The alkali modified MgO samples Li^+-MgO, K^+-MgO and Rb^+-MgO, were prepared by adding aqueous solution of LiOH, KOH and Rb_2CO_3 to MgO, respectively, followed by drying at 373K for 12h, and calcination at 873K for 5h in air. Total electron yield spectra were taken near the Mg K-edge at the soft X-ray absorption facility installed at the UVSOR BL7A Institute for Molecular Science. The monochromatizing crystal was a natural beryl with 2d=15.965Å. Fine powdered samples were evacuated at 823K for 2h, and placed on the first dinode of electron multiplier under N_2 atomosphere. All the measurements were performed below the pressure of ca 10^{-6}Pa and at room temperature.

RESULTS AND DISCUSSION Fig. 1 shows X-ray absorption spectra (total electron yield spectra) at Mg K-edge of MgO and Li^+-MgO, K^+-MgO, Rb^+-MgO. For alkali modified MgO, the fine structure of the spectra in the XANES region was similar to that of non-modified MgO. However, a significant difference in the intensity of the peak at the threshold was obviously observed.

In the absorption edge region, the fine structure of spectra reflects the distribution of unoccupied quantum state for absorbing atom. This sharp peak at absorption threshold can be assigned to a core exiton associated with the intra ionic allowed transition from 1s core state to 3p state of Mg[3]. Since the p state in the conduction band consists mainly of the electronic state of Mg cation in ionic crystal of MgO, a high peak at the absorption threshold for alkali modified MgO means that the partial charges of the Mg cation and O anion are extensively localized; an ionic nature of MgO is enhanced.

If MgO crystal becomes defective by addition of alkali metal cations, the charge localization between Mg cation and O anion on MgO must be weakened because Madelung potential decreases at coordinative unsaturated defects. Therefore, the enlargement of the peak at the absorption threshold shold not be caused by the contribution of defective sites.

As this spectral feature does not depend on the kind of alkali, it is adequate idea that the alkali of a low electron negativity compared with Mg interacts electrically with MgO matrix. X-ray absorption spectra at Mg K-edge revealed that the re-disribution of the charges on Mg cation, alkali metal cation and O anion take place around alkali added on MgO, and as a result, the electronic state of Mg becomes more cationic.

In fig. 2, X-ray absorption spectra at Mg K-edge of samples of Na^+-MgO prepared by adding aqueous solution of NaOH and ethanol solution of Na ethoxide are shown. The similarity of the fine structure of the spectra suggests that the qualitative change in the electronic state of MgO matrix is not influenced by the method of alkali modification.

In the chemical view point, it is concluded that a high base-catalytic performance of alkali modified MgO catalyst is owing to the increase in the ionicity on MgO surface; the highly localized partial charge on O anion of MgO surface contributes the enhancement of electron pair donor property.

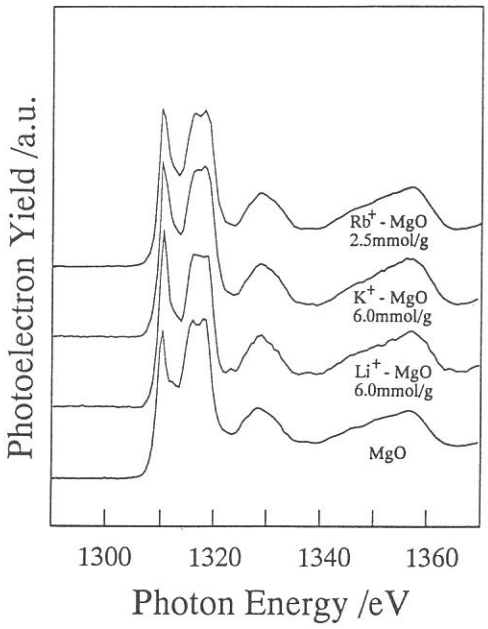

Fig. 1 Mg K-edge absorption spectra of MgO and various alkali modified MgO.

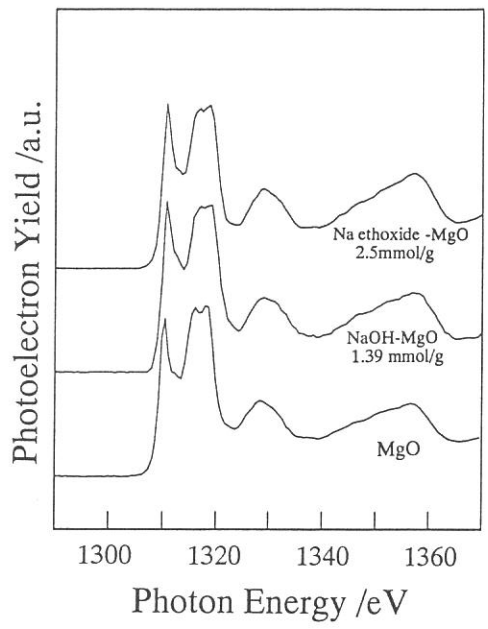

Fig. 2 Mg K-edge absorption spectra of MgO and Na+ modified MgO.

1) G. Zhang et al., Appl. Catal., 48 (1989) 63. 2) H. Tsuji et al., UVSOR activity report, (1990) 83.
3) T. Matsukawa et al., J. Phys. Soc. Jpn., 57 (1988) 2916.

Local Distortion of PO_4 Molecule in $KH_2(PO_4)_2$ Crystals

Hirofumi KASATANI, Yukio NODA[1], Hironobu MAEDA[2], Takashi UMEKI,
Yasuhiro YONEDA, Satoshi MURAKAMI[1], Yoshihiro KUROIWA[1] and Hikaru TERAUCHI

School of Science, Kwansei-Gakuin University, Nishinomiya 662
[1]Faculty of Science, Chiba University, Yayoi Chiba 263
[2]Faculty of Science, Okayama University, Okayama 700

1.Introduction

KDP family materials such as KDP(KH_2PO_4), ADP($NH_4H_2PO_4$), RDP(RbH_2PO_4) etc. show phase transitions at critical temperature T_c. When hydrogen atoms are replaced by deuterium atoms (abbreviated as DKDP), the transition temperature jumps up about 100K in these materials. So far, it has been believed that hydrogen ordering or softening of hydrogen tunneling mode plays an important role at the phase transition. However, recent works cast some doubts on the above tunneling model.

Hydrogen compound KDP transforms at T_c=123K. From the structural analysis, a PO_4 molecule distorts below T_c so that the bond length between P and O atoms splits to r_1=1.508Å and r_2=1.583Å from an undistorted state with r_0=1.538Å.[1)] Those numbers of DKDP are slightly different from ones in KDP, and it is known that T_c=213K, r_0=1.544Å, r_1=1.509Å and r_2=1.578Å.[2)]

The purpose of the present work is to investigate the local structure of PO_4 atoms to reveal the existence of disordering state by means of the XAFS technique. The key point we have to reveal is whether a PO_4 molecule distorts or not at high temperature phase. If the PO_4 molecule already distorts at above the transition temperature, the system must be treated as an order-disorder phenomenon of PO_4 molecules.

2. Experiments and Analysis

XAFS experiments around the K-absorption edge of phosphate atoms in KDP and DKDP were carried out at Wiggler beam line BL-7A of UVSOR. Since the energy of K-absorption edge of a phosphate is very low, special attention was paid to prepare the sample. Fine gel-like powder samples were made by dropping a saturated aqueous solution in to ethanol. The powder sample was entangled on a Cu-mesh and retained by collodion. Transmission XAFS measurements were performed in ultra high vacuum at various temperature. An InSb crystal was used as a monochromater. An example of an absorption coefficient observed in DKDP is shown in Fig.1a), in which XAFS signal around a phosphate atom and around a potassium atom is shown.

XAFS signal $k^3\chi(k)$ is obtained from the observed absorption coefficient by the standard procedure. The signal to noise ratio

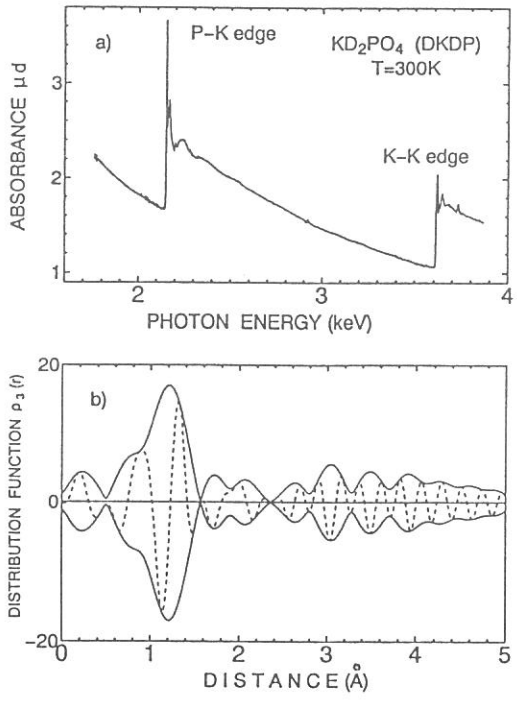

Fig.1 a) An example of XAFS signal in DKDP.
b) Fourier transformed distribution $\rho_3(r)$ of observed $k^3\chi(k)$ in DKDP at 199K.

is still poor so that we can use the k range from k=3.8Å^{-1}(with 2π unit) to 14.0Å^{-1} in $k^3\chi(k)$. In Fig.1b), Fourier transformed distribution function $\rho_3(r)$ of observed $k^3\chi(k)$ in DKDP at 199K is shown. The first peak reflects the oxygen atoms around the probed phosphate atom. Fourier filtered $k^3\chi(k)$ is recalculated by using the r range from r=0.32Å to 1.65Å in $\rho_3(r)$, and then this observed Fourier filtered $k^3\chi(k)$ is compared with two alternative models, one shell model and two shell model. For one shell model, the coordination number is fixed as N=4 and the bond length between P and O atoms(r_0) is a fitting parameter. On the other hand, in two shell model, the coordination numbers are fixed as $N_1=N_2=2$ and the bond lengths r_1 and r_2 are fitting parameters reflecting the local symmetry of the distorted PO_4 molecules.

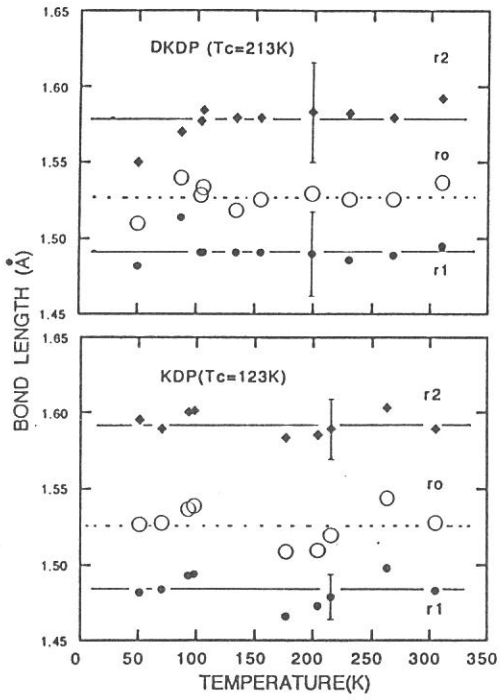

Fig.2 Bond length between P and O atoms in KDP and DKDP. r_0 denotes the bond length of undistorted PO_4 molecules, while r_1 and r_2 denote those of the distorted molecules.

3. Results and Discussion

Obtained bond lengths of KDP and DKDP are shown in Fig.2 as a function of temperature, for both one shell model and two shell model. Obviously, the PO_4 molecule in the low temperature phase distorts. However, least square fitting procedure gives almost the same discrepancy factor (R-factor) for two alternative models through all temperature region in KDP and DKDP. The ratio of R-factor between R_1 of one shell model and R_2 of two shell model indicates that it is difficult to distinguish which model is favorable, partially because the XAFS data of KDP is still poor and we could not measure enough range in k space in order to obtain the sufficient resolution. The bond lengths obtained in this experiments, however, are well consistent with the data of structural analysis noted in the previous section, both in high temperature and low temperature phases. Averaged data given by the present experiments are r_0=1.527(10)Å, r_1=1.484(10)Å and r_2=1.593(8)Å in KDP and r_0=1.528(8)Å, r_1=1.492(8)Å and r_2=1.578(11)Å in DKDP.

It is hardly to conclude that a PO_4 molecule is in a disordered state in KDP because of the insufficient resolution in the present experiments.

References

1) G.E.Bacon and R.S.Pease : Proc. Roy. Soc. (London), Ser. **A230** (1955) 259.
2) J.Nakano, Y.Shiozaki and E.Nakamura : Ferroelectrics **8** (1974) 483.

EXAFS STUDY ON LOCAL STRUCTURES NEAR THE PHASE TRANSITION OF PEROVSKITES

Yasuo NISHIHATA, Osamu KAMISHIMA, Kenji OJIMA, Jianhua ZHUAN
and Akikatsu SAWADA

Faculty of Science, Okayama University, Okayama 700

Many cubic perovskite crystals undergo phase transitions, where they transform to slightly distorted structure from the ideal perovskite structure. The phase transitions are concerned with the condensation of phonon modes. However, an overdamping of the phonon mode and central peak suggest that these phase transition cannot be regarded simply as displacive type ones. Recently, structure refinements by diffraction study on some perovskites of single crystals ($BaTiO_3$, $SrTiO_3$ and $PbTiO_3$ [1,2]) suggest the disorder of atoms. The purpose of this work is to study local structure and reveal whether or not there is a disordered nature in the crystals by EXAFS (Extended X-ray Absorption Fine Structure) technique. We measured x-ray photoelectron yield spectra for some kinds of powder samples; $KMnF_3$, $KNbO_3$ and $KTaO_3$.

In $KMnF_3$, successive phase transition occurs at 186 and 91 K, and caused by the condensation of the zone-boundary mode associated with the rotation of the MnF_6 octahedra [3]. X-ray photoelectron yield spectra, I, were taken near the K-K edge by the use of the double crystal monochromator (DXM) constructed at BL-7A of UVSOR. The Ge(111) plane was used as a monochromator. Signals from the powder sample which was mounted on a cryostat was very weak. Then, the powder samples were put on the first dinode of a photomultiplier with carbon paste. Figure 1 shows the spectrum of $KMnF_3$ at room temperature. Here, the spectrum was normalized by the x-ray photoelectron yield spectra from Au, I0. The quality of EXAFS spectra is not good enough to analyze the local structure around K atom. The intense x-ray using a superconducting wiggler enables us to obtain well-defined EXAFS signals.

[1] K. Itoh et al., Ferroelectrics, 63, 29 (1985).
[2] R. J. Nelmes, R. O. Piltz, W. F. Kuhs, Z. Tun and R. Restori, Ferroelectrics, 108, 165 (1990).
[3] K. Gesi, J. D. Axe, G. Shirane and A. Linz, Phys. Rev. B5, 1933 (1972).

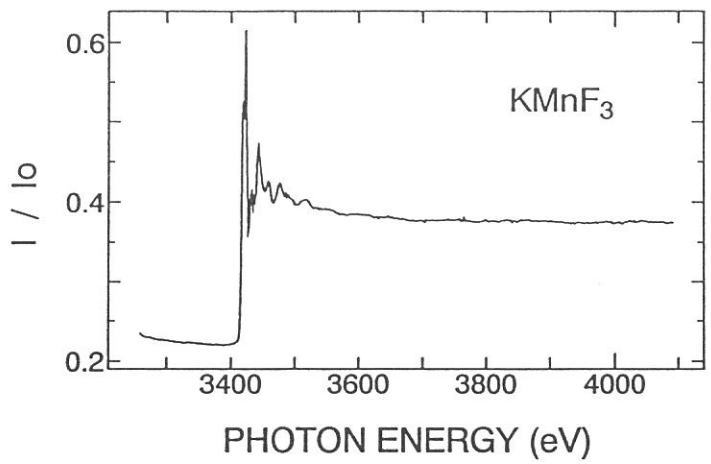

Fig. 1. X-ray photoelectron yield spectrum near the K-K edge of $KMnF_3$ at room temperature.

CORE ELECTRON ABSORPTION SPECTRA OF POLYESTER FILMS

Isuke OUCHI, Ikuo NAKAI, Masao KAMADA*, Shin-ichiro TANAKA* and Tsuneo HAGIWARA†

Department of Physics, Faculty of General Education, Tottori University,
Koyama, Tottori 680
*Institute for Molecular Science, Meidaiji, Okazaki 444
†Tokyo Research Laboratories, Teijin Limited, Hino, Tokyo 191

Polyethylene terephthalate (PET) is a typical polyester having a benzene ring in the main chain; its electronic spectra in UV region have been analyzed in detail[1] and its XPS have been reported[2]. In this work, the absorption spectra of core electrons of PET, together with those of polyethylene 2,6-naphthalate (PEN), were obtained; PEN has a naphthalene ring instead of benzene in the main chain.

The polymers for the samples were supplied from Teijin Limited. Thin amorphous films were made by casting a trichloro-hexafluoro-isopropanol solution. Uniaxially drawn films were obtained by stretching the cast films by an Instron tensile tester at 90°C. Biaxially drawn films of 0.7 microns were fabricated by Film Laboratories of Teijin Limited.

Absorption measurements were done at BL2B1 of UVSOR facilities. The samples were held between copper frames and put in a monochromatized radiation either normal to the beam or at 25° incidence. The transmited beam intensity through the sample or the blank was always corrected by detecting the photo-electrons from the Au mesh placed before the measurement chamber to eliminate the effects of the beam fluctuation and contaminations ; the absorbance of the sample was a ratio of the corrected blank intensity and the corrected sample intensity. The corrected blank intensity could change as much as ± 15% in a day: this was one of the sources of the possible errors.

The photon energy of the incident beam was corrected by the dips of the blank spectra without Au mesh correction at 284.7 and 291.0 eV originated from the carbon contamination, as described by Stohr et al[3].

The grating of the Grasshopper monochrometer had 600 lines per mm in the earlier experiments but later was replaced by that of 1200/mm; the resolution and the stray light were significantly improved. The comparison between the spectra obtained by use of these gratings is shown in Fig. 1.

The conspicuous absorption peaks at 285.5 eV and 289.1 eV of PET and PEN look to correspond to the absorption maxima at 285.5 eV and 287.4 eV, respectively, in the spectra of C_{60} [4]; they also correspond to the strong absorption of benzene adsorbed on Pt(111), peaking at 286 ev with a broad tail[5]. The absorption at 285.5 eV is consistent with the absorption at 285.5 eV of polycrystalline and microcrystalline graphites[6], amorphous carbons[7] and carbon films made by CVD [8]. These peaks have all been assigned to the transitions of C 1s to * state; therefore, the absorptions of PET and PEN at 285.5 eV and 289.1 eV must have occurred from the transitions of C 1s to *, although the peak at 289.1 eV

may be related not to C=C but to C=O.

The benzene ring in PET, as well as the naphthalene ring in PEN, tends to be alligned parallel to the film plane when drawn uniaxially, or, in particular, biaxially. If the parallelism be perfect, the normal incident light would not give rise to any intense peak at these photon energies; in actuality, there are small amount of non-parallel components even in the biaxially stretched films. Also, the films mounted oblique to the incident light exhibited stronger absorption at 289.1 eV. Therefore, the above assignment for these two peaks may be conceivable.

The other broad peaks at 293.4 eV, 296.6 eV and 304 eV should be related to * transitions, also after conjectured from the spectra of the above compounds.

The oxygen absorptions were found at 528.5 eV (shoulder), at 536.6 eV (main peak) and at 547 eV.

Detailed analysis is still to be made.

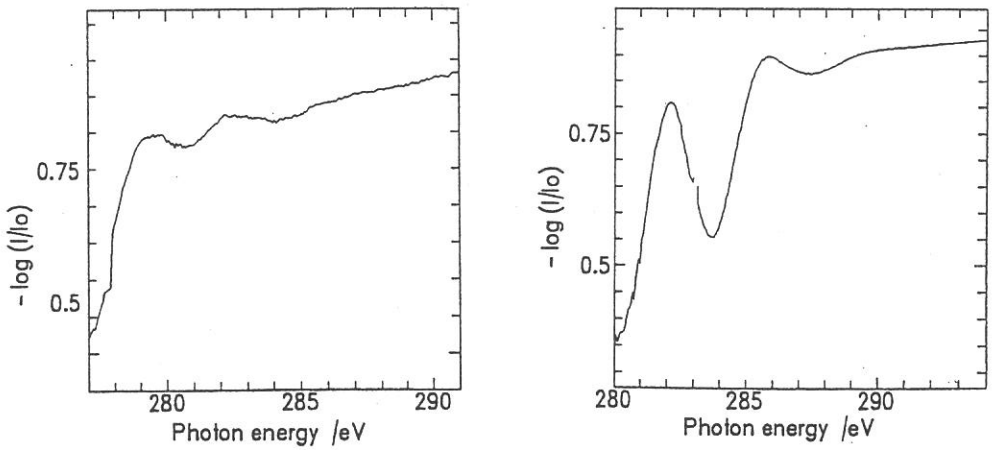

Fig.1 Comparison between the absorption spectra of biaxially oriented PET obtained by a monochrometer with a grating of 600/mm (left) and 1200/mm (right).

1) I. Ouchi: Polym. J. 15 (1983) 225.
2) ex. D.W. Dwight, J.E. McGrath and J.P. Wightman: J. Appl. Polym. Sci. Symp., 34 (1978) 35.
3) J. Stohr and R. Jaeger: Phys. Rev. B, 26 (1982) 4111.
4) H. Shinohara, H. Sato, Y. Saito, K. Tohji and Y. Udagawa: Jpn. J. Appl. Phys. 30 (1991) L848.
5) A.L. Johnson and E.L. Muetterties: J. Am. Chem. Soc. 105 (1983) 7183.
6) D. Denley, P. Perfetti and D.A. Shirley: Phys. Rev. B 21 (1980) 2267.
7) G. Commelli, J. Stohr, C.J. Robinson and W. Jark: Phys. Rev. B 38 (1988) 7511
8) K. Edamatsu, Y. Tanaka, T. Yokoyama, K. Seki, M. Tohnan, T. Okada and T. Ohta Jpn. J. Appl. Phys. 30 (1991) 1073.

PHOTOELECTRON-YIELD SPECTRA OF DYE-DOPED POLYMER SYSTEM

Masaya KAWASE+, Shunsuke NAKANISHI and Hiroshi ITOH

+Department of Chemistry and Department of Physics, Faculty of Education, Kagawa University, Saiwai-cho, Takamatsu 760

Organic dye-doped polymer system attracts much attention because of its optical properties and possibility of application for a functional optical memory. Optical dephasing of the dye-doped polymer system was reported previously[1,2].

In these studies using the incoherent photon echo technique, it was found that the optical dephasing time(T_2) of the doped dye molecule showed the host-dependence. That is, T_2 of the organic dye doped in the crosslinked polyvinyl alcohol derivatives (PVA-SbQ, PVA-SPPIα and PVA-SPPIIα) was longer than T_2 of the organic dye doped in polyvinyl alcohol (PVA). A study of Fourier-transform spectroscopy for photon echos, combined with the persistent hole-burning (PHB), has shown that the photon echo decay includes all information obtained in PHB [3]. This study suggests that the system with long T_2 shows the narrow hole-spectrum and is suitable for a functional optical memory.

As introduction of the cross-link in PVA was performed by photochemical reaction, there was the possibility to form the covalent bond between the doped dye and the host polymer. In order to investigate this point, we measured the soft X-ray photoelectron-yield spectra of the systems employed in this study.

In this report, we will present the results obtained by using BL7A.

As mentioned above, there is the possibility to form the covalent bond between the doped dye and the host polymer in photochemical reaction to crosslink the host polymer. In this study, DTCI was used as the doped organic dye. PPP-MO calculation showed that the frontier electron density was higher on hetero atom (S) than on other atoms around S atom. Therefore, if the covalent bond between the doped dye and the host polymer was formed in photochemical reaction, the soft X-ray photoelectron-yield spectra of S in the dye-doped crosslinked PVA systems must be different from that of the dye-doped PVA system [4]. The spectra of all systems tested in this study had the same shape displayed in Fig. 1. These results suggest that the covalent bond between the doped dye and the host polymer is not formed in the systems employed here. This study using BL7A shows that the host-dependence of T_2 is not caused

by the change of the structure of the doped dye molecule but that of the effective TLS density around the void space which entraps the dye molecule. Our model in the host dependent optical dephasing using the effective TLS density [1,2] is strongly supported by this study.

We would like to acknowledge Prof. Ichimura, Tokyo Institute of Technology, for providing us the crosslinked PVAs. We also thank to Dr. Watanabe, UVSOR, for his invaluable suggestion.

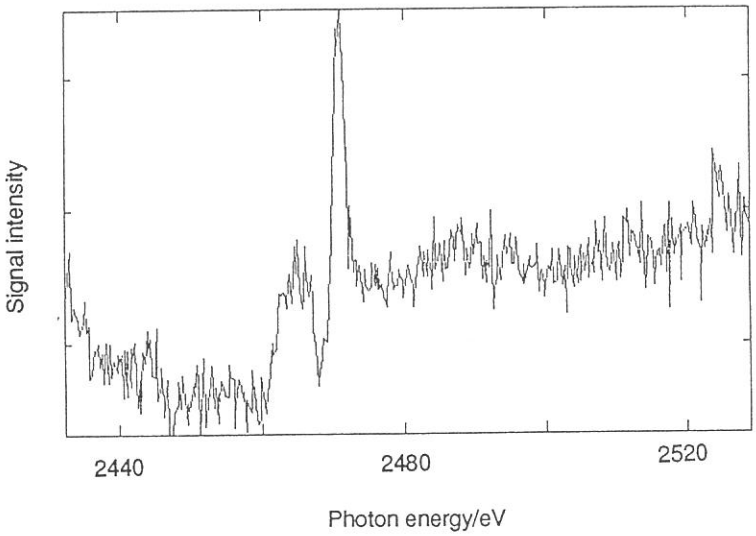

Fig. 1 Soft X-ray photoelectron-yield spectrum of the dye-doped polymer system

References

1. M. Kawase, S. Fujiwara, S. Nakanishi and H. Itoh, Chem. Phys. Lett., **194**, 268 (1992)
2. S. Nakanishi, M. Kawase and H. Itoh, in Ultrafast phenomena, in press.
3. S. Saikan, T. Nakabayashi, Y. Kanamatsu and N. Tato, Phys. Rev. B, **38**, 7777 (1988)
4. W. Gudat and C. Kunz, Phys. Rev. Lett., **29**, 169 (1972)

Photoemission Study of an Al-Pd-Mn Icosahedral Phase

M. MORI, S. HASEGAWA†, T. ISHIMASA, K. SAITO, S. MATSUO and H. INOKUCHI†

College of General Education, Nagoya University, Chikusa, Nagoya 464-01
†Institute for Molecular Science, Myodaiji, Okazaki 444

Since the discovery of an icosahedral phase (i-phase), there has been increasing interest in the electronic properties of icosahedral materials in spite of remaining the arrangement of the atoms unclear. Very recently, a dip-like anomaly in the DOS structure at E_F was confirmed with the UPS experiment. The dip-width and the depth were estimated to be 0.35eV and 70% of a normal DOS, respectively[1]. Successively, the CIS spectra at the binding energy region between 0 – 2eV show resonant characteristic[3]. The Fe 3d band is located in the region ranging from E_F to 2 – 2.5 eV below it with the maximum contribution at around 0.7eV in the binding energy. The smaller binding energy, exactly Fe 3d states sitting just below E_F, is consistent with Friedel's suggestion. The dip structure was interpreted in terms of the nearly-free-electron-like energy gap inferred from strong diffraction spots, which may be related to the stability of the i-phase. It has been known that in an Al-Pd-Mn alloy is a stable i-phase with a high quasicrystalline quality as well as an Al-Cu-Fe system[2]. This principal purpose is the check that the above-mentioned anomaly in DOS at E_F also exists in the Al-Pd-Mn i-phase.

An $Al_{68}Pd_{23}Mn_9$ i-phase specimen was a quasicrystalline ingot prepared by the method[2]. Preliminary checking of the sample was carried out by electron microscope and powder x-ray diffraction methods. The analyzer resolution was about 0.14eV at photon energy 35eV defined with a width of a Gaussian function. The clean surface of the specimen was obtained by scraping with a file in a vacuum of $2 - 4\times10^{-8}$ Pa. Immediately, the sample was transferred to the UPS experimental chamber and measured in a vacuum of $0.5 - 2\times10^{-8}$ Pa. A spectral dependence of incident radiation was determined from a photoelectric yield of gold which was prepared as a film.

UPS experiments were performed making a high resolution (0.14eV=ΔE defined as the width of Gaussian function) with the incident photon energy 35eV, in order to examine the detailed structure of DOS near the E_F. The dotted curve of Fig. 2 is the UPS spectum of Al-Pd-Mn i-phase sample. Well-defined Fermi edge of gold was observed, but Fermi edge of Al-Pd-Mn i-phase was not clearly observed as shown in Fig. 2, which has qualitatively a feature similar to the Al- Cu-Fe i-phase with the pseudo-gap structure[1].

Let us consider a model to reproduce spectra near E_F to obtain a quantitative estimation of the dip structure on the assumption that the observed spectrum is proportional to DOS and the DOS near E_F is linearly dependent on the energy. The DOS additionally has the dip of which shape is assumed to be a Lorentzian function having the center on E_F and a half width as showing in Fig. 1. The observed intensity $I(E)$ is given as follows.

$$I(E) = \int (ax + b) \cdot (1 - \frac{C\Gamma^2}{(x - E_F)^2 + \Gamma^2}) \cdot f(x) \cdot G\exp(-(x - E)^2/(\Delta E)^2)dx,$$

where $(ax + b) \cdot (1 - C\Gamma^2/\{(x-E_F)^2 + \Gamma^2\}$ shows the electronic DOS near E_F at energy x with the dip of the DOS near Fermi edge. In the case of C=0 a system has no anomaly (we call a normal DOS) and in the case of C=1 the system has no DOS at E_F; as C is the ratio of dip-depth and the normal, and C must be less than unity. $f(x)$ is the Fermi distribution function.

We consider the case of C=0 (the normal DOS case). We have tried to fit the spectrum of gold. The fitted was in good agreement with the observed curve using the energy resolution width ΔE=0.14eV and the fitting parameters a and b. But the calculated curve could not be fitted with the dotted curves as shown in Fig. 1, and it is noted that the calculated curve drops more abruptly near E_F than the experimental curve. At a final step, we tried to fit the spectrum of the Al-Pd-Mn i-phase, adding the additional fitting parameter C. The solid curve of Fig. 1 is the most adequately fitted calculation curve with C=0.67 and Γ=0.135eV. The solid curve of Fig. 2 shows that the calculated curve using this fitting model is in good agreement with the observed spectrum. Supposing the dip is approximately the Lorentzian function subtracting from the normal DOS structure, the dip-width is given as about 0.135±0.01eV and the DOS on E_F becomes 0.33±.05 of the normal DOS without the dip. The clear observation of the dip at E_F is consistent with UPS result of the Al-Cu-Fe i-phase[1]. These values should be taken as rough quantitative guess as to the dip width and depth because of somewhat arbitrary assumption of the Lorentzian form. Therefore, it is regarded that this 'dip' model is a good approximation to the DOS near E_F of this Al-Pd-Mn i-phase. A width of the dip is given as about 0.135 ±0.005eV and the DOS on E_F becomes 33±5% of the normal DOS. Comparing the UPS result of the Al-Pd-Mn i-phase with it of the Al-Cu-Fe i-phase, the dip depth is almost same and the width is sharper by the 3 times. The dip model is also supported by the present result. This non-well-defined Fermi edge is also an intrinsic property of this i-phase sample.

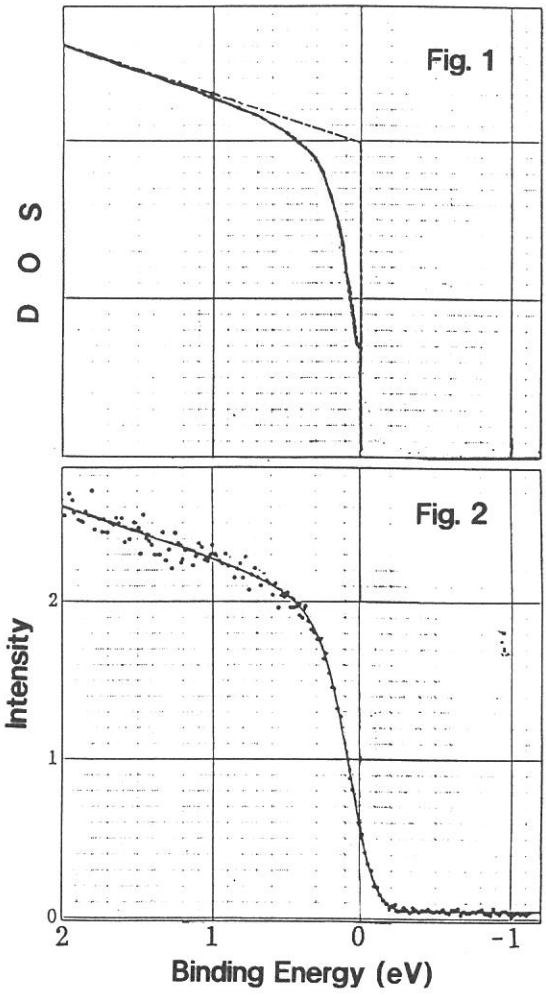

1) Mori M, Matsuo S, Ishimasa T, Matsuura T, Kamiya K, Inokuchi H and Matsukawa T, J. Phys.: Condens. Matter **3** (1991) 767
2) Ishimasa T and Mori M, Phil. Mag. **B66** (1992) 513
3) Mori M, Kamiya K, Matsuo S, Ishimasa T, Nakano H, Fujimoto H and Inokuchi H, J. Phys.: Condens. Matter **4** (1992) L157

FIG. 1. The DOS model of Al-Pd-Mn i-phase for fitting is made up at T=0K by subtracting the dip from the normal DOS (broken curve). Solid curve is in the case of C=0.67 and Γ=0.135eV.

FIG. 2. Dotted curve is the observed UPS near E_F for incident photon energy 35eV at room temperature. Solid curve is the calculated curve supposing that the DOS is like as the solid curve of Fig. 1.

UPS STUDY ON $NiPS_3$ CRYSTAL BY USING SYNCHROTRON RADIATION

H. Fujimoto
Department of Environmental Science,
The Graduate School of Science and Technology, Kumamoto University,
Kumamoto 860, Japan

H. Nakahama, M. Takashima, and K. Ichimura
Department of Chemistry, Faculty of Science, Kumamoto University,
Kumamoto 860, Japan

S. Hasegawa and H. Inokuchi
Institute for Molecular Science (IMS), Okazaki 444, Japan

Metal tricalcogeno-phosphate MPX_3 (M stands for a divalent metal ion and X is either S, Se, or Te) forms a large family of layered compounds. These compounds have attracted much attention due to their capability of intercalation with alkali metals and application to Li-based batteries [1]. Piacentini *et al.* [2] suggested that the Ni d states contribute primarily to the upper part of the valence band in the X-ray photoemission spectra. The resonant photoemission technique has been used to identify the origin of the valence band structures of $NiPS_3$ and $FePS_3$ [3,4]. In this report, we carried out a study of $NiPS_3$ crystals by ultraviolet photoemission spectroscopy (UPS) using synchrotron radiation to get further insight by carefully investigating the valence band electronic structure. We used the resonant-photoemission (RPS) and the constant-initial-state (CIS) spectroscopies to identify the contributions of each element to the valence band of $NiPS_3$.

All spectral measurements were performed at the UVSOR Facility of IMS. The photon energy ($h\nu$) was changed widely from 15 to 90 eV. The Fermi energy (E_F) of the instrument was determined by using the Fermi edge of gold films evaporated *in situ*. CIS spectra were obtained by measuring the $h\nu$ dependence of the electron counting rate and normalizing against the photon number. The photon number was determined by the emission current from a gold mesh placed in the light path and the emission yield of gold. $NiPS_3$ crystals were prepared from elemental mixtures of metal, phosphorus, and sulfur with the atomic ratio of 1:1:3 as reported previously [5]. The synthesized crystals were identified by means of powder X-ray diffraction and Raman spectroscopy. The elemental contents in the crystals were determined by an electron microscope analysis. The single crystal was fixed on a copper substrate by silver resin and was scraped by a diamond file or cleaved in vacuum. RPS and CIS spectra were measured on these clean surfaces.

The $h\nu$ dependence of UPS spectra is shown in Fig.1. Several features can be observed at 1.1, 2.1, 3.0, 4.2, 7.0, 8.2, and 10.0 eV from E_F. UPS spectra taken at high $h\nu$ are similar with the X-ray photoemission spectrum [2]. From the atomic subshell photoionization cross sections [6], the p character is enhanced at low $h\nu$. Taken into account of the atomic ratio between sulfur and phosphorus, the structure at 4.2 eV would mainly come from the sulfur 3p orbitals. Moreover, the structures observed at the high $h\nu$ can be assigned to the main and satellite bands of Ni 3d states.

Figure 2 shows CIS spectra of the valence band structures. Among the features of the valence band, the structures located at 2.1, 3.0, 7.0, and 10.0 eV show strong resonance at the 3d threshold energy of Ni; and the weak resonance is observed at the structures of 1.1 and 8.2 eV, and no resonance occurs in the features at 4.2 eV. The 4.2, and 8.2 eV structures are also

intensified at the photon energy of 30 eV. Therefore, the structures at 2.1, 3.0, 7.0, and 10.0 eV are mainly from Ni 3d orbitals, and the Ni 3d orbitals partly contribute to the features at 1.1 and 8.2 eV. Moreover, there is no 3d character in the 4.2 eV band.

From these observations, we conclude that the top of the valence band contains contributions from Ni atoms and P_2S_6 clusters. This is consistent with the observation that the photoionization threshold energy of $NiPS_3$ is almost same as that of $ZnPS_3$ and $FePS_3$.

References

[1]R. Brec, G. Ouvrard, A. Lousy, J. Rouxel, and A. Le Mehaute, *Solid State Ionics*, **6**, 185 (1982).

[2]M. Piacentini, F. S. Khumalo, G. Leveque, C. G. Olson, and D. W. Lynch, *Chem. Phys.*, **72**, 61 (1982).

[3]M. Piacentini, V. Grasso, S. Santangelo, M. Fanfoni, S. Modesti, and A. Savoia, *Il Nuvo Cimento*, **4D**, 444 (1984).

[4]M. K. Kelly, R. R. Daniels, G. Margaritondo, and F. Lévy, *Solid State Commun.*, **50**, 233 (1984).

[5]K. Ichimura and M. Sano, *Synth. Metals*, **45**, 203 (1991).

[6]J. J. Yeh and I. Lindau, *Atomic Data and Nuclear Data Tables*, **32**, 1 (1985).

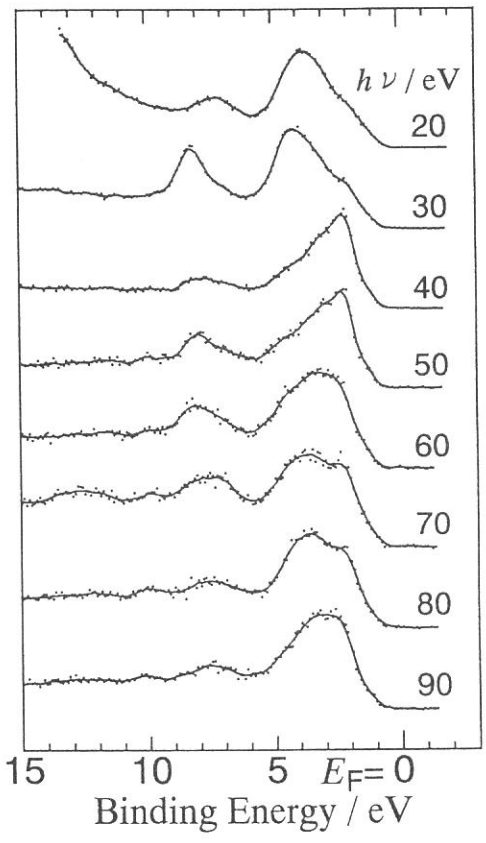

Fig.1 UPS spectra of the scaped $NiPS_3$ crystal.

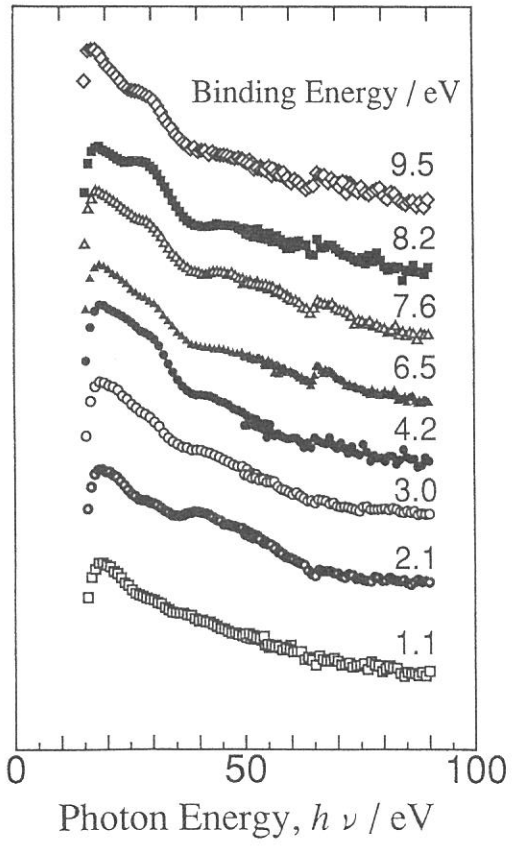

Fig.2 CIS spectra of the valence band structures.

Photoemission Study of $SrLaFeO_4$

Takahisa Omata, Naoyuki Ueda, Kazushige Ueda, Takuya Hashimoto, Hiroshi Kawazoe, Shinji Hasegawa* and Kazuhiko Seki**

Reseach Laboratry of Engineering Materials, Tokyo Institute of Technology, Midori-ku, Yokohama 227
**Institute for Molecular Science, Myodaiji, Okazaki 444*
***Department of Chemistry, Faculty of Science, Nagoya University, Chigusa-ku, Nagoya 464*

Electrical insulator of 3d transition-metal compounds are usually classified into Mott-Hubbard type or charge-transfer type. It has been clarified recentry that the compounds of Cu, Ni and Co are described as charge-transfer insulator. In this report, the electronic structure of $SrLaFeO_4$ with K_2NiF_4 structure has been studied by ultraviolet photoemission spectroscopy. It will be concluded that $SrLaFeO_4$ is a charge-transfer insulator if the bottom of the conduction band is composed of unoccupied Fe3d character.

Photoemission measurements were performed at the beam line BL8B2. The sample was a sintered pellet that was prepared by heating at 1500 °C for 48h in O_2 flow. It was scraped under a vacuum of 6×10^{-8} Torr with a diamond file. All spectra were normalized to the photon flux obtained from experimental and theoretical Au yield.

Fig.1 shows photoemission spectra in the valence band region for various photon energies of excitation. The valence band (2～12 eV band) consists of two feautures around 7.8 and 10.4 eV. The emission cross section of O2p steeply increases toward lower photon energies, while that of Fe3d emission becomes more dominant for higher photon energies ($h\nu$ > 40 eV)[1]. However, the line shape has unchanged for the whole photon energy in contrast with such different photon energy dependences of Fe3d and O2p. CIS spectra for various binding energies in the valence band spectra are shown in Fig.2. It is noted that the intensities of 7.8 and 10.4 eV bands steeply decrease toward higher photon energies and are enhanced for the excitation around $h\nu$～40 eV. Because of the fact that

Fe 3d cross section becomes maximum around $h\nu \sim 40$ eV, 7.8 and 10.4 eV bands are considered to be a mixture of Fe3d and O2p character. On the other hand CIS spectra for 4.0 and 5.0 eV bands do not show such enhancement and monotonously decrease toward higher photon energies. This suggests that O2p character is more dominant around valence band maximum rather than 7.8 and 10.4 eV bands.

Consequently we conclude that $SrLaFeO_4$ is a charge-transfer insulator if the bottom of the conduction band is composed of unoccupied Fe3d character.

1) J.J.Yeh and I.Lindau, At. Data Nucl. Data Tables, 32, 1(1985).

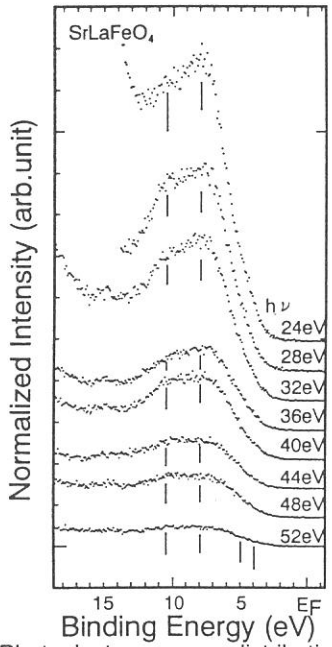

Fig.1 Photoelectron energy distribution curves taken at various photon energies on $SrLaFeO_4$

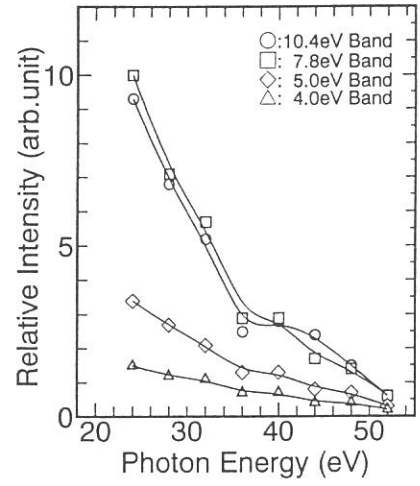

Fig.2 CIS spectra for various binding energies of the valence band spectra of Fig.1

Ultraviolet Photoelectron Spectra of C_{76} and K_xC_{76}

Shojun Hino
Department of Image Science, Faculty of Engineering, Chiba University, Chiba 260, Japan

C_{76} is one of the cage-like carbon compounds (fullerenes) isolated from carbon soot as C_{60}. Alkali metal dosed fullerenes often show high electric conductivity. The photoelectron spectra of both pristine and alkali metal dosed fullerenes will give a clew to understand the origin of their high conductivity. We have measured the ultraviolet photoelectron spectra of C_{76} and potassium dosed C_{76} at BL8B2.

Photoelectron spectra of pristine C_{76}

Figure 1 shows the photon energy dependence of the photoelectron spectra of C_{76}. Eight distinct structures denoted A – H in the figure are observed. There is no sudden appearance or disappearance of the structure in the spectra, as has often been observed in the UPS of the strict **k**-vector conserved system. The spectral onset locates at 1.3 eV below the Fermi level, which is smaller than those of C_{60} (1.9 eV) [1,2] and C_{70} (1.8 eV) [2,3] and the same as that of C_{84} (1.3 eV) [4].

The change of the spectral onset from C_{70} to C_{76} (only 6 atoms are added) is larger than that from C_{60} to C_{70} (10 carbon atoms increased). As the band gaps of fullerenes estimated from the photoemission spectra do not coincide with those estimated from their absorption spectra, the Fermi level of fullerenes does not seem to lie at the middle of the band gap. Actually inverse photoemission studies of C_{60} [5,6] and C_{70} [2] reveal that the Fermi level lies near the conduction band and the band gap is wider than the HOMO – LUMO gap.

A very strong intensity oscillation due to the incident pohoton energy tuning has been found in the first two bands of the spectra of C_{60} [1,7], C_{70} [2] and C_{84} [4]. However, there is no explicit intensity oscillation among the photoelectron structures induced by the incident photon energy change. The behavior of C_{76} seems to be different from the other fullerens.

A theoretically calculated density of states (DOS) of C_{76} using tight-binding approximation [8] expanded by 0.5 eV wide gaussian functions is also shown in Fig. 1. The calculated DOS is shifted so that both first bands coincide at the same energy position. The geometry used in the theoretical calculation is D_2 symmetry which was proposed by Ettl et al. from a NMR experiment [9]. The basis of their conclusion is 19 equal intensity lines in the NMR spectrum. As C_{76} has only one possible structure of D_2 symmetry, the structure of C_{76} is determined uniquely. The calculated DOS shows a very good correspondence with the photoelectron spectra. This agreement also supports the D_2 geometry of C_{76}.

Photoelectron spectra of potassium dosed C_{76}

Figure 2 shows the spectral change of the upper part of the valence band upon potassium dosing. At first stage of potassium dosing ($x = 0.13$ and 0.31), the valence band peaks shift far from the Fermi level by 0.15 eV, while the spectral onset shifts 0.1 eV. This peak shift dissolves at higher potassium dosage ($x = 3.0$). When potassium

dosage is 1.1, a new structure is observed as a small tail to the structure A. As the dosage increases, the new structure grows up between the structure A and the Fermi level to be observed as a distinct peak. At x = 2.1 and 3.0 the spectral onset is 0.15 eV, which is the closest position to the Fermi level in all the photoelectron spectra of potassium dosed C_{76}. The intensity of the new structure increases as the dosage increases. However, the spectral onset shifts away from the Fermi level. The spectral onset is about 0.2 eV at x = 3.6 – 5.5, and it increases to 0.3 eV at x = 6.5. Existence of a gap between the spectral onset and the Fermi level is a direct evidence of the band gap between the conduction and valence bands even though it is small. Therefore, K_xC_{76} is a narrow gap semi-conductor and may not be metallic or super-conductive.

REFERENCES

1. J. H. Weaver *et al.*,, Phys. Rev. Letters. **66**, (1991) 1741.
2. T. Takahashi *et al.*, Physica C **185–189**, (1991) 417.
3. M. B. Jost *et al.*, Chem. Phys. Letters. **184**, (1991) 423.
4. S. Hino *et al.*, Chem. Phys. Letters **190** (1992) 169.
5. P. J. Benning *et al.*, Science **252**, (1991) 1417.
6. T. Takahashi *et al.*, Phys Rev. Letters. **68**, (1992) 1232.
7. P. J. Benning *et al.*, Phys. Rev. B **44**, (1991) 1962.
8. S. Saito, S. Sawada and N. Hamada, Phys. Rev. B, in press.
9. R. Ettl *et al.*, Nature **353**, (1991) 149.

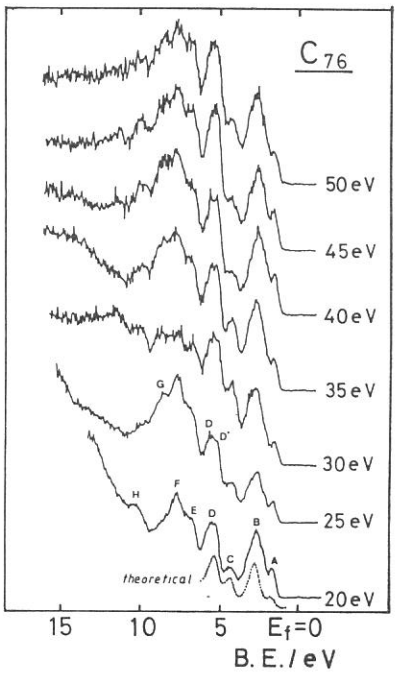

Fig. 1 The incident photon energy dependence of UPS of C_{76}.

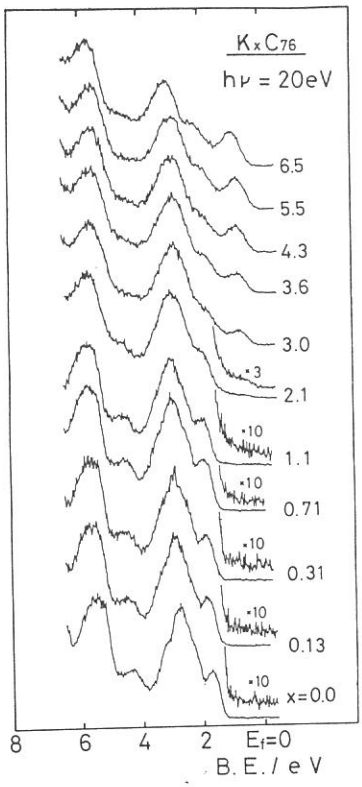

Fig. 2 Spectral change induced by potassium dosing.

Nonradiative decay processes of Cl 2p core exciton in LiCl and NaCl

K. Ichikawa, Y. Taguchi, K. Soda, K. Joda, S. Tanaka, O. Aita,
M. Kamada* and S. Tanaka*

College of Engineering, University of Osaka Prefecture, Gakuen-cho, Sakai 593
**Institute for Molecular Science, Okazaki 444*

We have investigated the nonradiative decay processes of the Li 1*s* core exciton in lithium halides[1,2] and the Na 2*p* core exciton in sodium halides[3,4] by using resonant photoemission. The enhancement of emission intensities of the valence band and the Auger peak was observed at the excitation energies of the Li 1*s* and Na 2*p* core excitons. In addition, kinetic energies of the Auger electron measured at excitation energy of the core exciton are slightly greater than those of ordinary one. The bottom of the conduction band is mainly composed of *s* states of alkali ions in LiCl and NaCl. Thus the Li 1*s* core exciton and the Na 2*p* core exciton are well localized in the alkali ion. On the other hand, the Cl 2*p* core exciton may somewhat be screened by valence electrons compared with the above excitons. The purpose of the present study is to investigate nonradiative decay processes of the Cl 2*p* core exciton in LiCl and NaCl. In this study, we anticipate different results from the previous studies on the core excitons well localized in the alkali ions.

A double stage cylindrical-mirror electron energy-analyzer at BL-2B1 was used to measure photoelectrons. Thin films of LiCl and NaCl were prepared *in situ* by evaporation onto gold substrates. The spectral distribution of incident radiation was determined from a photoelectric yield spectrum of gold.

Figure 1 shows the total photoelectric yield (TY) spectrum of NaCl. This spectrum shows sharp peaks at 201.4, 203.8, 205.9, and 208.2 eV and several broad peaks in the higher energy region. Early works on the absorption spectra have concentrated on interpretation of the first few peaks up to about 9 eV above the threshold. Because of the uncertainty of the absolute transition energies in calculations, the energy of the calculated band-structure has been shifted arbitrarily in order to get a reasonable correspondence between theoretical and experimental peaks. For this reason the first peak has sometimes been assigned to a transition to states in the conduction band[5] and sometimes to a core exciton.[6] At present, the first peak is interpreted in terms of excitation of a core exciton.

Figure 2 shows a set of energy distribution curves (EDC's) of NaCl obtained with the excitation photon energies around the Cl 2*p* threshold. Excitation photon energies ($h\nu$) are indicated on the right-hand side of each spectrum. The ordinates are proportional to the number of photoelectrons per photon flux. The abscissa represents the kinetic energy of electrons. The Cl $L_{2,3}VV$ Auger lines and Cl 3*s* levels are seen in this figure. The Cl 3*s* levels are indicated by arrows. It is noticed that the shape of Auger lines changes drastically with increasing the excitation energy. At $h\nu$ =200.4 eV, which corresponds to the low energy tail of the first absorption peak, the Cl 3*s* level is seen. Two Auger peaks are observed at 175 and 177 eV in the EDC's at $h\nu$ =201.0 and 201.4 eV, while four Auger peaks are seen at 172, 174.5, 175.5, and 178.5 eV in the EDC's measured between $h\nu$ =202.2 and 203.7 eV. At higher excitation energy than 220 eV a broad Auger line is always seen at the kinetic energy of 175 eV.

The change of the Auger shape is limited in the excitation energy range between the first and second peaks in the TY spectrum. The intensity of the 177-eV Auger peak has a maximum at $h\nu$ =201.4 eV which is the first peak energy in the TY spectrum as seen in Figs. 1 and 2. However, 178.5-eV Auger has its maximum intensity at $h\nu$ =202.8 eV

which does not coincide with TY peak. It is noted that the spin–orbit splitting of the Cl $2p$ level is about 1.6 eV from the photoelectron spectra and this value corresponds well to the difference of excitation energies where each Auger peak shows maximum intensity. But the energy separation between the first and second peaks in the TY spectrum is about 2.4 eV. Thus, the second peak in the TY spectrum is not a spin–orbit partner of the first peak and it can be assigned to a transition to states in the conduction band.

The 177-eV and 178.5-eV Auger peaks are observed only in the excitation energy region of the Cl $2p$ core exciton and on the higher energy side of the ordinary one by about 2 eV. These Auger peaks can be attributed to the decay of the core exciton. In the final state of the Auger-decay process of the core exciton, a photoexcited electron and two valence holes form some bound state and reduce the correlation energy from a two-hole state caused by the ordinary Auger transition. This bound state may split into a few levels and causes the 177-eV and 178.5-eV Auger peaks at the excitation energy of the core exciton.

In contrast to the Li $1s$ and Na $2p$ core excitons, no enhancement of the valence-band emission was observed at the excitation energy of the core exciton. Detailed analysis of the experimental results is under way.

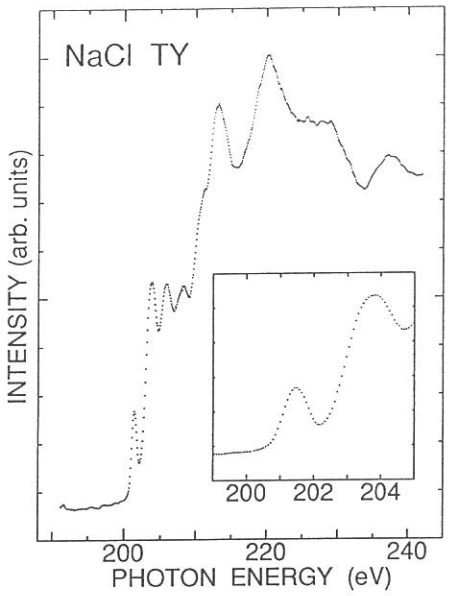

Fig. 1. Cl $L_{2,3}$ TY spectrum of NaCl. Inset shows the TY spectrum in the energy region of Cl $2p$ core excitons in expanded scale.

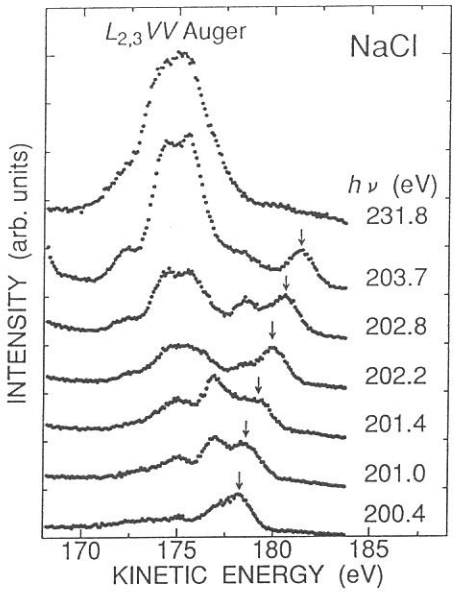

Fig. 2. A set of EDC's of NaCl. Excitation energies are indicated on the right-hand side of each spectrum. Arrows indicate the Cl $3s$ level.

1) M. Kamada *et al.* Phys. Rev. B **28**, 7225 (1983).
2) K. Ichikawa *et al.* Phys. Rev. B **32**, 8293 (1985).
3) M. Kamada *et al.* Phys. Rev. B **36**, 4962 (1987).
4) O. Aita *et al.* Phys. Rev. B **38**, 10079 (1988).
5) F. C. Brown *et al.* Phys. Rev. B **2**, 2126 (1970).
6) O. Aita *et al.* J. Phys. Soc. Jpn. **30**, 1414 (1971).

PHOTOEMISSION STUDY OF SUPERCONDUCTIVE AND NON-SUPERCONDUCTIVE ALKALI-DOPED C_{60}

Takashi TAKAHASHI[1], Takashi MORIKAWA[1], Shinji HASEGAWA[2], Hiroo INOKUCHI[2], and Yoji ACHIBA[3]

[1]*Department of Physics, Tohoku University, Sendai 980*
[2]*Institute for Molecular Science, Okazaki 444*
[3]*Department of Chemistry, Tokyo Metripolitan University, Tokyo 192-03*

Comparative photoemission measurements were performed on alkali (Rb , Cs) doped C_{60} to study the electronic structure, especially its change upon alkali-doping and the difference between the superconductor (Rb-C_{60}) and the non-superconductor (Cs-C_{60}). The photoemission measurement was done at BL2B. The photon energy used was 20 eV and the total energy resolution was about 0.15 eV.

Figure 1 shows the change of conductivity of a C_{60} film upon Rb- or Cs-doping. Pristine C_{60} film has a very low electrical conductivity in the range of 10^{-5} Scm^{-1} showing its insulating nature. However, upon the alkali-doping, the conductivity rapidly increases by 5 - 7 orders of magnitude until the calculated alkali content (x) reaches 3 - 4, then gradually decreases upon further doping.

Figure 2 shows change of photoemission spectrum in the vicinity of the Fermi level of C_{60} upon Rb-doping. As shown in the figure, the HOMO band located at about 2.3 eV, which originates in the six-fold degenerate h_u molecular orbital, shifts toward the high-binding-energy direction by about 0.3 eV upon a slight Rb-doping (from x=0.0 to x=0.5). The most striking feature in the spectrum upon the doping is appearance of a new band near the Fermi level, whose intensity is almost proportional to the doping amount. We ascribe this new band to the LUMO band of a C_{60} molecule which originates in the three-fold degenerate t_{1u} molecular orbital. We find that the density of states at the Fermi level gradually increases upon the Rb-doping in accordance with the growth of the occupied LUMO band near the Fermi level until x=3.7 (here, it should be reminded that the present study overestimates the x's by about 20 %, so that the actual composition is almost Rb_3C_{60} at x=3.7), then the density of states at the Fermi level decreases upon further doping as the occupied LUMO band gradually moves away from the Fermi level. This tendency of the density of states at the Fermi level shows a quite good correspondence to the change of the conductivity in Fig. 1.

Figure 3 shows the change of photoemission spectrum of C_{60} upon Cs-doping. The gross feature of change in the photoemission spectrum upon doping is similar between Rb and Cs, although one of them (Rb-C_{60}) becomes a superconductor while the other (Cs-C_{60}) not. In spite of the gross similarity, there is a small but distinct difference in the spectral intensity, namely the density of electronic states at the Fermi level. This is much more clearly seen in Fig. 4 where the photoemission spectra are displayed in an expanded scale. We find in Fig. 4 that the density of states at the Fermi level at the compositions of x=3 - 4 is much reduced (by a factor of about 5) in Cs-C_{60} compared with those in Rb-C_{60}. This is in good agreement with the conductivity measurement in Fig. 1 where the maximum conductivity in Cs-C_{60} is about a half order smaller than that of Rb-C_{60} at the composition of x=3 - 4. The observed lack of efficient density of states at the Fermi level would account for the absence of superconductivity in Cs-C_{60}.

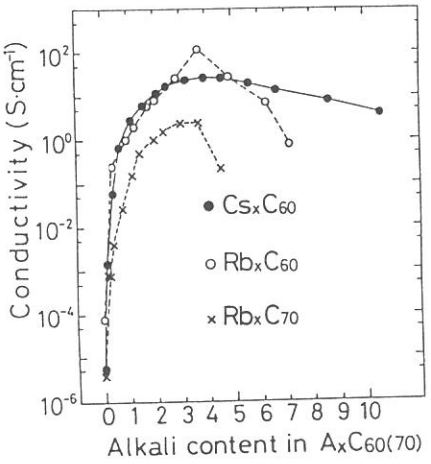

Fig.1 Change of the electrical conductivity of a C_{60} film upon Rb- or Cs-doping. The alkali content in film was calculated on an assumption that deposited alkali atoms distribute uniformly in the film.

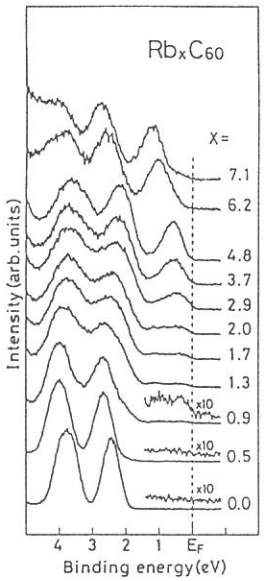

Fig. 2 Change of photoemission spectrum of C_{60} upon Rb-doping

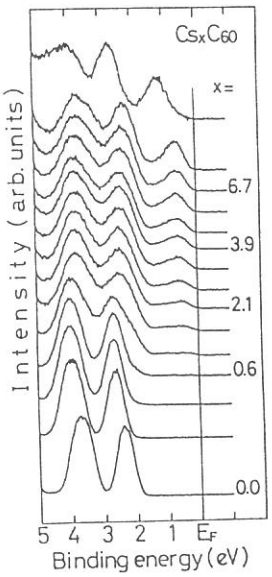

Fig. 3 Change of photoemission spectrum of C_{60} upon Cs-doping

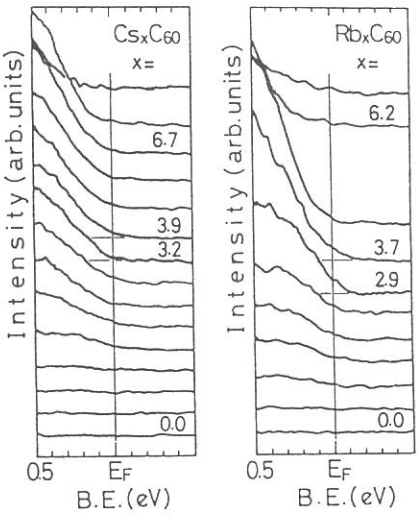

Fig. 4 Comparison of photoemission spectra in the vicinity of the Fermi level between Cs-C_{60} and Rb-C_{60}. The photoemission intensity is normalized with respect to the total intensity of the HOMO and HOMO+1 bands.

Molecular Orientation in Thin Films of Bis(1,2,5-thiadiazolo)-*p*-quinobis(1,3-dithiole) on Graphite Studied by Angle-Resolved Photoelectron Spectroscopy

S. Hasegawa, S. Tanaka, Y. Yamashita, H. Inokuchi,
H. Fujimoto[a)], K. Kamiya[b)], K. Seki[b)], N. Ueno[c)]

Institute for Molecular Science [a)]Department of Environmental Science, Kumamoto University [b)]Department of Chemistry, Nagoya University [c)]Department of Materials Science, Chiba University

Angle-resolved ultraviolet photoelectron spectra (ARUPS) using synchrotron radiation were measured for oriented thin films of bis(1,2,5-thiadiazolo)-*p*-quinobis(1,3-dithiole) (BTQBT) on cleaved graphite surface. The observed take-off angle dependence of photoelectron intensity was analyzed by using independent-atomic-center(IAC) approximation and MNDO molecular orbital calculation. The calculated results agree well with the experimental ones. From the comparison between these results, the molecules in the thin film are estimated to lie flat with the inclination angle $\beta \leq 10°$ to the HOPG surface. This analysis method is useful as a first step to a quantitative analysis for angular distribution of photoelectrons from thin films of large and complex organic molecules.

The experiments were carried out at UVSOR Facility (beamline 8B2). The incidence photon energy was hν= 40eV and the total energy resolution of the spectra was 0.15eV. The take-off angle (θ) dependence of photoemission intensity was measured at incidence angle of photons $\alpha = 0°$, BTQBT[1, 2] was carefully evaporated on HOPG substrate (Union Carbide ZYA-grade) at the deposition rate of 0.2 Å/min. The film thickness was estimated to be about 30 Å. The sample was then transferred to the measurement chamber ($\simeq 4 \times 10^{-10}$ Torr) under vacuum for *in situ* ARUPS measurements.

In Fig.1, the θ dependence of ARUPS spectra is shown in the binding energy region of $0 \sim 3.5$ eV. In this figure, three significant differences are observed: (1) the intensity of HOMO^{-1} band (A) exhibits a maximum at $\theta_{max} \simeq 37.5°$, while the HOMO (B) band gives a maximum at $\theta_{max} \simeq 45°$, (2) the maximum intensity of HOMO^{-1} band is more intense than that of HOMO band, and (3) the FWHM (full width at half maximum) of HOMO band is much larger than that of HOMO^{-1} band.

In IAC approximation by Grobman [3], a molecule is regarded as a set of independent atomic emitters. The total amplitude of photoemission is contributed to the atomic orbital coefficient of molecular orbital, the phase factor due to the difference in the path length to the detector from each atoms, and the atomic factor for optical excitation from an initial state to final continuum states. For the atomic factor, we used the values by Goldberg *et al.* [4].

In the calculation, we introduced the inclination angle β at which the molecular plane is inclined to the substrate surface and the molecular azimuthal angle ϕ_m specifying the azimuthal orientation in the molecular plane, as shown in Fig.2. In Fig.3 (a)$\sim$ (d), the calculated angular distributions of photoelecrtons for HOMO^{-1} state at inclination angles β= 0°, 5°, 10° and 20° are shown, where the dotted, broken and solid lines in each figure are the results at molecular azimuthal angles ϕ_m= 0°, 30° and 90°, respectively. The experimental results are also shown by open circles. The calculated distribution curve at β= 5° and ϕ_m= 90° (Fig.(b), solid line) give the best agreement

with the experimental results. By considering the experimental error and neglect of various scattering effects in the calculation, the BTQBT molecules were estimated to lie with the inclination angle $\beta \leq 10°$ to the HOPG substrate. The discussion for the HOMO band will be reported elsewhere[5].

For more complete analysis, it should be necessary to use exact values of atomic factors [4], and to take account of intermolecular interaction, surface barrier effect by inner-potential, and scattering of photoelectrons by neighboring atoms or molecules [6].

References

[1] Y. Yamashita, S. Tanaka, K. Imaeda and H. Inokuchi, Chem. Lett., 1213 (1991).
[2] K. Imaeda, Y. Yamashita, Y. Li, T. Mori, H. Inokuchi and M. Sano, J. Mater. Chem., **2**, 115 (1992).
[3] W. D. Grobman, Phys. Rev. B, **17**, 4573 (1978).
[4] S. M. Goldberg, C. S. Fadley and S. Kono, J. Electron Spectrosc. Relat. Phenom., **21**, 285 (1981).
[5] S. Hasegawa, *et al.*, (submitted to Phys. Rev. B).
[6] A. Liebsch, Phys. Rev. B, **13**, 544 (1976).

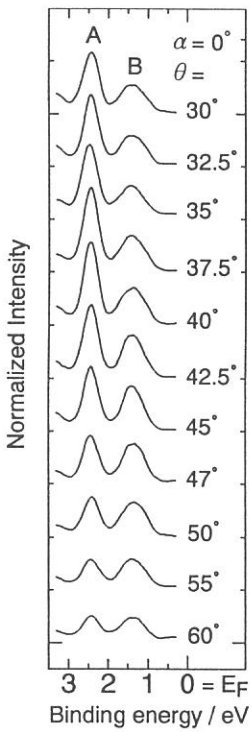

Fig. 1 The take-off angle (θ) dependences of ARUPS spectra. The HOMO^{-1} and HOMO bands are indicated by A and B.

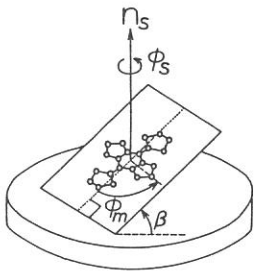

Fig. 2 Illustration of a BTQBT molecule with inclination angle β to the substrate. Molecular azimuthal angle ϕ_m is defined in the molecular plane.

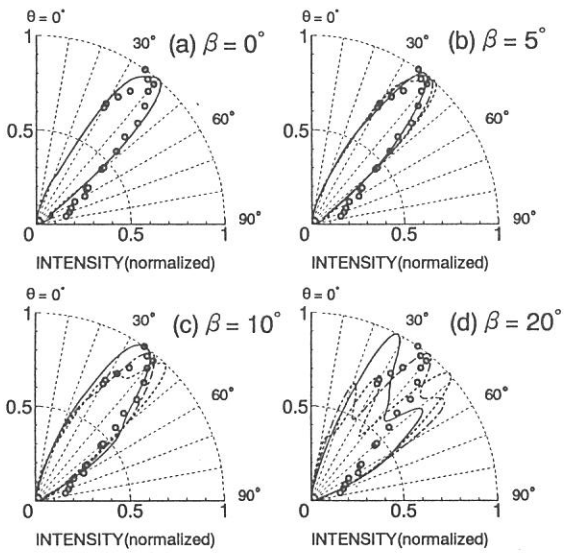

Fig. 3 The take-off angle (θ) dependences of photoemission intensities for the HOMO^{-1} band at $\alpha = 0°$.

Quantitative Analysis of Photoelectron Angular Distribution from Thin Films of Metal-Free Phthalocyanine

Nobuo UENO[a], Katsumi SUZUKI[a], Shinji HASEGAWA[b], Kazuhiko SEKI[c]
and
Hiroo INOKUCHI[b]

[a]*Faculty of Engineering, Chiba University, Yayoi-cho, Inage-ku, Chiba 263*
[b]*Institute for Molecular Science, Okazaki 444*
[c]*Faculty of Science, Nagoya University, Chikusa-ku, Nagoya 464*

The angular distribution of photoelectrons from thin films of organic crystals involves information on the molecular orientation in the film as well as on the wave functions of valence electron. Therefore, the quantitative analysis of the photoelectron angular distribution from a valence state gives a detailed information on the molecular orientation in ultrathin films of functional organic molecule, when the initial-state wave function is known. An advantage of the angle-resolved ultraviolet photoelectron spectroscopy (ARUPS) in determining the molecular orientation is that it introduces less radiation damages into the organic films in comparison with other surface sensitive techniques with electron beams. However, the quantitative analysis of the angular distribution from thin films of large organic molecules is very difficult, and no one has performed the quantitative analysis of the angular distribution after a challenging work by Permien *et al.* [1], which was reanalyzed by Richardson [2], on thin films of lead phthalocyanine. In our work on ARUPS of thin films of large organic molecules, we have found that the angular distribution calculated with the theoretical model used by Richardson [2] gave poor agreement with our experimental results on thin films of copper phthalocyanine.

In the present study, metal free phthalocyanine (H_2Pc) was selected as a sample, since (i) MNDO molecular orbital calculation is possible for this molecule, (ii) the molecule is large enough, (iii) phthalocyanine molecules were known to show flat-lie orientation on various single crystal surfaces [3,4], and the valence electronic states can be well approximated by those of isolated molecule because of the weak intermolecular interaction. For the calculation of the photoelectron angular distribution we used the independent atomic center (IAC) approximation presented by Grobman [5] and the initial-state wave function obtained by MNDO molecular orbital calculation.

Take-of-angle (θ) dependencies of the photoelectron spectra of H_2Pc film (8.6Å thick) on MoS_2 single crystal and HOPG graphite surfaces are shown in Figs. 1a and 1b for the normal incidence condition (the incidence angle $\alpha=0°$) at $h\nu=40$ eV. For both cases, the intensity of the peak A, which originates in the HOMO band consisting of single π orbital, shows prominent θ

dependence. In Figs. 2a and 2b, θ dependence of the intensity of the peak A is plotted for H_2Pc on MoS_2 and H_2Pc on HOPG, respectively. Sharp and similar angular distribution was obtained for both samples. It is notable that the angular distribution is very sharp and the angle θ_{max} giving the highest intensity is 34–38°. These characteristics can not be explained by the model calculation used by Permien *et al.* [1] and Richardson [2]. The angular distribution calculated by IAC approximation and MNDO molecular orbital calculation is also shown in Figs. 2a and 2b. In the calculation, the flat-lie orientation of the molecules and a complete polarization of the incidence photons were assumed, and the scattering of photoelectrons by the substrate and other molecules was neglected. An excellent agreement was obtained between the observed and calculated angular distributions, indicating that the analysis method using IAC approximation and molecular orbital calculation is successfully applicable to the quantitative analysis of the angular distribution of photoelectrons from thin films of large organic molecules.

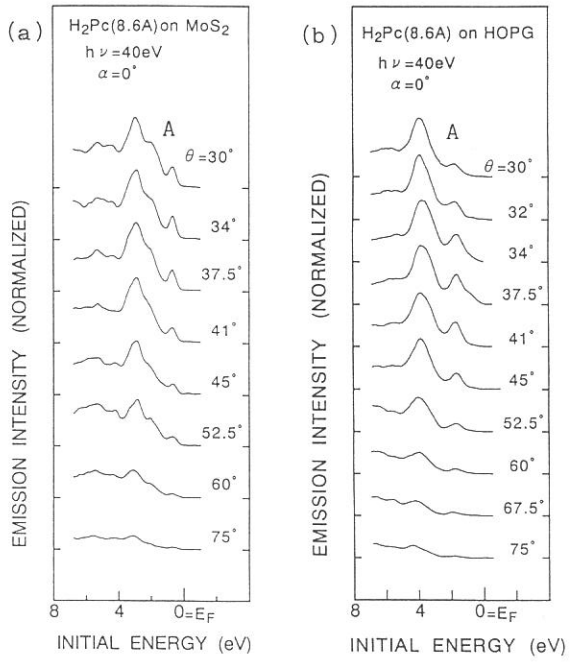

Fig. 1 Take-off-angle (θ) dependence of ARUPS spectra of thin films (8.6 Å) of metal-free phthalocyanine (H_2Pc) on MoS_2 (a) and on HOPG graphite (b) at hν=40eV and α=0°.

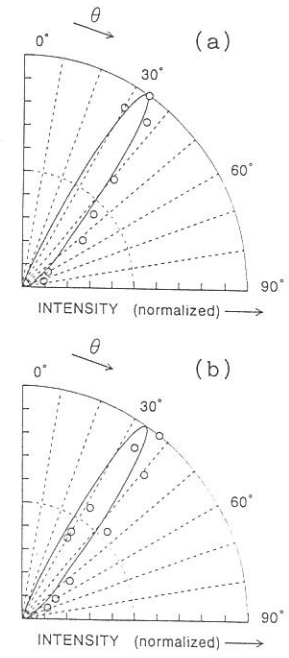

Fig. 2 Take-off-angle (θ) dependence of the intensity of HOMO band A. (a)H_2Pc on MoS_2. (b) H_2Pc on HOPG graphite. The calculated results are shown by solid curves.

References

[1] T. Permien, R. Engelhardt, C. A. Feldmann and E. E. Koch, Chem. Phys. Lett. **98** 527 (1983).
[2] N. V. Richardson, Chem. Phys. Lett. **102** 390 (1983).
[3] J. C. Buchholz and G. A. Somorjai, J. Chem. Phys. **66** 573 (1977).
[4] M. Hara, H. Sasabe, A. Yamada and A. F. Garito, Jpn. J. Appl. Phys. **28** L306 (1989).
[5] W. D. Grobman, Phys. Rev. B**17** 4573 (1978).

Photoelectron Spectroscopy of Polysilanes, Polygermanes, and Si-Ge Copolymers

Akira Yuyama, Satoru Narioka, Hisao Ishii, Toshihiro Okajima, Kazuhiko Seki, Shinji Hasegawa,* Masaie Fujino,**Hiroaki Isaka,** Michiya Fujiki,** Nobuo Matsumoto**

Department of Chemistry, Faculty of Science, Nagoya University, Chikusaku, Nagoya 464-01
**Institute for Molecular Science, Myodaiji, Okazaki 444*
***Basic Research Laboratories, Nippon Telegraph and Telephone Corporation, Midoricho, Musashino 180*

Polysilanes, which are polymers with Si backbones with organic substituents, have attracted attention as a new class of conducting polymers, photoresists, and also due to various interesting properties such as thermochromism. Such functions of polysilanes are not found in saturated organic polymers with C backbones. In this project, we have measured the whole valence band of five polysilanes, two polygermanes, and three Si-Ge copolymers by ultraviolet photoelectron spectroscopy (UPS) to investigate their electronic structures.

The UPS spectra were measured at BL8B2 of UVSOR. The samples were prepared by spin-coating on Cu substrates in a glove bag under N_2 flow. These films were transferred into the vacuum chamber without exposing to air, evacuated, and measured. The obtained spectra are of higher quality than those previously reported for several compounds[1] in showing fine structures and being free from charging.

The UPS spectra of a typical alkylpolysilane, PMPS (Poly(methylpropylsilane)), is shown in Fig.1(a). The abscissa is the binding energy relative to the vacuum level. To compare with the spectrum of PMPS, in Fig.1(b)-(f) we show the UPS and XPS spectra of propane[2)3)] and methane[4)], and the UPS spectrum of $Si_4(CH_3)_{10}$[5)] as a model compound of Si backbone. It is seen that the spectrum of PMPS corresponds well to those of constituent parts; the electronic structure of PMPS can be regarded as an overlap of those of methane, propane, and $Si_4(CH_3)_{10}$. The UPS spectra of polygermanes and block copolymer also correspond to those of $Si_4(CH_3)_{10}$ and $Ge_4(CH_3)_{10}$[6)] as in the case of polysilane, but the spectra of random polymers are not in so good correspondence to $Si_4(CH_3)_{10}$ and $Ge_4(CH_3)_{10}$ because of the contribution of Si-Ge bonding.

The UPS spectra of PMϕS (Poly(methylphenylsilane)), which is a typical arylpolysilane, is shown in Fig.2(a). Compared with PMPS, the spectrum of PMϕS is not in so good correspondence to $Si_4(CH_3)_{10}$ as for PMPS in the uppermost part of the valence band. We suppose that this is caused by σ–π interaction between the πHOMO states of benzene and the Si σHOVB states of the Si backbone. This result corresponds to that of theoretical band calculation reported by Takeda et.al.[7)]

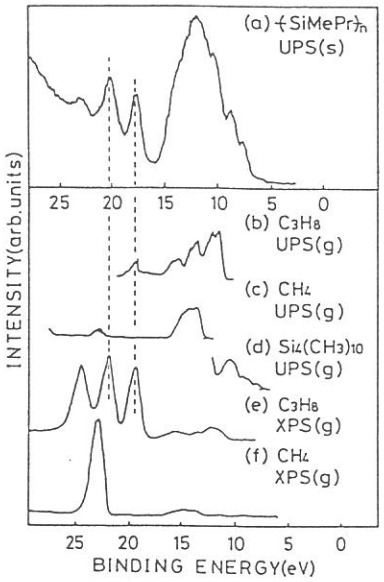

Fig.1 UPS and XPS spectra of PMPS and related compounds. (s) and (g) stand for solid and gaseous states, respectively.

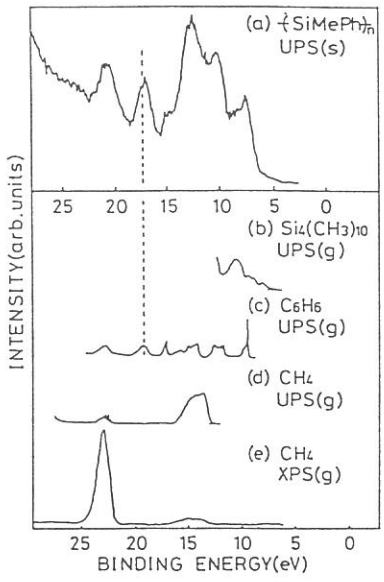

Fig.2 UPS and XPS spectra of PMϕS and related compouds. (s) and (g) stand for solid and gaseous states, respectively.

References

(1) G.Loubriel and J.Zeigler, Phys. Rev., B33, 4203 (1986)
(2) K.Kimura, S.Tatsumata, Y.Achiba, T.Yamazaki, and S.Iwata, Handbook of HeI Photoelectron Spectra of Fundamental Organic Molecules, Japan Scientific Societies Press, Tokyo (1980)
(3) J.J.Pireaux, S.Svenson, E.Basilier, P.Å.Malmqvist, U.Gelius, R.Coudano, and K.Siegbahn, Phys. Rev., A14, 2133 (1976)
(4) A.W.Potts, T.A.Williams, and W.C.Price, Faraday Disc. Chem. Soc., 54, 104 (1972)
(5) H.Bock and W.Ensslin, Angew. Chem. Internat. Ed., 10, 404 (1971)
(6) S.Tokura, K.Mochida, S.Masuda, Y.Harada, 63th Ann. Meeting of Chem. Soc. Jpn., 3 c 33 (Osaka, 1992)
(7) K.Takeda, H.Teramae, and N.Matsumoto, J. Am. Chem. Soc., 108, 8186 (1986)

TEMPERATURE DEPENDENCE ON THE FLUORESCENCE LIFETIMES OF HETEROGENEOUS TRYPTOPHAN RESIDUES IN HEAVY MEROMYOSIN POWDERS

Mieko TANIGUCHI and Masaya KATO
Department of Physics, Faculty of Science, Nagoya University, Chikusa-ku, Nagoya 464-01

Heavy meromyosin (HMM) is a subfragment of myosin which is one of the main proteins of muscle. HMM has an ability of ATP hydrolysis and interacts with actin filaments during muscle contraction. Therefore, it is important to get information whether any conformational changes take place in HMM. In most studies of protein conformation, temperature is a good indicator for monitoring their dynamical properties. The static and dynamic properties of tryptophan luminescence in HMM powders were investigated over wide temperature ranges under high vacuum conditions using synchrotron radiation from UVSOR. HMM was prepared from rabbit muscle. The apparatus was set up, as illustrated schematically in Fig. 1. A cryostat chamber was connected to a excitation monochromator in BL7B beam line. The vacuum pressure was about 1×10^{-7} torr. The samples were placed in a cryostat. A copper-constantan thermocouple was connected to the cell holder. The excitation and emission lights were focused by UV lens, respectively. Fluorescence decay times were measured by using the technique of time-correlated single photon counting under the single bunch operation. The signals from a microchannel plate photomultiplier were received by multichannel analyzer and then sent to microcomputer. Data were analyzed by a least-squares iterative convolution method. The fluorescence emission spectrum has a peak at 330 nm, when excited at 295 nm. The result means short-wavelength fluorescence from buried tryptophan residues. The decay times have three components (comp. 1 = 4.3-5.2 ns, comp. 2 = 2.5 ns and comp. 3 = 0.2 ns) and these values are independent of temperature. The fraction of these components depend on temperature. Fig. 2 show temperature dependence on the total and components of decay-associated emissions, respectively. The results show that the component 1 depends on temperature.

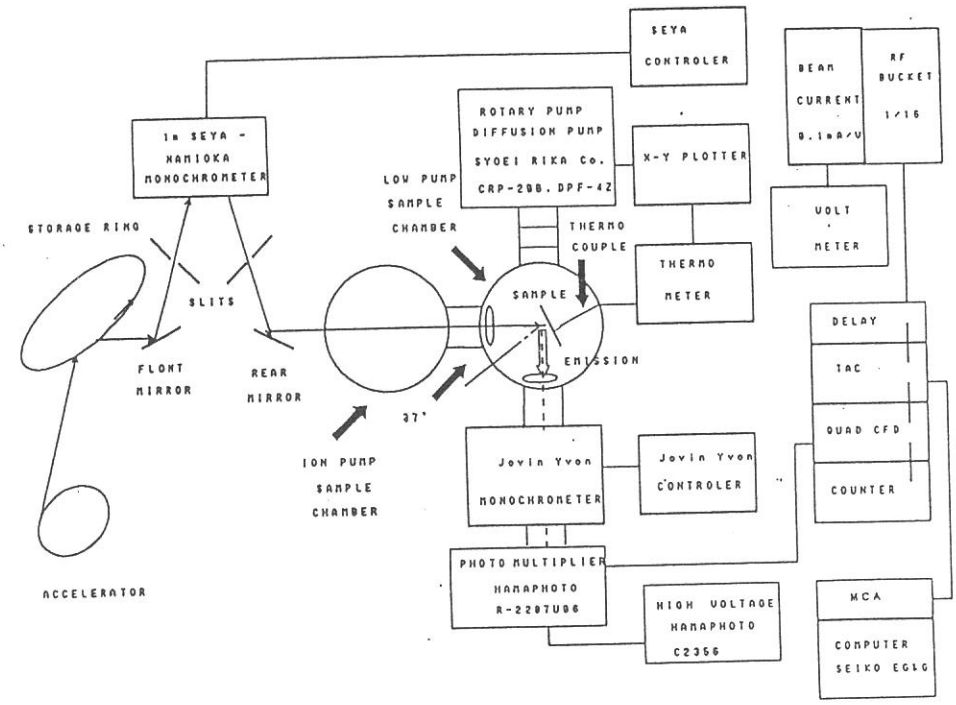

Fig. 1 A schematic drawing of apparatus for time-resolved fluorescence experiments.

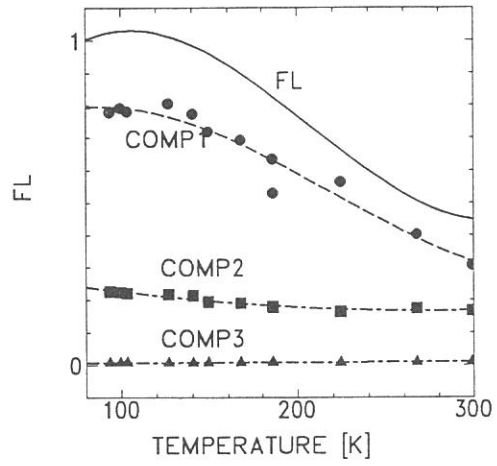

Fig. 2 Temperature dependence on the decay-associated emissions of HMM powders.
Excitation at 295 nm. Emission at 330 nm. ---, total intensity
Comp. 1 = 4.7-5.2 ns, comp. 2 = 2.5 ns, and comp. 3 = 0.2 ns.

Coadsorption of K and Cl on the Si(100)(2x1) surface

Shin-ichiro TANAKA, Masao KAMADA and Yukihiro TAGUCHI*

Institute for Molecular Science, Okazaki 444
* College of Engineering, University of Osaka Prefecture, Mozu, Sakai, Osaka 591

Coadsorption of K and Cl on the Si(100)(2x1) surface has been studied by the use of core-level photoemission and absorption spectroscopy. All experiments were performed in an UHV chamber equipped with a double-pass CMA, a LEED optics etc, at BL2B1· where the 'grasshopper' monochromator was installed. The sample was a Si(100) wafer (p-type, B-doped, 10 Ωcm). Cleaning was achieved by heating the sample at >1350K, and was checked by LEED and AES. A commercial getter was used for the evaporation of potassium, and an electrochemical AgCl cell was used for the exposure to chlorine. All spectra were recorded at room temperature. The surface-sensitive absorption spectra were recorded in the Auger electron yield mode with a double-pass CMA, and divided by the photoelectron yield from a gold mesh positioned across the incident light beam in order to eliminate effects due to the transmission function of the monochromator.

Figures 1 show the Si-2p spectra of (a): the clean Si(100) surface, (b): the Si(100) surface covered with a potassium monolayer [denoted as Si(100)/K hereafter], (c): the Si(100) surface with a potassium monolayer and subsequently exposed to chlorine [Si(100)/K/Cl], and (d): the Si(100) surface exposed to chlorine (without a potassium layer) [Si(100)/Cl]. The photon energy was 130 eV and the overall resolution was 0.3 eV. It is noted that both coverages of potassium on Si(100)/K and chlorine on Si(100)/Cl are estimated to be 1 according to previous references. Dots are experimental data, lines are least square fits, and dotted lines are backgrounds. Each component has two peaks due to the spin-orbit splitting. All spectra have components at similar binding energies, which are ascribed to the 'bulk' Si atoms (Si_{bulk}). [Figs. 1(a)-1(d)] Other components are ascribed to the 'surface' Si atoms, and they have different binding energies and shapes. The components denoted as Si_{up} and Si_{down} for the clean surface are assigned to the emissions from the upper atoms and the lower atoms, respectively, of the buckled dimers on the reconstructed Si(100)(2x1) surface [Fig. 1(a)]. The shift of the binding energies from the

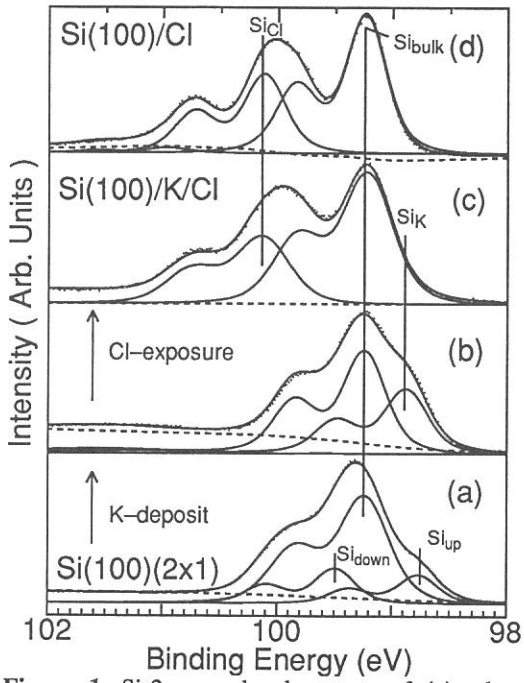

Figure 1. Si-2p core-level spectra of (a): clean Si(100)(2x1), (b): Si(100)/K, (c): Si(100)/K/Cl. (d): Si(100)/Cl. Photon energy was 130 eV.

'bulk' components are ascribed to the charge transfer associated with the reconstruction. The Si_K and Si_{Cl} components for Si(100)/K and Si(100)/Cl are ascribed to the Si atoms bonded to the potassium and chlorine atoms, respectively [Figs. 1(b) and 1(d)]. The shifts of the binding energies for these surface atoms are interpreted to indicate the charge transfer between the substrate atoms (Si) and the adsorbate atoms (K and Cl), which is caused by their different electronegativity. It is noted that the intensity ratio of the surface components to the bulk components observed for Si(100)/Cl is similar to that for Si(100)/K/Cl. Therefore, the coverage of atoms is estimated to be 1 on Si(100)/K/Cl.

For the Si(100)/K/Cl system, the Si_K component which is observed for Si(100)/K is extinguished. The binding energy of the surface components for Si(100)/K/Cl is similar to that of Si_{Cl} component observed for Si(100)/Cl. Thus, it is considered that the configuration of the chemical bond between the Si atom and the Cl atom in the Si(100)/K/Cl system is similar to that in the Si(100)/Cl system, where the atom is bonded to the Si atom via a partially ionized covalent bond.

Figures 2 show K $L_{2,3}$ core-level absorption spectra of (a): Si(100)/K, (b): Si(100)/K/Cl, and (c): plolicrystalline KCl film evaporated on an Au substrate (recorded in the total electron yield mode). The splitting of the main two peaks (2.8 eV) observed in all spectra are ascribed to the spin-orbit interaction. These doublets are ascribed to the transition $2p^6 \rightarrow 2p^5 4s$ and $2p^6 \rightarrow 2p^5 3d$ (not resolved). The peaks observed for Si(100)/K are broad. [Fig. 2(a)] It may be related to the metallic character of the Si(100)/K surface and the formation of 4s and 3d bands on the surface. These peaks are sharpened for Si(100)/K/Cl and are very similar to those of the KCl film. This indicates that the chemical nature of K on Si(100)/K/Cl is similar to that in KCl crystal. Thus, it is considered that K is ionized in the Si(100)/K/Cl system.

These results show that Cl atoms are partially ionized and bonded to Si atoms, and K atoms are ionized in the Si(100)/K/Cl system. The coverages of K and Cl are estimated to be 1:1. It is noted that the (2x1) LEED pattern was observed for Si(100)/K/Cl, indicating that there is a ordered structure on this surface. These results are consistent with the other results of the core-level photoemission spectra (Cl2p, K2p and K3p) , and the Si $L_{2,3}$ absorption spectra. (not shown) Thus, it is concluded that a quasi two-dimensional alkali halide layer is produced on the Si(100)(2x1) surface.

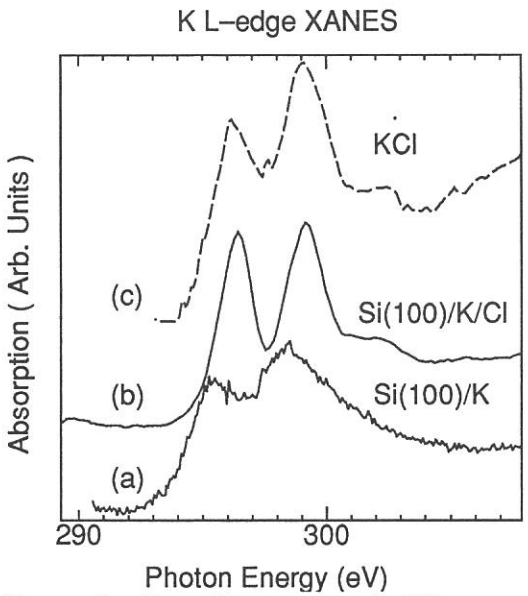

Figure 2. Absorption spectra of K-$L_{2,3}$ core levels for (a): Si(100)/K, (b): Si(100)/K/Cl, and (c): KCl film. (a) and (b) were recorded in the Auger electron yield mode, and (c) were recorded in the total electron yield mode.

DESORPTION OF METASTABLE Ne FROM THE SURFACE OF RARE GAS SOLID BY PHOTON IMPACT

Takato HIRAYAMA*, Akira Hoshino*, Daniel E. WEIBEL*, Ichiro ARAKAWA* and Makoto SAKURAI**

*Department of Physics, Gakushuin University, Mejiro, Tokyo 171
**National Institute for Fusion Science, Chikusaku, Nagoya 464

We have studied the desorption of metastable Ne atoms from thin Ne film on solid Ar, Kr, and Xe by photon impact (photon stimulated desorption: PSD) to reveal the mechanism of the desorption induced by electronic transitions (DIET). Experiments have been carried out using a synchrotron radiation at the beam line BL5B in UVSOR, Institute for Molecular Science. Details of the experimental setup and procedure have been previously described.[1]

Kloiber and Zimmerer[2] have proposed two types of models to describe the desorption of excited neutral atoms; "cavity-ejection (CE)" and "excimer-dissociation (ED)" mechanisms. Because the CE process, where the excited atom is desorbed due to the repulsive force from the surrounding atoms in ground state, strongly depends on the electron affinity (EA) of the matrix, the desorption via CE mechanism is expected to take place in solid Ne and Ar (EA < 0), which was experimentally observed[3,4], but not in solid Kr and Xe (EA > 0). We have investigated the desorption of metastable Ne atoms from thin Ne film on solid Ar, Kr, and Xe to clarify the cavity ejection mechanism.

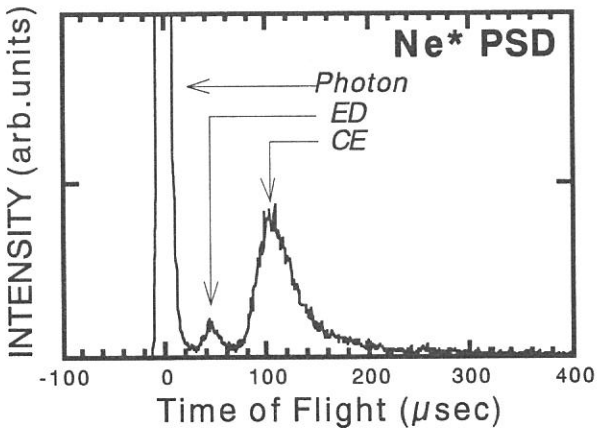

Fig.1. Typical TOF spectrum of Ne metastables desorbed from solid Ne by photon impact.

Figure 1 shows a typical time-of-flight spectrum of desorbed metastable Ne (Ne*) from the surface of solid Ne by photon excitation. Two peaks due to the CE and ED mechanisms are clearly shown in the spectrum together with a photon peak, which is used as an origin of the flight time.

Figure 2 shows a dependence of kinetic energies of Ne* desorbed by the CE mechanism on the thickness of the Ne film on solid Ar, Kr, and Xe at the photon energy corresponding to the 1st order surface exiton. The kinetic energies of the Ne metastables are calculated from the flight time and the flight length. The gradual shift of the kinetic energy to the CE peak energy of pure Ne (0.18 eV) shows that Ne* in the Kr and Xe matrix, whose electron affinities are positive, can desorb from the surface via the CE mechanism.

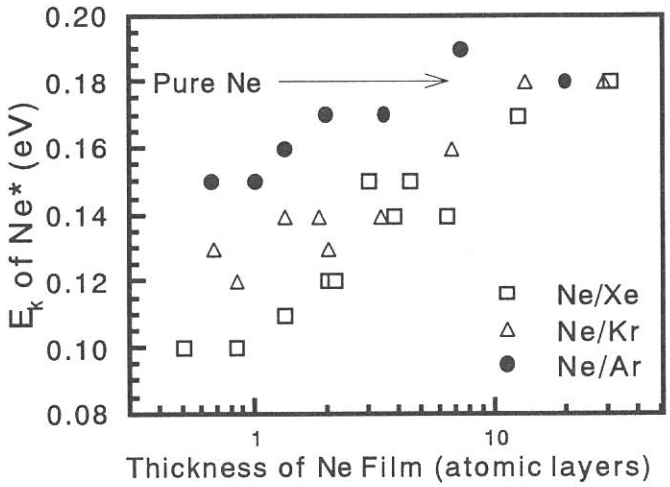

Fig.2. Dependence of kinetic energies of Ne* desorbed through the CE mechanism on the thickness of a Ne film on solid Ar, Kr, and Xe.

REFERENCES

[1]M. Sakurai, T. Hirayama, and I. Arakawa, Hosyakou **5**, (1992) 13. (in Japanese): M. Sakurai, T. Hirayama and I. Arakawa, Vacuum **41**, (1990) 217.

[2]T. Kloiber and G. Zimmerer, Rad. Eff. Def. Sol. **109**, 219 (1988).

[3]F. Colletti, J. M. Debener, and G. Zimmerer, J. Phys. (Paris) Lett. **45**, L467 (1984): T. Kloiber and G. Zimmerer, Physica Scripta **41**, 962 (1990).

[4]I. Arakawa, M. Takahashi, and K. Takeuchi, J. Vac. Sci. Technol. **A7**, 2090 (1989): D. J. O'Shaughnessy, J. W.Boring, S. Cui, and R. E. Johnson, Phys. Rev. Lett. **61**, 1635 (1988)

Time Response of Exited-State Na Desorption from SR-Irradiated Na-Halides

Sayumi Hirose and Masao Kamada
Institute for Molecular Science, Myodaiji, Okazaki 444

Bombardment of solids by energetic electron- or photon-beams causes the ejection of constituent species from the surface. There are numerous studies of the electron-stimulated desorption (ESD) from alkali halides. However few groups have studied the photon-stimulated desorption (PSD) of excited species.[1] The purpose of present study is to get a better understanding of the PSD mechanism. Time response of excited-state Na desorption from SR-irradiated Na-halides has been investigated by using a method of time-correlated single photon counting.

Experiments were performed at a PGM beam line 6A2. The interval of successive SR pulses was 178 ns and the full-width at half-maximum of a bunch was 500 ps. Time response measurements were carried out with a time-correlated single photon counting method. Single crystals were cleaved with a knife edge in sample chamber and were excited with the zeroth-order light through the aluminum film.

Emission spectra of Na halides are composed of the atomic emission (so-called Na D-line) at about 2.1 eV due to the transition from desorbed excited-state Na atoms and broad bands.[2] Therefore, in order to obtain the time response of the excited-state Na desorption, atomic line was separated from the broad band with using the time response data observed at 2.07, 2.10 and 2.14 eV. The results obtained after the separation are shown in figure 1. These time responses are composed of fast and slow components. The fast component is in the time scale of nano-second and the slow component is between 178 ns and 3 ms. The slowest limit was determined with the mechanical chopper method. The time response of ground-state Na atoms has been regarded to be in the scale of μs to ms by Kanzaki et al.[3] and Loubriel et al.[4]. Kanzaki et al.[3] have observed the decay time and the temperature dependence of PSD of neutrals from alkali halides, and proposed that the desorption process of ground-state alkali atoms is related to the diffusion of Vk centers and the surface reaction of F centers and alkali ions. Loubriel et al.[4] have studied the time dependence of ESD of ground-state Li from LiF, and explained the persistence of the Li emission in terms of the slow diffusion of bulk F centers. From the comparison between the time response of excited- and ground-state alkali desorption, the slow component of excited-state alkali desorption is seemed to be

in the time scale of ground-state alkali desorption. Therefore, the slow desorption of excited-state alkali atoms may be due to the same mechanism as that of ground-state alkali atoms. On the other hand, the fast component of excited-state alkali desorption is in the time scale of nano-second, and so the fast desorption may be related to the lattice defect formation (for example STE, F-H pair formation, and so on) due to the electronic excitation in the surface layer and the charge transfer to alkali ions.

It should be noted that the time response of NaF (Fig. 1a) is much different from that of NaCl (Fig. 1b). That is, the ratio of fast and slow components is about 1.5 and 3 for NaF and NaCl, respectively. The decay time of fast component of NaCl is 1.2 times larger than that of NaF. These differences may be related with the substance dependence reported previously.[2)]

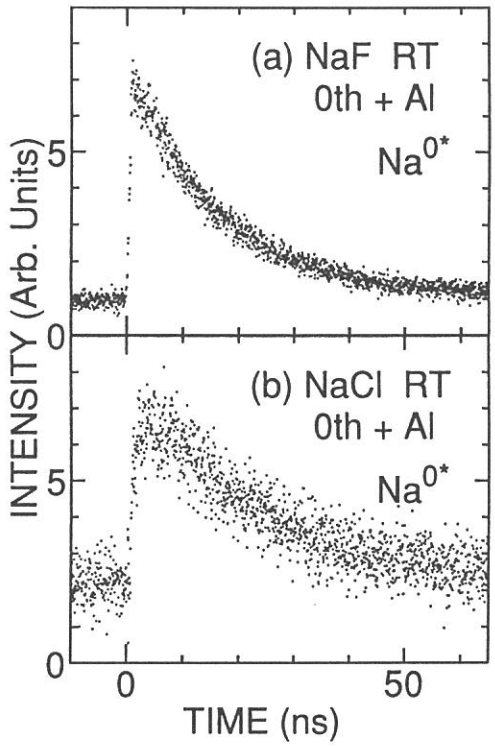

Fig.1 Time response of excited-state Na atom desorption from NaF (a) and NaCl (b) excited with the zeroth-order light through the aluminum film at room temperature.

References

1) Desorption Induced by Electronic Transitions (DIET IV), edited by G. Betz and P. Varga (Springer, Berlin, 1990).

2) S. Hirose and M. Kamada, J. Phy. Soc. Jpn., 60, 4376, (1991)

3) H. Kanzaki and T. Mori, Phys. Rev. B29, 3573 (1984)

4) G. M. Loubriel, T. A. Green, N. H. Tolk and R. F. Haglund, Jr., J. Vac. Sci. Technol. B5, 1514 (1987)

THERMAL AND PHOTODECOMPOSITION OF IRON PENTACARBONYL ADSORBED ON TITANIUM AND OXIDIZED TITANIUM SURFACES

Masahiko MOROOKA*, Sadao HASEGAWA*, Tadashi HASEGAWA*, Shosuke TERATANI*, Shinri SATO**, and Yuji UKISU**

**Department of Chemistry, Tokyo Gakugei University, Koganei, Tokyo 184, Japan*
***Institute for Molecular Science, Myodaiji, Okazaki 444, Japan*

Irradiation of iron pentacarbonyl, $Fe(CO)_5$, adsorbed on solid surfaces leads to formation of a variety of products depending on the type of surface.[1] On insulator surfaces, a dimer or a trimer of $Fe(CO)_5$ is formed depending on acid-base property of the surface, while complete photodecomposition occurs at room temperature on semiconductor or metal surfaces.[1] To study a detailed mechanism of the photolysis of $Fe(CO)_5$ adsorbed on metal surfaces, a reaction intermediate has been investigated by a low-temperature adsorption method using IR reflection absorption spectroscopy (IRAS), X-ray photoelectron spectroscopy (XPS), and temperature programmed desorption (TPD) technique.

In the present study a Ti polycrystal plate was used as a substrate. Since Ti oxides show the property of semiconductor, the Ti sample was oxidized in oxygen at 1000K and then used as another substrate to examine a difference in a reaction mechanism between metal and semiconductor surfaces. All the experiments were conducted in the UHV chamber of BL-4A, which had been constructed for the study of surface photochemistry[2]. Because surface impurities give crucial effects on the adsorption state of $Fe(CO)_5$, the sample surface was cleaned by repeating Ar ion sputtering at 673K for 1 hr followed by annealing at 900K for 5 min. SOR light was passed through a sapphire filter which cutoff wavelength is ca. 150 nm. The coverage of $Fe(CO)_5$ on the surface is about monolayer unless otherwise stated.

It is very important to examine adsorption states of reactants in surface photochemistry, since electronic states as well as geometrical structure of adsorbed molecules are often quite different from those observed in the gas phase. Fig. 1 shows the C_{1S} XPS spectra of $Fe(CO)_5$ adsorbed on a clean Ti surface at 100K: The peaks at the binding energies of 282, 286, and 288eV are assigned to the carbons of carbide, carbonyl in subcarbonyl species, and carbonyl in $Fe(CO)_5$, respectively.[3] This result indicates that $Fe(CO)_5$ adsorbed directly on Ti undergoes thermal decomposition even at 100K to form partially decarbonylated species, $Fe(CO)_{5-x}$ (x = 1 - 4), and carbide. The formation of carbide implies thermal dissociation of CO released from $Fe(CO)_5$ and therefore remarkable reactivity of a Ti surface. Fig. 1 also shows temperature dependence of the C_{1S} spectrum; adsorbed $Fe(CO)_5$ decomposes further with rise in temperature. Fig. 2 shows the thermal desorption spectra recorded after the adsorption of $Fe(CO)_5$ on the clean Ti sample. The solid line denotes CO^+ produced from $Fe(CO)_5$ and CO in a quadrupole mass spectrometer, and the dotted line Fe^+ exclusively from $Fe(CO)_5$. The peaks below 120K is due to the desorption from a heater of the sample holder. Because these spectra involve contribution from the back of sample, which was not cleaned by Ar ion sputtering, the desorption peak of $Fe(CO)_5$ at ca. 150K is attributable to the

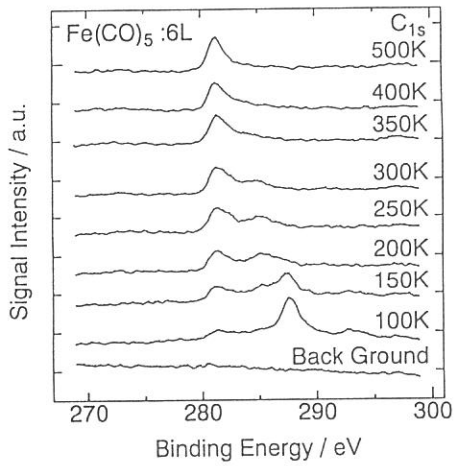

Fig. 1. C1s XPS spectra of $Fe(CO)_5$ adsorbed on the Ti sample.

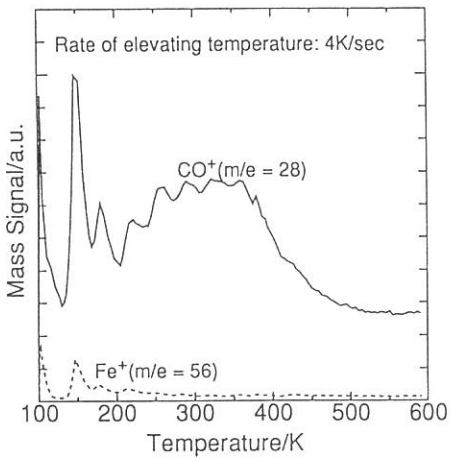

Fig. 2. Thermal desorption spectra of $Fe(CO)_5$ adsorbed on the Ti sample.

uncleaned surface, on which $Fe(CO)_5$ physisorbs. The $Fe(CO)_5$ desorption peak at ca. 180K is ascribable to physisorbed $Fe(CO)_5$ which may exist on a carbided surface produced by thermal dissociation of carbonyl. The multiple desorption peaks of CO at temperatures above 200K arise from decomposition of decarbonylated (intermediate) species, and suggest that various states of the intermediate species are yielded. The IRAS spectrum of adsorbed $Fe(CO)_5$ (not shown here) exhibits a single CO stretching band, suggesting that a trigonal-bipyramidal form in the gas phase is changed to a square pyramidal form on the surface, and the broad shoulder in lower frequencies is indicative of the presence of decarbonylated species. With rise in temperature the main band assignable to physisorbed $Fe(CO)_5$ disappears below 180K in agreement with the result of TPD.

Irradiation of the adsorbed $Fe(CO)_5$ with SOR (>150 nm) light leads to evolution of CO, but no photodesorption of $Fe(CO)_5$ was observed. XPS, IRAS, and TPD spectra show that physisorbed $Fe(CO)_5$ rapidly undergoes photo-decarbonylation to form partially decarbonylated intermediate. When the substrate is heated, the intermediate species shows similar behaviors to the thermally decarbonylated species. Neither composition nor geometry of the photo-product, however, has been determined since the decarbonylated species produced by thermal decomposition already presents too much on the surface. To avoid the thermal decomposition of $Fe(CO)_5$, the Ti sample was oxidized. After the oxidation, TPD analysis shows that the thermal decarbonylation is greatly suppressed, while IRAS indicates that the adsorption state of $Fe(CO)_5$ is quite different from that observed for metal surfaces. Further investigation is under progress.

References

1) S. Sato, Hyomen Kagaku, **13**, 225(1992).

2) S. Sato, Y. Ukisu, E. Nakamura, T. Kinoshita, A. Hiraya, and M. Watanabe, UVSOR Report 11(1991).

3) S. Sato and Y. Ukisu, Surf. Sci., in press.

Photodecomposition of Iron Pentacarbonyl Adsorbed on Silver Surfaces

Yuji UKISU, Hisashi OGAWA, and Shinri SATO
Institute for Molecular Science, Myodaiji, Okazaki 444, Japan

Surface photochemistry of organometallic compounds has received increasing attention because of its application to production of a variety of functional materials. For a deeper understanding of a mechanism of surface photochemical reactions, information on structure and geometry of adsorbed molecules becomes indispensable. This paper reports observation of the photolysis of iron pentacarbonyl adsorbed on silver surfaces using IR reflection absorption spectroscopy (IRAS), temperature-programmed desorption (TPD) technique and X-ray photoelectron spectroscopy (XPS).

Experiments were done with a UHV chamber at BL-4A.[1] Silver samples used were a polycrystalline plate and cleaned by Ar ion sputtering. Monolayer coverage was achieved by 6-8 L dosing of $Fe(CO)_5$ (L = Langmuir, 10^{-6} torr/sec). SOR light was irradiated to the sample through a sapphire or glass cutoff filter.

Figure 1 shows the IRAS spectra of $Fe(CO)_5$ adsorbed on Ag surface at 100 K before and after irradiation of SOR (>150 nm) light at different coverages. In the spectrum after irradiation at coverages below monolayer, a new C-O stretching band due to subcarbonyl species assignable to $Fe(CO)_4$ or $Fe(CO)_3$ is observed at lower frequencies. In multilayer $Fe(CO)_5$, the photolysis leads to appearance of a broad band at higher frequencies, indicating formation of oligomers such as $Fe_2(CO)_9$ and $Fe_3(CO)_{12}$.

Figure 2 shows TPD spectra of CO^+(m/e=28) before and after the photolysis. A desorption peak at around 180 K is due to the desorption of physisorbed $Fe(CO)_5$ in multilayer and peaks above 200 K are attributable to the thermal decarbonylation of adsorbed species bound strongly to the surface and photoproducts. The average composition of photoproducts can be estimated from a change in peak areas between the low and high temperature peaks, and the result shows that the CO/Fe ratio is about 4 at nearly monolayer coverage and decreases to less than 3 with further increase in coverage, indicating the extent of photo-decarbonylation depends upon coverages.

XPS spectra of C_{1s}, O_{1s} and Fe_{2p} (Fig.3) show that their binding energies shift to lower energies after irradiation. This indicates again formation of subcarbonyl species. From the comparison of peak areas of C_{1s} and Fe_{2p}, the photoproduct is assumed to be $Fe(CO)_4$. After heating up to 330 K, C and O signals disappear and deposition of Fe metal is observed.

We conclude that an intermediate of the photolysis is $Fe(CO)_4$ stabilized due to strong interaction between the carbonyl ligands and the surface, and the intermediate undergoes further photo-decarbonylation to form oligomers at multilayer coverages.

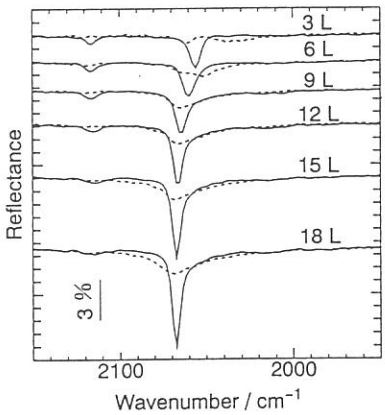

Fig.1. IRAS spectra of $Fe(CO)_5$ adsorbed on Ag at different coverages before (solid line) and after (dotted line) irradiation (>150 nm) for 10 min.

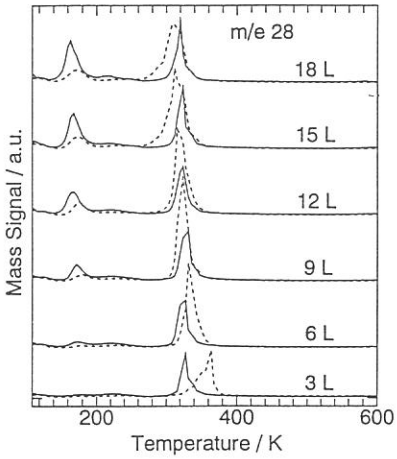

Fig.2. TPD spectra of CO^+ (m/e=28) from $Fe(CO)_5$ adsorbed on Ag at different coverages before (solid line) and after (dotted line) irradiation (>150 nm) for 10 min.

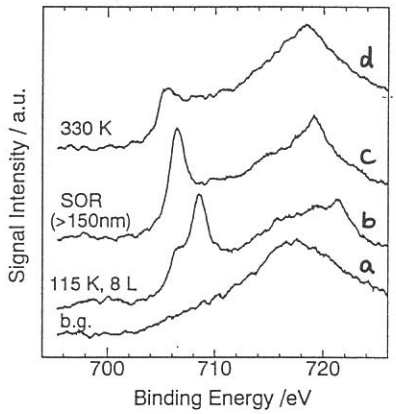

Fig.3. XPS Fe_{2p} spectra of $Fe(CO)_5$ adsorbed on Ag; (a) before adsorption; (b) after 8 L dosing; (c) after irradiation (>150 nm) for 30 min; (d) after heating to >330 K.

References

1) S.Sato, Y.Ukisu, E.Nakamura, T.Kinoshita, A.Hiraya, and M.Watanabe, UVSOR Activity Report, p.11 (1991).

SYNCHROTRON RADIATION EXCITED ETCHING OF SILICON SURFACE STUDIED BY VELOCITY DISTRIBUTION MEASUREMENTS OF DESORBED SPECIES

Haruhiko OHASHI, Kiyohiko TABAYASHI and Kosuke SHOBATAKE

Institute for Molecular Science, Myodaiji, Okazaki 444, Japan

The neutral species desorbed from the surface in the etching reaction of crystalline Si(100) have been identified from the measurements of their velocity distributions using a time-of-flight (TOF) technique combined with an electron bombardment ionization mass spectrometry. The preliminary measurements of the velocity distributions indicate that the desorbed species formed in the etching reactions of Si with XeF_2 are essentially identical for the undulator on and off although irradiation of synchrotron radiation (SR) promotes the etching reaction.

In the present study very reactive etchant XeF_2 gas was used to avoid the etchant gas pressure to exceed 1.0×10^{-4} Torr in the reaction chamber and yet to supply enough F atoms to the surface. The schematics of the apparatus is shown in Fig. 1.

The reaction chamber is connected to the undulator beam line BL3A1. The gap length of the undulator magnets was 60 mm where the peak energy of the 1st order light is 35.8 eV. The incident angle of the undulator light was 75 degrees and the species desorbing into the direction of 15 degrees were monitored. The undulator beam is perpendicular to the axis of quadrupole mass filter. The desorbed species enters the chopper chamber through an aperture. A molecular beam of the desorbed species which is modulated with a correlation copper enters the mass spectrometer chamber. The beam molecules are

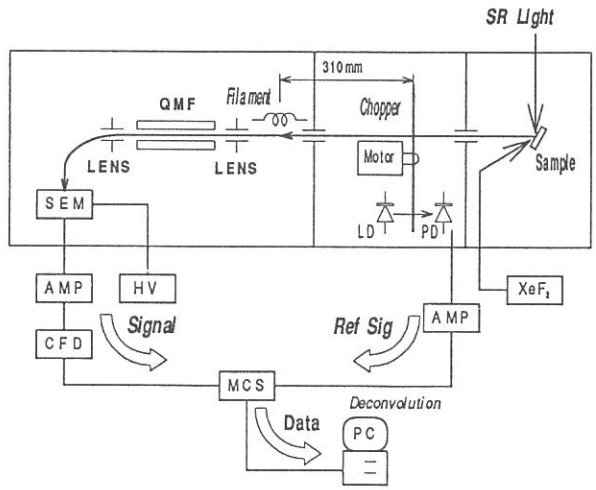

Fig.1 Schematic of the apparatus for the measurements of the velocity distributions of the desorbed species formed in the etching reaction of SiO_2 and Si with XeF_2.

detected by an electron bombardment ionization quadrupole mass spectrometer. Since the ion energy is much larger than the thermal translational energy of the neutral species, the time spent from the moment of a neutral species passing the chopper to that of ion detection is essentially equal to the neutral flight time (from the chopper to the ionizer). The flight length from the chopper to the ionizer was 31.0cm.

The velocity distributions of the desorbed species from the substrate surface were measured at masses m/e = 47, 66, 75, and 85 with the undulator beam on and off. From the TOF distributions of the desorbed species we conclude that the only products with relatively heavy masses M > 100 are desorbed. The typical TOF spectra measured at ion mass m/e = 85 (SF_3^+) with SR on and off are illustrated in Fig. 2. The substrate was kept at room temperature (27℃) and the XeF_2 pressure was at 1.1×10^{-5} Torr. The solid lines are the calculated Maxwell-Boltzmann distributions with a functional form in the time space for the neutral flight time $t = L/v$:

$$F(t)\propto\left(\frac{v}{\alpha}\right)^4 \exp\left(-\left(\frac{v}{\alpha}\right)^2\right)$$

where α is the most probable velocity $\alpha = \{2RT/M\}^{1/2}$ for translational temperature T = 300 K and a neutral mass M = 104 which corresponds to SiF_4. If a mass of the desorbed species M = 85 (SiF_3) is assumed the calculated distribution does not fit well to the observed one. From the results mentioned above we conclude that the parent molecule detected at m/e = 85 is not SiF_3 but SiF_4 even for the beam on. This is an important observation since the species desorbed from the surface on a repulsive potential energy surface or kept at a higher temperatures than room temperature just after photoexcitation, can exhibit a velocity distribution for T higher than the room temperature. In fact from Fig. 2 one finds that 1) the distributions for the beam on and off are basically identical with each other except for the higher intensity for the SR beam on, and 2) the product intensity is higher for the SR beam on than for the beam off within the experimental error.

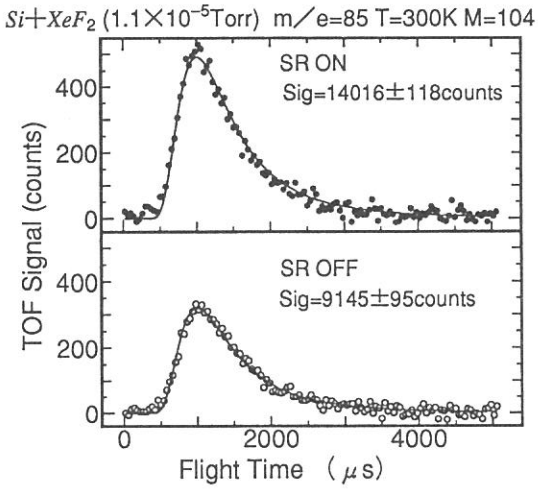

Fig.2 TOF spectra of desorbed species detected at mass m/e = 85 with SR beam on and off. The solid curves corresponds to calculated Maxwellian for mass M = 104.

Synchrotron radiation assisted epitaxial growth of compound semiconductor using metalorganic sources

Hiroshi OGAWA, Mitsuhiro NISHIO, Makoto IKEJIRI,
Toshihiro OGATA, and Akira YOSHIDA*

Department of Electronic Engineering, Faculty of Science and Engineering, Saga University, 1 Honjo, Saga 840, Japan
*Institute for Molecular Science, Myodaiji, Okazaki 444, Japan

The synchrotron radiation (SR) seems to provide a new light source in low-temperature growth process. In order to demonstrate its usefulness, we have investigated the growth of ZnTe, which is a II-VI compound semiconductor. In this report, we describe the first successful growth of compound semiconductor using metalorganic sources by the SR irradiation.

The apparatus used in the present experiment is illustrated schematically in fig. 1. This apparatus was connected with the differential pumping chamber system in the beam line BL-8A of UVSOR facility at Institute for Molecular Science. Diethylzinc and diethyltelluride were used as source materials. As a carrier gas, hydrogen was employed. The substrate was (100) oriented GaAs. The growth was carried out in the same manner as previously reported[1] except that the substrate holder was not heated. That is, the introduction of source gases into the chamber, formation of adsorbed layer and decomposition of adsorbed source molecules by the SR iradiation (one cycle for growth) were repeated.

Figure 2 shows the microphotograph of the film deposited on the substrate and the corresponding result measured with a surface-roughness meter. The film has a relatively smooth and featureless surface morphology. The boundary between the film is estimated to be 1000 to 1500 A. This value corresponds to 5 to 8 A/cycle in average, implying the surprising slow growth of atomic layer order.

Both the Zn 2p core level XPS signal and the Te 3d signal were distinctly observed in the grown layer, showing that the film is ZnTe.

Until the growth exceeds 15 cycles, the RHEED pattern of the film exhibits streak pattern. The pattern changes to the spotty one after 15 cycles and then retains it through the experiment. Figure 3 shows the RHEED pattern (20 keV, [011] azimuth) of ZnTe film on (100) GaAs substrate when the number of growth cycles is 190. The distinct and clear spot pattern clearly shows the single crystalline film and excellent crystallinity. Furthermore, as shown in fig. 3b, the array of diffraction spots confirms the epitaxial layer.

The substrate temperature rise due to the SR irradiation itself is probably negligible because of the use of low power less than 0.3W and

the intermittent introduction of SR light. Hence, it can be concluded that the SR irradiation offers the epitaxial growth at room or low temperature using metalorganic sources.

1)H. Ogawa, M. Nishio and M. Ikejiri, UVSOR activity report (1992).

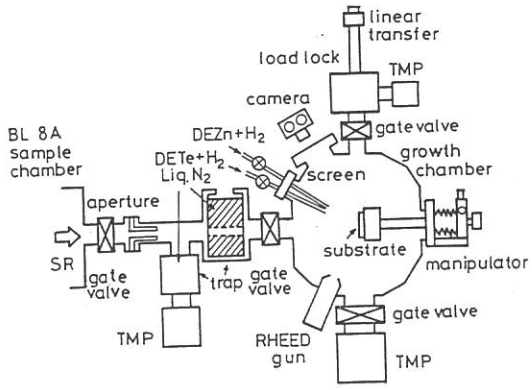

Fig. 1. Schematical experimental apparatus.

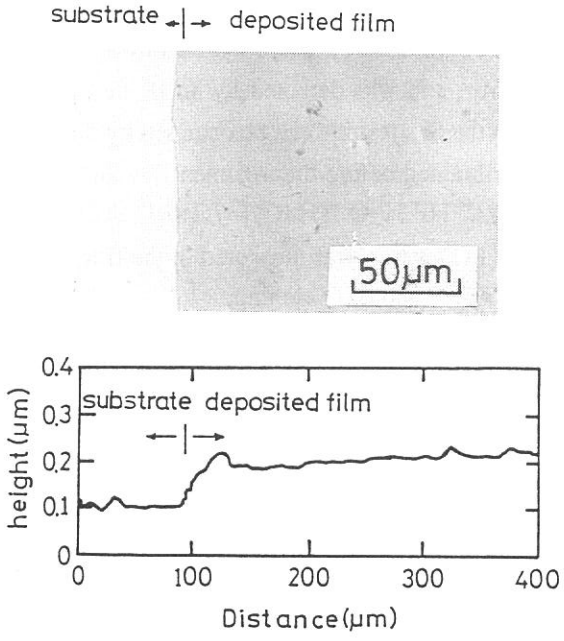

Fig. 2. The microphotograph of the film deposited on the substrate and the result measured with surface roughness meter.

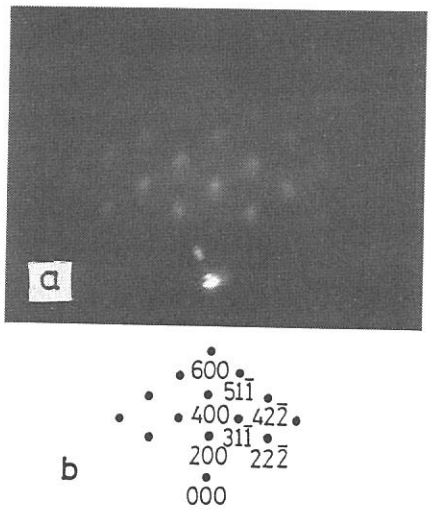

Fig. 3. A typical RHEED pattern of the deposited film (a), and the array of the diffraction spots expected for ZnTe crystal with an (100) surface (b).

OPTICAL CHARACTERIZATION OF Si SURFACE BY HIGH-SENSITIVITY INFRARED REFLECTANCE SPECTROSCOPY

Masanori OKUYAMA, Masahiro NISHIDA, Junko IZUMITANI, Takeshi KANASHIMA

Department of Electrical Engineering, Faculty of Engineering Science, Osaka University, Toyonaka, Osaka 560, Japan

Atomic bondings and morphology on the Si surface have attracted much attention with respect of microfabrication of Si integrated devices, because Si atomic layer steps and/or oxide on the Si surface change the electrical properties of the prepared Si or SiO_2 film, and affect basic characteristics of the fabricated devices. High-sensitivity infrared reflection spectroscopy has a sufficient sensitivity to give detailed information about the chemical state of the substrate and deposited film during in-situ deposition. We investigated Si(111) surface in-situ using high-sensitivity infrared reflection spectroscopy, and studied the surface reaction and atomic condition of Si treated with O_2 or H_2 gas and wet etching with and without irradiation in a vacuum chamber.[1)]

A Si wafer of 4-inch diameter was supported in a vacuum chamber of 500 mm ϕ diameter and 400 mm length. An infrared beam from a fourier-transformation infrared (FT-IR) spectrometer was concentrated by a concave mirror and applied to the Si wafer through a window plate in a vacuum chamber. The reflected infrared beam exited through the other window, was concentrated by a focusing mirror, and was detected by an IR detector. The absorption induced by species and molecules on the Si substrate can be obtained by dividing the spectrum measured after the treatment by that obtained before the treatment. A Si(111) wafer was etched with 5% HF solution or BHF(NH_4F:HF:H_2O:NH_4OH=7:1:6:1) solution after RCA cleaning. Reflectance spectrum of the Si(111) wafer was measured in the film treated at 200°C in 5Torr O_2 ambience for 100min after 5%HF and BHF etching.

Three main absorption peaks are found in the spectrum, and are attributed to absorptions corresponding to SiO stretching (~1080cm^{-1}), SiOH deformation (~950cm^{-1}) or SiO bending (~840cm^{-1}). Intensities of the three peaks as a function of O_2 treatment time are shown for the film etched by BHF in Fig.1. Obvious steplike increases in the absorption intensities may indicate a process of layer-by-layer oxidation. The plateaus in the steplike behavior are seen more clearly and their values are smaller in the sample etched with BHF in comparison to that with 5%HF. It is considered that there are many atomic steps on the Si (111) substrate surface after 5%HF or BHF solution etching. The terraces on the Si surface are well passivated with strong chemical Si-H bonds. Although a part of the Si on the terrace can be oxidized vertical to the substrate surface, it is difficult to oxidize Si on the terrace because of formation of monohydrides. Oxygen can attack reactive sites, such as step edges and dislocations, whose chemical bondings are weak. The nearest neighbor atoms to the oxidized

atom are also attacked easily by oxygen due to the stress. The surface layers of Si parallel to the substrate surface suffer stress from oxidized neighbor atoms and are oxidized more easily than those vertical to the substrate surface. Deeper Si layers require more time for oxidation than shallower layers due to the difficulty of oxygen diffusion. Then, one layer of the substrate surface is oxidized and becomes quasi-stable till oxygen's next attack. A consequent delay in oxidation occurs, and causes the plateaus shown in Fig.1. Moreover, Fig.1 indicates that the plateaus obtained in the surface etched by BHF are longer than those etched by 5%HF; thus, the surface treated by the BHF etching is flatter atomically than that by the 5%HF.

Si wafers were irradiated by UVSR to study photochemical reaction for hydrogen termination and Si oxidation. Absorption peaks of Si-O(~1080cm^{-1}) was not changed by irradiation of UVSOR light in O_2 or H_2 ambient. Figure 2 shows spectral change induced by UVSOR irradiation in H_2 ambient. Si-H absorption on Si(~ 2070cm^{-1}) and Si-H absorption in SiO_2 film(~2270cm^{-1}) increase with inceasing irradiation time in H_2 ambient. H_2 is dissolved by the UVSOR irradiation and becomes to proton(hydrogen ion). This proton might increase hydrogen terminating Si, and also get into SiO_2 layer easily.

References
1) M. Nishida, Y. Matsui, M. Okuyama and Y. Hamakawa: to be published in Jpn. J. Appl. Phys.

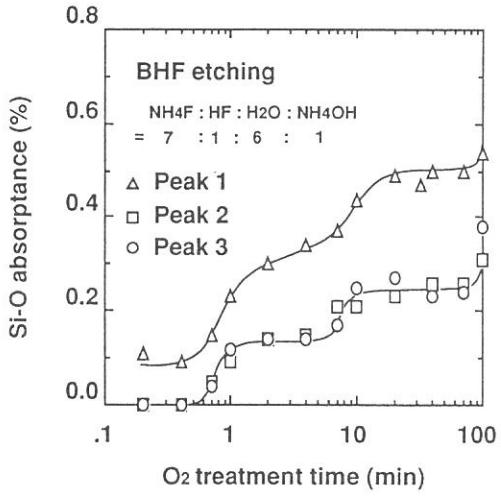

Fig. 1. Intensities of three absorption peaks as a function of oxidation time. Si wafers were etched with BHF. Circles, squares and triangles are absorption intensities at ~840cm^{-1}, ~950cm^{-1} and ~1080cm^{-1}, respectively.

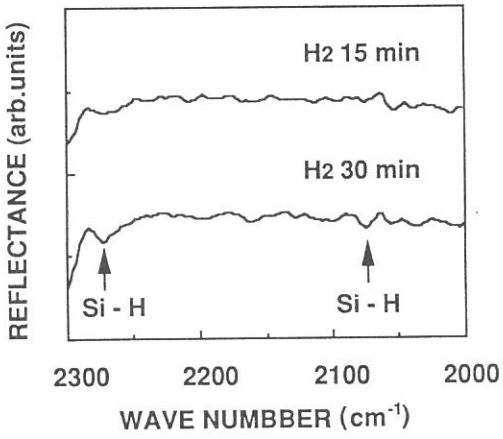

Fig. 2. Relative reflectance spectra of Si surface irradiated in H_2 ambient for 15 and 30 min by direct light of UVSOR.

FABRICATION OF SILICON FILMS USING UNDULATOR RADIATION

Masahiro TOMIDA, and Akira YOSHIDA*

Toyohashi University of Technology, Toyohashi 441
*Institute for Molecular Science, Okazaki 444

Undulator radiation(UR) emitted from a mulipole wiggler is qusi-monochromatic and contains vacuum-ultraviolet light which is suitable to decompose the material gases in semiconductor industry. Therefore, it is a promising light source in phto-CVD(chemical vapor deposition) for future LSI processing. However, there are few reports on phto-CVD utilizing UR. We have fabricated silicon films for the first time using UR as a light source. In this report, the experimental results of UR-CVD of silicon thin films are presented.

<EXPERIMENTAL>

The experiments were carried out at BL3A1 in UVSOR. The undulator gap was adjusted to 45, 60, and 75 mm :the fundamental lines of photon energy are 19, 36, 50 eV, respectively. The experimental apparatus consists of a differential pumping system that prevents any gases from flowing into the beam line, and of a growth chamber. A nickel mesh was installed 10 mm away over the substrate. Substrates were Si wafers and glass. Disilane gas was introduced to the growth chamber. The flow rate was 2 sccm through a mass flow controller and the growth pressure was kept at 15 mTorr. The substrate temperature was varied from room temperature to 100 ℃.

<RESULTS>

The photograph of the film is shown in Fig. 1. The film was deposited only at the irradiated areas, suggesting that surface reactions dominant. Moreover, some small fringes were found inside each squares. This is due to Fresnel diffraction in which the mesh acts as a slit.

A typical result of Auger electron spectroscopy(AES) is given in Fig. 2. The Si(LVV) peak at 92 eV and Si(KLL) peak at 1619 eV are observed. The contamination due to carbon and oxygen is not found.

Fig. 3 shows the temperature dependence of the growth rate. From this result, the growth rate decreases as the substrate temperature increases:i.e., the actviation energy is apparently negative. This fact suggests that the depositon is due to adsorption-controlled process.

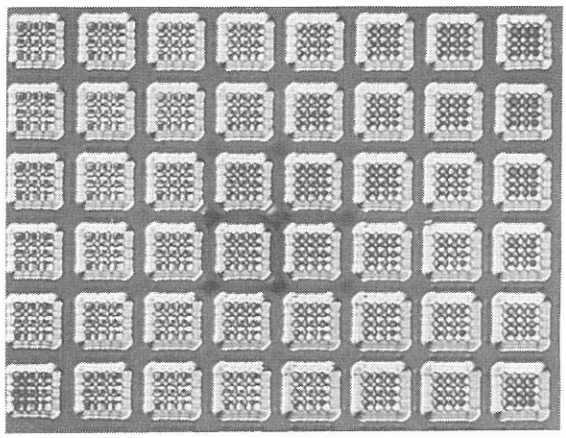

Fig. 1. Photograph of silicon film deposited on glass. The substrate temperature was 25℃, and UR gap was 45 mm.

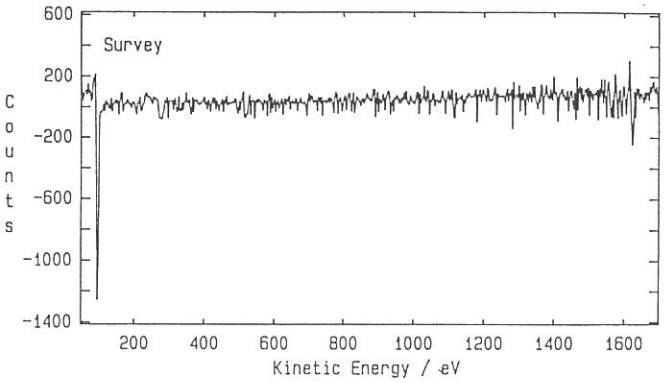

Fig. 2. AES spectra of the specimen deposited on Si at room temperature. UR gap was 60 mm.

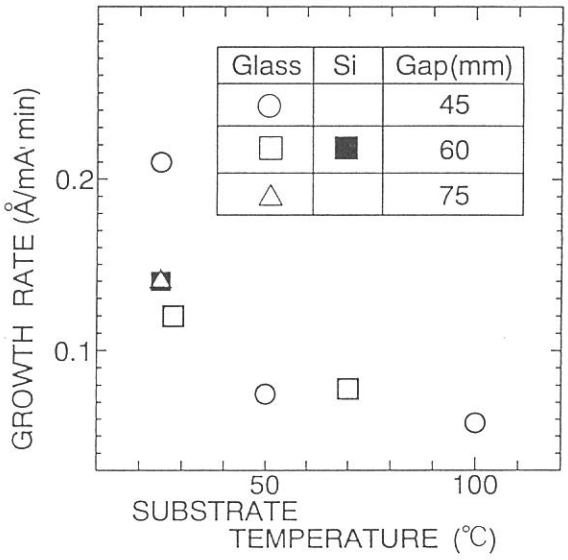

Fig. 3. Substrate temperature dependence of growth rate.

Reflectance of Multilayer Gratings in the Soft X-ray Region

Eiji ISHIGURO, Tsutomu KAWASHIMA, Koujun YAMASHITA*, Hideyo KUNIEDA*, Yuzuru TAWARA*, Takashi YAMAZAKI*, Hidenori YOSHIOKA*, Akihiro FURUSAWA*, Kuninori SATO#, Masaru KOEDA$, Tetsuya NAGANO$ and Kazuo SANO$

Department of Applied Physics, Osaka City University, Sumiyoshiku, Osaka 558
*Department of Physics, Nagoya University, Chikusaku, Nagoya 464-01
#National Institute for Fusion Science, Chikusaku, Nagoya 464-01
$Optical Devices Dept., Shimadzu Corporation, Kyoto 604

The reflectance for a laminar Pt/C multilayer grating has been measured in the region from 1.2 keV to 2.8 keV by using monochromatized light from a crystal monochromator in the BL7A beamline of UVSOR. The grating comprises 10 layers of Pt and C with 2d=100 Å on a SiO_2 laminar grating which was produced by means of a holographic exposure and reactive ion-beam etching. The groove density was 1200 l/mm and the groove depth 100 Å.

Examples of angular distributions of diffracted light for various incident angle at the photon energy of 1.2 keV are shown in Fig.1. It can be seen that the intensities of the m=0,+1, and −1 spectral orders vary depending on the incident glancing angle. In Fig.2(a), the reflectance of each order are plotted as a function of the glancing angle, together with the total reflectance measured with a detector having a large acceptance angle and that of a multilayer mirror which was fabricated at the same time when the multilayer was deposited on the grating. A high total reflectance at the glancing angle less than 2 deg. are due to the total reflection of Pt, and a peak around the glancing angle of 5.8 deg. to Bragg reflection of the multilayer.

The dependence of the reflectance of the spectral orders in the Bragg peak on the glancing angle can be qualitatively interpreted by a kinematical theory of multilayer gratings[1];

$$I=\frac{1}{N^2}\frac{\sin^2\{N\pi D/\lambda(\cos\theta-\cos\theta')\}}{\sin^2\{\pi D/\lambda(\cos\theta-\cos\theta')\}}\times\frac{1}{M^2}\frac{\sin^2\{M\pi d/\lambda(R_\theta\sin\theta-R_\theta\sin\theta')\}}{\sin^2\{\pi d/\lambda(R_\theta\sin\theta-R_\theta\sin\theta')\}}$$
$$\times\left|\frac{1}{D}\int_0^L\exp\{2\pi ix(\cos\theta-\cos\theta')/\lambda\}dx\right|^2 \qquad (1)$$

The symbols in this formula are referred to the reference (1). Fig.2(b) shows a comparison of the experimental results in the Brag region with those calculated from eq.(1).

The maximum reflectance of m=0, +1 and −1 order in the Bragg region were 6.4 %(5.8°), 1.8 %(5.7°) and 1.6 %(6.2°), respectively, at E=1.2 keV, 9.0 %(4.1°),2.1 %(4.3°) and 1.6 %(4.3°) at E=1.7 keV, 6.4 %(3.5°), 1.2 %(3.3°) and 1.3 %(3.2°) at E=2.0 keV, and 8.8 %(2.5°), 1.5 %(2.2°) and 1.4 %(2.0°) at E=2.8 keV.

Reference

1)W.K.Warburton, Nucl.Instrum. and Methods A291, 278 (1990)

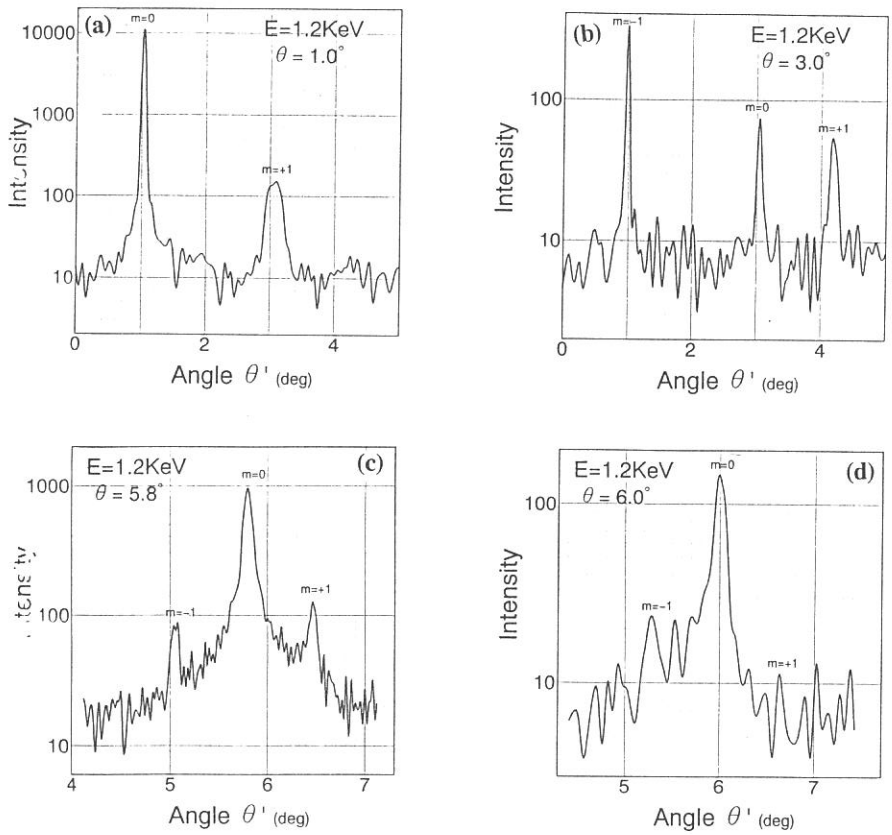

Fig.1 Angular distribution of diffracted light from a multilayer grating for various incident glancing angles θ at the photon energy of 1.2 keV.

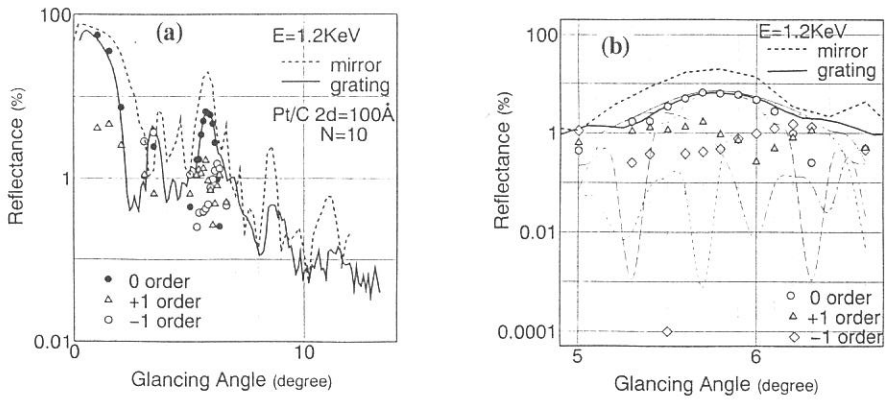

Fig.2 Reflectance of the m=0, +1 and −1 spectral orders as a function of the , incident glancing angle, together with the total reflectance of the grating(——), and that of a multilayer mirror(----). The Brag peak around the glancing angle of 5.8° is shown in an enlarged scale in fig.(b) for a comparison with theoretical results of eq.(1) for the reflectance of m=0( ), +1( ), and −1( ).

Heat Load Resistivity of SiC Gratings for High-Power Synchrotron Radiation

Eiji ISHIGURO, Makoto SAKURAI[1], Hideki MAEZAWA[2], Mihiro YANAGIHARA[3], Makoto WATANABE[4], Masaru KOEDA[5], Tetsuya NAGANO[5], Kazuo SANO[5], Yasuhiro AKUNE[6] and Kichiya TANINO[6]

Department of Applied Physics, Osaka City University, Osaka 558

[1]Department of Physics, Kobe University, Kobe 657

[2]National Laboratory for High Energy Physics, Ibaraki 305

[3]Research Institute for Scientific Measurements, Tohoku University, Sendai 980

[4]Institute for Melecular Science, Okazaki 444

[5]Shimadzu Corporation, Kyoto 604

[6]Nippon Pillar Packing Co., LTD., Hyogo 669-13

High resistivity against the heat load of synchrotron radiation is required for diffraction elements in grating monochromators which will be installed in VUV and soft x-ray beam lines of a high-brilliance next-generation storage ring. It has been reported that SiC gratings withstand high power beam emitted from an undulator.

We fabricated ion-beam etched SiC gratings and examined them about the resistivity against radiation from a multipole wiggler (EMPW #28) installed on the Photon Factory storage ring. High quality of surface finish is essential, and CVD-b SiC is considered to be one of the best mirror materials. We have developed CVD-SiC in which individual grains are strongly oriented to the (220) plane. For the fabrication methods, crystallographic orientation, polishability and etching characteristics of CVD-SiC, we described in detail elsewhere[1].

Diffraction efficiencies of two SiC gratings with groove density of 1200 l/mm were measured by using monochromatized lights in the region of 17-300 Å from a plane grating monochromator installed at the BL5B of UVSOR. One (#1) has a groove depth of 75 Å and a width-to-spacing ratio of 0.33 and the other (#2) a groove depth of 100 Å and a width-to-spacing ratio of 0.45. Through the wavelength region in the present experiment, the maximum efficiencies of the +1 order are 5-20 % for the gratings coated with Au.

The grating #1 without coating and the grating #2 coated with Au of 200 Å thickness were tested for the radiation of EMPW #28. The comparison of diffraction efficiency between Au coated and without coating revealed that the coating improves it especially just over C-K and Si-L edges. The total power which the grating absorbed was 277 W and the power density at the center of the wiggler beam was estimated to be 2.7 W/mm^2. No visible damage was observed for the grating #1, on the other hand a discoloration was observed in a limited portion around the center of irradiation for the grating #2 (Fig. 1). SEM photographs of both gratings clearly show the difference in thermal strength (Figs. 2 and 3). No deformation of the grooves was found for the grating #1, however, the grooved pattern of the grating #2 can hardly be recognized after irradiation for 40 min.

Figure 4 shows angular distributions of the diffraction light for the both gratings. The efficiencies of the grating #2 can be regarded to be unchanged after irradiation, as well as for the grating #2. However, increase of the scattered light components was observed for the grating #2 irradiated for 40 min. This is due to the disappearance of the groove pattern in the central part and relatively large deformation of the Au layer in the portion except the center.

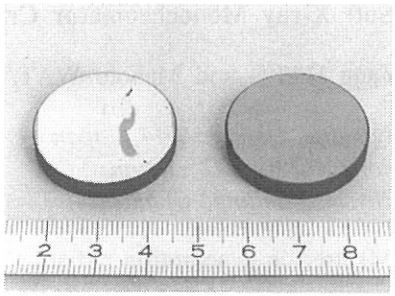

Figure 1 SiC gratings after irradiation of wiggler beams; the right side is grating #1 and the left grating #2. The left and right halves of each grating were irradiated for 4 and 40 min, respectively.

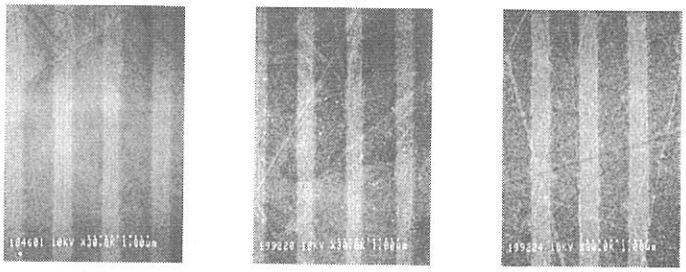

(a) (b) (c)

Figure 2 SEM photographs of the grating #1 (a) before irradiation, (b) after irradiation for 4 min and (c) after irradiation for 40 min.

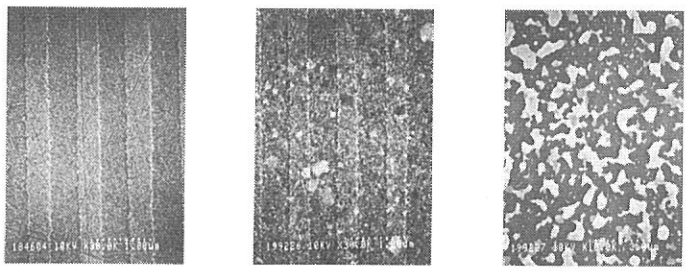

(a) (b) (c)

Figure 3 SEM photographs of the grating #2 (a) before irradiation, (b) after irradiation for 4 min and (c) after irradiation for 40 min.

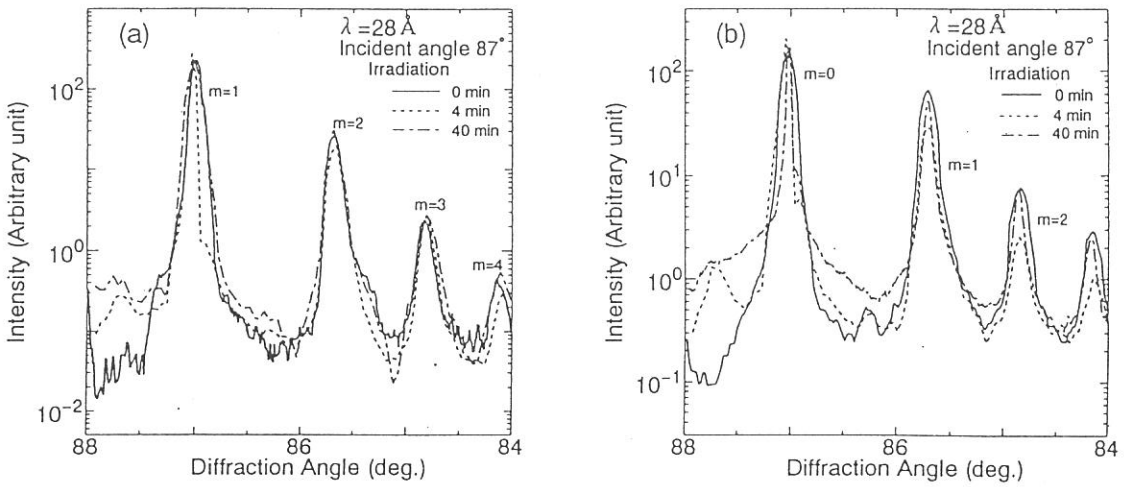

Figure 4 Angular distribution of diffraction intensities before and after irradiation for (a) the grating #1 and (b) the grating #2.

[1]E. Ishiguro, H. Maezawa et al., Proc. SPIE (to be published).

Performance Check of β-Alumina as a Soft X-ray Monochromator Crystal

Atsunari HIRAYA, Kazunori MATSUDA*, Yang HAI**, and Makoto WATANABE

Institute for Molecular Science, Myodaiji, Okazaki 444, Japan
**Naruto University of Education, Naruto 772, Japan*
***Institute of High Energy Physics, Beijing, China*

For double crystal monochromators (DXM) used in synchrotron radiation facilities, only beryl crystal can be used steadily in the region below 1.5 keV. However beryl has several disadvantages such as weakness to radiation damage and difficulty to obtain a good natural specimen. Therefore, there are interest and need for crystals that can be used below 1.5 keV, especially the lower energy region than that covered with beryl crystal. We tried to use a synthesized inorganic crystal β-alumina ($Na_2O{\cdot}(Al_2O_3)_{11}$, 2d = 22.53 Å) as a monochromator crystal of DXM and compared the resolution and intensity from β-alumina with those from beryl.

A pair of β-alumina crystals were prepared from a block of re-crystallized alumina firebrick (Toshiba Monoflux) by cleaving flat area (ca. 2 × 2 cm^2) and used without further polishing. Measurements were carried out by setting two β-alumina crystals in the DXM at BL1A beamline equipped with a focusing pre-mirror. Figure 1 shows a throughput spectra of DXM obtained with β-alumina, beryl, quartz-Y, InSb, and Ge-111 crystals with the same detection system (electron multiplier tube with Au first dynode, high voltage = 1.5 kV). The β-alumina crystal covers the energy region from 580 to 1740 eV (Bragg angle 71.5° ~ 18.5°) with more than ten times higher intensity than beryl crystal. Resolution of the pair of β-alumina crystals used is estimated to be 0.75 eV at about 900 eV which is enough narrow for some experiments such as EXAFS, though broader than that of beryl (0.46 eV). No degradation in intensity and resolution were observed even after 1 month exposure to synchrotron radiation under normal operation conditions. Since this resolution was obtained for as-cleaved crystal, improvement in both intensity and resolution are expected after proper treatment such as polishing and annealing. As an example of measurement with using β-alumina, figure 2 shows an absorption spectrum, obtained by a transmission method, of NaF film (2000 Å) deposited on a polyester film.

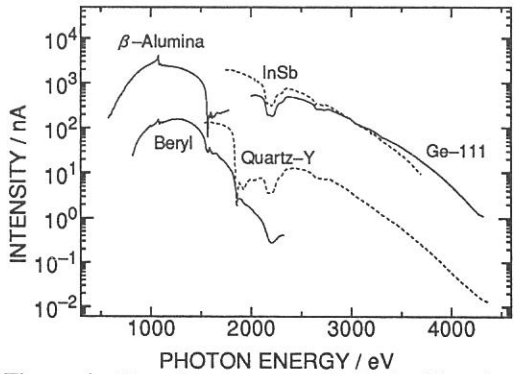

Figure 1. Throughput spectra obtained with using β-alumina, beryl, quartz-Y, InSb, Ge-111 crystals.

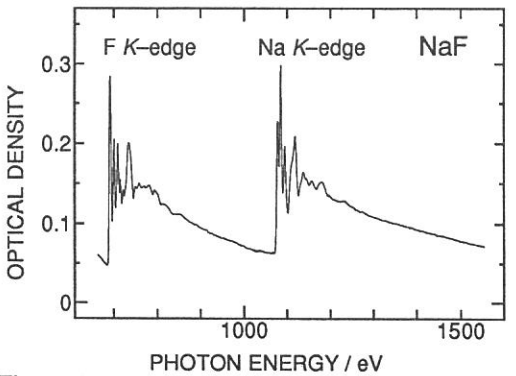

Figure 2. F-*K* and Na-*K* absorption spectrum of NaF thin film (2000Å).

X-Ray Reflectivity of Thin Foil Mirrors for X-Ray Telescope

K. Yamashita, H. Kunieda, Y. Tawara, Y. Kamata, K. Iwasawa, T. Yamazaki, A. Furusawa and H. Yoshioka

Department of Physics, Nagoya University, Nagoya 464-01

The grazing incidence X-ray telescope for ASTRO-D, the fourth Japanese X-ray astronomy satellite, is made of two stages multi-nested thin foil conical mirrors in order to reduce the weight and to get high throughput in the energy region up to 10 keV. Conical mirrors are simulated to Wolter type I. The telescope's specifications are: outer (and inner) diameter, 344 mm (and 120 mm); glancing angle of 0.25 deg at inner to 0.7 deg at outer; mirror length, 100(x2) mm; focal length, 3500 mm; total number of mirrors, 120; mirror substrate, aluminum foil (0.15 mm thick) coated with acrylic laquer and gold for the reflecting surface; angular resolution, 3 arcmin (half power diameter, HPD); and effective area of 300 cm2 at 1.5 keV, 180 cm2 at 4.5 keV and 100 cm2 at 8 keV. Aluminum foil substrates are bent in a proper shape by using a hot-press method with vacuum chucking to a conical mandrel. All the mirrors are precisely aligned at coaxial and confocal positions by 1 mm pitch in average in order to obtain sharp image at the focal plane.

The X-ray reflectivity of thin foil mirrors against glancing angles was measured by using a double crystal monochromator at BL-7A in the energy range of 0.8 - 2.3 keV with beryl and 1.7 - 4 keV with InSb. The glancing angle was changed in the range of 0.5 - 1.4 deg. A conical mirror was fixed at the sample holder

keeping in right shape. The observed results are shown in figure 1. The degradation of the reflectivity was not recognized in comparison with a standard gold mirror deposited on superpolished glass[1]. Therefore it turned out that the reflecting surface is smooth enough for X-ray reflection, whereas the surface figure is not flat enough for the image formation as expected.

This measurement is very important to derive the effective area of the telescope against X-ray energies, especially around M absorption edge of gold.

References

1. K. Yamashita et al., UVSOR Activity Report 1991, p.112.

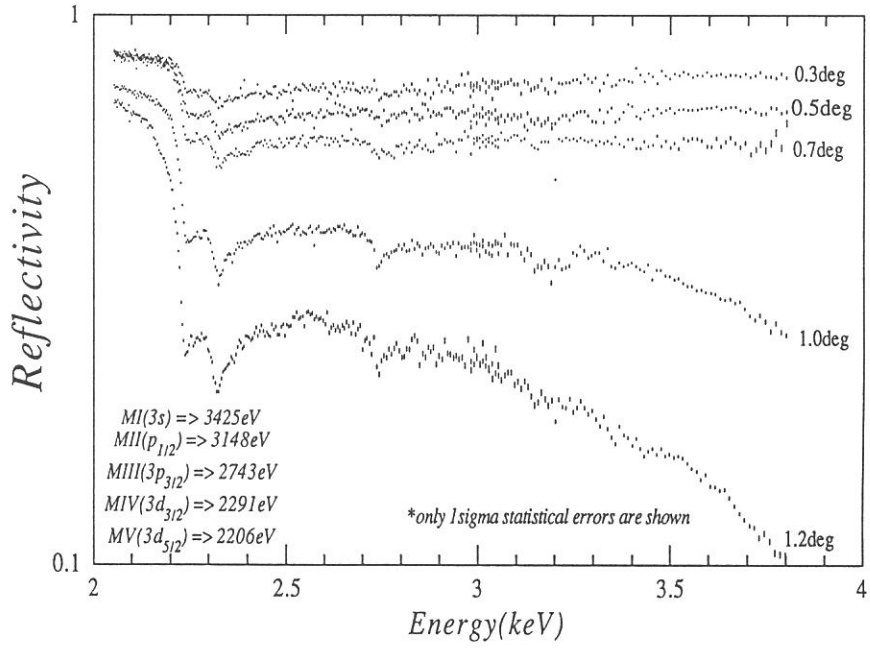

Fig.1 Reflectivity of thin foil gold mirror vs. X-ray energy. Incident angles to the reflecting surface are written in the figure.

Soft X-Ray Imaging Microscope with Sub-optical Resolution at UVSOR.

N. Watanabe[1], S. Aoki[1], Y. Shimanuki[2], K. Kawasaki[2], M. Taniguchi[3], E. Anderson[4], D. Attwood[4], D. Kern[5], S. Shimizu[6], H.Nagata[6], and H.Kihara[7]

1) Department of Applied Physics, Tsukuba University, Tsukuba
2) Department of Oral Anatomy, Tsurumi University, Yokohama
3) Department of Physics, Nagoya University, Nagoya
4) Lawrence Berkeley Laboratory, Berkeley, CA
5) IBM Research Center, Yorktown Heights, NY
6) Nikon Corp., Nishi-ooi, Shinagawa-ku, Tokyo
7) Jichi Medical School, School of Nursing, Tochigi 329-04

A soft x-ray imaging microscope with zone plates was set up at UVSOR BL8A, and imaging tests were performed at 3.2nm. This microscope is basicaly the same with the last type[1], but with great improvements on resolution, as objective zone plates of high resolution became available.

The system consists of an upstream pinhole (UPH; $100\mu m\phi$-$400\mu m\phi$ or not used), a filter (SiN, thickness: 100nm and Ti, thickness: 55nm), a condenser zone plate (($4.3mm\phi$, the outermost zone width: $0.25\mu m\phi$. The third order radiation was used for illumination.) or ($2.4mm\phi$, the outermost zone width: $0.44\mu m\phi$. The first order radiation was used for illumination.), a pinhole (SPH; $10\mu m\phi$ or $30\mu m\phi$), a specimen, an objective zone plate (OZP; $50\mu m\phi$, the outermost zone width: 45nm), a micro-channel plate (MCP) and a fluorescent plate. The magnification ratio is 750-800. A photographic view of the microscope is shown in Fig.1

The resolution was estimated to be $0.21\mu m$ from the edge profile of an image of a zone plate used as a specimen (10%-90% of the total contrast). This is worse than the theoretical one (55nm), which would be mainly due to low spatial resolution of MCP. A 78nm line and 78nm space pattern of a Ni zone plate (thickness: 135nm) was resolved as shown in Fig.2. Experiments using photographic films instead of MCP are currently under way.

Dry biological specimens, such as diatoms (of which image is shown in Fig.3), rabbit and crab myofibrils (of which image is shown in Fig.4), collagen fibers, chromosomes, sperms, Synechocystis, Porphyridium cruentum, Chlamydomonas, Euglena gracilis, and soybean protoplasts, were observed.

Acknowledgements

The authors are grateful to the help and encouragements by Prof. M. Watanabe, Mr. T. Kinoshita and other staffs of the Institute for Molecular Science. They also express their sincere thanks to all sample suppliers; rabbit myofibril (Prof. S. Ishiwata of Waseda Univ.),

crab myofibril and sperms (Prof. Y. Hamaguchi of Tokyo Inst. of Technology), collagen fibers (Dr. K. Furuya of Inst. of Physiol. Sci.), chromosomes (Dr. Y. Kinjo of Tokyo Metropolitan Inst. for Isotope Research), Synechosystis PCC6714, Porphyridium cruentum, Chlamydomonas (Dr. S. Nakamura of Inst. for Basic Biology) and Euglena gracilis (Prof. M. Watanabe of Inst. for Basic Biology).

Reference

1) N. Watanabe, Y. Shimanuki, M. Taniguchi, and H. Kihara (1992) UVSOR Activity Report, 1991, 72-73.

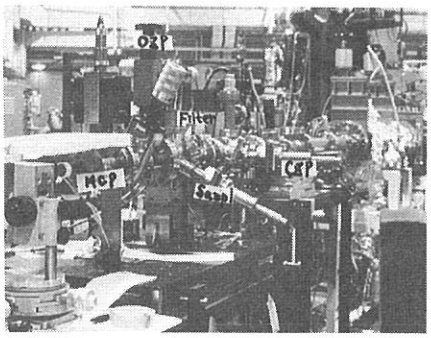

Fig.1 Photographic view of the microscope.

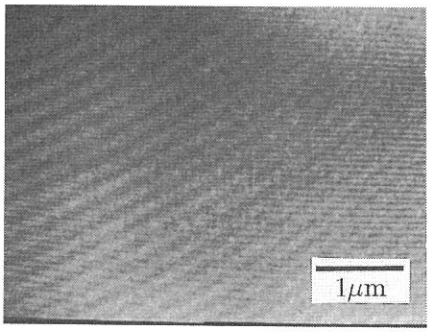

Fig.2 Image of the specimen zone plate at 3.2nm.

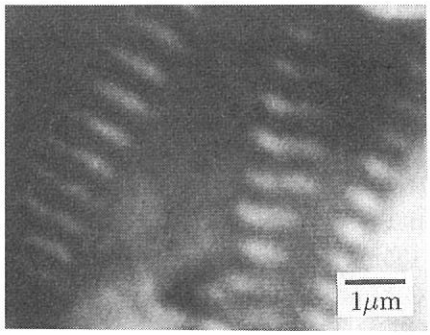

Fig.3 Image of a diatom at 3.2nm.

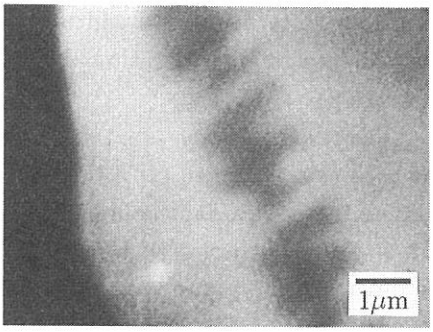

Fig.4 Image of a rabbit myofibril at 3.2nm.

Some Characteristics of a Solid State Detector at Soft X-ray Region

Hiroshi TSUNEMI, Kiyoshi HAYASHIDA, Keisuke TAMURA
Akira HIRANO and Hiroyuki MURAKAMI
Department of Earth and Space Science, Faculty of Science, Osaka University
1-1 Machikaneyama-cho, Toyonaka, Osaka, 560

We carried out a experiment to test a solid state detector, EG & G ORTEC Si(Li) detector. The entrance window of the detector is about 4 mm in diameter while we placed a pinhole of about 0.5 mm in diameter in front of the detector to restrict the position of X-rays at the detector center. We also placed an X-ray shutter to control the incident X-ray flux on the detector. All the measurements were done at an intensity level about 2000 counts/sec.

Figure 1 shows pulse height distributions for various X-ray energies. They can be well expressed with two gaussian profiles: one represents a main peak profile while the other represents a tail next to the main peak. There is a clear difference in the shape of the pulse height distribution just below the Si-K edge energy (1.84 keV) and that just above it. The ratio between the main peak and the tail part is correlated not to the incident X-ray energy but to the mean absorption length of

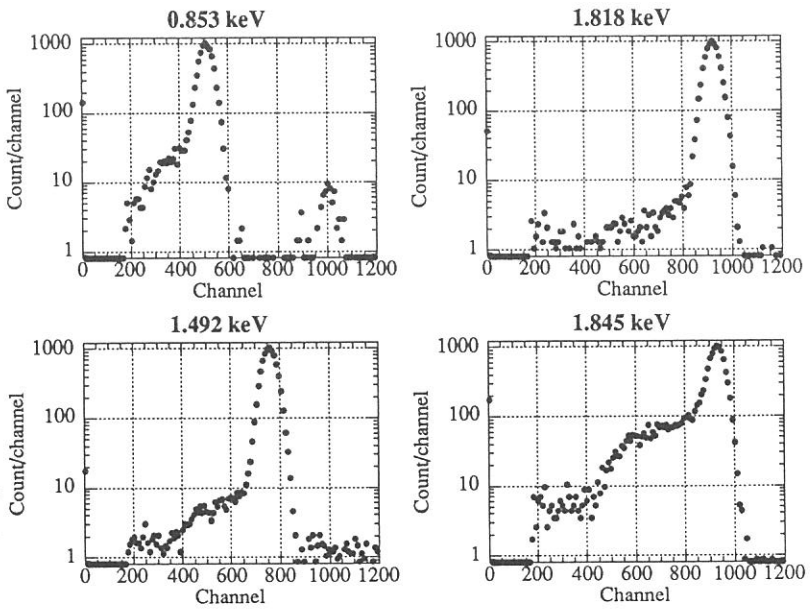

Fig. 1. Pulse height distributions obtained with the SSD at various X-ray energies. The shorter the mean absorption length is, the bigger the tail part next to the main peak. There is a big difference just above and below the Si-K edge energy.

the X-ray in silicon. The mean absorption length just above the Si-K edge is only 1.2 μm while that just above it is about 14 μm.

Taking into account the electric field applied inside the Si and the electron mobility, some charge is lost at the earth electrode due to the diffusion process. Therefore, the shorter the mean absorption length is, the bigger the tail part compared to that of the main peak. Since the mean absorption length of the X-ray below 0.7 keV becomes shorter than that at 1.84 keV, the tail part will grow until we lose the main peak. The solid state detector may not work well at sub-keV range even if we replace the beryllium window with other thin material.

Figure 2 shows the relation between the incident X-ray energy and the peak position of the main peak. In general, the linearity of the detector is good. However, there is a clear jump at the Si-K edge energy. The discrepancy is about 8 eV. The X-ray just above it is absorbed through the K-absorption while that below it is absorbed through the L-absorption. The final charge state of the atom depends on the absorption process. The average ionization degree of the atom after its K-electron vacancy is bigger than that after its L-electron vacancy. The ionization process of the photoelectron in the silicon is independent of the incident X-ray energy. This means that the average ionization energy for the X-ray just above the Si-K edge becomes bigger than that for the X-ray just below it.

We found the characteristics of Si SSD as follows.

(1) It will produce a deformed pulse height distribution when the X-ray mean absorption length is short.

(2) There is a non linearity of about 8 eV at the Si-K edge energy.

Fig. 2. The linearity of the SSD between the incident X-ray energy and the peak position of the main peak. A wide energy range is shown in the left while that around the Si-K edge is in the right. There is a non-linearity effect about 8 eV at the Si-K edge energy seen.

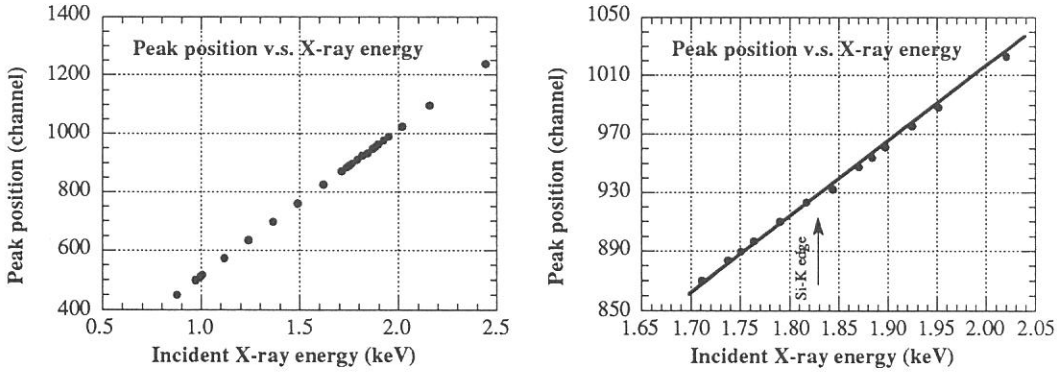

Calibration of the GIS Detectors on board the ASTRO-D Satellite

Kazuo MAKISHIMA, Yoshiki KOHMURA, Makoto TASHIRO, Yasushi IKEBE,
Takaya OHASHI*, Koujun YAMASHITA#, Yoshihiro UEDA#,
and the GIS Team

Department of Physics, University of Tokyo, Bunkyo-ku, Tokyo 113.
* Department of Physics, Tokyo Metropolitan University, Hachioji, Tokyo 192-03.
# Institute of Space and Astronautical Science, Sagamihara, Kanagawa 229.

The cosmic X-ray satellite ASTRO-D, to be launched in February 1993, will carry on board two sets of imaging gas scintillation proportional counters, called GIS (Gas Imaging Spectrometer). The GIS detectors have a circular working area of 50 mm diameter, a wide sensitivity range (0.7-15 keV), a moderate energy resolution (8% FWHM at 6 keV), and a position resolution of 0.5 mm (FWHM) because they are used as focal plane imaging X-ray detectors. The GIS detectors also have very low background level suitable for observations of very faint cosmic X-ray sources.

Because of these superior but complex capability of the GIS, it is essential to calibrate their pulse-height and position responses all over the sensitive energy range in detail before launch. The calibration needs highly monochromatic and well collimated X-ray beam of sufficient brightness. Furthermore calibration below about 4 keV is difficult to perform in the atmosphere.Therefore the UV SOR provides an ideal mean of the GIS calibration.

We used the BL7A beam line of the UV SOR to calibrate a protomodel GIS detector. Using a Ge(111) and a Beryl crystal spectrometers to cover energy ranges of 2.0-5.8 and 0.83-2.41 keV respectively, we performed detailed two-dimensional scans over the sensitive area of the detector at various beam energies. We obtained the following results. These results provide valuable contribution to the GIS project which aims at a novel research in the high energy astrophysics.

(1) We measured relation between the GIS output pulse-height and the incident beam energy (see Figure). In particular, we determined small jumps in the pulse-height vs. energy relation at L-edges of Xenon, which is used as a working gas in the GIS.

(2) We obtained deteailed calibration data of the GIS down to about 0.8 keV, which is close to its energy lower boundary.

(3) Through these calibration experiments, we confirmed that the GIS high voltage components (up tp 8 kV) work properly in the vacuum, and that the signal processing electronics (placed outside the chamber) can properly analyze the GIS analog signals down to the lower-level discriminator.

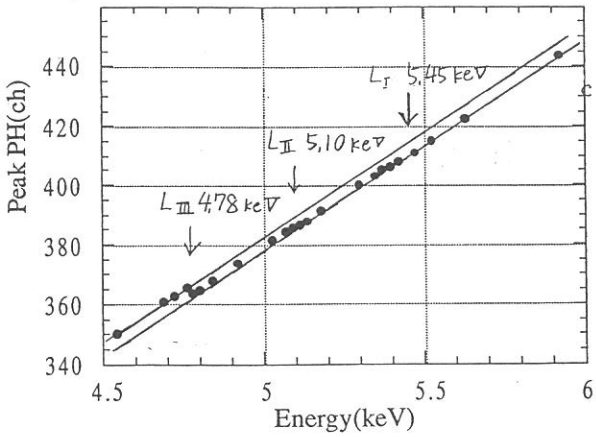

Figure: relation between the GIS output pulse height and the incident beam energy.

Finally, we deeply thank the UV-SOR staff for their kind help and cooperation

FAR-INFRARED REFLECTION SPECTRA OF MONOCLINIC ZnP_2

Osamu ARIMOTO, Mitsuru SUGISAKI, Masaru EGUCHI,
Makoto WATANABE,* and Kaizo NAKAMURA

Department of Physics, Okayama University, Okayama 700
**Institute for Molecular Science, Okazaki 404*

Monoclinic zinc diphosphide (β-ZnP_2) shows a very clear hydrogen-like exciton series near the fundamental absorption edge. Recently we have observed two closely separated resonant Raman (RR) lines with energies of 260 and 252 cm^{-1} under excitation into the exciton resonance region at 2 K.[1] From comparison with the infrared reflection spectra at room temperature (RT),[2] they are tentatively assigned to be due to the scattering of exciton polaritons by the longitudinal optical (LO) phonons with those energies. However, there is no data of infrared spectra at low temperatures. The unit cell of β-ZnP_2 contains 8 zinc atoms and 16 phosphorous atoms, giving rise to 72 phonon branches. Of these, 33 modes are infrared-active and 36 modes are Raman-active.

In the present study, we have measured far-infrared reflection spectra of β-ZnP_2 at temperatures 300, 80, and 10 K. Experiments were performed at the beam line BL6A. A Si-disk was used as the beam splitter of the interferometer, by which the spectral region is extended up to ~ 300 cm^{-1}. Figure 1 shows reflection spectrum (solid curve) for the *E//b* polarization at RT. Two prominent reflection bands labelled A and B of the B_u mode are seen, whose reflection peaks locate at 214 and 245 cm^{-1}. For the *E//c* polarization, one reflection band of the A_u mode is observed at 228 cm^{-1}. The broken curve shows the calculated spectrum obtained by using a many-oscillator model, in which the dispersion of the complex dielectric constant is given by the expression

$$\varepsilon(\omega) = \varepsilon_1(\omega) + i\varepsilon_2(\omega) = \varepsilon_\infty + \sum_j \frac{\varepsilon_\infty(\omega_{Lj}^2 - \omega_{Tj}^2)}{\omega_{Tj}^2 - \omega^2 - i\omega\Gamma_j},$$

where ε_∞ is the high frequency dielectric constant. The parameters ω_{Tj} and ω_{Lj} are the transverse (resonance) and longitudinal frequencies of the j-th oscillator. The Γ_j is the damping

constant. Two oscillators are assumed for the calculation. The measured spectrum is normalized to the calculated reflectivity at their peaks. The agreement is fairly good.

In Fig. 2 is shown reflection spectrum (solid curve) for the *E//b* polarization at 10 K. The reflection bands A and B are shifted to the high energy side by about 5 cm^{-1}, as compared with those at RT (Fig. 1). The intensities of the bands become larger and the widths become narrower as temperature is lowered. The third band labelled C is recognized at 238 cm^{-1} as a shoulder of the B band. Tha calculated spectrum (broken curve) was obtained by assuming three oscillators in the energy range shown. The LO phonon energies used in the calculation are 256 and 247 cm^{-1} for the B and C bands. These are in rough agreement with the energies of the scattering lines 260 and 252 cm^{-1} obtained from the RR experiments. In the RR spectrum, the intensity ratio of the sacttering line of 260 cm^{-1} to that of 252 cm^{-1} is about 2,[1] so that ratio of the oscillator strength of the phonon modes corresponding to the B and C bands was assumed to be 2 in the calculation. The calculated spectrum well reproduces the observed spectrum. Thus it is considered that two LO phonons with nearly equal energies of about 260 cm^{-1} are resolved also in the infrared reflection spectrum at low temperatures.

References

1) O. Arimoto, H. Takeuchi, and K. Nakamura: to be appeared in Phys. Rev. B**46** (1992).
2) H. Sobotta, H. Neumann, N.N. Syrbu, and V. Riede: Phys. Status Solidi (b)**115** (1983) K55.

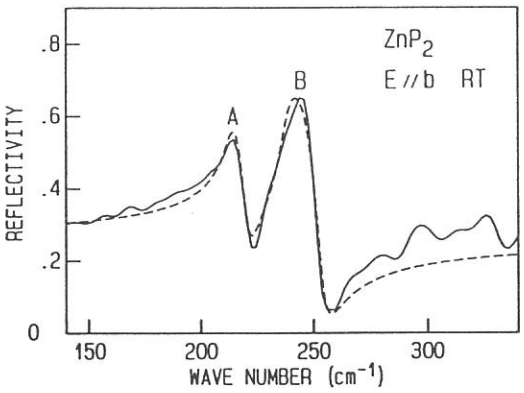

Fig.1. Reflection spectrum for *E//b* at RT.

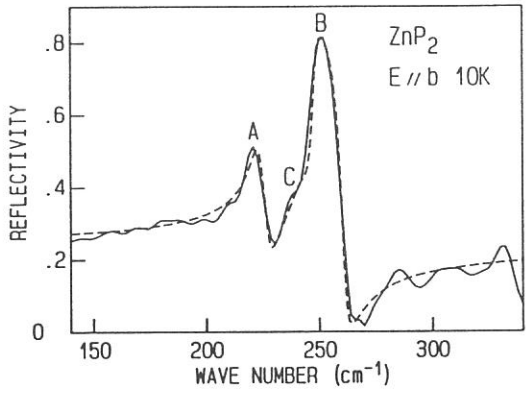

Fig.2. Reflection spectrum for *E//b* at 10 K.

Optical Phonon in YbB_6

S. Kimura, T. Nanba[+], S. Kunii[++] and T. Kasuya[++]
Research Institute for Scientific Measurements, Tohoku University, Aoba-ku, Sendai 980
[+]Department of Physics, Faculty of Science, Kobe University, Nada-ku, Kobe 657
[++]Department of Physics, Faculty of Science, Tohoku University, Aoba-ku, Sendai 980

Almost all rare-earth hexaborides (RB_6's) behave like monovalent metals because the rare-earth ion is trivalent and the valence of B_6 molecule is -2. On the other hand, however, YbB_6 becomes a narrow-gap semiconductor due to Yb^{2+} ion in YbB_6. Therefore the infrared active phonon modes, which are not seen in trivalent RB_6, are expected to be observed in YbB_6 because a strong Drude absorption which is seen in trivalent RB_6 may be much reduced due to very low concentration of conduction electron in YbB_6. Now, we measured the reflectivity spectrum of YbB_6 in the photon energy range from 1 meV to 40 eV at 300 K and 9 K for the purpose of obtaining the information of infrared active phonons.

The reflectivity was measured in the photon energy range from 1 meV to 40 eV. In the far-infrared region from 1 meV to 30 meV, the measurement was done by two different methods. One is by using the beam line BL6A1 of UVSOR and the other using a normal far-infrared spectrophotometer system. The same reflectivity spectrum was obtained by both methods.

YbB_6 becomes a narrow gap semiconductor ideally as mentioned above. However this material actually has a few number of conduction electrons because of the defect of Yb ion. This fact was seen in the reflectivity spectrum in Fig. 1. The Drude like reflectivity spectrum was observed in the energy range below 0.2 eV. From the fitting of the Drude model, the effective number of conduction electron was estimated to be 0.87 % / f. u. at 300 K and 0.96 % / f. u. at 9 K. The result of the weak temperature dependence is consistent with the result of the Hall effect qualitatively [1]. In the spectrum, two definite peaks indicated by A and B were observed. These peaks are discussed below.

From the Kramers-Kronig transformation of the reflectivity spectrum, we obtained the imaginary part of the dielectric constant (ε_2). Fig. 2 shows the ε_2 spectra of peaks A and B. Both of the peaks show simple Lorentzian shapes.

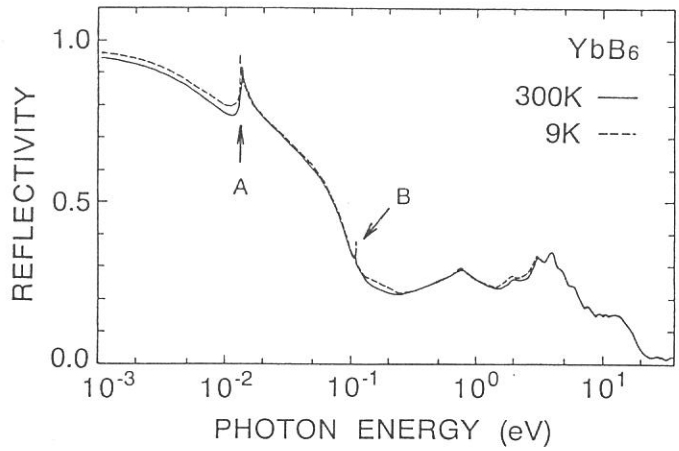

Fig. 1 Reflectivity spectrum of YbB_6 in the photon energy range from 1 meV to 40 eV at 300 K and 9 K. The peaks indicated by A and B are two kinds of optical phonons.

The phonon dispersion curve of YbB_6 was calculated by Takegahara *et al.* [2] According to the calculation result, the phonon energies of two kinds of t_{1u}–modes at Γ–point of Brillouin zone were given as 18 meV and 108 meV. These theoretical values agree with the experimental results qualitatively. Therefore it was seen that the peak A was the mode due to the relative motion between Yb and B_6 and the peak B an intra–molecular vibration in B_6. These two kinds of t_{1u}–modes are shown in Fig. 3 schematically. For the peak B, the experimentally obtained phonon energy was quite indicated to the theoretical value which reproduced the result of Raman measurement. On the other hand, however, the energy position of the peak A was about 30 % lower than that of the calculation. This means that the actual second derivative of the binding energy between Yb and B_6 is smaller than that estimated in the calculation. Since the bottom of conduction band consists of bonding states between Yb–$5d(e_g)$ and B_6–$2p(t_{2u})$, the hybridization between these states is considered to give an influence to the binding energy between Yb and B_6.

References

[1] J. M. Tarascon, J. Etourneau, P. Dordor, P. Hagenmuller, M. Kasaya and J. M. Coey, J. Appl. Phys. **51** (1980) 574.

[2] K. Takegahara and T. Kasuya, Solid State Commun. **53** (1985) 21.

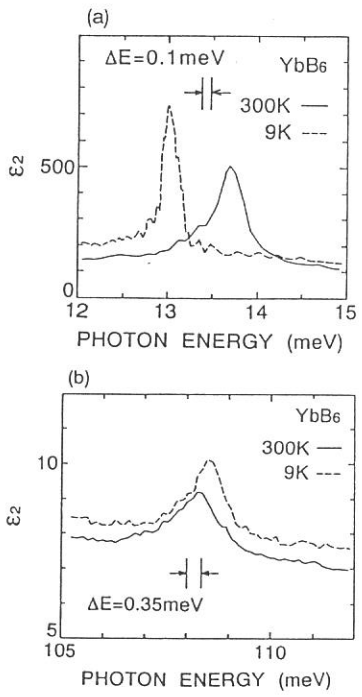

Fig. 2 Imaginary part of dielectric constant (ε_2) of two kinds of phonon absorption structures at 300 K and 9 K; (a) is for the peak A at about 13 meV. This peak is assigned to be due to the t_{1u}–mode between Yb and B_6. (b) is for the peak B at about 108 meV which is assigned to be due to the t_{1u}–mode in B_6–octahedron.

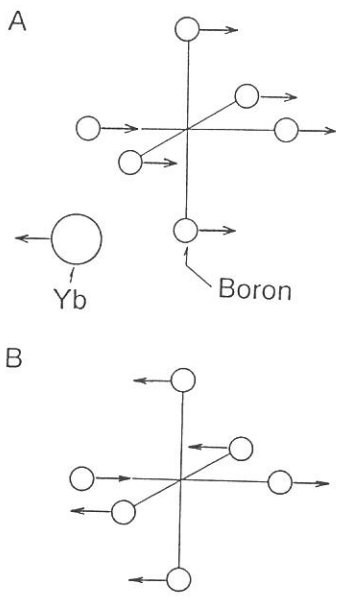

Fig. 3 Schematic pictures of two kinds of t_{1u}–modes of infrared active phonon. A is the mode between Yb and B_6 and B is the mode of intra B_6–octahedron.

IONIC PLASMON IN SUPERIONIC COPPER CONDUCTOR

Teruyoshi AWANO, Takao NANBA* and Mikihiko IKEZAWA**

Department of Applied Physics, Tohoku Gakuin University, Tagajo 985
*Department of Physics, Kobe University, Kobe 657
**Research Institute for Scientific Measurements, Tohoku University, Sendai 980

We have studied ionic motion in superionic conductors, which have very high ionic conductivity at solid phase. Absorption structure due to translational motion of mobile ions is expected to appear at the spectral range less than a few tens wave numbers considering from the mass of conduction ion and the potential barrier for conduction ion. The brilliance of the UVSOR light in this spectral region made it possible to measure the reflectivity or absorption spectra of small superionic crystals precisely. We had measured reflectivity spectra of some silver ion conductors of the form of MAg_4I_5 (M=Rb, K and NH_4). Shoulder peaks in energy loss function (imaginary part of dielectric constant) were observed in the spectral region below 10 cm^{-1} in these crystals. We have assigned these peaks as being due to ionic plasma oscillation.[1] In this work we have investigated copper ion conductors $Rb_4Cu_{16}Cl_{13}I_7$ and Cu_2HgI_4 to compare the plasma frequency with that of silver ion conductors. The former crystal has the same structure as MAg_4I_5 and has the highest ionic conductivity among all of the superionic conductors at room temperature. It is expected that the plasma frequency is proportional to the inverse of the root of the mass of conduction ion.

Reflectivity spectra were measured and transformed into optical constants by Kramers-Kronig analysis.

Fig. 1 shows conductivity spectra of $Rb_4Cu_{16}Cl_{13}I_7$ obtained from the reflectivity spectra. One peak near 40 cm^{-1} at 300 K split into two peaks at 15 K. This peaks seems to be due to the attempt vibration of copper ion in the cage of iodine ions and chlorine ions. The splitting seems to be due to the different shape of the potential cage by iodine ion from that by chlorine ion. The shoulder on the low energy side of this 40 cm^{-1} peak grows when the temperature rises. This phenomenon was observed also in the case of MAg_4I_5 and be due to translational motion of conduction ions. Fig. 2 shows energy loss function spectra obtained from the reflectivity spectra. The dashed and dotted curves show calculated one by the ionic Drude model. Parameters of curve fitting are listed in table 1. The agreement is good at 300 K although it is not good at 150 K. The cooperative motion which is noted as "ionic plasmon" seems to be impossible at low temperature because of strong scattering by immobile ions. Increase of dielectric constant at high energy side (ε_∞) seems to be due to the relative increase of vibrational motion of ions. Obtained plasma frequency is in good agreement with that estimated from mass and number of conduction ions.

Fig. 3 shows energy loss function of Cu_2HgI_4. The transition temperature to the superionic phase is 340 K. These shoulders disappeared at 77 K. As shown in table 1. plasma frequency is almost the same as that of $Rb_4Cu_{16}Cl_{13}I_7$. Small difference of ω_γ and ε_∞ from those of $Rb_4Cu_{16}Cl_{13}I_7$ seems to be due to the difference of potential barriers and the number of conduction ion in both crystal.

1) T.Awano, T. Nanba and M. Ikezawa, Solid State Ionics, 53-56 (1992) 1269

Table 1. Parameters in the Drude curve fitting.

$Rb_4Cu_{16}Cl_{13}I_7$	Temp. (K)	ω_p (cm^{-1})	ω_γ (cm^{-1})	ε_∞
	300	42	75	10
	230	42	85	11
	150	40	95	13
Cu_2HgI_4	Temp. (K)	ω_p (cm^{-1})	ω_γ (cm^{-1})	ε_∞
	320	49	95	8
	300	53	110	9

Fig. 1. Conductivity spectra of $Rb_4Cu_{16}Cl_{13}I_7$.

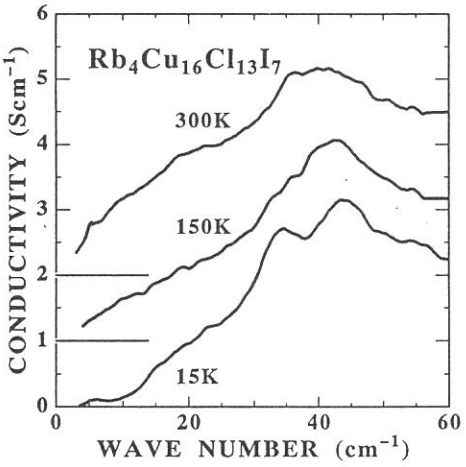

Fig. 2. Energy loss function spectra of $Rb_4Cu_{16}Cl_{13}I_7$.

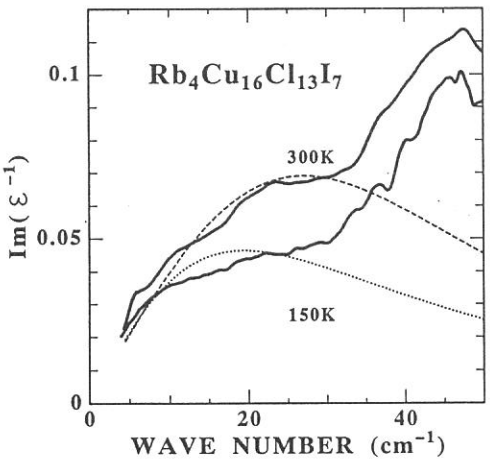

Fig. 3. Energy loss function spectra of Cu_2HgI_4.

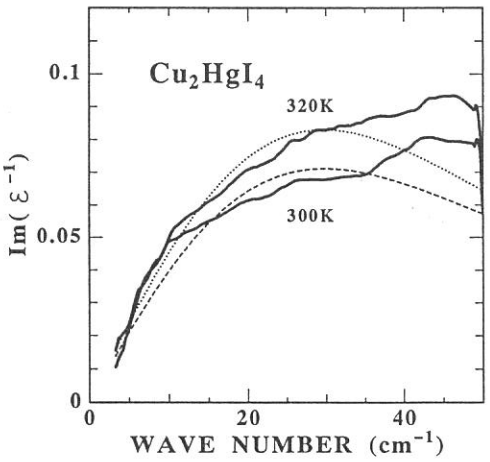

Far Infrared Absorption of NaCl Microcrystal under Pressure

T.Nanba,T.Matsuya and M.Motokawa

Department of Physics, Faculty of Science, Kobe University, Nada-ku, Kobe 657

The far infrared absorption spectrum of the NaCl microcrystal was measured at room temperature. As the crystal size decreases to a microcrystal, a so-called surface phonon mode can be induced because of the important role of the atoms which exist at the surface. The absorption due to such surface phonon mode under atmospheric pressure is known to be very sensitive to the shape and the size of the microcrystal. Such phenomena has been well explained by the continuum theory [1]. The purpose of the present study is to make clear the behavior of the surface phonon mode of the microcrystal under pressure.

The spherical NaCl microcrystal was obtained by a conventional gas evaporation techniques and its shape and size distribution were determined by an electron microscopic observation. The average size of microcrystals was 0.5-2 um. On the other hand , the cubic-shaped NaCl microcrystal was obtained by griding of the bulk NaCl down to the powders. The size distribution was also confirmed to be 1-3 um by the electron microscopic method. The sizes of both spherical and cubic samples are much smaller than the far infrared wavelength (40-400 um). A small amount of microcrystals were mixed with a transparent medium (apiezon grease-N) in the far infrared region and enclosed in the diamond anvil cell for the transmission measurement under high pressure at the BL6A1 of the UVSOR.

Observed peak positions of the absorption due to the surface phonon of the microcrystals were plotted as the function of the applied pressure to the sample and shown in Fig.1 in comparison with the peak positions of those absorption due to the bulk TO phonon mode of NaCl which were measured independently with thin films. We found that the energies of the surface phonons are quite different even at P=0 between a spherical (denoted as the "spherical" in the figure) and a cubic-like microcrystal (the "cubic").

According to the continuum theory [1], the surface phonon mode of the microcrystal in the spherical shape occurs at the frequency (ωs) which fills the equation

$$\varepsilon(\omega s) = -2 * \varepsilon m .$$

Here, ε is the dielectric function of the material comprising the sphere and εm the dispersionless dielectric constant of the medium surrounding the sphere. Similar theory was developed to the case of the cubic-shaped microcrystal by Fuchs [2] and he obtained that the energy of the dominant surface phonon mode in the the cubic microcrystal is given by the equation of

$$\varepsilon(\omega s) = -3.68 * \varepsilon m.$$

The difference in the surface phonon energies of the microcrystals in both shapes seen at P=0 in the figure can be explained by considering the difference in these two conditions. The phonon modes of all samples showed a blue shift with the applied pressure and the pressure dependences are different each other. We extended the above continuum model which has been developed only at P=0 to the case of the microcrystals under high pressure and revealed that the difference in the pressure dependence of the phonon energies of the microcrystal on its shape can be explained if we consider the increase of the dielectric constant of the surrounding medium with the pressure.

References

[1] L.Genzel and T.P.Martin: Surface Science **34**(1973) 33.
[2] R.Fuchs: Phys.Rev.**B11**(1975)1732.

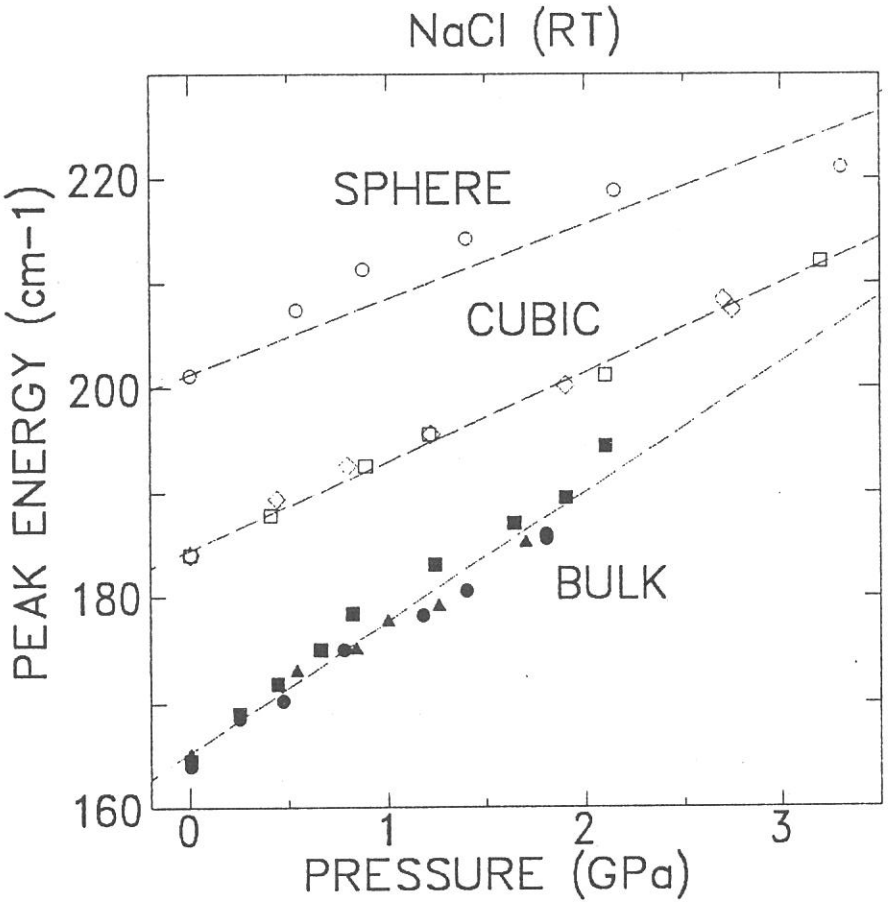

Fig.1
Pressure dependences of the peak positions of the absorption bands due to the surface phonon modes of the microcrystals in the different shapes with the applied pressure. The names of "SPHERE", "CUBIC" and "BULK" in each curve correspond to the shape of the microcrystals,respectively.

PROTON ORDER-DISORDER PHASE TRANSITION IN HIGH PRESSURE PHASE OF ICE OBSERVED BY VIBRATIONAL SPECTRA

M. KOBAYASHI, T. NAKAI, T. NANBA* and M. KAMADA

Faculty of Engineering Science, Osaka University, Toyonaka, Osaka 560
*Department of Science, Kobe University, Rokkodai, Kobe 657
Institute for Molecular Science, Myodaiji, Okazaki 444

Recently we reported far-infrared absorption spectra of high pressure phases in ice for the first time by using a diamond anvil cell and the synchrotron radiation [1]. We have extended the measurements by changing sample thickness in order to determine more precise spectral shapes.

Ice VII and VIII have almost the same atomic structure regarding arrangements of oxygen ions, while protons in VII and VIII have disordered and ordered structures, respectively. Figure 1 shows the absorption spectra of H_2O and D_2O ice in VII and VIII phases. In ice VII a broad absorption band whose peak locates at 140 cm^{-1} is observed. We designate this band as A. The band A disappears completely in ice VIII. Our former data showed that a weak absorption band still remains near at 120 cm^{-1} in ice VIII (cf. Fig. 1 of ref. [1]). This absorption turned out, however, to be only apparent arising from the Fabry-Perot interference between both the sides of sample, since the peak position changes depending on the sample thickness, and when we used thick enough sample, the absorption disappeared. On the other hand, another absorption band whose peak locates at 200 cm^{-1} appears in ice VIII at 3 GPa. We designate this band as B.

We measured pressure dependence of the spectra in ice VIII. Figure 2 plots the pressure dependence of the center position of the band B. When we assume a linear relation between the energy and the pressure, it gives a pressure coefficient of 18.2 cm^{-1}/GPa. When the relationship is extrapolated to the zero pressure, the energy of the band B becomes 153 cm^{-1}. This value is comparable to 162 cm^{-1}, which was obtained in pressure quenched sample of ice VIII by Tay et al. [2] and ascribed to the translational mode $\nu_T E_u$ [2]. Taking into consideration of the restricted numbers of experimental points and the experimental error, we conclude that the band B is ascribed to $\nu_T E_u$ mode. Our measurements correspond to the in situ observation of $\nu_T E_u$ mode at high pressures. The pressure quench is impossible for ice VII. Therefore, the in situ observation is indispensable to elucidate the effect

of proton ordering, because one should compare the spectra for both the phases at high pressure.

The band A in ice Ⅶ is ascribed to the absorption induced by random motion of protons. Ice Ⅶ and Ⅷ have almost the same lattice constants and densities. Therefore, both the phases show common elastic characteristics. Since the atomic arrangements of oxygen ions are almost invariable during the Ⅶ – Ⅷ transition, the Brillouin zone itself is definite in ice Ⅶ. The random motion of protons in ice Ⅶ breaks, however, the translational symmetry, which results in the non-conservation of the crystal momentum. Thus the whole phonon branches become optically active and therefore the absorption spectra reflects the density of states [3]. The peak A is presumably ascribed to the maximum of the density of states corresponding to the zone boundaries.

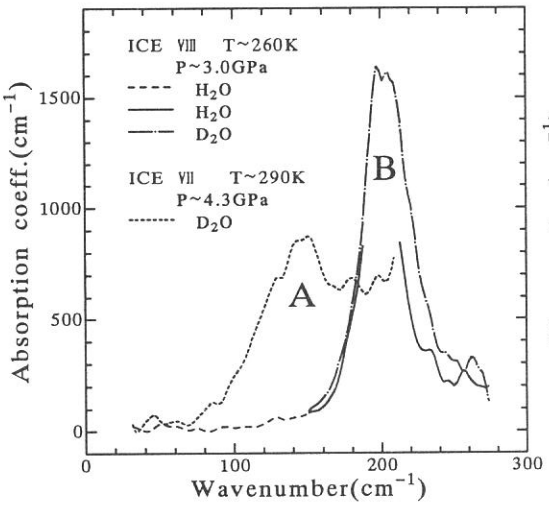

Fig.1 Far-infrared absorption spectra of ice Ⅶ and Ⅷ at high pressures.

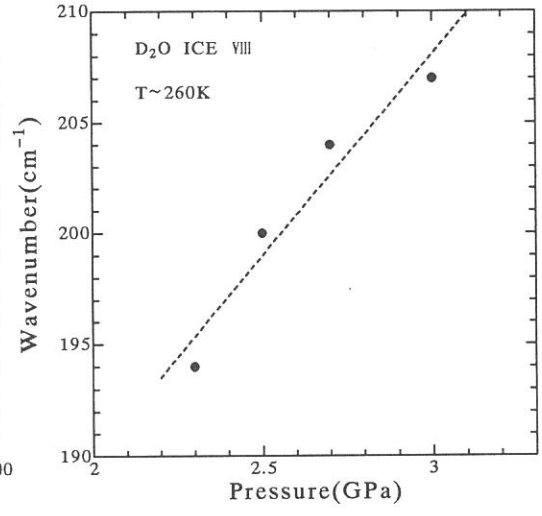

Fig.2 Pressure dependence of the energy of band B in ice Ⅷ.

REFERENCES

[1]M. Kobayashi, S. Morita, T. Nakai, T. Nanba and M. Kamada, UVSOR Activity Rep. (1991) 62.

[2] S. P. Tay, D. D. Klug and E. Whalley, J. Chem. Phys. 83 (1985) 2708.

[3] E. Whalley and J. E. Bertie, J. Chem. Phys. 46 (1967) 1264.

Far-infrared absorption of non-polar liquids and liquid C_6H_6 - C_6F_6 mixtures

Yoshitaka FUJITA and Shun-ichi IKAWA

Department of Chemistry, Faculty of Science, Hokkaido University, Sapporo 060

Previously, we measured the far-infrared collision-induced absorption(CIA) of liquid CS_2, CCl_4, C_6H_6 and C_6F_6 under pressure and observed that average induced dipole moments of the system $\sqrt{\langle\mu^2\rangle}$ obtained from the zeroth moment of the CIA bands decreased with increasing pressure, while the second moments M_2 increased[1]. In this study the CIA bands of liquid C_6H_6, C_6F_6 and $C_6H_3F_3$ have been measured in the pressure ranges 1 to 1250 bar, 540 bar and 890 bar, respectively, to further confirm the pressure dependence of $\sqrt{\langle\mu^2\rangle}$. In addition, we have measured liquid mixture of C_6H_6 and C_6F_6 at temperatures in the 13 ~ 45 °C range.

The high-pressure cell and the method of the analysis were described previously[1),2)]. For measurements of the liquid mixtures at ambient pressure, a liquid cell with Si windows of 3mm and 4mm thicknesses was used, and the sample thicknesses were 2 ~ 6.5mm. Fig.1 shows the resulting $\sqrt{\langle\mu^2\rangle}$ and M_2 plotted against pressure with the results for CS_2 and CCl_4. Obviously $\sqrt{\langle\mu^2\rangle}$ decrease while M_2 increase with increasing pressure, and freezing strengthens this tendency. Recently we have carried out the molecular dynamics simulation of liquid CS_2 at higher pressures and found the similar decrease in $\sqrt{\langle\mu^2\rangle}$ near the pressure of freezing, which is due to increase in the intermolecular correlation of the induced dipole moments.

Fig.2 shows the observed spectra of the equimolar mixture of C_6H_6 and C_6F_6. All the spectra of the mixture were measured with an InSb detecter and $\sqrt{\langle\mu^2\rangle}$ were obtained from the curves fitted to the spectral densities $\alpha(\nu) / \nu^2$ using a

function $1/(a+bv^2+cv^4+dv^6)$. The resulting $\sqrt{\langle\mu^2\rangle}$ values plotted against temperature are shown in fig.3. The large value of $\sqrt{\langle\mu^2\rangle}$ for the solid phase indicates the strong interaction between these two molecules[3].

References

1) Y.Fujita, T.Cho and S.Ikawa, UVSOR Activity Report 1991, p84.

2) Y.Fujita, T.Oba and S.Ikawa, Can.J.Chem.,69,1745(1991).

3) C.S.Patrick and G.S.Prosser, Nature 187.1021(1960).

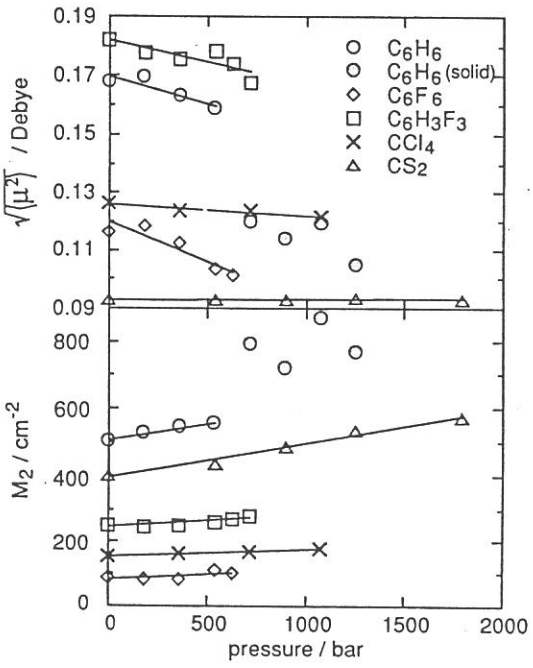

Fig. 1 $\sqrt{\langle\mu^2\rangle}$ and $M_2 = \int \alpha(\nu)\, d\nu$ of liquid CS_2, CCl_4, C_6H_6, C_6F_6 and $C_6H_3F_3$ plotted against pressure.

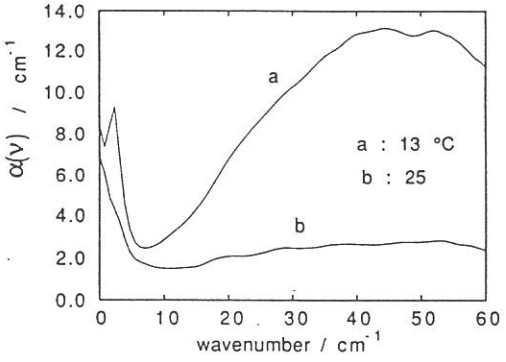

Fig. 2 Far-infrared spectra of the equimolar mixture of C_6H_6 and C_6F_6.

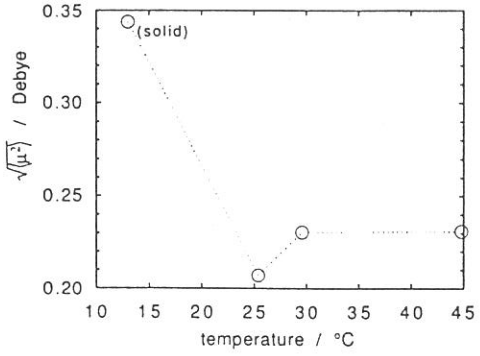

Fig. 3 $\sqrt{\langle\mu^2\rangle}$ plotted against temperature.

ABSTRACTS

THE 46TH OKAZAKI CONFERENCE

The 46th Okazaki Conference on Application of Synchrotron Radiation to Molecular Science: Present Status and Future Prospects

Institute for Molecular Science, December 16-18, 1992
(Room 101, Office Bldg.)

December 16 (Wed.), 1992

Chairperson: Takehiko Ishii (ISSP, Univ. of Tokyo)

12:55 Welcome Address: Kyuya Yakushi, Director (UVSOR, IMS)

13:00 - 13:50 Samuel Krinsky (NSLS, BNL)
"Development of the VUV Storage Ring and Plans for a UVFEL"

13:50 - 14:15 Hisashi Kobayakawa (Photon Factory, KEK)
"Present Status of the Photon Factory Storage Ring"

14:15 - 14:40 Yukihide Kamiya (ISSP, Univ. of Tokyo)
"Present Status of SOR-Ring and Future Plans of a High-Brilliant VUV Ring"

14:40 - 15:05 Goro Isoyama (UVSOR, IMS)
"Present Status and Recent Developments of the UVSOR Storage Ring"

15:05 - 15:35 Coffee Break

Chairperson: Hideo Onuki (Electrotechnical Lab.)

15:35 - 16:25 Walter Braun (BESSY)
"Recent Instrumental Developments and Experimental Highlights at BESSY I, Future Prospects for BESSY II"

16:25 - 16:50 Masaki Yamamoto (Tohoku Univ.)
"Soft-X-Ray Multilayers for the Uses with Synchrotron Radiation"

16:50 - 17:15 Makoto Watanabe (UVSOR, IMS)
"Review of Recent Progress in Soft X-Ray Monochromators and Their Dispersive Elements"

Chairperson: Yoshihiko Hatano (Tokyo Inst. of Tech.)

17:15 - 17:40 Kiyohiko Tabayashi (IMS)
"VUV Photochemistry of Rare Gas-Dihalogen van der Waals Complexes Studied by Absorption and Fluorescence Spectroscopy"

17:40 - 18:40 Yuan T. Lee (Univ. of California, Berkeley)
"Application of VUV Undulator Beam Line to Chemical Dynamics at ALS"

19:00 - 20:45 Reception (Faculty Club, 2-nd Floor)

December 17 (Thur.), 1992

Chairperson : Inosuke Koyano (Himeji Inst. of Tech.)

9:00 - 9:30 Yukinori Sato (Tohoku Univ.)
"Resonance-Auger-Electron-Photoion Coincidence Studies on State-to-State Dissociation Dynamics of Inner-Shell-Excited Molecules"

9:30 - 10:00 Pascal Lablanquie (LURE, Univ. Paris Sud)
"Multiphotoionization Following Innershell Excitation"

10:00 - 10:40 Yoshihiko Hatano (Tokyo Inst. of Tech.)
"Spectroscopy and Dynamics of Superexcited Molecules"

10:40 - 11:10 Coffee Break (Room. 201) + Group Photo

Chairperson : Noriaki Itoh (Nagoya Univ.)

11:10 - 11:35 Koichiro Mitsuke (IMS)
"Negative-Ion Formation from Molecules, Clusters, and Condensed-Gas Surfaces"

11:35 - 12:25 Georg Zimmerer (DESY-HASYLAB, Univ. of Hamburg)
"Spectroscopy of Molecules in Gaseous and of Molecular Centers in Condensed Phase"

12:25 - 13:30 Lunch

Chairperson: Tadaoki Mitani (IMS)

13:30 - 13:55 Yoshinori Tokura (Univ. of Tokyo)
"Polarized Absorption Spectroscopy on σ-Conjugated Polymer: Polysilanes and Polygermanes"

13:55 - 14:20 Nobuo Ueno (Chiba Univ.)
"Molecular Orientation in Thin Films of Functional Molecules by Means of Angle-Resolved Photoemission"

14:20 - 14:45 Ken-ichi Kan'no (Kyoto Univ.)
"Time-Resolved Spectroscopic Study on the Self-Trapped Excitons in Alkali Halide Crystals"

14:45 - 15:10 Masao Kamada (UVSOR, IMS)
"Present and Future of Photoelectron and Photodesorption Spectroscopic Studies at UVSOR"

15:10 - 15:45 Coffee Break (Room 201)

Chairperson: Akito Kakizaki (ISSP, Univ. of Tokyo)

15:40 - 16:30 Ingolf Lindau (MAX-Lab, Univ. of Lund)
"High Resolution Photoelectron Spectroscopy on Solids: Past, Present and Future"

16:30 - 16:55 Akio Kotani (ISSP, Univ. of Tokyo)
"Can We Obtain X-Ray Absorption Spectra beyond the Core-Hole Lifetime Broadening?"

16:55 - 17:20 Tsuneharu Koide (Photon Factory, KEK)
"Magnetic Circular Dichroism in Core-Level Absorption of Magnetic Materials"

17:20 - 17:45 Takao Nanba (Kobe Univ.)
"Far Infrared Spectroscopy of Rare Earth Hexaborides"

17:45 - 19:00 Dinner

Chairperson: Masao Kamada (UVSOR, IMS)

19:00 - 21:00 Poster Session + (Laboratory Tour)

December 18 (Fri.), 1992

Chairperson: Shinri Sato (IMS)

9:00 - 9:25 Syozo Kono (Tohoku Univ.)
"A Future Direction of Synchrotron-Radiation Photoemission Study of Solid Surfaces"

9:25 - 9:50 Toshiaki Ohta (Univ. of Tokyo)
"XAFS Studies of Molecular Adsorbates on Metals"

9:50 - 10:40 Peter Weightman (Univ. of Liverpool)
"New Directions in the Study of Electronic Structure Using Synchrotron Radiation"

10:40 - 11:10 Coffee Break

Chairperson: Kosuke Shobatake (IMS)

11:10 - 11:35 Kenichiro Tanaka (Photon Factory, KEK)
"Photon Stimulated Desorption by Core Electron Excitation"

11:35 - 12:00 Tsuneo Urisu (IMS)
"Science and Engineering in Synchrotron Radiation-Excited Semiconductor Process"

12:00 - 12:10 Closing Remarks: Hiroo Inokuchi, Director-General (IMS)

Poster Session (December 17, 19:00 - 21:00)

Chairperson: Masao Kamada (UVSOR, IMS)
Place: Office Bldg. Room 201

PS-I. P. M. Raja Rao, B. N. Raja Sekhar, N. C. Das, S. Padmanabhan, P. S. Murty, G. D. Saksena, S. V. N. Bhaskara Rao, S. S. Bhattacharya, V. B. Kartha, A. K. Sinha, and S. Bhat (Bhabha Atomic Res. Cent., India)
"Design and Development of Spectroscopy Beam Lines at Indus I"

PS-II. P. -K. Tseng (Natl. Taiwan Univ. and SRRC, Taiwan)
"Present Status and Future Perspective of Synchrotron Radiation Center"

PS-III. C. Y. Xu (HESYRL, China and Riken)
"Present Status of HESYRL"

PS-IV. D. Xian, E. Tang, and Y. Hai (Beijing SR Facility, China)
"BSRF Status and Research Opportunities"

PS-V. S. Y. Rah, Y. Chung, and T.-N. Lee (Postech, Korea)
"Current Status of the PLS Project"

PS-VI. M. Watanabe (IMS)
"Synchrotron Radiation Sources in Japan"

PS-1. K. Yamashita (Nagoya Univ.)
"X-Ray Reflectivity of Au, Pt and Pt/C Multilayer"

PS-2. M. Sakurai (Kobe Univ.)
"VUV and Soft X-Ray Radiometry on the NIFS Beam Line BL5B"

PS-3. E. Ishiguro (Osaka City Univ.)
"Reflectance of Multilayer Gratings in Soft X-Ray Region"

PS-4. N.Watanabe (Univ. of Tsukuba)
"Soft X-ray Microscope with Zone Plates III"

PS-5. I. Ouchi (Tottori Univ.)
"Core Electron Absorption Spectra of Polyester Films"

PS-6. W.-F. Pong (Tamkang Univ., Taiwan)
"Soft X-Ray Absorption Studies of Diluted Magnetic Semiconductors $Zn_{1-x}Y_xS$ (Y=Mn, Fe, Co)"

PS-7. S. Nakai (Utsunomiya Univ.)
"Polarized Cu L Absorption Spectra of $Bi_2Sr_2Ca_{1-X}Y_XCu_2O_8$ (x=0.06)"

PS-8. S. Hasegawa, S. Tanaka Y. Yamashita, H. Inokuchi (IMS), H. Fujimoto (Kumamoto Univ.), K. Kamiya, K. Sekiya (Nagoya Univ.) and N. Ueno (Chiba Univ.)
"Molecular Orientation in Thin Films of Bis(1,2,5-thiadiazolo)-p-quinobis(1,3-dithiole) on Graphite Studied by Angle-Resolved Photoelectron Spectroscopy"

PS-9. T. Masuoka (Osaka City Univ.)
"Dissociative Double Photoionization of Carbonyl Sulfide (OCS)"

PS-10. K. Furuya (Kyushu Univ.)
"Dissociation Dynamics of CH_4^+ in the A State Region"

PS-11. H. Yoshida, H. Hattori, and K. Mitsuke (IMS)
"Positive Ion-Negative Ion Coincidence Spectroscopy of Diatomic Molecules"

PS-12. H. Hattori, H. Yoshida, and K. Mitsuke (IMS)

"Ion-Pair Formation from Hydrocarbons by Predissociation of the Rydberg States with C-2s Hole Characters"

PS-13. H. Yasumatsu, T. Kondow (Univ. of Tokyo), K. Tabayashi, K. Suzuki, and K. Shobatake (IMS)
"Dissociative Excitation of Alkali Cyanide Molecules"

PS-14. M. Kono, K. Tabayashi, and K. Shobatake (IMS)
"Photodissociative Excitation Process of ClCN Studied by Fluorescence Polarization Measurements"

PS-15. H. Ogawa (Saga Univ.)
"Synchrotron Radiation Assisted Epitaxial Growth of ZnTe Using Metalorganic Sources"

PS-16. A. Yoshida, S. Umeda, and Y. Saito (IMS)
"Synchrotron Radiation-Induced Degradation of Metal-Insulator-Semiconductor Devices"

PS-17. S. Hirose and M. Kamada (IMS)
"Sputtering of Excited Alkali Atoms from Alkali-Halides Irradiated with Synchrotron Radiation"

PS-18. Y. Ukisu, H. Ogawa and S. Sato (IMS)
"Mechanism of the Photolysis of Iron Pentacarbonyl Adsorbed on Silver"

PS-19. S. Tanaka and M. Kamada (IMS)
"Co-Adsorption of K and Cl on the Si(100)(2x1) Surface"

PS-20. H. Nishikawa (Waseda Univ.)
"Photoluminescence and VUV Absorption Spectra in SiO_2 Glass"

PS-21. H. Kawazoe (Tokyo Inst. of Tech.)
"Crystal Structure and Electronic Structure-Design of Transparent Electrode Materials"

PS-22. M. Itoh (Shinshu Univ.) and H. Itoh (Kagawa Univ.)
"Light Amplification due to Population Inversion between the Valence and Outermost-Core Bands in BaF_2"

PS-23. H. Nakagawa (Fukui Univ.)
"Self-Trapped Excitons in $CdBr_2$ and $CdCl_2$"

PS-24. K. Nakagawa (Kobe Univ.)
"Origin of Photocurrent Structures of Anthracene Doped in Super Critical Xenon"

PS-25. S. Kubota (Rikkyo Univ.)
"Variation of Decay Curves for Auger-Free Luminescence in CsCl and BaF_2 against Exciting Photon Energies"

PS-26. M. Taniguchi (Nagoya Univ.)
"Time-Resolved Luminescence Spectroscopy of HMM Powders"

PS-27. T. Dodo (Ehime Univ.)
"Absorption and Reflection of FIR by Concentrated Electrolyte Solutions"

PS-28. M. Kobayashi (Osaka Univ.)
"Proton Order-Disorder Phase Transition in Ice Observed by Vibrational Spectra"

PS-29. H. Ohashi, K. Tabayashi, and K. Shobatake (IMS)
"Synchrotron Radiation-Excited Etching of Semiconductor Material Surface Studied by Velocity Distribution Measurements of Desorbed Species Using an Electron Bombardment Ionization Mass Spectrometer Detector"

PS-30. H. Hama, S. Takano, and G. Isoyama (IMS)
"Control of the Bunch Length on the UVSOR Storage Ring"

DEVELOPMENT OF THE VUV STORAGE RING AND PLANS FOR A UVFEL

Samuel Krinsky
National Synchrotron Light Source
Brookhaven National Laboratory
Upton, NY 11973

Abstract

The NSLS was initially funded in 1977 and VUV storage ring operations began in 1982. During the Phase II upgrade program in 1986, two insertion devices and an infrared beamline were installed. In 1989, a prototype real time global orbit feedback system was commissioned, stabilizing the orbit for all beamlines utilizing a single feedback system based upon harmonic analysis of the orbit fluctuations and correction dipole magnetic fields. The orbit feedback is facilitated by new RF receivers for processing the signals from the ring's pick-up electrodes. These receivers have a noise level below 10 microns. In 1992, RF receivers had been installed for all of the VUV ring's pick-up electrodes, allowing a real time orbit display. Also, the prototype global orbit feedback system was replaced by new horizontal and vertical orbit feedback systems with improved performance. Fast (5 Hz) and slow (once every two minutes) orbit histories are now logged on the computer to help follow up on user problems related to orbit stability.

The electron beam lifetime in the VUV ring, which operates at 750 MeV and is filled to 900 ma, is limited by Touschek (intrabunch) scattering. The lifetime was doubled in 1990 by installing a fourth harmonic RF cavity (211 MHz) and operating it passively in a manner to increase the electron bunch length. In Spring 1993, we plan to power the harmonic cavity and obtain an additional 50% increase in lifetime. We are also investigating the possibility that a further increase in lifetime can be achieved by increasing the ring's horizontal aperture.

Beamline development is continuing on the VUV ring. The success of the infrared beamline U4IR, has led to the building of a second infrared line on U2. The instrument of choice for high resolution soft x-ray spectroscopy is the spherical grating monochromator which was developed by AT&T Bell Labs on U4. This year the new SGM on the U13 undulator is supporting an active scientific program. Work has begun on the development of a beamline using the U13 undulator and standard normal incidence optics, for high resolution angle resolved photoemission in the 5 to 30 eV photon energy range. The normal bending magnet port on the VUV ring collects less than 50 milliradians of radiation. Consideration is being given to the development at ports U5 and U6 of special optics to collect and time focus close to 500 milliradians of radiation. This would provide an optimized source for projection x-ray lithography, and could also be used as a universal ionizer for state-of-the-art pump-probe experiments.

At the NSLS we are pursuing the development of a free electron laser operating in the wavelength range of 75-300 nm. Nanocoulomb electron pulses will be generated at a laser photocathode RF gun. The 6 ps pulses will be accelerated to 250 MeV in an s-band SLAC-type LINAC. We consider a subharmonically seeded single pass FEL amplifier utilizing two wiggler magnets separated by a dispersion section. To be specific, suppose the seed to be laser light at 300 nm. A first wiggler is

used to energy modulate the electron beam. This is followed by a dispersion section to produce spatial bunching, and a second wiggler resonant to 100 nm. Upon passing through the second wiggler the prebunched electron beam first radiates coherently, and then this radiation is exponentially amplified. Finally, a tapered section is used to extract additional power from the electron beam. In this manner we can achieve radiation pulses of 6 ps duration with 1 mJ energy per pulse in 10^{-4} bandwidth, with continuously tunable wavelength in the range 75-300 nm.

A proof-of-principle experiment in the infrared is presently in preparation to be carried out at the Accelerator Test Facility at BNL. In this experiment we will triple the frequency of a CO_2 seed laser by using two superconducting wigglers and a dispersion section. We plan to study the evolution of the various growth mechanisms as well as the coherence of the tripled and amplified radiation.

Present Status of the Photon Factory Storage Ring

Hisashi Kobayakawa

Photon Factory

National Laboratory for High Energy Physics

Oho, Tsukuba, Ibaraki 305, Japan

Abstract

The Photon Factory is a user-based facility for synchrotron-radiation research at the National Laboratory for High Energy Physics (KEK). Accelerators consist of a 2.5-GeV linear accelerator and a 2.5-GeV storage ring. Operating beam is positron. Initial stored current is 350-360 mA for user-runs and the beam lifetime is in excess of 60 hours at 300 mA. The average current is about 300 mA in 24-hour fill lengths. The injection rate of the positron beams is presently very high, 0.5-1.0 mA/sec. In 1991, 208 hours were provided for single-bunch users. The beam lifetime at 50 mA is 10-20 hours, which is limited by the Touschek effect. By using this vertical tune shifts, the beams in the neighboring buckets are cleaned to a factor of 10^{-5}-10^{-6}

Twenty-one beamports have been equipped with beamlines. Fifty-nine experimental stations are now operational; thirty-two of these are for X-ray studies, twenty-seven for VUV and soft X-rays and one for photon-beam position monitoring for diagnosis. Four beamlines were built by private companies. Six insertion-device beamlines have been operational.

Number of users is about 2300 including more than 500 users from industries. 69% of users is from universities, 7% is from national laboratories, and 24% is from industries. Number of proposals submitted every year is about 250; 48% of which is solid state physics and material science, 23% is chemistry and atomic or molecular sciences, 15% is biology or biochemistry, 6% is for technology or industrial uses.

The storage ring has been operational since 1982. Major upgrades made on the storage ring are (1) low emittance operation from 1987 in order to increase the brightness of synchrotron radiation, and (2) positron operation from 1988. A product of beam current and lifetime ($I\tau$) is a good standard of storage-ring performance. $I\tau$'s in present runs are very large more than 1000 Ampere·min.

An FEL-project using the Photon Factory storage ring is underway. This project involves FEL-research for developing the shorter-wavelength region. A gain measurement at 177-nm is our present goal.

We are planning to upgrade the storage ring with reducing the beam emittance by a factor of 5 and increase the brightness of synchrotron radiation by a factor of approximately 10. The present emittance is 130 nmrad, and new emittance will be 27 nmrad at 2.5 GeV. In this plan, we must add new quadrupole- and sextupole-magnets, which have smaller bore radius of 40 mm (present bore radius is 55 mm), and also their side-yokes are opened for the beamline ports. Since the bending magnets will not be changed, source points and lines of the synchrotron light do not change.

Present Status of SOR-Ring and Future Plans of a High-brilliant VUV Ring

Yukihide KAMIYA
ISSP, The University of Tokyo

Abstract

Presented in this talk are two subjects; SOR-Ring status and future project of a high-brilliant light source. First I will give a talk about an overview of the SOR-Ring, operational status of the ring, and some accelerator studies and problems. Next I will report the future plans of a light source; an overview, accelerator parameters and ongoing accelerator R&D.

The SOR-Ring is located in the site of the Institute for Nuclear Study (INS) in the northwestern part of Tokyo Metropolitan, and operated by the Synchrotron Radiation Laboratory of ISSP. The construction of the SOR-Ring began in 1971, following productive activities of the INS-SOR, which utilized synchrotron light extracted from the ES, 1.3-GeV Electron Synchrotron. After the construction completed, the operational time of the ring was gradually increased and became up to about 2000 hours in the fiscal year of 1991. The ring is usually operated from morning to night and the weekly schedule is from Tuesday to Friday. There are five beamlines in the SOR-Ring, three of which are active ones: BL1 is for the experiments of photon reflection and absorption, BL2 for photoelectron spectroscopy, and BL5 is specifically dedicated to ultraviolet photobiology.

The injection energy and storage energy of the ring are 308 MeV and 380 MeV, respectively. The ring with an RF frequency of 120.83 MHz has 17.4-m circumference and consists of eight bending magnets and four quadrupole triplets. At 380 MeV the beam emittance is around 320 nm·rad and the critical photon energy 110 eV. In this summer shutdown, beam position monitors (BPM's) along with beam steerings have been installed to measure the closed orbits and to correct them. In this talk, I will present the BPM system, some results of orbit correction and also recent measurement of other machine parameters. Further I will talk about the accelerator problems in the SOR-Ring; ion-trapping phenomena, vacuum pressure growth around the RF-cavity and longitudinal instability presumably caused by a higher-order-mode in the RF-cavity. As every component of the SOR-Ring is aging rapidly, we eagerly hope to construct a new facility.

Our future project of a high-brilliant light source is one of the future plans for the whole ISSP, which is expected to move to a new campus in Kashiwa located northeast of Tokyo. The accelerator scheme of the new light source consists of a 50-MeV linac, a 1.5-GeV booster synchrotron and a 1.5-GeV storage ring that has a circumference of about 240 m, twelve long straight sections and an emittance of several nm·rad. Further presented in this talk are a plan view of the facility buildings, a layout of beamlines, principal parameters of the accelerators, photon brilliance and so forth. Because of the very small emittance and relatively low energy of the beam, the beam lifetime will be mainly determined by the Touschek effect even for muti-bunch operation. The lifetime is then estimated to be around 10 hours.

Two accelerator R&D's are now under way. One is a BPM system with PIN diodes used as signal switching, being intended to be more high-speed and reliable than ever. This BPM system is already working in SOR-Ring. Relative accuracy of the system obtained so far is the order of a few microns, but large unevenness of BPM data that would unexpectedly occur for mechanical switches has never been observed. The other R&D is that for RF-cavities, the purposes of which are to find out a suitable cavity structure not so as to cause coupled-bunch instabilities, and to adopt a simple structure in order to get a reliable operation at high RF power. The specific feature of the present design is that resistive material, SiC, is attached on the beam pipes near a cavity to damp some higher-order-modes that are propagated out of the cavity. A cold model of cavity has already been delivered from a company and its test is about to begin this December. I will report some details of these R&D's and beam instabilities related to this designed cavity.

Present Status and Recent Developments of the UVSOR Storage Ring

Goro ISOYAMA
UVSOR Facility, Institute for Molecular Science
Myodaiji, Okazaki 444

The accelerator system of the UVSOR facility is introduced, and recent developments of the control system and a superconducting wiggler are described. The present status, experiments of control of the bunch length and a free electron laser on the storage ring are given in other parts of this report.

Construction of the accelerator system started in 1981, and the first electron beam was stored on November 10, 1983. Since then, the light source has been running for 9 years. The accelerator system consists of a 750 MeV electron storage ring and a 600 MeV injector synchrotron with a 15 MeV linac. The magnetic lattice of the storage ring is the double bend achromat. There are four long straight sections of 3.5 m long, where a superconducting wiggler and two undulators are installed.

Recently, a new control system was installed for the accelerator system. It is a distributed control system based on two mini-computers as process computers. One of the computers controls the storage ring and the other takes care of the beam transport line from the synchrotron. The system was designed with the emphasis on its reliability and flexibility. To ensure reliability, the dual disk system was employed. It is possible to operate the accelerator system with one computer though performance of the control system becomes slightly worse. To ensure flexibility, we employed a file-operating system. In a conduct file, names of data files are written, while names and setting values of devices are written in data files.

A 4 T superconducting wiggler of the wavelength shifter type was recently installed on the storage ring. Two thermal shielding plates for the helium vessel are cooled with one of the refrigerators equipped on the top, and evaporated helium gas is liquefied again with the other refrigerator. Therefore, this wiggler can be operated without adding liquid helium.

Recent Instrumental Developments and Experimental Highlights at BESSY I, Future Prospects for BESSY II

W. Braun
Berliner Elektronenspeicherring-Gesellschaft für Synchrotronstrahlung m.b.H. (BESSY)
Lentzeallee 100, D(W)-1000 Berlin 33, Germany

The BESSY company was founded in 1979 after the federal government had decided to build a dedicated 800 MeV XUV source in Berlin. The purpose of the company is the operation and development of synchrotron radiation sources for basic and applied research as well as technology: in particular microlithography for microelectronics and micromechanics and radiometry for the federal governments standards institute. The first beam was stored in December 1981 and user operation started already in February 1982. From mid 1985 onwards the storage ring was operated in the small emittance mode. About 130 user groups perform their experiments at BESSY per year. These groups originate from national and international (mainly European) universities, research institutes, industry and the national institutes of standards. Presently BESSY operates 33 experimental stations with 25 monochromators and 2 X-ray microscopes in the basic research area, 5 experimental stations with 5 monochromators are operated by the Physikalisch-Technische Bundesanstalt (German standards institute) and 4 white light beam lines are dedicated for X-ray lithography purposes.

In the following some recent developments and highlights will be discussed. After commissioning in 1986, the first undulator (a 35 period device) was equipped with two toroidal grating monochromators. These instruments are now used for photoemission spectroscopy in surface and solid state physics as well as for atomic and molecular physics. In particular two photon experiments to determine the angular distributions of photoelectrons of laser excited aligned atoms are performed with high count rates and high resolution (1000 cts/sec and 17.5 meV at 31 eV in the gas phase). In 1992 very high resolution (4 meV at 65 eV) was obtained in first order with a plane grating monochromator (SX-700 II) at a dipole source using a 2400 ℓ/mm grating. Theoretically predicted but hitherto unseen Rydberg states of doubly ionized He were observed [1]. Magnetic X-ray dichroism of deep core levels was observed for the first time in photoelectron spectroscopy [2]. In 1991 the first crossed undulator (6.5 and 7.5 periods) of the Nikitin-Kim type [3] went into operation and its polarization characteristics were determined. As expected, the quality of the circular polarization of this device is determined by the emittance of the storage ring and also decreases as the wavelength decreases, as theoretically predicted. The spherical grating monochromator beam line optimized for operation on this undulator showed its excellent performance. A resolving power in exess of 17000 was obtained at 65 eV. The combination of these devices makes new experiments like magnetic circular dichroism possible, not only in the solid state but also in the gas phase.

Even spin resolved measurements will be possible for photon energies between 30 eV and 200 eV.

A special plane mirror device was developed by H. Petersen and M. Willmann of BESSY to select right and left handed circular polarization from a dipole magnet source. This device was combined with a standard SX-700 monochromator to produce circularly polarized light up to 1000 eV. The degree of circular polarization as a function of off plane angle was determined at 265 eV using a multilayer polarimeter [4]. The measured Stokes parameter S_3 clearly follows the theoretically expected curve. A commercial photoelectron microscope was adapted to this beam line. With this instrument H^+-ion bombarded organic films as well as magnetic domains of ion single crystals have been imaged. In the latter, topography effects can be eliminated by measuring the domains with different helicities. Thus, photoelectron microscopy will help to study magnetic domain properties. Recently, the X-ray microscopes of Prof. Schmahl's group from Göttingen have been further developed. Now specimens can be put in a special preparation chamber and brought into the light path in air. The implementation of a CCD camera helped to reduce the measuring time per picture to below 200 msec. New developments at BESSY also include the test of new designs of monochromators such as Rowland circle and variable line spacing monochromators. Test stations will be set up in the near future.

In July 1992 the construction of the 1.7 GeV third generation synchrotron radiation source, BESSY II, was approved. The project started already in September 1992 in Berlin-Adlershof in the former GDR. New science will be possible in atomic and molecular physics, depth lithography, high resolution X-ray microscopy and photoelectron microscopy for applications in particular in material sciences, catalysis and biology. It will be a storage ring of double achromate symmetry with two different length straight sections. The emittance of that new storage ring will be about 6×10^{-9} m·rad, an order of magnitude smaller than that for the present ring BESSY I. The first beam is scheduled for end of 1997.

[1] M. Domke, G. Remmers and G. Kaindl, Phys. Rev. Lett. 69, 1171 (1992)

[2] L. Baumgarten, C.M. Schneider, H. Petersen, F. Schäfers and J. Kirschner, Phys. Rev. Lett. 65, 492 (1990)

[3] K.-J. Kim, Nucl. Instrum. Meth. 222, 11 (1984)
M.B. Moisev, M.M. Nikitin and N.I. Fedosov, Sov. Phys. Journal 21, 332 (1984)

[4] S. DiFonzo, W. Jark, F. Schäfers, H. Petersen, A. Gaupp and J. Underwood, SRN 6, 16 (1993)

Soft-X-Ray Multilayers for the Uses with Synchrotron Radiation

Masaki Yamamoto and Mihiro Yanagihara

Research Institute for Scientific Measurements, Tohoku University, 2-1-1 Katahira, Aoba-ku, Sendai 980 Japan

Soft-x-ray multilayers have been used as novel optical elements such as a refection filter, a power filter, a polarizer, and a phase shifter. With development of fabrication technique, the multilayer structure is made possible to realize constructive interference of soft-x-ray[1].

The multilayer differs from that in visible region in two respects. Absorption of layer elements limits the attainable reflectance level and interface roughness scatters light, which necessitates a use of super-polished substrate. At present, we can fabricate a multilayer mirror having a high enough reflectance over 50% for various applications at a photon energy up to 100eV.

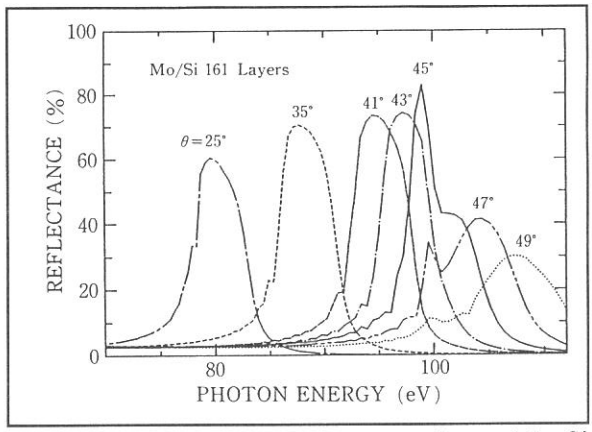

Figure 1 S-reflectance spectra of a Mo-Si multilayer at various angles of incidence

Figure 1 shows reflectance spectra of Mo-Si multilayer measured at various angles of incidence with s-polarization. Such a multilayer can be used as a reflection filter with a 10eV FWHM pass band whose center is tunable by adjusting the angle of incidence. This has been utilized at beamline 11A, PF-KEK, where a multilayer reflection filter delivers high flux photon to a station of photo CVD experiments[2]. In these application with SR, multilayers have been proved to be durable for irradiation of SR of a bending section at a power level of 20W/cm^2. For a power filter application to reduce heat load to beamline optics, irradiation test was carried at BL-28 multipole wiggler, PF-KEK. A Mo/BN multilayer was found survived after 10min exposure of 2.3W/mm^2 irradiation[3].

Another use of the multilayer is in polarization measurements. At near 45° angle of incidence, a multilayer acts as a polarizer since p-reflectance is much smaller than s-reflectance. At a photon energy of 97eV, polarizance of over 97% is easily obtained[4]. With the polarizer, we evaluated the state of polarization of SR coming out of a grasshopper monochromator at BL11A, PF-KEK. It was found that the alignment of beamline optics to the maximum intensity gave elliptical polarization whose axis was not horizontal[5]. This demonstrated that for the best alignment to linear polarization at the center of SR, polarization should be observed.

References

1)T. W. Barbee, Jr., Phys. Scr. **T31**, 147 (1990).
2)M. Yamamoto, *et al*, Phys. Scr. **41** 21 (1990).
3)M. Yanagihara, K. Mayama, S. Asaoka, and H. Maezawa, Proc. SPIE **1739** (1992) in print.
4)T. Maehara, *et al*, Appl. Opt. **30** 5018 (1991).
5)H. Kimura, *et al*, Rev. Sci. Instrum. **63** 1379 (1992)

Review of Recent Progress in Soft X-Ray Monochromators and Their Dispersive Elements

M. Watanabe
UVSOR, Institute for Molecular Science

The soft X-ray region from 40 Å to 6 Å had been somewhat dark. The soft X-ray optics is now being developed from two sides, one of which is long wavelength side using grating monochromators and, the other, short wavelength side using crystal monochromators. It had been suggested that grating monochromators can supply monochromatic light down to 6 Å.[1] Recently, high resolution spectrum of K-absorption on condensed N_2 was obtained with $E/\Delta E$ of 10^4 by the use of Dragon monochromator.[2] The high resolution has been achieved by the use of a grating with a large radius. Further high resolution will be realized by the use of gratings with high groove density or varied space.[3]

In Japan, two types of SiC gratings have been developed. One is the mechanically ruled grating on Au film evaporated on SiC substrate.[4] The other is the holographic grating with the grooves directly ruled on the SiC substrate by ion-beam etching and coated with Au.[5] In both cases, the SiC substrate is durable against the heat load of undulator radiation, but the Au coating is not. Effective cooling system should be developed.

Usually, double crystal monochromators equipped with beryl crystals have supplied monochromatic light with $E/\Delta E$ of 10^3 below 15 Å. Since the beryl is not strong against highly bright radiation, new crystals of β-alumina[6] and YB_{66}[7] have been developed. However, it is a future subject to grow large crystals with good crystallinity.

References

1) H. Petersen : Nucl. Instr. Meth. Phys. Res. A**246** (1986) 260.
2) C. T. Chen and F. Sette : Rev. Sci. Instr. **60** (1989) 1616.
3) M. C. Hetterick : Appl. Opt. **29** (1990) 4531.
4) T. Kita et al. : Rev. Sci. Instr. **63** (1992) 1424.
5) E. Ishiguro et al. : Rev. Sci. Instr. **63** (1992) 1439.
6) J. Wong et al. : Nucl. Instr. Meth. **195** (1982) 133.
7) F. Schafers et al. : Synch. Rad. News **5** (1992) No. 2, 28.

VUV Photochemistry of Rare Gas-Dihalogen van der Waals Complexes Studied by Absorption and Fluorescence Spectroscopy

Kiyohiko TABAYASHI, Atsunari HIRAYA, and Kosuke SHOBATAKE
Institute for Molecular Science, Myodaiji, Okazaki, 444 Japan

One of the merits for the application of SOR light to photochemistry of van der Waals (vdW) complexes lies in that spectral measurements for both direct absorption and fluorescence can be easily carried out in the wide vacuum UV energy regions. In the VUV regions, however, not much work has been done for all a variety of the excited states and opening of new reactive channels for the excited vdW complexes.

Present paper summarizes current VUV photochemical studies[1,2] of rare gas-dihalogen Rg-Cl_2(Rg=Xe,Kr) complexes made in UVSOR(BL2A) using both absorption and fluorescence excitation spectroscopy. As the topics, two types of new vdW bands for Rg-Cl_2 are presented and principal decay processes from the relevant excited states are proposed on the basis of the fluorescence quantum yields determined.

Both bands observed are originated from (1:1)Rg-Cl_2 complex and are attributed to the excitation in Cl_2 moiety. Broad absorption band in the 125-150nm region is assigned to a transition to the excited state of ion-pair $RgCl^+Cl^-$ type. Low fluorescence quantum yield ≤ 0.05 for the band indicates predominant dissociation of the photoexcited vdW complex to the non-fluorescent products,

$$XeCl_2 + h\nu \rightarrow XeCl^+Cl^-(v'=m) \rightarrow Xe + 2Cl$$

Another complex band in the fluorescence excitation spectrum in the 138-145nm region has a vibrational structure ($\Delta\nu \sim 640$ cm^{-1}) and can be assigned to the excitation to the Cl_2^* state of Rydberg character. We propose two kinds of excimer formation channels contribute to the observed emission in the 230-400 nm region,

$$XeCl_2 + h\nu \rightarrow XeCl_2^* \rightarrow XeCl^*(B) + Cl$$
$$\rightarrow Xe + Cl_2^*(3^3\Pi_g)$$

It should be complemented that BL2A was designed to conduct both absorption and fluorescence measurements for gaseous samples such as molecules in a gas cell and molecular complexes in free jets. Although a LiF window has been placed to eliminate higher order of excitation light and isolate sample region from the vacuum systems, fundamental but important spectroscopic data have been accumulated[2] in the energy region below the LiF cut-off. Since detection efficiency of absorption measurements is generally not so high, special precautions have been taken to cover the present experiments, by increasing and controlling the concentration of the complexes and clusters. In order to check directly on the complex size distribution, beam characterization such as TOF photoion-mass analysis should be next programmed in the separate measurements. Ionization of the complexes and clusters without LiF window might be required for the characterization of such kind. Users outside our Institute also have a request to extend the energy range upward, then modification of the setup and measurements without window are our next future projects for BL2A.

References

[1] K. Tabayashi, A. Hiraya, and K. Shobatake, to be published.
[2] K. Shobatake, A. Hiraya, and K. Tabayashi, and T. Ibuki, in *Vacuum Ultraviolet Photoionization and Photodissociation of Molecules and Clusters*, C. Y. Ng ed. (World Sci. Pub. Co. Singapore, 1991), p. 503.

APPLICATION OF VUV UNDULATOR BEAM LINE TO CHEMICAL DYNAMICS AT ALS

Andrew H. Kung and Yuan T. Lee
Department of Chemistry, University of California
and Chemical Sciences Division
Lawrence Berkeley Laboratory, Berkeley, California 94720 USA

Purpose

A new program will be initiated at the Lawrence Berkeley Laboratory (LBL) to explore applications of synchrotron radiation at LBL's Advanced Light Source (ALS) in chemical dynamics, which encompasses all phenomena in which molecules undergo energetic or chemical transformations and to provide the experimental facilities needed for the exploration. The ALS will be used as a photo-analysis source to produce high yields of vacuum ultraviolet photoionized products. If operated in conjunction with powerful lasers, the Light Source will additionally be a powerful tool for the study of chemical processes induced by multiphoton absorption. Its time structure permit the study of ultrafast processes. These studies will culminate in research to determine the microscopic details of the mechanisms and dynamics of primary dissociation processes and elementary chemical reactions, to explore the chemistry of molecules excited to a Rydberg state or to other superexcited states, to study the structure, energetics and chemical reactivity of highly reactive polyatomic radicals and unusual transient species, to probe the nature of inter- and intra-molecular energy relaxation, and to search for bond-selective means to modify and manipulate chemical reactivity.

Approach

The experimental approach involves combining a synchrotron radiation source, lasers, molecular beams, and molecular and spectroscopic detection techniques to carry out the proposed research. The ALS U8.0 undulator beamline will be modified and a new branchline constructed to deliver a high intensity (10^{15}) photons/sec), low resolution (2.5%) VUV beam for selective photoionization and product detection in primary photodissociation and photofragmentation studies. This branchline will feature a differentially pumped gas filter to suppress unwanted orders of the undulator radiation, and torroidal mirrors that focuses the synchrotron light to a spot of ~100 μm. The ability to focus a small spot size is a special characteristic of undulator radiation. It will lead to highly improved mass and energy resolution in ion and electron detection in the proposed experiments.

Standard lasers in the IR, Visible, and UV, and specially fabricated high-power, high-resolution lasers in the mid-IR and VUV will be used in conjunction with the undulator beamline to carry out pump-probe and state-to-state selective dynamics experiments throughout the optical region of the electromagnetic spectrum.

Projects of 1993

1. Design and fabrication of branchline at the ALS U8.0 undulator beamline. It is necessary to modify the existing U8.0 beamline so that VUV photons can be deflected, filtered, and refocused into the molecular beam chamber. A new torroidal mirror and associated

vacuum chamber will be inserted as the deflector that also serves to squeeze the photon beam through a differentially-pumped high-order suppressor. This high-order suppressor is used to absorb unwanted high energy photons that are found in abundance in the undulator beam. A second torroidal mirror then recollimates the beam to a cross-section of the order of 100 μm x 0.5 mm located at the detector ionization region or at the point where two molecular beams cross in the sample chamber. The VUV beam is then sent through a normal incidence monochromator to provide light for experiments that require higher resolution than the undulator can produce.

2. Design and fabrication of molecular beam experimental station. Two stations are planned. One will be designed for experiments requiring the highest available VUV fluxes and one will be for experiments that need to utilize higher resolution than the 2.5% bandwidth that the U8.0 undulator normally provides. It is anticipated that the majority of experiments will fall in the former category.

The first station will be a universal rotating-source crossed-molecular-beam apparatus designed to use the ALS as a photoanalysis source. The tunable output from the U8.0 undulator will be used directly, without additional frequency filtering. The apparatus will be designed for studying primary photochemical processes and the dynamics and reactivity of polyatomic molecules, ions and clusters, using photofragmentation translational spectroscopy. The ALS beam will be shaped and transmitted through the ionizer region of the conventional TOF mass analyzer and serves to ionize photodissociation products. This unique approach is advantageous for product detection because it provides both improved species selectivity and reduced background detection. Alternatively, for certain experiments, the ALS beam will be directed to the molecular-beams interaction region to be used as an excitation source. In this case, an electron impact ionizer will be used in the same TOF apparatus. Differential pumping will be employed extensively to protect against systematic and accidental contamination of the synchrotron beamline and storage ring apparatus.

Experiments that require a higher resolution that the 2.5% bandwidth that the U8.0 undulator can provide will be performed in a second station. The ALS beam exiting from the first station will be passed through a 1-m normal incidence monochromator to obtain a 100-fold improvement in wavelength resolution. This monochromatized beam will be collimated and delivered to a molecular beam apparatus. The apparatus will be "conventional" in design, equipped with a TOF mass spectrometer and a zero-electron-kinetic-energy (ZEKE) spectrometer. Since this station will be located further downstream from the storage ring, the vacuum protection requirements will be less stringent. This station will be particularly useful for studying VUV and IR spectroscopy of superexcited molecules, free radicals, and other transient species.

Molecular source chambers for generating radicals, ions and clusters, both CW and pulsed, will be constructed to be used at both stations. Oil-free vacuum equipment will be employed for all chambers. Tunable lasers for pump-probe experiments will be included.

This work was supported by the Director, Office of Energy Research, Office of Basic Energy Sciences, Chemical Sciences Division, of the U.S. Department of Energy under Contract No. DE-AC03-76SF00098.

RESONANCE-AUGER-ELECTRON–PHOTOION COINCIDENCE STUDIES ON STATE-TO-STATE DISSOCIATION DYNAMICS OF INNER-SHELL-EXCITED MOLECULES

Yukinori Sato

Research Institute for Scientific Measurements, Tohoku University, Sendai 980, Japan

Decay of a core-excited molecule is a complex of a variety of processes including the electronic processes as well as the relaxation in nuclear degrees of freedom. In most cases, the primary decay of a core-excited molecule occurs electronically with the ejection of Auger electrons, and the resultant cation may then be subject to dissociation processes. We have started a series of coincidence experiments between the Auger electrons and the photofragment ions of core-excited molecules, using the SR of the 2.5 GeV storage ring at the Photon Factory of KEK in Tsukuba [1-3]. I present here the study on the decay of the core-excited resonance of BF_3 produced by the photoexcitation of the B-K electron into the lowest unoccupied $2a_2''(2p_{z,B})$ orbital [3].

The time-of-flight mass-analysis of the fragment ions is performed in coincidence with the energy analysis of the B:KVV normal- and resonance-Auger electrons as well as the valence photoelectrons. The results are summarized as follows:

(a) Direct photoionization of the valence electrons or the participant-resonance-Auger decay of the core-excited resonance results in the BF_3^+ states with one hole in an outer-valence orbital. The resultant BF_3^+ states dissociate to yield the BF_2^+ ion.

(b) The spectator-resonance-Auger decay of the core-excited resonance results in the excited BF_3^+ states having one excited (a_2'') electron and two outer-valence holes. The resultant BF_3^+ states dissociate to yield the B^+ ion as the predominant ionic fragment.

The results (a) and (b) demonstrate a dramatic change of dissociation induced by one electron excitation from an outer-valence orbital to the a_2'' orbital in the BF_3^+ states.

(c) The excited BF_3^+ states having one excited (a_2'') electron, one outer-valence hole, and one inner-valence hole are energetically allowed to autoionize into the dicationic BF_3^{++} states but are subject to a primary fast dissociation before the autoionization.

(d) The spectator-resonance-Auger-final BF_3^+ states have been assigned to have two types of two-hole locations; one is localized at a single F atomic site and the other at different F atomic sites. However, no significant difference is observed in dissociation between the two types of two-hole locations.

In conclusion, the coincidence measurements between the resonance-Auger electrons and the fragment ions provide us with a new method to investigate the state-to-state dissociation dynamics of various excited monocationic states.

1. E. Shigemasa, T. Koizumi, Y. Itoh, T. Hayaishi, K. Okuno, A. Danjo, Y. Sato, and A. Yagishita, Rev. Sci. Instrum. **63**, 1505 (1992).

2. Y. Sato, K. Ueda, H. Chiba, E. Shigemasa and A. Yagishita, Chem. Phys. Lett., **196**, 475 (1992).

3. K. Ueda, H. Chiba, Y. Sato, E. Shigemasa, and A. Yagishita, Phys. Rev. A **46**, R5 (1992).

MULTIPHOTOIONISATION FOLLOWING INNERSHELL EXCITATION

M.Simon, M.Lavollée, R.Thissen, D.Thomas, P.Morin and P.Lablanquie

LURE, Bâtiment 209D, Fac des Sciences, 91405 ORSAY Cédex FRANCE

Multiphotoionisation processes have recently become the subject of many detailed investigations. Here we will just stress a part of this wide field, and give a few examples to illustrate the special case where they are produced through innershell excitation. As opposed to the "direct" multiphotoionisation case in the valence region (where the dominent process is single photoionisation), it is a very intense and effective way to create multicharged ions.

As suggested in the title, a useful guide to describe the processes is to use the time evolution of the system, which can be considered to occur in the following successive steps: 1) photon absorption giving rise to the excitation of an innershell electron 2) electronic relaxation -or "creation" of a multicharged species- 3) nuclear motion -that is vibration, rotation and possibly dissociation of the excited ion. Here are given some examples extracted from the work performed in our laboratory, to illustrate this description and its limits:

-1) the different kinds of innershell excitation processes can be visualised through absorption measurement; due to the high energy range (typically 100 to 1000eV) such high resolution experiment have only recently been possible[1]. In LURE, a high resolution plane grating monochromator in the 20-200 eV photon energy range was constructed recently. Its high resolving power (routinely 5000) enables to study the broadening of these innershell resonances, and consequently gives us the lifetime of the transient excited state; for H_2S, the excited state vibrational structures could also be resolved for the first time[2].

-2) The well known Auger effects (resonant or not) then give lead to the formation of multicharged ions. Though studied since a long time, we just begin to have a clear view ofthe branching ratios between the different production mechanisms and ionisation degrees of the final state. An example is the relaxation of the $3d_{5/2}$ –> 5p transition in Krypton; we showed[3] that its relaxation gives dominently doubly charged ions, produced in a 2 step electron emission.

Electronic relaxation in molecules is futhermore complicated by the nuclear motion of the squeleton. However, in a good first approximation, it can generally be considered that electronic relaxation occurs with nuclei fixed, the subsequent motion of these ocurring later, in the

multicharged environment. Caution is however essential: P.Morin et al[4] showed that in HBr, rapid loss of an H atom can sometimes efficiently compete with the electronic relaxation. Since then, other examples have been found, usually envolving a rapid H release prior to electronic relaxation.

-3) The multicharged molecule we then obtain is usually, (but not always) unstable. It is precisely the mechanisms of these dissociations we want to analyze. In order to visualize all ionization degrees and dissociation paths, we developped a multidimension mass spectroscopy experiment "EPICE" described in ref [5] whose advantage is to be able to detect, in coincidence, all the ionic fragments from the same ionisation event, and their time correlation. Analysis of these correlations is a very powerful tool to observe the dissociation mechanisms, it was first developped by John Eland, and deeper understanding is constantly gained[6].

As an example we will mention here the case of the $Fe(CO)_2(NO)_2$ molecule. We were interested to see whether excitation of an innershell electron from the metal Fe or from one of the ligands NO or CO gave rise to a specific dissociation process, or in other terms whether some selective fragmentation could be initiated. Our results[7] showed that extensive fragmentation is experienced, that occurs through successive evaporation of the ligands (charged or not); moreover whatever the innershell electron we excite, the same final state is observed; it shows that the memory of the excitation route is lost at the end; explanation is that, after electronic relaxation, the multicharged ion has time to vibrate and redistribute its internal energy in vibrational modes, prior to a statistical dissociation.

As a conclusion, we showed that the innershell photoexcitation mechanism is a powerful means to produce multicharged species in order to investigate their dissociation mechanisms. Coincidence technique is essential and will certainly be greatly developped in the future. One such extension is the Auger electron / ion(s) coincidence experiment developped in Tsukuba, USA and also in LURE.

REFERENCES

1) M.Watanabe, Progress Report in this conference
2) D.Thomas, M.Coville, R.Thissen & P.Morin *Synchrotron Radiation News*, 5 n°3 (1992) 8
3) P.Lablanquie & P.Morin *J.Phys.B* 24 (1991) 4349
4) P.Morin & I.Nenner *Phys.Rev.Lett.* 56 (1986) 1913
5)M.Simon, T.LeBrun, P.Morin, M.Lavollée and J.L.Maréchal *Nucl.Instr.& Meth.* B62(1991)167
6) J.Eland *Acc. Chem. Res* 22(1989)381 M.Lavollee & H.Bergeron *J.PhysB* 25 (1992) 3101
7) M.Simon, M.Lavollée, T.LeBrun, J.Delwiche, M.J.Hubin and P.Morin *Conf.Proc. "Synchrotron Radiation and Dynamic Phenomena , Grenoble 1991, A.I.P.(accepted)*

Spectroscopy and Dynamics of Superexcited Molecules

Yoshihiko HATANO
Department of Chemistry
Tokyo Institute of Technology
Meguro-ku, Tokyo 152, Japan

A survey is given of the entitled subject based mainly on the author's recent review articles and talks[1-4].

After introducing briefly a historical background of the entitled subject such as the Platzman's theoretical idea of a scheme of the formation and decay of superexcited states AB',

$$\begin{array}{l} AB + \text{energy} \\ \quad (> Ip) \end{array} \rightleftarrows AB^+ + e^- \qquad AB' \rightleftarrows AB^+ + e^- \quad (\searrow\ A + B)$$

and the electron impact studies of this scheme[5], recent advances in synchrotron radiation studies of the spectroscopy and dynamics of superexcited molecules are surveyed by choosing some typical examples of molecules from the recent investigations by the author's group summarized as follows.

(1)Dissociation dynamics of doubly excited molecular hydrogen[6,7],
(2)Angular momentum population of excited hydrogen atoms produced by the dissociation of H_2[8],
(3)Dissociation dynamics of N_2[9], O_2[10], CO_2[11], SiH_4[12], Si_2H_6[13], and C_2H_2[14] in the superexcited states, and
(4)Absolute measurements of photoabsorption cross sections, photoionization cross sections, photodissociation cross sections, and photoionization quantum yields of hydrocarbons[14-17], Si-containing molecules[12,13], ethers[17-19], and alcohols[17-19].

It is concluded from these investigations that the electronic structure of superexcited molecules is characterized with their decaying processes of the dissociation into neutral fragments in competing with antoionization and is classified into the following four types.

1)Vibrationally excited,
2)Doubly excited, or
3)Inner-core excited high Rydberg states converging to each ion state, or
4)Inner-core excited non-Rydberg states.

Finally, comments on future prospects and problems as divided into those of experimental techniques and research objectives are presented from the viewpoint of the application of synchrotron radiation to molecular science.

References

1)Y.Hatano, "The Chemistry of Synchrotron Radiation" in "Radiation Research", ed., E.M.Fielden, J.F.Fowler, J.H.Hendry, and D.Scott, Taylor & Francis(1987), p.35.

2)Y.Hatano, "Dynamics of Superexcited Molecules" in "Dynamics of Excited Molecules", ed., K.Kuchitsu, Elsevier, in press.

3)Y.Hatano, "Dissociation Dynamics of Superexcited Molecules", Invited paper, 14th Int.Symp.Mol.Beams,Asilomer(1992).

4)Y.Hatano, "Dynamics of Superexcited Molecules", Invited talk, Gordon Res.Conf.on Radiat.Chem.,Newport(1992).

5)Y.Hatano, Comments on At.Mol.Phys.,13,259(1983).

6)S.Arai, T.Yoshimi, M.Morita, K.Hironaka, T.Yoshida, H.Koizumi, K.Shinsaka, Y.Hatano, A.Yagishita, and K.Ito, Z.Phys.D;Atoms, Molecules, and Clusters,4,65(1986).

7)S.Arai, T.Kamosaki, M.Ukai, K.Shinsaka, Y.Hatano, Y.Ito, H.Koizumi, A.Yagishita, K.Ito, and K.Tanaka, J.Chem.Phys.,88,3016(1988).

8)N.Kouchi, N.Terazawa, Y.Chikahiro, M.Ukai, K.Kameta, Y.Hatano, and K.Tanaka, Chem.Phys.Lett.,190,319(1992).

9)M.Ukai, K.Kameta, N.Kouchi, Y.Hatano, and K.Tanaka, Phys.Rev.A,46 (11),(1992),in press.

10)M.Ukai, N.Kouchi, K.Kameta, N.Terazawa, Y.Chikahiro, Y.Hatano, and K.Tanaka, Chem.Phys.Lett.,195,298(1992).

11)M.Ukai, K.Kameta, N.Kouchi, K.Nagano, Y.Hatano, and K.Tanaka, J.Chem.Phys.,97,2835(1992).

12)K.Kameta, M.Ukai, R.Chiba, K.Nagano, N.Kouchi, Y.Hatano, and K.Tanaka, ibid.,95,1456(1991).

13)K.Kameta, M.Ukai, N.Terazawa, K.Nagano, Y.Chikahiro, N.Kouchi, Y.Hatano, and K.Tanaka, ibid.,95,6188(1991).

14)M.Ukai, K.Kameta, R.Chiba, K.Nagano, N.Kouchi, Y.Hatano, H.Umemoto, Y.Ito, and K.Tanaka, ibid., 95,4142(1991).

15)H.Koizumi, T.Yoshimi, K.Shinsaka, M.Ukai, M.Morita, Y.Hatano, A.Yagishita, and K.Ito, ibid.,82,4856(1985).

16)H.Koizumi, K.Shinsaka, and Y.Hatano, Radiat.Phys.Chem.,34,87(1989).

17)H.Koizumi, K.Shinsaka, T.Yoshimi, K.Hironaka, S.Arai, M.Ukai, M.Morita, H.Nakazawa, A.Kimura, Y.Hatano, Y.Ito, Y.Zhang, A.Yagishita, K.Ito, and K.Tanaka, ibid.,32,111(1988).

18)H.Koizumi, K.Hironaka, K.Shinsaka, S.Arai, H.Nakazawa, A.Kimura, Y.Hatano, Y.Ito, Y.Zhang, A.Yagishita, K.Ito, and K.Tanaka, J.Chem.Phys.,85,4276(1986).

19)K.Kameta, M.Ukai, T.Kamosaki, K.Shinsaka, N.Kouchi, Y.Hatano, and K.Tanaka, ibid.,96,4911(1992).

Negative-Ion Formation from Molecules, Clusters, and Condensed-Gas Surfaces.

Koichiro Mitsuke
Department of Vacuum UV Photoscience,
Institute for Molecular Science, Myodaiji, Okazaki 444

Ion-pair formation is a very common process of highly-excited molecules in the photon energy range of 10 - 50 eV. Negative-ion mass spectrometry (NIMS) enables us to study ion-pair processes in various molecules:[1] diatomic [O_2, H_2, CO, NO], triatomic [N_2O, OCS, CO_2, SO_2], saturated and unsaturated hydrocarbons [C_nH_{2n+2} ($1 \leqq n \leqq 5$), C_2H_4, C_2H_2], and halogenides [SF_6, CF_4, CH_3F, CH_3Cl, CH_3Br]. We have measured the efficiency curves of negative ions using monochromatized synchrotron radiation. A series of works demonstrates that NIMS provides a sensitive probe to investigate the properties of Rydberg states lying in the vacuum ultraviolet —— not only their spectroscopy but also their dynamical behavior in predissociation —— if the ion-pair continuum interacts strongly with these discrete states. A great interest has also been taken in the dynamics of the ion-pair formation as half-collisional version of the electron-transfer reaction. In the case of clusters or condensed gas-surfaces, it is probable that the ion-pair formation plays an important role in the vacuum UV photoscience, since the electronic couplings with the neighboring molecules or substrate change the high-energy relaxation dynamics in superexcited states. For example, the $O^+ + O^-$ production from quasi-bound positive-energy excitons has been observed in the condensed oxygen.[2]

Last year, We developed a new coincidence technique, PINICO, which utilizes the flight-time correlation of a pair of positive and negative ions produced by single photon excitation.[3] This method is likely to prove eminently useful to study the ion-pair formation process. In this conference, we presented our molecular-beam photoexcitation apparatus, recent results on NIMS and PINICO, discussion on the spectroscopy and dynamics of molecular superexcited states, and future prospects of applying these experimental methods to clusters and condensed-gas surfaces.

References

1) K. Mitsuke, S. Suzuki, T. Imamura, and I. Koyano, *J. Chem. Phys.* **92,** 6556 (1990); *ibid.* **93,** 1710 (1990); *ibid.* **93,** 8717 (1990); *ibid.* **94,** 6003 (1991); *ibid.* **95,** 2398 (1991); *ibid.* **96,** 7550 (1992); J. Org. Mass Spectrom. to be published.
2) G. Dujardin, L. Hellner, L. Philippe, R. Azria, and M. J. Besnard-Ramage, *Phys. Rev. Lett.* **67,** 1844 (1991).
3) K. Mitsuke, H. Yoshida, and H. Hattori, to be published.

SPECTROSCOPY OF MOLECULES IN GASEOUS AND OF MOLECULAR CENTERS IN CONDENSED PHASE

Georg ZIMMERER

II. Institute of Exp. Physics, The University of Hamburg
2000 Hamburg 50, Germany

Very early luminescence experiments on rare gas solids (RGS) and rare gas liquids yielded close similarities between the dense gaseous phase and the condensed phases [1]. The similarities arise from the fact that an emitting center in the condensed phases exists which corresponds to a rare gas dimer, R_2^*, embedded into a matrix of the same kind of atoms. This was the starting point for spectroscopic investigations of the emitting species with SR of the storage ring DORIS at DESY, Hamburg. It turned out that time- and spectrally resolved luminescence spectroscopy under selective photon excitation is a powerful method to investigate the properties of the R_2^* molecules in the gas phase and of the R_2^*-type centers in the solid phase. After an initial period of experiments at the HIGITI station of HASYLAB, the experimental station SUPERLUMI was constructed for this purpose [2].

Another starting point was the unique contribution of Toyozawa at the VUV-4 conference in 1974 [3]. In Toyozawa's theory, the formation of the R_2^* centers was attributed to the peculiarities of exciton lattice interaction. Moreover, the co-existence of free excitons (FE) in the unrelaxed lattice, and of so-called selftrapped excitons (STE) like the R_2^* centers in a locally distorted lattice was predicted. This co-existence should show up in the luminescence spectra, and, indeed, was found lateron. The early work has been described elsewhere [4]. Several examples of our gas-phase work have been published in [5].

In this contribution, a few very recent solid-state results are presented which are of great relevance for the fundamental properties of RGS-excitons.

(i) FE-spectroscopy: in the early work [4], an order-of-magnitude discrepancy between the intensity ratio of FE versus STE luminescence on one side, and the measured FE-lifetime was reported. Very recently, it was possible to prepare Xe samples in which the FE line is so intense that this discrepancy can be removed [6]. Fig. 1 shows that the peak-to-peak ratio is $\cong 50$, and the ratio of the wavelength-integrated spectra is $\cong 1$. A typical decay curve of the FE line is shown in the inset, together with a time-resolved spectrum of the STE band. Superimposed to a background originating from the triplet state, a signal with fast rise and decay is observed (singlet state of STE). The temporal behaviour of the singlet emission can be quantitatively fitted convoluting the temporal FE-spectrum with the exponential singlet decay. In other words, in a high-quality Xe crystal, the STE precursor is indeed the FE. Only then it is possible to deduce the self-trapping rates from the intensity ratio and the FE decay rate [6].

(ii) Exciton-induced desorption: The microscopic mechanism of desorption of neutral atoms from the surface of a pure or a rare gas doped RGS is closely ralated to exciton-lattice interaction [7]. Luminescence spectroscopy is especially well suited to detect desorbed excited atoms which emit resonance fluorescence after desorption. The SUPERLUMI station is so sensitive that even desorption from doped systems can be investigated. Metastable and neutral ground-state atoms have been detected as well [7]. It was even possible to measure the partial yield spectra of each desorption channel. First theoretical calculations of the interaction potentials of an excited Kr sur-

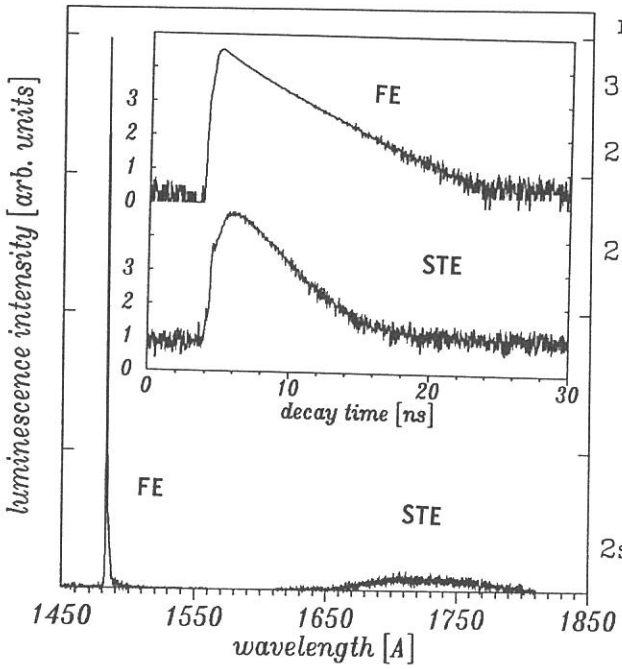

Fig. 1 Luminescence of solid Xe at T= 4.7K, excited with 1400Å-light. Note the logarithmic intensity scale of the inset.

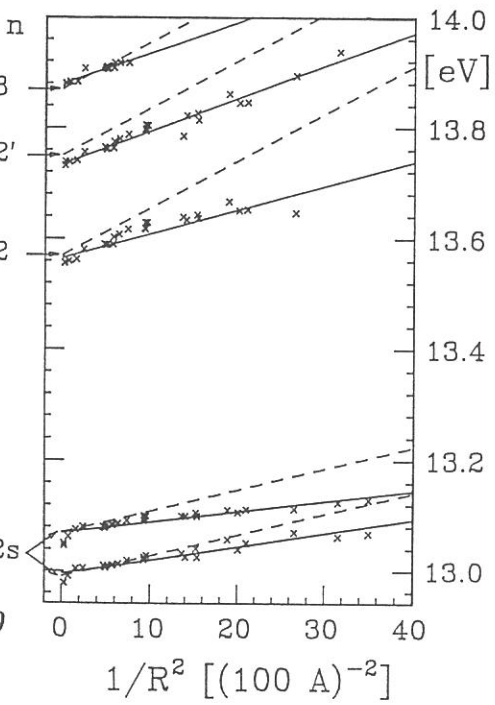

Fig. 2 Energetic positions of excitons in Ar clusters. R = cluster radius

face atom with an Ar host have been carrried out leading to a microscopic understanding of the sputtering process [8].

(iii) Confined excitons in rare-gas clusters: it is a fundamental question, how the Wannier-type excitons of RGS develop as a function of particle size starting from the atoms or molecules. A powerful cluster-beam apparatus has been constructed in which the skimmed beam is crossed with monochromatized SR. The emitted clusterluminescence is detected either wavelength-integrated or spectrally and even time resolved [9]. Fig. 2 shows the energetic positions of surface (n=2(s) and of bulk Wannier-type excitons (n=2,2';3) of Ar clusters as a function of $1/R^2$ (R: cluster radius) [10]. The straight lines observed can be explained with confinement models. The luminescence methods can be used as well to investigate fragmentation and relaxation processes.

[1] J.Jortner, L.Meyer, S.A.Rice and E.G.Wilson, J.Chem.Phys.42 (1965) 4250
[2] G.Zimmerer, Nucl. Instr. Meth. in Phys. Res. A308 (1991) 178
[3] Y. Toyozawa: in Vacuum Ultraviolet Radiation Physics, ed. by E.E.Koch, R. Haensel and C. Kunz (Vieweg-Pergamon, Braunschweig, 1974) p. 317
[4] G.Zimmerer: in Excited-State Spectroscopy in Solids, ed. by U.M.Grassano and N. Terzi (North-Holland, Amsterdam, 1987)
[5] T. Möller and G. Zimmerer, Physica Scripta T17 (1987) 177
[6] D. Varding et al. (to be published)
[7] T.Kloiber and G.Zimmerer, Rad. Eff. Def. in Solids 109 (1989) 219
[8] M. Runne et al. to be published in Nucl. Instr. Meth. (B. Section)
[9] T. Möller: in Progress and Application of Synchrotron Radiation to Molecules and Clusters, ed. by A. Ding (Cambridge University Press), in preparation
[10] J. Wörmer, M. Joppien, G. Zimmerer, and T. Möller, PRL 67 (1991) 2053

Polarized Absorption Spectroscopy on σ-Conjugated Polymers: Polysilanes and Polygermanes

Y. Tokura

Department of Physics, University of Tokyo, Tokyo 113, Japan

Polysilanes (and polygermanes) are extended Si (Ge) polymers with organic substituent in which σ electrons are considered to be delocalized on the Si (Ge) backbones. Ideal polymer structures with regular sequences may be viewed as ultimate quantum wires made of Si (Ge). To elucidate their overall electronic structures, polarized absorption spectra on highly oriented films of polysilanes and polygermanes have been investigated over a wide photon-energy region by utilizing synchrotron radiation from the UV-SOR ring at IMS.

Polarized absorption spectra (77K) with polarization parallel (E//) and perpendicular (E$\perp$) are shown in Fig. 1 for the trans planar forms of polydihexylsilane (PDHS) and polydihexylgermane (PDHG). The both spectra show very common features for spectral shapes, polarization dependence and energy positions, indicating nearly identical electronic structures. The polarized absorption spectra can be well compared with the theoretical band calculation, as demonstrated in Fig. 2. The results indicated that the one-dimensional (1D) band model works well in polysilanes and polygermanes. Detailed results and discussion have been reported in the references listed below.

H. Tachibana, Y. Kawabata, S. Koshihara, T. Arima Y. Moritomo and Y. Tokura, Phys. Rev. B 44, 5487 (1991).

H. Tachibana, K. Kawabata, A. Yamaguchi, Y. Moritomo, S. Koshihara and Y. Tokura, Phys. Rev. B 45, 8752 (1992).

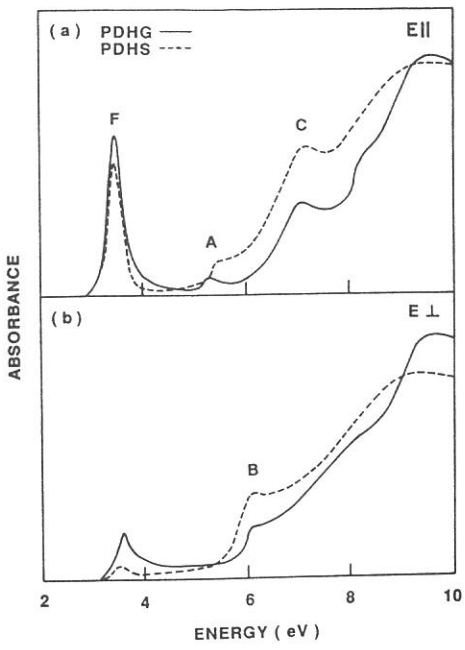

FIG. 1. Polarized absorption spectra of highly oriented films of *trans*-planar PDHG (solid line) and PDHS (dashed line) at 77 K.

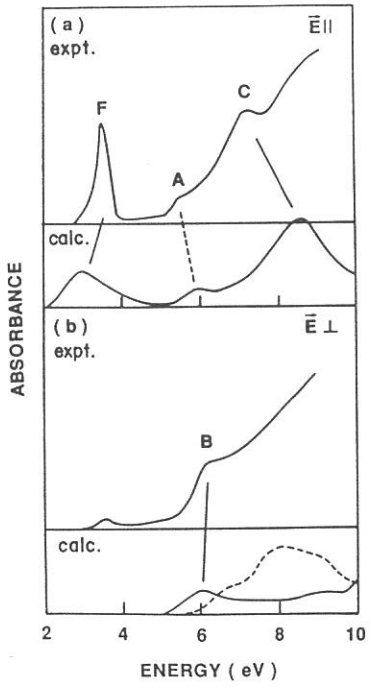

FIG. 2. Observed and calculated absorption spectra polarized parallel (a) and perpendicular (b) to the polymer chain. For the calculated spectra polarized perpendicular to the polymer chain, solid and broken line represent absorption for the polarizations parallel and perpendicular to the plane of the Si backbone, respectively.

Molecular Orientation in Thin Films of Functional Molecules by Means of Angle Resolved Photoemission

Nobuo UENO

Department of Materials Science, Faculty of Engineering, Chiba University
Yayoi-cho, Inage-ku, Chiba 263, Japan

The angular distribution of photoelectrons from thin films of organic crystals involves information on the molecular orientation in the film as well as on the wave functions of valence electrons. Therefore, the quantitative analysis of the photoelectron angular distribution from a valence state gives a detailed information on the molecular orientation in ultrathin films of functional organic molecule, when the initial-state wave function is known. An advantage of the angle-resolved ultraviolet photoelectron spectroscopy (ARUPS) in determining the molecular orientation is that it introduces much less radiation damages into the organic films than other surface sensitive techniques with electron beams. However, the quantitative analysis of the angular distribution from thin films of large organic molecules is very difficult, since the molecule consists of many atoms. Hence the analysis has been mainly performed by a symmetry consideration on the photoemission process with the dipole selection rule, and no one has performed the quantitative analysis of the angular distribution since a challenging work by Permien *et al.* [1] on thin films of lead phthalocyanine and Richardson's successful analysis [2] on their ARUPS data. In our work on ARUPS of thin films of large organic molecules, however, we found that the angular distribution calculated with the theoretical model used by Richardson [2], where the molecule was considered to be a point emitter of photoelectron, gave poor agreement with our experimental results on thin films of copper phthalocyanine [3] which showed a very sharp angular distribution.

In this talk, it is shown that the experimental ARUPS results on thin films of metal free phthalocyanine on MoS_2 crystal surface, where the molecules lie flat on the surface, can be quantitatively explained by a calculated photoelectron angular distribution using the independent atomic center (IAC) approximation [4] combined with MNDO molecular orbital calculation. The results indicate that IAC approximation combined with molecular orbital calculation is useful in the quantitative analysis of photoelectron angular distribution from thin films of large organic molecules. Further, an example of the determination of the molecular orientation with ARUPS is presented for thin films of BTQBT [bis(1,2,5-thiadiazolo)-*p*-quinobis(1,3-dithiole)] evaporated on graphite (HOPG) surface.

REFERENCES

[1] T. Permien, R. Engelhardt, C. A. Feldmann and E. E. Koch, Chem. Phys. Lett. **98** 527 (1983).
[2] N. V. Richardson, Chem. Phys. Lett. **102** 390 (1983).
[3] N. Ueno *et al.*, unpublished.
[4] W. D. Grobman, Phys. Rev. B**17** 4573 (1978).

Time-Resolved Spectroscopic Study on the Self-Trapped Excitons in Alkali Halide Crystals

Ken-ichi Kan'no
Department of Physics, Kyoto University

In the last few years, a new stage has been brought to understanding self-trapped exciton (STE) luminescence in alkali halide crystals with relation to the adiabatic instability of STE's.[1] The important point made clear is that the STE emission bands are classified into three types, I, II and III, irrespective of the traditional classification into two categories (σ and π bands).[2] This suggests that there appear, at most, three distinct local minima in the adiabatic potential energy surface (APES) of the lowest energy, corresponding to the on-center (I) and two different off-center (II,III) configurations. One of the urgent topics to be studied is to see how the shape of the APES is, and how the population is fed into each minimum.

We have studied the origin of the short lifetime singlet σ emission band, and its relation to the longer lifetime triplet π luminescent state. Decay curves of the type I emission bands, that is, σ emission bands in NaCl, KBr, RbBr, KI and RbI and π emission bands in NaBr and NaI, were measured using TAC method at UVSOR under single-bunch operation.[3] Counting photons over four orders of magnitude have revealed that every σ emission band involves a phosphorescent component with a lifetime longer than 100 ns, in addition to the main fluorescent component. The phosphorescent component shows almost the same emission and excitation spectra as those of the fluorescent one. This evidences that the σ emission band originates from the lowest orbital state of the the STE. Thus, it becomes clear that type I emission results, in general, from radiative decays of nearly degenerate singlet-triplet manifolds of the on-center STE. Simultaneous detection through two different time windows discloses a split in the peak energy of the singlet and triplet components, suggesting a slight difference in the location of the minima in the APES for the singlet-triplet STE pair. Based on these results, a new scheme for the dynamics of exciton self-trapping are proposed.

1) W.B. Fowler and N. Itoh (editors), Rev. Solid State Sci. 4, 357-465 (1990).
2) K. Kan'no, K. Tanaka and T. Hayashi, Rev. Solid State Sci. 4, 383 (1990).
3) T. Matsumoto, T. Kawata, A. Miyamoto, and K. Kan'no, J. Phys. Soc. Jpn. 61, 4229-4241 (1992).

Present and Future of Photoelectron and Photodesorption Spectroscopic Studies at UVSOR

Masao Kamada

Institute for Molecular Science, UVSOR

Myodaiji, Okazaki 444, Japan

The photoelectron (UPS) experiments have been carried out at three beam lines (2B1, 6A2, and 8B2), and photodesorption (PSD) has been measured at three beam lines (3A1, 5B, and 6A2).

UPS has been applied to many materials and surfaces in order to know binding energy, p-DOS, k-dispersion, and so on. Now, UPS is recognized to be useful, standard, and powerful method for Molecular Science. Tunability and polarization of SR are very effective in UPS. Moreover, it is stressed that UPS presents new concepts to optical and PSD spectroscopies, and also it is the other way around. Therefore, new science is expected on the crossing between UPS, optical, and PSD. As an example, UPS studies of core-exciton decay on wide-band gap materials are presented.

Among lots of attractive subjects for future of UPS, spin-resolved UPS with circular polarized SR on non-magnetic materials is interesting and promising, since the spin-resolved electronic states and the spin-dependent decay processes can be clearly understood. The planning of the spin-resolved UPS studies is presented with the design of a spin detector.

PSD is also a young and attractive spectroscopy, since it is related with basic science and engineering. Tunability, high intensity, and pulsive nature of SR are very powerful to PSD. The interesting results of time-response of the excited-state alkali desorption are shown on SR-irradiated sodium halides. The planning of the high-sensitive detection system is proposed for one of the future PSD experiments.

High Resolution Photoelectron Spectroscopy on Solids: Past, Present and Future

I. Lindau

MAX-Laboratory, Lund University, Lund, Sweden
and
Stanford Synchrotron Radiation Laboratory, Stanford University, Stanford, USA

ABSTRACT

In 1964 electron spectroscopy of inner core levels had reached sufficiently high energy resolution that chemical shifts [1] were detected for the first time for sulphur in some sodium compounds: the technique of electron spectroscopy for chemical analysis (ESCA) was born. About ten years later, Gelius et al [2] published a paper where monochromatized Al Kα radiation made it possible to resolve vibrational levels in the carbon ls level of CH_4. Since the mid-1970's, synchrotron radiation has played an increasingly important role in high resolution core-level spectroscopy. The instrumental resolution has been improved to well below 100 meV for core levels with binding energies below about 200 eV. In this talk, we will review some recent high resolution core level work at MAX-Lab, Lund University, Sweden, and we will discuss future opportunities with the next generation of synchrotron radiation sources.

From an instrumental point of view it is argued that it is extremely important to have an optimal match between the synchrotron radiation source, the monochromator/optical system, the electron spectrometer and the detector. The system in its entirety will not perform better than its weakest component. The centerpiece of MAX-Lab is a 550 MeV storage ring, with fairly low emittance: 40 nm-rad horizontally. The beam current is typically 100-200 mA and the lifetime 3-4 hours. The work reported here was done on a bending magnet beamline, equipped with a modified SX-700 plane grating monochromator [3]. With a typical source size of 100 microns (vertical) x 400 microns (horizontal), the photon spot on the sample is about 0.5 mm x 3 mm. This spot size is well matched to the acceptance of the energy analyzer which is of the hemispherical type, developed and manufactured at the Institute of Physics at Uppsala University (under the leadership of Prof. N. Mårtensson) in close collaboration with Scienta [4,5].

The beam line covers the spectral region from 20 eV to 1000 eV. The resolving power of the monochromator at for instance 240 eV is 4000. For core levels with binding energies below 100 eV extremely good resolution and intensity can be achieved, as demonstrated by the 2p core level spectra from a single crystal of Al(100). With a total instrumental resolution of 50 meV and a data accumulation time of less than 20 minutes, a surface core-level shifted peak can be determined with high accuracy,-96 ± 5 meV [6]. On the (111) surface, no core-level shifted peak is observed to within 15 meV. These observations are state-of-the-art experimentally and pose challenges for future theoretical calculations.

Measurements of surface core level shifts play an important role in the understanding of both the electronic and structural properties of surface layers. Furthermore, surface core level shifts can be correlated with thermodynamical properties of the surface, like solution, segregation, and adhesion energies. With the new experimental capabilities at MAX-Lab, it has been possible to study the 3d core levels of the 4d transition metals with high resolution: 0.2-0.3 eV

total instrumental resolution for photon energies 380-450 eV [7]. For a Pd (100) single crystal, a surface core-level shift of 0.44 ± 0.03 eV towards lower energy has been determined for the Pd 3d core level (binding energy 335 eV). Adsorption of CO on the very same surface results in three different ordered structures dependent on the CO coverage. High resolution spectra of the Pd 3d and C 1s core levels (instrumental resolution of 270 meV and 220 meV, respectively) make it possible to establish a direct relation between the detailed geometry of the CO overlayer and differently shifted peaks in the Pd 3d spectra [8]. From the C 1s spectra, it is furthermore possible to establish and confirm earlier reports that CO only occupies bridge sites on Pd (100).

It has been commonly assumed that no intermixing occurs for alkali metal chemisorption onto free-electron like metals: in all models, the alkali atoms have been thought to reside on top of the surface. Recent work at MAX-Lab on the Al 2p [instrumental resolution ΔE= 40 meV] and Na 2p [ΔE = 60 meV] core levels for different ordered structures of Na/Al (111) clearly demonstrates that intermixing does occur [9]. All previous models must therefore be discarded, and a new picture is emerging for the surface structures of these prototypical systems.

A final example of high resolution core-level spectra is illustrated with recent work by Landemark et al [10] on the clean Si(001) surface. Judged from the Si 2p core-level spectra (total instrumental resolution better than 70 meV) the local structure appears very similar for the two reconstructions 2x1 and c(4x2), respectively. Surface core-level components from both the up and down Si surface atoms in the asymmetric dimers as well as the second-layer Si atoms can be identified, removing some ambiguity in earlier work. The large chemical shift (0.55 eV) between the two dimer-atom components further points to a substantial charge transfer within the dimers.

Based on core-level spectroscopy with a total instrumental resolution of 40-250 meV, as illustrated with a few examples above, it is argued that it makes sense to improve the resolution another order of magnitude for the instrumentation being planned for the third generation of synchrotron radiation sources. Even if the instrumental response function can be deconvoluted (if it is known accurately enough) form the recorded core-line, it is highly advantageous if it is sufficiently small, so that it can be neglected compared to other broadening mechanisms. For investigations of small chemical shifts and subtle changes in line-shapes it can be advantageous to have a total instrumental resolution which is only a small fraction of the inherent line-width.

References

1. S. Hagström, et al, Phys. Lett. 9, 235 (1964).
2. U. Gelius, et al, Chem. Phys. Lett. 28, 1 (1974).
3. R. Nyholm, et al, Nucl. Instrum. and Meth. A 246, 267 (1986).
4. J.N. Andersen, et al, Synchrotron Radiation News 4, (4), 15 (1991).
5. U. Gelius, et al, J. Electron Spectrosc. and Relat. Phenom. 52, 747 (1990).
6. R. Nyholm, et al, Phys. Rev. B 44, 10987 (1991).
7. R. Nyholm, et al, J. Phys. C 4, 277 (1992).
8. J.N. Andersen, et al, Phys. Rev. Lett. 67, 2822 (1991).
9. J.N. Andersen, et al, Phys. Rev. Lett. 68, 94 (1992).
10. E. Landemark, et al, Phys. Rev. Lett. 69, 1588 (1992)

Can We Obtain X-Ray Absorption Spectra beyond the Core-Hole Lifetime Broadening?

A. Kotani

Institute for Solid State Physics, The University of Tokyo
Roppongi, Minato-ku, Tokyo 106, Japan

Recently, Hämäläinen *et al.*[1] observed experimentally the excitation spectrum of L_3M_5 X-ray emission of Dy compounds in the region of Dy L_3 absorption edge, and found a dramatic improvement in resolution far beyond the limit of the L_3 core-hole lifetime width. We analyze theoretically this excitation spectrum on the basis of the coherent second order optical formula with multiplet coupling effect.[2] The width of the calculated spectrum is determined by the M_5 core-hole lifetime, instead of the shorter L_3 lifetime. A fine pre-edge structure of L_3 edge due to $L_3N_{6,7}$ quadrupole transition can be seen in the excitation spectrum, while this structure is quite invisible in the conventional XAS. We discuss the relationship between the excitation spectrum and the conventional XAS, and possible applications of this new technique.

1) K. Hämäläinen, D.P. Siddons, J.B. Hastings and L.E. Berman: Phys. Rev. Lett. **67**, 2850 (1991).
2) S. Tanaka, H. Ogasawara, K. Okada and A. Kotani: to be published in Jpn. J. Appl. Phys. (Proc. of The 7th Intl. Conf. on X-Ray Absorption Fine Structure, Kobe, 1992).

Magnetic Circular Dichroism in Core-Level Absorption of Magnetic Materials

T. Koide Photon Factory, National Laboratory for High Energy Physics

Magnetic circular dichroism (MCD) in core-level absorption is element specific and site selective. Thus it can provide valuable information about local magnetic states in compounds and alloys as well as in metals. We present the results of MCD studies around the Fe, Co, and Ni $M_{2,3}$ core edge and Pt $N_{6,7}$ and $O_{2,3}$ edges for Ni and Fe metals, and an Fe_{50} Pt_{50} alloy, and two ferrites (Fe_3O_4 and $CoFe_2O_4$).

The experiments were performed with a bulk-sensitive reflection method[1,2] by utilizing circularly polarized synchrotron radiation from both a bending-magnet source (BL-11D) and a helical undulator (BL-28U) at the Photon Factory. The direction of the magnetic field was reversed with the photon helicity fixed.

The MCD spectrum of Ni showed a large negative peak followed by a small positive one with photon energy around the $M_{2,3}$ edge.[1,2] A satellite feature in MCD was also observed several eV above the edge. The MCD spectrum of Fe exhibited a nearly antisymmetric shape at the $M_{2,3}$ edge with no satellite structure; this is in contrast to the MCD of Ni. The result for Ni could be favorably compared with the calculations by Yoshida and Jo[3] and van der Laan and Thole.[4]

The MCD spectrum of an ordered Fe_{50} Pt_{50} alloy showed a clear negative peak at the Fe $M_{2,3}$ and Pt N_6 edges and a positive peak at the Pt N_7 edge. Positive and negative MCD signals were also observed at the Pt O_2 and O_3 edges, respectively. The observation of MCD at the Pt core edges indicates induced magnetic moment in the 5d electron states in Pt. Comparison with theoretical consideration of MCD for the $p \rightarrow d$ and $f \rightarrow d$ transitions shows that the magnetic moment in Pt is parallel to that in Fe; i.e., the interaction between the 3d electrons in Fe and the 5d electrons in Pt is ferromagnetic. Two causes can be responsible for no observation of a positive MCD peak at the $M_{2,3}$ edge. First, the negative broad MCD signal due to the Pt O_3 edge spreads over this region, resulting in a cancellation of the possible positive MCD at the $M_{2,3}$ edge. Second, the Fe 3d orbital angular momentum in the alloy could be less quenched than in metal Fe.

For Fe_3O_4 and $CoFe_2O_4$, the MCD of multiplet structures in the Fe $M_{2,3}$ prethreshold region was studied in detail using circularly palarized undulator radiation. Three high-lying MCD peaks are common to two compounds while two low-lying MCD features are seen only in Fe_3O_4. This observation leads to the assignment that the former is attributed to multiplet transitions in the Fe^{3+} ions and the latter is due to transitions in the Fe^{2+} ions. Abundance of features observed in the MCD spectra of Fe_3O_4 and $CoFe_2O_4$ in the Fe $M_{2,3}$ prethreshold region demonstrates the capability of MCD to reveal structures obscured in unpolarized spectra.

References

1) T. Koide et al., Phys. Rev. B44, 4697 (1991).
2) T. Koide et al., Rev, Sci. Instrum. 63, 1371 (1992).
3) A. Yoshida and T. Jo, J. Phys. Soc. Jpn. 60, 2098 (1991).
4) G. van der Laan and B. T. Thole, J. Phys.: Condens. Matter 4, 4181 (1992).

Far Infrared Spectroscopy of Rare Earth Hexaborides

T.Nanba
Department of Physics,Kobe University,Kobe 657

S.Kimura
Research Institute for Scientific Measurements,
Tohoku University, Sendai 980

S.Kunii and T.Kasuya
Department of Physics, Tohoku University, Sendai 980

Reflectivity spectra of trivalent rare earth (R=La, Ce, Pr, Nd, Gd, Dy and Ho) hexaborides were systematically measured in the wide energy region from 1meV to 40 eV. Optical conductivity spectrum was obtained from the reflectivity spectrum by a Kramers-Kronig transformation. A broad infrared absorption band was found at 0.5-0.7 eV in common with the rare earth elements except La which exhibits a normal metallic property The energy position of the infrared absorption band was almost independent of the kind of the rare earth element but its intensity strongly depended on it. We found that the intensities are nearly proportional to the occupied 4f electron numbers of the rare earth element. This means that the infrared absorption is strongly correlated with the total 4f-angular momentum of these materials.

Up to now, some models on the origin of the infrared absorption have been proposed by other group. The first model was a so-called "f-d model" which suggests that the infrared absorption band originates from the absorption due to the optical excitation between the 4f and the 5d states of the rare earth element. According to the XPS data of the some trivalent rare earth hexaborides, however, the position of the occupied 4f level of the rare earth element below the Fermi level changes with the element although the 5d state is almost unchangeable. This result means that if the "f-d model" holds the energy position of the infrared absorption should change with the element. But this is strictly in contrast with the present results.

The other is the excitonic model. In this model the infrared absorption was considered to be due to the optical transition between the bonding and the antibonding states which are composed of the boron 2p and 2s electrons. This prediction, however, can not explain that the intensity is proportional to the occupied 4f electron numbers of the rare earth element.

Then, considering our experimental results and also the results of the recent band calculation on LaB6 [1], we propose that the infrared absorption is due to the optical excitation between the saddle points, 1 of the valence band and 25 of the conduction band of which transition is mediated by the exchange interaction between the 4f-conduction electrons. The energy separation between these points in the B.Z. coincides with the energy of the observed infrared absorption.

References

[1] H.Harima et al:Solid State Commun. **66**(1988)603.

A Future Direction of Synchrotron-Radiation Photoemission Study of Solid Surfaces

Shozo Kono
Research Institute for Scientific Measurements, Tohoku University
Sendai 980, Japan

It is known that the binding energies of core-levels in the selvedge region of solid surfaces are shifted sightly from those of the bulk atoms (called surface core-level shift; SCLS). This SCLS can be best detected by synchrotron-radiation photoemission in the photoelectron energy region for the shortest mean-free-path, which can be attained by tuning the energy of synchrotron-radiation. Both clean and alkali-metal saturated Si(001) surfaces were chosen as examples. For the clean Si(001)2×1 surface, the situation was quite controversial until a recent high-resolution photoemission study of Landemark et al.[1] appeared. Recent and unpublished results of synchrotron-radiation photoemission study of the author's group for both the clean and potassium- saturated Si(001)2×1 surfaces were introduced[2]. It was indicated that an interpretation of the our results following the result by Landemark et al. [1] shows that the photoelectron intensity for the upper dimer Si atoms is dependent on photoelectron emission-angle. This angular dependence is indicative of photoelectron diffraction effect for the SCLS component. A future direction of synchrotron-radiation photoemission study of solid surface was raised, i.e., photoelectron diffraction of SCLS for semiconductor surfaces.

There have been several studies of SCLS photoelectron diffraction for metal surfaces but only a few attempts have been made for semiconductor surfaces. An recent example by Gota et al.[3] was introduced. In their work, azimuthal photoelectron diffraction patterns for In 4d SCLS of an InP(110)1×1 surface were measured and analyzed based on the well-understood zigzag relaxation of the (110) surface of III-V semiconductors. The analysis showed a promising feature of the SCLS photoelectron diffraction as a means of surface structure-analysis although it was too premature to be conclusive.

The key factors of SCLS photoelectron diffraction in future would be the following.

(1) High photon flux and/or high efficiency in photoelectron detection.
(2) How easy or how difficult is the analysis of SCLS photoelectron diffraction?

References

[1] E. Landemark, C.J. Karlsson, Y.-C. Chao and R.I.G. Uhrberg, Phys. Rev. Lett. 69(1992)1588.
[2] The experiment was performed on the ISSP BL-18A at Photon Factory, KEK.
[3] S. Gota, D. Sebilleau, C. Guillot, J. Lecante, E.L. Bullock, A. Quemerais and G. Jezequel, Surf. Sci. 251/252(1991)437.

XAFS Studies of Molecular Adsorbates on Metals

T.Ohta

Dept. of Chemistry, Fac.Science, The Univ. of Tokyo,Bunkyo-ku, Tokyo, 113,Japan

The adsorption behaviors of S-containing molecules, ,thiophenol(C_6H_5SH), and thiophene(C_4H_4S) on clean Ni(100) have been studied by polarization dependent S K-edge XANES and EXAFS at BL 11B soft X-ray double crystal monochromator station in the Photon Factory. Clean Ni(100) surface was dosed with each molecule at 100 K and heated up to some temperatures subsequently. S K-edge absorption spectra were measured by the fluorescence and total electron yields at each stage.

(1)*Thiophenol on Ni(100)*

Heating up to 200 K, physisorbed molecules desorb and the surface is covered by only monolayer, judging from the signal to background ratio. From the polarization dependence of the XANES peak characteristic of the σ^*(S-C) transition , we found that the S-H bond is cleaved and the remained phenyl thiolate (C_6H_5S-)stands on the surface almost perpendicularly. Polarization dependence of S K-edge EXAFS shows that sulfur atom of phenyl thiolate sits on the 4-fold hollow site. Heating the sample further, phenyl rings are removed from the surface and S atoms remained on the 4-fold hollow sites. On the other hand, it turned out that thiophenol at very low coverage(0.075 ML) lies down flat on the surface and heating induced dissociation and left S atoms at the hollow site without passing the process of phenyl thiolate formation.

(2)*Thiophene on Ni(100)*

Heating up to 145-160K, physisorbed molecules desorb and monolayer species remain on the surface, which consist of thiophene and atomic S. Further increase of the temperature induces the gradual dissociation and only atomic S exists on the surface at 180 K. On the other hand, remarkable polarization dependence appears in the XANES spectra of submonolayer species at 100 K, suggesting the thiophene molecule lying parallel to the surface.

High resolution spectra of S K-edge XANES from thiophene on O precovered Ni(100) and clean Ni(100) were measured at the undulator beamline BL 2A in the Photon Factory. It was revealed that the first prominent peak consists of $\pi^*$and σ^* transitions with 0.6 eV splitting for thiophene on O-precovered surface, while the splitting is 1.4 eV for thiophene on clean surface at low coverage(0.05 ML). The σ^* peak remains at the same energy. and the π^* peak shifts lower by 0.8 eV. This indicates that the charge transfer occurs from nickel substrate to S in thiophene. At the slightly higher coverage(0.1ML), additional peak appears at the grazing incidence spectrum, whose position is almost same as that of π^* peak from thiophene on O precovered Ni(100). This result suggests the second layer begins to adsorb at this coverage.

Above results demonstrate the usefulness of the XAFS technique for the investigation of adsorption behavior of molecules on metal surfaces.

New Directions in the Study of Electronic Structure using Synchrotron Radiation.

P. Weightman
Physics Department and IRC in Surface Science, University Of Liverpool,
Oxford Street, Liverpool L69 3BX, UK.

A brief review will be given of some of the opportunities for the study of electronic structure which are opening up as a result of recent and future developments in synchrotron radiation. Of primary importance is the construction of new sources of synchrotron radiation and an account will be given of the new beamline constructed on the Daresbury Synchrotron by the UK IRC in Surface Science. The construction of the beamline is being organised by Dr G. Thornton of the Chemistry Department of the University of Manchester in close collaboration with staff at the SERC Daresbury Laboratory. The beamline will have two stations; 4.1 with an energy range of 15 eV to 250 eV and which is scheduled for completion in February 1993 and 4.3 covering the energy range 640 eV to 1 keV and which is currently being commissioned.

Improvements in the resolution and sensitivity of monochromators of synchrotron radiation offer obvious ways in which the study of electronic structure will be advanced. It is suggested that the development of monochromators capable of matching the resolution and sensitivity of the best of current laboratory instruments should be a high priority. Current commercial x-ray photoelectron spectrometers (XPS) have the sensitivity to measure core level spectra with good signal to noise from significantly less than 1% of a monolayer of adsorbates using monochromated Al Kα radiation with a resolution of ~0.25 eV. The development of monochromators of synchrotron radiation with equivalent performance in the energy range of ~ 1 keV to 2 keV offers the possibility of obtaining important new information on local electronic structure from the linewidths and lineshapes of photoelectron lines. This would be particularly important in the study of "shallow buried interfaces" which are of technological importance in the semiconductor and magnetic

recording industries and are difficult to study with other techniques. The results of a recent study [1] of Cooper minimum photoemission from Ag impurities in Cd and Al will be used to illustrate the potential of improvements in sensitivity for the study of the wavefunctions of adsorbates.

It will be argued that important advances in the study of electronic structure are also likely to come from coordinated studies combining a variety of synchrotron and laboratory based techniques. This will be illustrated by a case study of a decade of research on the link between the physical and electronic structure of CuPd alloys [2,3].

Finally it will be argued that there is always scope for the development of new theoretical approaches which can advance the understanding of electronic structure by offering new ways of interpreting the results of standard experimental techniques. An example will be given of a new approach to the interpretation of Auger parameter shifts which offers insight into mechanisms of charge transfer and electron screening in alloys [4], semiconductors [5] and interfaces [6].

1 "Solid state effects on Ag in dilute alloys revealed by Cooper minimum photoemission."
J. Cole, J.A. Evans, L. Duo, A.D. Laine, P.S. Fowles, P. Weightman, G. Mondio and D. Norman. Phys. Rev. B **46** 3747 (1992).

2 "Experimental Determination of the Pd and Cu Densities of States in $Cu_{75}Pd_{25}$"
H. Wright, P. Weightman, P. Andrews, W. Folkerts, C.F.J. Flipse, G.A. Sawatzky, D. Norman and H. Padmore, Phys. Rev. B **35** 519 (1987)

3 "Local Lattice Expansion Around Pd Impurities in Cu and its influence on the Pd Density of States: An EXAFS and Auger Study"
P. Weightman, H. Wright, S.D. Waddington, D. van der Marel, G.A. Sawatzky, G.P. Diakun and D. Norman, Phys. Rev. B **36** 9098 (1987)

4 "Valence Electronic Structure of AuZn and AuMg Alloys Derived from a new way of Analysing Auger parameter Shifts"
T.D. Thomas and P. Weightman, Phys. Rev. B, 33, 5406-13 (1986)

5 "Charge transfer and core-hole screening in PbTe."
S.D. Waddington, P. Weightman, J.A.D. Matthew and A.D.C. Grassie. Phys. Rev. B **39** 10,239 (1989).

6 "Charge transfer across the As/Si(100)-2x1 Interface."
J.A. Evans, A.D. Laine, P. Weightman, J.A.D. Matthew, D.A. Woolf, D.I. Westwood and R.H. Williams. Phys. Rev. B **46** 1513 (1992).

PHOTON STIMULATED DESORPTION BY CORE ELECTRON EXCITATION

Kenichiro TANAKA[1,2], Hiromi IKEURA[1,2], Tetsuhiro SEKIGUCHI[1,3], Kinichi OBI[3], Nobuo UENO[4] and Kenji HONMA[5]

1 *Photon Factory, National Laboratory for High Energy Physics, Tsukuba, 305 Japan*
2 *Department of Chemistry, University of Tokyo, Hongo, Tokyo, 113 Japan*
3 *Department of Chemistry, Tokyo Institute of Technology, Meguro, Tokyo, 152 Japan*
4 *Department of Materials Science, Chiba University, Chiba, 260 Japan*
5 *Department of Material Science, Himeji Institute of Technology, Akoh, Hyogo, 678-12 Japan*

The photon stimulated ion desorption (PSID) from the adsorption system of H_2O on the Si(100) surface has been studied in the range 500-700 eV. Experiments have been carried out at the Photon Factory of the National Laboratory for High Energy Physics using the grasshopper monochromator beamline (BL11A). Ions were detected and analyzed by a time of flight (TOF) spectrometer utilizing pulsed synchrotron radiation (turn time: 624ns, width: 100ps) from the Photon Factory storage ring in single bunch mode operation.

H^+ ion is dominant in all investigated region and O^+ ion is also observed in the TOF spectrum which is strongly energy-dependent. The relative ion yield curves of these ions indicate characteristic behavior near and above the O K-edge (539.7 eV); H^+ ion exhibits sharp rises at ca. 530 eV and two broad peaks below (ca. 535 eV) and above (ca. 555 eV) the O K-edge, O^+ exhibits a delayed threshold at ca. 570 eV and gradual increase up to 700 eV.

To explain these experimental results and to elucidate the mechanism of PSID, the O_{KLL} auger electron yield (AEY) spectrum and the photoion-photoion coincidence (PIPICO) spectrum between H^+ and O^+ in this energy region have also been obtained. The results are discussed in terms of the primary excitation followed by the Auger decay and the modification of charge state of desorbing species. Our experimental results are consistent with a mechanism of formation of multiple charged OH^{m+} ($m \geq 3$) ions followed by reneutralization of the excess of charge with strong interactions with the substrate and finally desorption as single charged H^+ and O^+ ions.

Science and Engineering in Synchrotron Radiation-Excited Semiconductor Process

Tsuneo Urisu
Institute for Molecular Science,
Yuichi Utsumi, Jun-ichi Takahashi, Housei Akazawa, and Hakaru Kyuragi
NTT LSI Laboratories

Abstract
Recent results of the Synchrotron Radiation excited Semiconductor process experiments are reviewed. Unique material selectivity is observed both in the etching and CVD reactions. As a possible explanation for these material selectivity, a generation of reactive centers with certain lifetime is proposed.

1. Introduction

It can be said that the surface photochemical reaction induced by the vacuum ultraviolet light is started by the appearance of the synchrotron radiation (SR). Since the first experiment of the SR etching(1) and CVD(2) are reported, studies of this field have become more active year by year. The study of the SR semiconductor process contains not only engineering interests of exploring the future new process technologies, but also scientific interests of developing a new scientific field of VUV surface photochemistry. In the present report, several interesting phenomena as a problem of photochemistry observed in the SR etching and CVD experiments are introduced and the reaction mechanisms are briefly discussed.

2. Material selectivity observed in SR etching and CVD.

Under the reaction gas SF_6+O_2 or without reaction gases, SiO_2, Si_3N_4 and poly- or amorphous Si can be etched (or evaporated) by electronically exciting the substrate surface by SR irradiations. In this etching, the unique difference of the etching rate among materials were found (1,3). The tendency of the material selectivity is roughly similar between etching (with reaction gas) and evaporations (without reaction gas). In a detailed comparison, however, it has been found that the etching rate is significantly enhanced by the existence of the reaction gas in the case of Si_3N_4 and poly-Si. The temperature dependence is also quite different between etching and evaporations. The evaporation rate increases with increasing temperature. But, the etching rate decreases with increasing temperature.

Concerning to the CVD, similar kind of material selectivity is observed.(4) Silicon nitride film is deposited from the mixture gas SiH_4 + NH_3 by the SR irradiation. In this system, it has been found that while the film composition (N/Si) increases in proportion to the partial pressure ratio of NH_3/SiH_4 (P) initially , it rapidly increases nonlinearly at around 1 of P. The position (value of P) of this sharp increase is slightly lower in insulating substrate than in c-Si substrate. This phenomena indicates that the incorporation efficiency of nitrogen is larger in insulating materials than in c-Si.

At the present stage, the reaction mechanisms for these etching and CVD reactions are not explained clearly yet. A possible explanation is that a reactive center resulting in the fluorination reaction or nitridation reaction is generated by the SR irradiation on the substrate surface, and the material selectivity is due to the difference of the lifetime of the reactive center.

Acknowledgement
Thanks are given to staffs of KEK Photon Factory for their collaboration with these experiments.

References
(1)T. Urisu, and H. Kyuragi; J. Vac. Sci. and Tech. B5 (1987) 1436.
(2)H. Kyuragi and T. Urisu: J. Appl. Phys. 61 (1987) 2035.
(3)J. Takahashi, Y. Utsumi, and T. Urisu; J. Appl. Phys. 70 (1991) 2958.
(4)H. Kyuragi and T. Urisu; J. Electrochem. Soc. 138 (1991) 3413.

DESIGN AND DEVELOPMENT OF SPECTROSCOPY BEAM LINES AT INDUS-1

P.MEENAKSHI RAJA RAO,B.N.RAJA SEKHAR,N.C.DAS,S.PADMANABHAN,
P.S.MURTY,G.D.SAKSENA,S.V.N.BHASKARA RAO,S.S.BHATTACHARYA
V.B.KARTHA,A.K.SINHA* AND S.BHAT*

SPECTROSCOPY DIVISION,BHABHA ATOMIC RESEARCH CENTRE,TROMBAY,
BOMBAY -400085,INDIA

ABSTRACT:INDUS-1 IS THE FIRST SYNCHROTRON RADIATION SOURCE BEING BUILT AT CENTRE FOR ADVANCED TECHNOLOGY(CAT),INDORE,INDIA.THIS SOURCE,A STORAGE RING, OPERATES AT 450 M eV ENERGY AND HAS A CRITICAL WAVELENGTH OF 61 Å.THE CRITICAL WAVE LENGTH WILL BE 30 Å WITH THE USE OF A WIGGLER.THUS INDUS-1 IS AN INTENSE SOURCE OF PHOTONS,THEIR ENERGIES RANGING FROM SOFT X-RAYS TO INFRA RED.SEVERAL BEAM LINES ARE PLANNED AT INDUS-1 TO CARRY OUT STUDIES OF INTERACTION OF RADIATION WITH MATTER.SPECTROSCOPY DIVISION OF BARC,IS DESIGNING AND FABRICATING THREE OF THE BEAM LINES AND THE REQUIRED EXPERIMENTAL FACILITIES.ALL THE BEAM LINES OPERATE UNDER UHV CONDITIONS (PRESSURE $< 10^{-9}$ TORR.A BRIEF DESCRIPTION OF THE WORK IS GIVEN BELOW.

1.PHOTOPHYSICS BEAM LINE:THIS BEAM LINE MAKES USE OF PRE AND POST FOCUSING TOROIDAL MIRRORS AND A 1 METRE SEYA-NAMIOKA TYPE MONOCHROMATOR AS EXCITING MONOCHROMATOR AND 0.5 - 1 METRE MONOCHROMATORS AS ANALYSING MONOCHROMATORS.THIS BEAM LINE IS DESIGNED TO CARRY OUT STUDIES ON PHOTO ABSORPTION,PHOTO DISSOCIATION AND FRAGMENTATION,CLUSTERS ETC.MOST OF THE BEAM LINE COMPONENTS, BARRING UHV SLITS, MIRRORS AND GRATINGS,ARE INDEGENOUSLY BUILT.

2.HIGH RESOLUTION VUV BEAM LINE:THIS BEAM LINE HAS A FORE OPTICS CONSISTING OF THREE CYLINDRICAL MIRRORS.THE HIGH RESOLUTION INSTRUMENT IS A 6.65 METRE CONCAVE GRATING SPECROGRAPH/SPECTROMETER IN OFF-PLANE EAGLE MOUNT.A HIGH TEMPERATURE FURNACE AND ABSORPTION CELL ARE BEING FABRICATED TO CARRY OUT EXPERIMENTS ON SPECTRA OF ATOMS AND MOLECULES INVOLVING RYDBERG STATES,MULTIPLY EXCITED STATES AUTO IONIZING LEVELS ETC.MOST OF THE BEAM LINE COMPONENTS INCLUDING THE 6.65 M SPECTROGRAPH/SPECTROMETER IS BEING BUILT INDEGENOUSLY. HOWEVER,THE GRATINGS ,MIRRORS AND UHV SLITS WILL BE IMPORTED.

3.PHOTO ELECTRON SPECTROSCOPY BEAM LINE:THIS BEAM LINE MAKES USE OF PRE AND POST FOCUSING TOROIDAL MIRRORS , A TOROIDAL GRATING MONOCHROMATOR(TGM 1400) AND A SPHERICAL SECTOR ANALSER ELECTRON SPECTROMETER AND A SAMPLE CHAMBER.THIS BEAM LINE IS DESIGNED TO CARRY OUT EXPERIMENTS ON HIGH T_c MATERIALS,PARTIAL PHOTOIONIZATION CROSS SECTIONS ETC.THE BEAM LINE COMPONENTS ARE BEING DESIGNED.

*CENTRAL WORK SHOPS

Present Status and Future Perspective of Synchrotron Radiation Research Center

Presented by Poh-Kun Tseng
Physics Department National Taiwan University
and
Synchrotron Radiation Research Center
Hsin-Chu, Taiwan, R. O. C.

The Synchrotron Radiation Research Center (SRRC) is the name of new institute in Taiwan,R.O.C. for collaborative research center for scientific community in Taiwan area. Presently, the main facility of this center is, of course, a dedicated electron storage ring for synchrotron radiation researches.

The project of the SRRC was initialed and proposed by a feasibility study group in 1982. It was approved by authority in July,1983,and a task organization for the construction of main fascility was organized and the construction has been started.

The detailed parameters are shown in the table shown below.

The booster has been purchased from the Scantronix company and has been put in operation resently. The transport line has been constructed successfully. The main ring is almost having its shape. All magnet systems are placed and pre-aligned. All aluminum vacuum chambers will be installed by the end of this year. RF cavity has been installed and those high frequency power station and power transmission circuits are on construction.

We expect to commission the system by the middle of next year and three beam lines will be assembled by the end of next and start for research. By that time our organizaton will be a National facility of our scientific community. It will be welcomed international research collaborations in these variety application of the synchrotron light.

Nominal energy	1.3 GeV
Nominal circulating current	200 mA
Number of stored electron	5×10^{11}
Horizontal natural emittance	1.92×10^{-8} m-rad
Circumference	120 m
Revolution frequency	2498.27 kHz
Radio frequency	499.654 MHz
Harmonic number	200
Number of superperiods	6
Free long straight section length	6 m
Bending field	1.24 T
Bending radius	3.495 m
Horizontal tune	7.18
Vertical tune	4.13
Synchrotron tune	1.15×10^{-2}
Max. horizontal beta	18.43 m
Max. vertical beta	12.06 m
Bunch length (rms)	0.74 cm
Bending Magnet Beam size	
Horizontal σ_h	0.14 mm
Vertical σ_v	0.131 mm
Critical photon wavelength (dipole)	8.89 Å

Present Status of HESYRL

C. Y. Xu

Hefei Synchrotron Radiation Laboratory, University of Science and Technology of China, Hefei, Anhui 230026, P.R.China
(Scholar of the Spring-8 Team, RIKEN)

The Hefei synchrotron radiation laboratory (HESYRL) was completed and passed a technical examination organized by the Chinese Academy in October 1991. The current intensity has got to over 200 mA under 800 MeV and the beam lifetime has been 6 hours at keeping the current intencity over 10 mA each injecting. Now the HESYRL operates on schedule and 5 beamlines with stations are available to users to do experiments.

The HESYRL facility consists of three major systems: the 200 MeV electron Linac, the 800 MeV electron storage ring and photon beamlines with corresponding experimental stations. Fig.1 shows the general layout of the facility and Table 1 summarized its main parameters.[1] There are twelve dipoles, thirty two quadrupoles, fourteen sextupoles and four long straight sections in the storage ring.

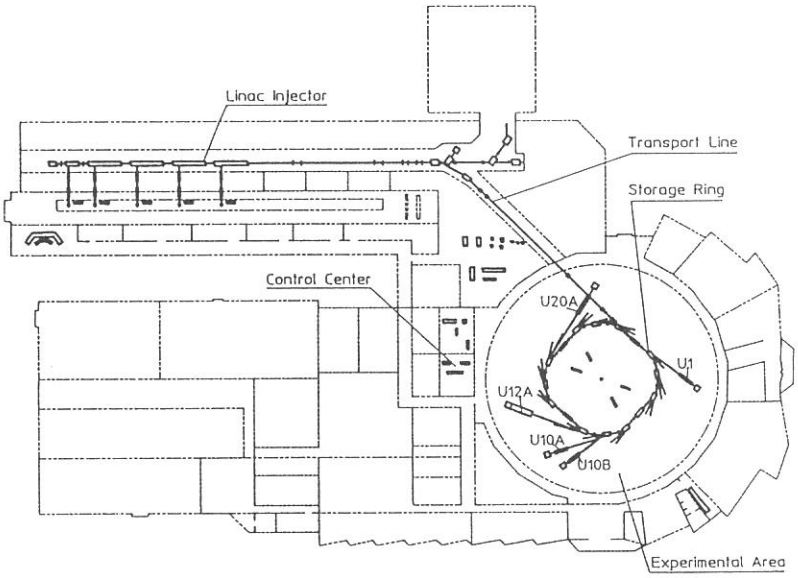

Fig.1 Layout of Hefei synchrotron radiation facility.

Three long straight sections will be used in the future for the installation of wigglers, undulators and free electron lasers. The Linac injector consists of four accelerating sectors and a preinjector. Each sector is composed of two 3 m long accelerating sections and is powered by a klystron of 15 MW. The preinjector is composed of a triode gun, a prebuncher and a 3 m long accelerating section and is powered by a klystron of 10 MW.[2]

The storage ring is installed in a hall 50 m in diameter and the experimental area is the floor that surrounds it as shown in Fig.1. The Hefei synchrotron radiation facility can produce a wide spectrum of radiation from the infrared to the soft X-ray region. Every bending magnet has two beam ports whose opening angles are 85 and 120 mrad in the horizontal direction, respectively. Therefore light from 24 ports in total can be extracted from the storage ring. Each beamline will be split two branch lines, so the storage ring can be equipped with about 50 beamlines, including ones from insertion devices, and corresponding stations.

Table 1 Parameters of Hefei synchrotron radiation facility

Storage ring	
Energy	800 MeV
Current intensity	100-300 mA
Circumference	66.13 m
bending magnets	12
Bending field	1.2T
Bending radius	2.222 m
Critical wavelength	24 A°
Total radiation power	4.89 kW
Energy loss per turn	16.3 keV
Working pressure	2×10^{-9} Torr
Linac injector	
Energy	200 MeV
Peak current	130 mA
Total length 35 m	

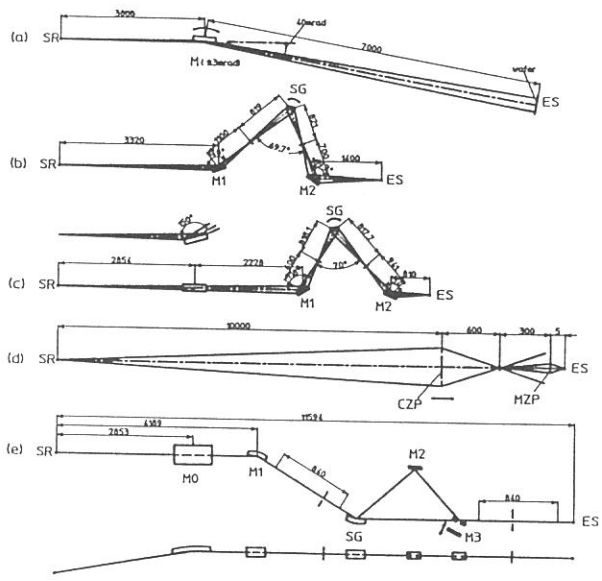

Fig.2 Optical layout of the beamlines.

Five beamlines and corresponding stations were constructed at the first stage. All of them were installed in the experimental hall and open to users to do experiments on X-ray lithography, photochemistry, time-resolved spectroscopy, soft X-ray microscopy and photoelectron spectroscopy since the end of last year. Fig.2 and Table 2 show their optical design and the main parameters.[3]

Table 2 Main optical parameters of the beamlines

Beamline	U1	U10A	U10B	U12A	U20A
Monochromator	none	1m Seya	1m Seya	linear	SGM
Grating(l/mm)		2400	2400	n=1506	1100
		1200	1200	1082	600
		600	600	770	500 200
Resolution(nm)		0.1 at 35 nm	0.1 at 35 nm	0.03	$\lambda/\delta\lambda=10^3$
Wavelength range(nm)	0.5-2	35-600	35-600	2-5.4	1-110
Pre-mirror		toroidal	spherical ellipsoidal		spherical
Post-mirror		toroidal	cylindrical		cylindrical
Accept. hxv(mrad)	15×0.6	25×5	25×5	0.27×0.27	20×2.5
Spot at sample hxv(mm)		2×1	3×0.2	0.2μm	3×1
Flux at sample(phs/s)	$0.1W/cm^2$	5×10^{11}	2×10^{11}	5×10^5	10^{10}

References

[1] He Duohui, Proc. 13th Int. Conf. Part. Accel., Novosibirsk, 280 (1986).

[2] Wang Defa, Pei Yuanji, He Duohui, Proc. 1986 Linac Conf., SLAC, (1986)

[3] Zhang Yunwu, Int. Conf. on SR Appli., Hefei, 303 (1989)

BSRF Status and Research Opportunities

Dingchang Xian, Esheng Tang and Yang Hai
Institute of High Energy Physics, Chinese Academy of Sciences
P. O. Box 918, 100039 Beijing, China

The Beijing Synchrotron Radiation Facility (BSRF) is a partly dedicated Synchrotron Radiation (SR) facility whose construction was started in 1985 and affiliated with the Beijing Electron Positron Collider National Laboratory (BEPC). It is located at the Institute of High Energy Physics (IHEP) in the west suburb of Beijing. BSRF is one of four constituents of BEPC. The other three are a 1.55 GeV linac injector, a 1.55-2.8 GeV storage ring (BEPC) and a particle spectrometer for high energy physics research. At present, most shifts are run for high energy physics research. The dedicated mode was commissioned at the end of 1989 and the storage ring energy is 2.2 GeV, and a horizontal emittance of 70 nm·rad was achieved[1]. The construction project of BSRF is divided into two phases. First phase was from 1985 to 1990. The second one is from 1991 to 1995.

The first phase of BSRF construction project consists of three beam ports, seven beamlines and nine stations[2]. one beam port is a wiggler port and the other two are bending magnet ports. The nine stations are the topography and microprobe fluorescence station with white beamline (4W1A), XAFS station with monochromatic beamline (4W1B), general purpose diffraction station with monochromatic and focusing beamline (4W1C), the diffraction and small angle scattering station with a monochromatic and focusing beamline (4B9A), photoelectron spectroscopy station with VUV/soft X-ray compatible beamline (4B9B), lithography studies station with soft X-ray beamline (3B1A) and biology spectroscopy station with monochromatic and focusing beamline (3B1B).

The second phase of construction project of BSRF has being designed[3]. It consists of two insertion devices, and four experiment stations. The first beam port is the wiggler port 1W1. The permanent magnet wiggler in designing is a 16 pole wiggler (17 kG). Two beamline 1W1A and 1W1B will be from this port. The beamline 1W1A is a unfocusing white and monochromatic beamline providing for diffraction at ultra-high pressure and microprobe X-ray fluorescence station. The beamline 1W1B is planned to be designed for nuclear resonance scattering station. The second is the undulator beam port 3U1. The insertion device is a 34 pole permanent magnetic undulator (5.2 kG). The preliminary design of the optical system of beamline 3U1 includes a horizontal focus mirror and a SX-700 type plane grating monochromator. The two stations will exploit this beamline. One is the atomic and molecular physics station. The other is the soft X-ray optics station. The third is a bending magnet beam port. The beamline 3B7 is a general purpose beamline which will be used for synchrotron radiation diagnostics and calibration of detectors etc.

Reference

1. D. C. Xian, *Nucl. Instum. Methods,* A282, 380(1989)
2. Esheng Tang and D. C. Xian, *Rev. Sci. Instrum.,* 63, 1575(1992)
3. BSRF Activity Report, 1991

Current Status of the PLS Project

Seung Yu Rah, Youngmin Chung and Tong-Nyong Lee

Pohang Accelerator Laboratory
P.O. Box 125, Pohang
Kyungbuk, 790-600, KOREA

The Pohang Light Source (PLS) project, which was started on April 1, 1988, is progressing smoothly. The PLS consists of a 2 GeV electron linear accelerator and an electron storage ring optimized at 2 GeV. The synchrotron radiation will cover from VUV to soft X-rays. The major parameters and the current status for the storage ring and the linear accelerator are described bellow:

Storage Ring

The nominal electron energy is 2 GeV, and the initial goal for the electron beam current is 100 mA for the multi-bunch mode and 7 mA for the single-bunch mode. The circumference of the ring is 280.56 m and the natural beam emittance is 12 $\times$ 10^{-9} m-rad. The ring has 12 straight sections. Ten of them are for insertion devices and other two sections are for injection system and RF system.
The prototype dipole and quadrupole magnets have been tested and approved for production. All magnets including sextupoles and correctors are scheduled to be completed by the end of 1993. Also, the test for the second prototype vacuum chamber have been completed.
Initially there will be two bending magnet beam lines, one for VUV and another for X-ray users. The monochromator for the VUV beam line will cover the energy range of 12-1230 eV and will be used for ARUPS, XPS and XAS. The X-ray beam line will provide the photons of energy 3-12 keV and will be used for X-ray diffraction, XAFS and X-ray standing wave experiments.

Linear Accelerator

The 2 GeV full energy linear accelerator, which is 150 m long, has 42 accelerating columns and are powered by 11 klystrons. The maximum output power of the each klystron is 80 MW. A 200 MW modulator will be installed to operate these klystrons.
The 60 MeV preinjector for the linac was commissioned in February, 1992. Eight accelerating columns for the second and third modules were installed. The second module was tested successfully at 200 MeV in December, 1992 and it is expected that the test for the third module will be done by the end of February, 1993. The installation of the linac system will be completed by the end of 1993.

Synchrotron Radiation Sources in Japan

M. Watanabe
UVSOR, Institute for Molecular Science

Table I is a list of the synchrotron radiation sources in Japan operated and under construction. The total number is 17. They are classified into two, one of which is belonging to the public institutes widely opened for scientific research (upper 6)[1] and the other, to the private companies used closedly for industrial purposes (lower 11)[2](with one exception). The sources in the planning stage are not given.

Table I Existing Synchrotron Radiation Sources in Japan

Machine	Location	Institution	E(GeV)	ε_c(keV)
TERAS	Tsukuba	ETL	0.8	0.57
PF	Tsukuba	KEK	2.5	4.0
AR	Tsukuba	KEK	6.5	26.4
SOR-RING	Tanashi	Univ.Tokyo	0.38	0.11
UVSOR	Okazaki	IMS	0.75	0.43
Spring-8*	Nishiharima	JAREI-RIKEN	8	28.3
HITACHI-I	Hitachi	HITACHI	0.2	0.026
JSR	Tokai	JAERI	0.3	0.072
NIJI-II	Tuskuba	ETL-SEI	0.6	0.342
NIJI-III	Tsukuba	SEI-ETL	0.62	1.057
NIJI-IV	Tsukuba	ETL-KHI	0.5	0.231
LUNA	Tsukuba	IHI	0.8	0.568
SORTEC	Tsukuba	SORTEC-ETL	1.0	0.792
AURORA	Tanashi	SHI	0.65	1.218
NAR	Atsugi	NTT-TOSHIBA	0.8	0.614
Super-ALIS	Atsugi	NTT-HITACHI	0.6	0.715
MELCO-II	Itami	MELCO	0.8	1.893

*Under construction

References

1) H. Kobayakawa and K. Huke : Rev. Sci. Instrum. **60** (1989) 2548.
2) T. Tomimasu : Rev. Sci. Instrum. **63** (1992) 722.

List of Participants

I. Lindau, Max-Lab, Lund, Sweden
W. Braun, BESSY, Berlin, Germany
Y. T. Lee, California Univ., USA
G. Zimmerer, Hamburg Univ., Germany
P. Weightman, Univ. Liverpool, UK
P. Lablanquie, LURE, Orsay, France
S. Krinsky, NSLS, Brookhaven, USA
S. Y. Rah, Postech, Pohang, Korea
Y. Chung, Postech, Pohang, Korea
P. M. Raja Rao, BARC, Bombay, India
P.-K. Tseng, Natl. Taiwan Univ., Taiwan
W.-F. Pong, Tamkang Univ., Taiwan
Y. Hai, IHEP, Beijing, China
C. Y. Xu, Riken (HESYRL, Hefei, China)
J. D. Bozek, Electro-Tech. Lab.
(Univ. Western-Ontario, Canada)
H. Kobayakawa, Photon Factory
Y. Kamiya, Univ. Tokyo
M. Yamamoto, Tohoku Univ.
Y. Hatano, Tokyo Inst. Tech.
Y. Sato, Tohoku Univ.
Y. Tokura, Univ. Tokyo
N. Ueno, Chiba Univ.
K. Kan'no, Kyoto Univ.
T. Koide, Photon Factory
A. Kotani, Univ. Tokyo
T. Nanba, Kobe Univ.
S. Kono, Tohoku Univ.
K. Tanaka, Photon Factory
T. Ohta, Univ. Tokyo
T. Ishii, Univ. Tokyo
A. Kakizaki, Univ. Tokyo
M. Itoh, Shinshu Univ.
N. Watanabe, Tsukuba Univ.
T. Masuoka, Osaka City Univ.
H. Ogawa, Saga Univ.
M. Taniguchi, Nagoya Univ.
K. Nakagawa, Kobe Univ.
H. Nakagawa, Fukui Univ.
H. Kawazoe, Tokyo Inst. Tech.
H. Nishikawa, Waseda Univ.
S. Nakai, Utsunomiya Univ
T. Dodo, Ehime Univ.
I. Koyano, Himeji Inst. Tech
I. Ouchi, Tottori Univ.
K. Yamashita, Nagoya Univ.
S. Kubota, Rikkyo Univ.
K. Furuya, Kyusyu Univ.
H. Yasumatsu, Univ. Tokyo
M. Sakurai, Kobe Univ.
K. Ichikawa, Univ. Osaka Prefecture
Y. Fujii, Osaka City Univ.
E. Ishiguro, Osaka City Univ.
N. Itoh, Nagoya Univ.
M. Kobayashi, Osaka Univ.
Y. Kihara, Jichi Medical School
K. Fukui, Fukui Univ.
N. Ohno, Osaka Elect.-Comm. Univ.
H. Onuki, Electro-Tech. Lab.
K. Kimura, JAIST, Hokuriku
I. Ochiai, Hitachi Co.
K. Yakushi, IMS
S. Hasegawa, IMS
H. Ogata, IMS
K. Shobatake, IMS
K. Okuyama, IMS
H. Ozeki, IMS
H. Ohashi, IMS
H. Yoshikawa, IMS
K. Tabayashi, IMS
M. Kono, IMS
T. Urisu, IMS
K. Mitsuke, IMS
K. Mase, IMS
H. Yoshida, IMS
H. Hattori, IMS
S. Sato, IMS
Y. Ukisu, IMS
H. Ogawa, IMS
T. Ogata, IMS
T. Kato, IMS
N. Morita, IMS
T. Suzuki, IMS
K. Iwano, IMS
K. Yoshihara, IMS
K. Sawabe, IMS
H. Petek, IMS
B. Kim, IMS
J. Lee, IMS
K. Fuke, IMS
F. Misaizu, IMS
T. Mitani, IMS
S. Asaka, IMS
M. Watanabe, IMS
G. Isoyama, IMS
M. Kamada, IMS
S. Tanaka, IMS
A. Hiraya, IMS
H. Hama, IMS
S. Ohara, IMS
K. Sakai, IMS
O. Matsudo, IMS
T. Kinoshita, IMS
M. Hasumoto, IMS
J. Yamazaki, IMS
E. Nakamura, IMS
S. Hirose, IMS

APPENDIX

ORGANIZATION

Staff

Director

Katsumi	KIMURA	Professor (–March 1992)
Kyuya	YAKUSHI	Professor (April 1992–)

Scientific Staff

Light Source

Goro	ISOYAMA	Associate Professor
Hiroyuki	HAMA	Research Associate
Shirou	TAKANO	Research Associate (–March 1992)

Beam Line

Makoto	WATANABE	Associate Professor
Masao	KAMADA	Associate Professor
Atsunari	HIRAYA	Research Associate
Shin–ichiro	TANAKA	Research Associate
Shigeo	OHARA	IMS Fellow (April 1992–)

Technical Staff

Kusuo	SAKAI	Section Chief Engineer
Osamu	MATSUDO	Unit Chief Engineer
Toshio	KINOSHITA	Engineer
Masami	HASUMOTO	Engineer
Jun–ichiro	YAMAZAKI	Engineer
Eiken	NAKAMURA	Engineer

Secretary

Eiko	ADACHI	(–June 1992)
Hisayo	HAGIWARA	(July 1992–)

Guest Scientist

Eiji	ISHIGURO	Adjunct Associate Professor from Osaka City Univ.

Graduate Student

Sayumi	HIROSE

Representative of Beam Lines

BL1A	Makoto	WATANABE	UVSOR
BL2A	Kosuke	SHOBATAKE	Dept. Vacuum UV Photoscience
BL2B2	Koichiro	MITSUKE	Dept. Vacuum UV Photoscience
BL3B	Koichiro	MITSUKE	Dept. Vacuum UV Photoscience
BL4A	Shinri	SATO	Dept. Vacuum UV Photoscience

BL4B	Tsuneo	URISU	Dept. Vacuum UV Photoscience
BL6B	Kyuya	YAKUSHI	Dept. Molecular Assemblies
BL6A2	Masao	KAMADA	UVSOR
BL8B2	Hiroo	INOKUCHI	IMS
Others	Makoto	WATANABE	UVSOR
	Masao	KAMADA	UVSOR

Steering Committee (April 1992 – March 1994)

Kyuya	YAKUSHI	IMS Chairman
Masahiro	KOTANI	Gakushuin Univ.
Kaizo	NAKAMURA	Okayama Univ.
Yukinori	SATO	Tohoku Univ.
Noriaki	ITOH	Nagoya Univ.
Akito	KAKIZAKI	Tokyo Univ.
Toshio	KASUGA	Hiroshima Univ.
Tadashi	MATSUSHITA	Nat. Lab. High Energy Phys.
Eiji	ISHIGURO	IMS and Osaka City Univ.
Keitaro	YOSHIHARA	IMS
Norio	MORITA	IMS
Koichiro	MITSUKE	IMS
Makoto	WATANABE	IMS
Goro	ISOYAMA	IMS
Masao	KAMADA	IMS

JOINT STUDIES (fiscal year 1992)

Special Project	: 2
Cooperative Research	: 39
Cooperative Research (Invited)	: 7
Use of Facility	: 107
Use of Facility (Private Company)	: 3
Users' Meeting	: 1
Workshop on Beam Dynamics and Free Electron Laser	: 1
Users' Time	: 43 weeks

LIST OF PUBLICATIONS (1992)

1) "Time Resolved Study of Photoluminescence from O_2^- Molecules in Alkali Halides"
   S. Hongo, H. Murata and R. Kato
   J. Lumi. **48** & **49** (1991) 807.
2) "Low Temperature Growth of SiO_2 Thin Film by Photo-CVD Using Synchrotron Orbital Radiation"
   Y. Matsui, R. Nagayoshi, M. Nakamura, M. Okuyama and Y. Hamakawa
   Proc. Symp. on Dry Process (The Institute of Electrical Engineers of Japan,1991) p.177.
3) "Structural Modification of a-C:H Films Caused by 2 MeV ^4He Ion Irradiation"
   K. Takahiro, T. Yamasaki, F. Nishiyama, Y. Osaka, S. Nagata and S. Yamaguchi
   Nucl. Instrum. Meth. Phys. Res. B**59/60** (1991) 1374.
4) "Cubic Boron Nitride Prepared by an ECR Plasma"
   Y. Osaka, M. Okamoto and Y. Utsumi
   Mat. Res. Soc. Symp. Proc. **223** (1991) 81.
5) "Energy Partitioning in the Dissociation Reaction $Ar_3^+ \rightarrow Ar_2^+ + Ar$"
   K. Furuya, K. Kimura and T. Hirayama
   J. Chem. Phys. **97** (1992) 1022.
6) "Millimeter Wave Spectroscopy and Color Centers of MAg_4I_5 (M=Rb, K and NH_4) Family"
   T. Awano, T. Nanba and M. Ikezawa
   Solid State Ionics **53-56** (1992) 1269.
7) "Gain Measurement of a Free Electron Laser on the UVSOR Storage Ring"
   S. Takano, H. Hama, G. Isoyama, A. Lin and N. A. Vinokurov
   Jpn. J. Appl. Phys. **31** (1992) 2621.
8) "Negative-Ion Mass Spectrometric Study of Ion-Pair Formation in the Vacuum Ultaviolet. VI. $CH_3X \rightarrow X^- + CH_3^+$ (X=F, Cl, Br)"
   S. Suzuki, K. Mitsuke, T. Imamura and I. Koyano
   J. Chem. Phys. **96** (1992) 7500.
9) "Characterization of Platinum-Carbon, Tungsten-Silicon and Tungsten-B_4C Multilayers"
   K. Yamashita, M. Watanabe, O. Matsudo, J. Yamazaki, I. Hatsukade, T. Ishigami,
   S. Takahama, K. Tamura and M. Ohtani
   Rev. Sci. Instrum. **63** (1992) 1217.
10) "Characterization of Multilayer Reflectors and Postition Sensitive Detectors in the 45-300 Å Region"
   K. Yamashita, S. Takahashi, S. Kitamoto, S. Takahama, K. Tamura, I. Hatsukade,
   M. Sakurai, M. Watanabe, A. Yamaguchi, H. Nagata and M. Ohtani
   Rev. Sci. Instrum. **63** (1992) 1513.

11) "Soft X-Ray Beamline BL7A at the UVSOR"
T. Murata, T. Matsukawa, S. Naoé, T. Horigome, O. Matsudo and M. Watanabe
Rev. Sci. Instrum. **63** (1992) 1309.

12) "Status of the UVSOR Facility-1991"
M. Watanabe, G. Isoyama, M. Kamada and K. Kimura
Rev. Sci. Instrum. **63** (1992) 1584.

13) "Fabrication and Characterization of Reactive Ion Beam Etched SiC Gratings"
E. Ishiguro, K. Yamashita, H. Ohashi, M. Sakurai, O. Aita, M. Watanabe, K. Sano, M. Koeda and T. Nagano
Rev. Sci. Instrum. **63** (1992) 1439.

14) "Photoelectron Spectroscopic Study of the Decay Process of Excited 4*d* States in Cesium Halides"
M. Kamada, O. Aita, K. Ichikawa, M. Okusawa and K. Tsutsumi
Phys. Rev. B **45** (1992) 12725.

15) "Design of an Instrument for Far-Infrared Microspectroscopy Using a Synchrotron Radiation Source"
A. Ugawa, H. Ishii, K. Yakushi. H. Okamoto, T. Mitani, M. Watanabe, K. Sakai, K. Suzui and S. Kato
Rev. Sci. Instrum. **63** (1992) 1551.

16) "Measurement of the Bunch Length on the UVSOR Storage Ring"
A. Lin, H. Hama, S. Takano and G. Isoyama
Jpn. J. Appl. Phys. **31** (1992) 921.

17) "Self-Trapped Exciton Luminescence in $KBr_{1-x}I_x$ and $RbBr_{1-x}I_x$ Solid Solutions"
T. Hayashi, T. Yanase, T. Matsumoto, K. Kan'no, K. Toyoda and Y. Nakai
J. Phys. Soc. Jpn. **61** (1992) 1098.

18) "Resonant Photoemission Study of the Al-Cu-Fe Icosahedral Phase"
M. Mori, K. Kamiya, S. Matsuo, T. Ishimasa, H. Nakano, H. Fujimoto and H. Inokuchi
J. Phys. : Condens. Matter **4** (1992) L157.

19) "Vacuum Ultraviolet Absorption Spectra and Photodissociative Excitation of $CHBr_2Cl$ and $CHBrCl_2$"
T. Ibuki, A. Hiraya and K. Shobatake
J. Chem. Phys. **96** (1992) 8793.

20) "Core Absorption Spectra of SnTe and PbTe in Crystalline and Amorphous Phases"
K. Fukui
J. Phys. Soc. Jpn. **61** (1992) 2018.

21) "UV Photoemission Studies on PbTe, SnTe and GeTe in Polycrystalline and Amorphous Phases"
K. Fukui
J. Phys. Soc. Jpn. **61** (1992) 1084.

22) "State Selective Ionization of O_2 in a Framework of van der Waals Molecules"
M. Ukai, K. Kameta, K. Shinsaka, Y. Hatano, T. Hirayama, S. Nagaoka and K. Kimura
Synchrotron Radiation and Dynamic Phenomena (Conf. Proc. No. 258, American Institute of Physics, 1992) p.179.

23) "Sensitivity Calibration of Surface Barrier Diodes for Soft X-Ray Observation of Plasma"
M. Sakurai, Y. Shimazu and N. Asakura
Rev. Sci. Instrum. **63** (1992) 832.

24) "Trapping and Probing of Multiply Charged Xe Ions Produced by Synchrotron Radiation"
M. Sakurai, M. Kimura, T. Sekioka, M. Terasawa, H. Yamaoka, T. Niizeki, Y. Awaya, T. Hirayama, J. Yoda, A. Ogata and S. Ohtani
Rev. Sci. Instrum. **63** (1992) 1186.

25) "Fast Decay Behaviors of Self-Trapped Exciton Luminescence in Ammonium Halides"
N. Ohno, M. Itoh and S. Hashimoto
J. Lumi. **53** (1992) 121.

26) "Focusing and Imaging Properties of a Nickel Phase Zone Plate"
H. Fujisaki, N. Nakagiri, H. Kihara, N. Watanabe, Y. Shimanuki and Y. Nagai
X-Ray Microscopy III (Springer Series in Optical Sciences **67**, Springer-Verlag, 1992) p.90.

27) "Construction of Focusing Soft X-Ray Beamline BL1A at the UVSOR"
A. Hiraya, T. Horigome, N. Okada, N. Mizutani, K. Sakai, O. Matsudo, M. Hasumoto K. Fukui and M. Watanabe
Rev. Sci. Instrum. **63** (1992) 1264.

28) "Electronic Structure of Bis [1,2,5,] thiadiazolo-*p*-quinobis (1,3-dithiole) (BTQBT) Studied by Ultraviolet Photoemission Spectroscopy"
H. Fujimoto, K. Kamiya, S. Tanaka, T. Mori, Y. Yamashita, H. Inokuchi and K. Seki
Chem. Phys. **165** (1992) 135.

29) "Core-Hole Migration and Relaxation Effect in Alkali Halide Excited by Synchrotron Radiation"
M. Itoh, N. Ohno and S. Hashimoto
Phys. Rev. Lett. **69** (1992) 1133.

30) "Pseudo-Gap and Electronic Structure Near the Fermi Level in Doped C_{60}"
T. Takahashi
Comments Cond. Mat. Phys. **16** (1992) 113.

31) "Time-Resolved Spectroscopic Study on the Type I Self-Trapped Excitons in Alkali Halide Crystals. I. Emission Spectra and Decay Behavior"
T. Matsumoto, T. Kawata, A. Miyamoto and K. Kan'no
J. Phys. Soc. Jpn. **61** (1992) 4229.

32) "Kinetic-Energy Release in the Dissociative Double Photoionization of OCS"
T. Masuoka, I. Koyano and N. Saito
J. Chem. Phys. **97** (1992) 2392.

33) "Observation of Wet Biological Specimen by Soft X-Ray Microscope with Zone Plates at UVSOR"
N. Watanabe, M. Taniguchi, Y. Shimanuki, M. Sugiyama, A. Ohba and H. Kihara
Jpn. J. Appl. Phys. **31** (1992) L1571.

34) "Low Energy Electronic State and Optical Phonon in YbB_6"
S. Kimura, T. Nanba, S. Kunii and T. Kasuya
J. Phys. Soc. Jpn. **61** (1992) 371.

35) "Ultraviolet Photoelectron Spectra of C_{84} and K_xC_{84}"
S. Hino, K. Matsumoto, S. Hasegawa, K. Kamiya, H. Inokuchi, T. Morikawa, T. Takahashi, K. Seki, K. Kikuchi, S. Suzuki, I. Ikemoto and Y. Achiba
Chem. Phys. Lett. **190** (1992) 169.

36) "Ultraviolet Photoelectron Spectra of C_{76} and K_xC_{76}"
S. Hino, K. Matsumoto, S. Hasegawa, H. Inokuchi, T. Morikawa, T. Takahashi, K. Seki, K. Kikuchi, S. Suzuki, I. Ikemoto and Y. Achiba
Chem. Phys, Lett. **197** (1992) 38.

37) "Orientation of Oxygen Admolecules on a Reconstructed Platinum(110)(1×2) Surface: a Near-Edge X-Ray-Absorption Fine-Structure Study"
Y. Ohno, T. Matsushima, S. Tanaka, E. Yagasaki and M. Kamada
Surf. Sci. **275** (1992) 281.

38) "Low-Temperature Growth of SiO_2 Thin Film by Photo-Induced Chemical Vapor Deposition Using Synchrotron Radiation"
Y. Matsui, R. Nagayoshi, M. Nakamura, M. Okuyama and Y. Hamakawa
Jpn. J. Appl. Phys. **31** (1992) 1972.

39) "X-Ray Microscope with Grazing Incidence Mirrors and a High Resolution X-Ray Imaging Apparatus"
S. Ohsuka, A. Ohba, M. Sugiyama, T. Hayakawa, T. Matsumura, K. Kinoshita, N. Watanabe, Y. Shimanuki, Y. Sano and H. Kihara
X-Ray Microscopy III (Springer Series in Optical Sciences **67**, Springer-Verlag, 1992) p.164.

40) "Comparative Photoemission Study of Rb_xC_{60}, Rb_xC_{70} and RbC_8. A Pseudo-Gap at the Fermi Level in the Fulleride"
T. Takahashi, T. Morikawa, S. Hasegawa, K. Kamiya, H. Fujimoto, S. Hino, K. Seki, H. Katayama-Yoshida, H. Inokuchi, K. Kikuchi, S. Suzuki, K. Ikemoto and Y. Achiba
Physica C **190** (1992) 205.

41) "Stimulated Ultraviolet Emission from BaF_2 under Core-Level Exutation with Undulator Radiation"
M. Itoh and H. Itoh
Phys. Rev. B **46** (1992) 15509.

42) "Vacuum-Ultraviolet-Light-Induced Defects in Hydrogenated Amorphous Silicon Films"
Y. Saito and A. Yoshida
Philos. Mag. B **66** (1992) 219.

43) "Carbon K-Edge XANES and EXAFS of C_{60}, C_{70}, and K_3C_{60}"
H. Shinohara, H. Sato, Y. Saito, M. Kobayashi, Y. Akahama, H. Kawamura and K. Tohji
Physics and Chemistry of Fine Systems:From Clusters to Crystals II (Kluwer Academic Publishers, 1992) p.1385

44) "Preparation and Characterization of Platinum-Carbon Multilayers"
K. Yamashita, G. S. Lodha, T. Suzuki, I. Hatsukade and M. Ohtani
Physics of Multilayer Structures (Technical Digest Series **7**, Optical Society of America, 1992) p.144.

45) "Structure and Reactivity of MoO_3-MgO Catalysts"
S. Hasegawa, T. Tanaka, M. Kudo, H. Mamada, H. Hattori and S. Yoshida
Catalysis Lett. **12** (1992) 255.

46) "Optical Properties of Silica Glasses Having O_2 and Cl_2 Molecules"
K. Awazu, H. Kawazoe and K. Muta
Mat. Res. Soc. Symp. Proc. **244** (1992) 21.

47) "Structural Imperfections in Silica Glasses with an Optical Absorption Peak at 3.8 eV"
K. Awazu, K. Harada, H. Kawazoe and K. Muta
J. Appl. Phys. **72** (1992) 4696.

48) "Soft X-Ray Microscopy with Zone Plates at UVSOR"
N. Watanabe, M. Taniguchi, Y. Shimanuki, K. Kawasaki, Y. Watanabe, Y. Nagai and H. Kihara
X-Ray Microscopy III (Springer Series in Optical Sciences **67**, Springer-Verlag, 1992) p.147.

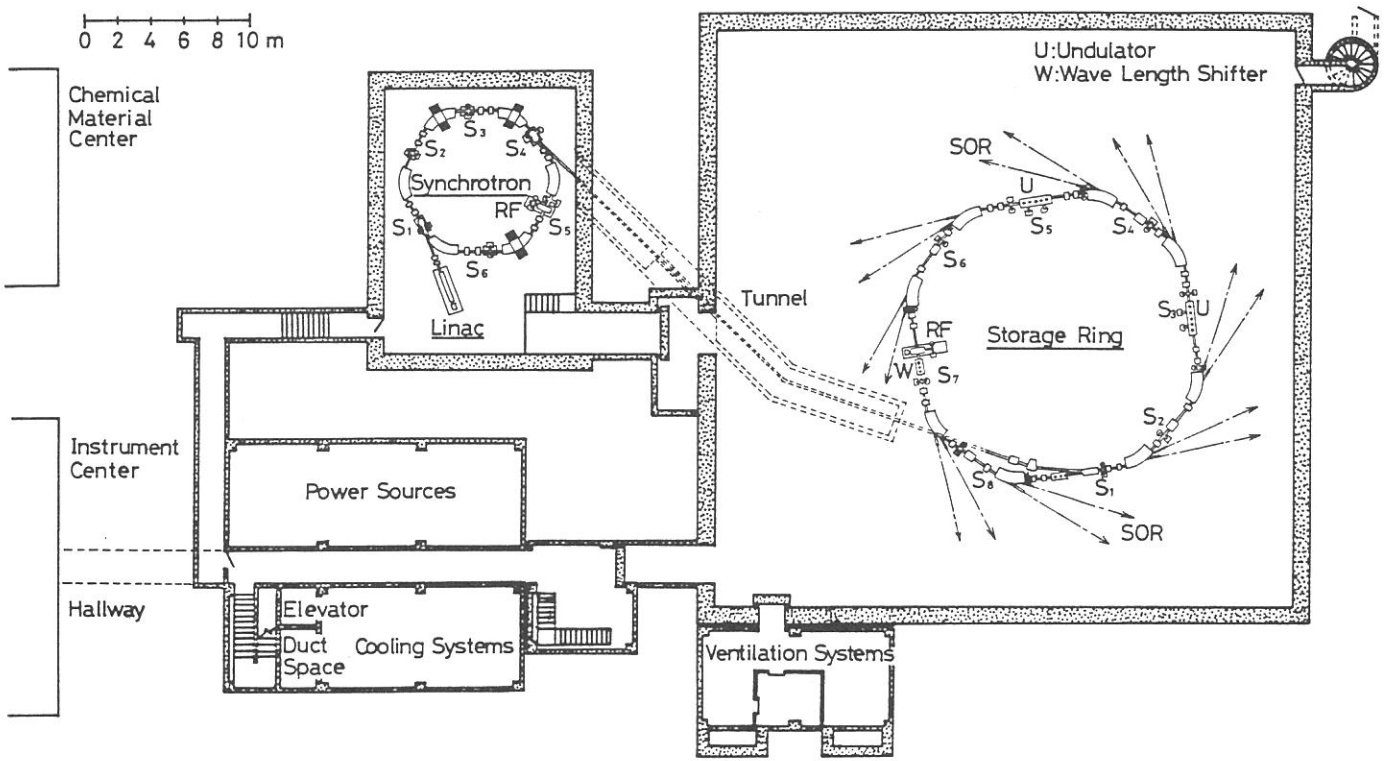

Ground plan of the basement of the UVSOR Facility

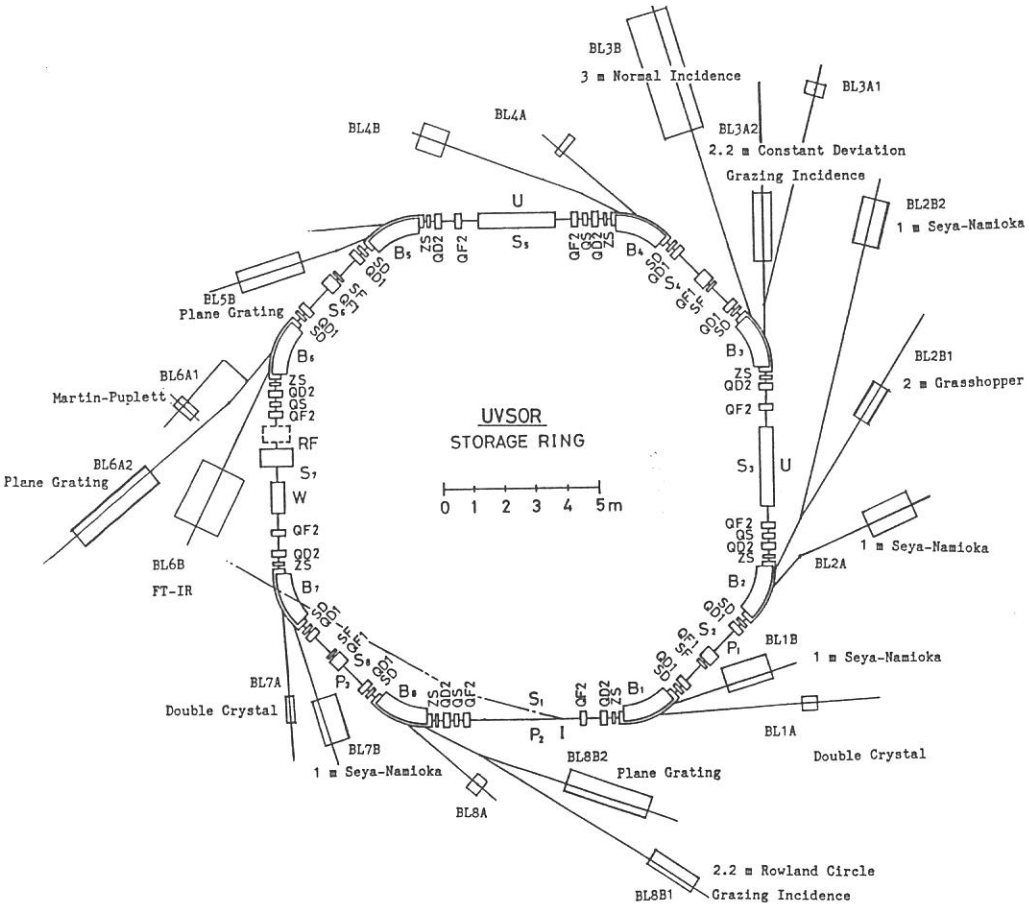

The UVSOR storage ring and the beam lines.

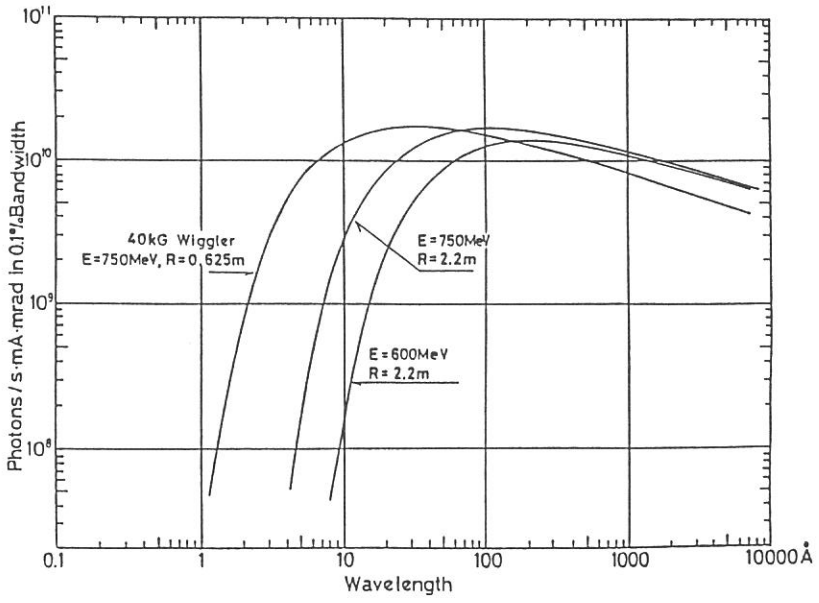

Intensity distribution of the UVSOR radiation.

Table 1. Main Parameters of the UVSOR Accelerator Complex

Linac	
Energy	$E = 15$ MeV
Frequency	$f_{RF} = 2.856$ GHz
Synchrotron	
Energy	$E = 600$ MeV
Beam Current	$I = 32$ mA
Circumference	$C = 26.6$ m
Superperiodicity	$N_{superperiodicity} = 6$
Bending Radius	$\rho = 1.8$ m
Harmonic Number	$h = 8$
RF Frequency	$f_{RF} = 90.115$ MHz
Repetition Rate	$f_{rep} = 2.6$ Hz
Storage Ring	
Energy	E=750 MeV
Critical Energy of SR	$\varepsilon_c = 425$ eV
Beam Current (Nominal)	
Multi-Bunch	$I = 200$ mA
Single-Bunch	$I = 50$ mA
Beam Lifetime	$\tau = 200$ min.at I=200 mA
Circumference	$C = 53.2$ m
Superperiodicity	$N_{superperiodicity} = 4$
Bending Radius	$\rho = 2.2$ m
Betatron Wave numbers	
Horizontal	$Q_x = 3.16$
Vertical	$Q_y = 2.65$
Momentum Compaction Factor	$\alpha = 0.032$
RF Frequency	$f_{RF} = 90.115$ MHz
RF Voltage	$V_{RF} = 50$ kV
Natural Emittance	
Horizontal	$\varepsilon_x = 1.15 \times 10^{-7}$ π m rad
Vertical[a)]	$\varepsilon_y = 1.15 \times 10^{-8}$ π m rad
Beam Sizes	
Horizontal	$\sigma_x = 0.39$ mm
Vertical[a)]	$\sigma_y = 0.27$ mm
Bunch Length	$\sigma_l = 170$ psec

a) 10 % coupling is assumed.

Table 2. Beam Lines at UVSOR

Beam Line	Monochromator, Spectrometer	Wavelength Region		Acceptance Angle(mrad)			Experiment
					Horiz.	Vert.	
BL1A	Double Crystal	15 – 8 Å			4	1	Solid
BL1B	1m Seya–Namioka	6500 – 300 Å			60	6	Gas &Solid
BL2A	1m Seya–Namioka	4000 – 300 Å			40	6	Gas
BL2B1	2m Grasshopper	600 – 15 Å			10	1.7	Gas & Solid
BL2B2	1m Seya–Namioka	2000 – 300 Å			20	6	Gas
BL3A1	None (Filter, Mirror)			(U)	0.3	0.3	Gas & Solid
BL3A2	2.2m Constant Deviation	1000 – 100 Å			10	4	Gas & Solid
	Grazing Incidence			(U)	0.3	0.3	
BL3B	3m Normal Incidence	4000 – 300 Å			20	6	Gas
BL4A	None				6	6	Irradiation
BL4B	None				8.3	6	Irradiation
BL5B	Plane Grating	2000 – 20 Å			10	2.2	Calibration#
BL6A1	Martin–Pupplet	5000 – 50 μm			80	60	Solid
BL6A2	Plane Grating	6500 – 80 Å			10	6	Solid
BL6B	FT–IR	2500 – 1 μm			70	25	Solid
BL7A	Double Crystal	15 – 8 Å			2	0.3	Solid
		15 – 2 Å		(W)	1	0.15	Solid
BL7B	1 m Seya–Namioka	6500 – 300 Å			40	8	Gas & Solid
BL8A	None (Filter)				25	8	Irradiation, User's Instrm.
BL8B1	2.2 m Rowland Circle Grazing Incidence	440 – 20 Å			10	2	Gas & Solid
BL8B2	Plane Grating	6500 – 80 Å			10	6	Solid

The BL5B constructed and used by National Institute for Fusion Science, will belong to UVSOR from the fiscal year 1993.

U: with an undulator (λ_u=85mm, N=25, λ_1=1500–235 Å), W: with a wiggler (4T).

LOCATION

Ultraviolet Synchrotron Orbital Radiation (UVSOR) Facility, Institute for Molecular Science (IMS) is located at Okazaki. Okazaki (population 300,000) is 260 km southwest of Tokyo, and can be reached by train in about 3 hours from Tokyo via New Tokaido Line (Shinkansen) and Meitetsu Line.

Address
UVSOR Facility, Institute for Molecular Science
Myodaiji, Okazaki 444, JAPAN

Telephone 0564-55-7402 (Secretary, UVSOR)
0564-52-6101 (UVSOR)
Fax 0564-54-7079 (UVSOR)
Telex 4537475 KOKKEN J (IMS)

Editors: M. Watanabe and A. Hiraya